Physics Reference Manual

Release 10.4

Geant4 Collaboration

Dec 8, 2017

CONTENTS:

1 Introduction **1**
- 1.1 Introduction . . . 1
  - 1.1.1 Scope of This Manual . . . 1
  - 1.1.2 Definition of Terms . . . 1
- 1.2 Monte Carlo Methods . . . 1
- 1.3 Particle transport . . . 2

2 Transportation **5**
- 2.1 Transportation . . . 5

3 Decay **7**
- 3.1 Decay . . . 7
  - 3.1.1 Mean Free Path for Decay in Flight . . . 7
  - 3.1.2 Branching Ratios and Decay Channels . . . 7

4 Electromagnetic **13**
- 4.1 Standard . . . 13
  - 4.1.1 Positron Annihilation into $\mu^+\mu^-$ Pair in Media . . . 13
  - 4.1.2 Positron - Electron Annihilation . . . 15
  - 4.1.3 Positron Annihilation into Hadrons in Media . . . 16
  - 4.1.4 Discrete Processes for Charged Particles . . . 17
  - 4.1.5 Compton scattering . . . 18
  - 4.1.6 Gamma Conversion into e $^+$ e $^-$ Pair . . . 20
  - 4.1.7 Bremsstrahlung . . . 24
  - 4.1.8 Ionization . . . 28
  - 4.1.9 Hadron and Ion Ionization . . . 31
  - 4.1.10 Single Scattering, Screened Coulomb Potential and NIEL . . . 35
  - 4.1.11 Multiple Scattering . . . 40
  - 4.1.12 Ion Scattering . . . 48
  - 4.1.13 Photoabsorption Ionization Model . . . 51
  - 4.1.14 PhotoElectric effect . . . 54
  - 4.1.15 Introduction . . . 55
  - 4.1.16 Ionization . . . 59
  - 4.1.17 Positron - Electron Annihilation . . . 62
  - 4.1.18 Polarized Compton scattering . . . 65
  - 4.1.19 Polarized Bremsstrahlung for electron and positron . . . 68
  - 4.1.20 Polarized Gamma conversion into an electron–positron pair . . . 70
  - 4.1.21 Polarized Photoelectric Effect . . . 71
  - 4.1.22 Photoabsorption Cross Section at Low Energies . . . 72
  - 4.1.23 Single Scattering . . . 73

4.1.24 Synchrotron Radiation . . . 74
4.1.25 MuPGen . . . 75
4.2 Low Energy . . . 81
4.2.1 Bremsstrahlung . . . 81
4.2.2 Compton Scattering . . . 84
4.2.3 Geant4-DNA processes and models . . . 85
4.2.4 Gamma Conversion . . . 85
4.2.5 Low energy extentions . . . 86
4.2.6 Electron ionisation . . . 90
4.2.7 Ionisation . . . 90
4.2.8 The MicroElec [1] extension for microelectronics applications . . . 91
4.2.9 Monash Low Energy Photon Processes . . . 92
4.2.10 Introduction . . . 93
4.2.11 Penelope physics . . . 94
4.2.12 Photoelectric effect . . . 104
4.2.13 PIXE . . . 106
4.2.14 Compton Scattering by Linearly Polarized Gamma Rays . . . 106
4.2.15 Pair production by Linearly Polarized Gamma Rays . . . 107
4.2.16 Rayleigh Scattering . . . 109
4.2.17 Atomic relaxation . . . 110
4.2.18 Triple Gamma Conversion . . . 111
4.3 Miscellaneous . . . 116
4.3.1 True Step Length . . . 116
4.3.2 Conversion from Cut in Range to Energy Threshold . . . 117
4.4 Muons . . . 119
4.4.1 Multiple scattering . . . 119
4.4.2 Bremsstrahlung . . . 120
4.4.3 Muon Ionization . . . 123
4.4.4 Muon Photonuclear Interaction . . . 124
4.4.5 Positron - Electron Pair Production by Muons . . . 126
4.5 Precision . . . 130
4.5.1 Overview . . . 130
4.5.2 Impact ionisation by hadrons and PIXE . . . 130
4.6 Utils . . . 132
4.6.1 Density effect . . . 132
4.6.2 Introduction . . . 133
4.6.3 Mean Energy Loss . . . 134
4.6.4 Energy Loss Fluctuations . . . 137
4.6.5 Correcting the Cross Section for Energy Variation . . . 140
4.7 Xrays . . . 141
4.7.1 Čerenkov Effect . . . 141
4.7.2 Scintillation . . . 141
4.7.3 Transition radiation . . . 142

5 Optical **159**
5.1 Interactions of optical photons . . . 159
5.1.1 Physics processes for optical photons . . . 159
5.1.2 Photon polarization . . . 160
5.1.3 Tracking of the photons . . . 160
5.1.4 Mie Scattering in Henyey-Greensterin Approximation . . . 163

6 Phonon **167**
6.1 Introduction . . . 167
6.2 Phonon Propagation . . . 167

6.3 Lattice Parameters . . . 168
6.4 Scattering and Mode Mixing . . . 168
6.5 Anharmonic Downconversion . . . 168

7 Hadronic **171**
7.1 Elastic . . . 171
7.1.1 Coherent elastic scattering . . . 171
7.2 Elastic_he . . . 171
7.2.1 Hadron-nucleus Elastic Scattering at Medium and High Energy . . . 171
7.3 LowEnergyChargedParticles . . . 173
7.3.1 Low Energy Charged Particle Interactions . . . 173
7.4 LowEnergyNeutrons . . . 186
7.4.1 Geant4 Low Energy Nuclear Data (LEND) Package . . . 186
7.4.2 Neutrons . . . 186
7.5 LPBias . . . 195
7.5.1 Leading Particle Bias . . . 195
7.6 Radioactive Decay . . . 197
7.6.1 Radioactive Decay . . . 197
7.7 Stopping . . . 199
7.7.1 Complementary parameterised and theoretical treatment . . . 199
7.7.2 Pion absorption at rest . . . 199
7.7.3 Interactions of Stopping Particles . . . 200
7.8 Theory-Driven . . . 200
7.8.1 Abla . . . 200
7.8.2 AbrasionAblation . . . 201
7.8.3 BinaryCascade . . . 207
7.8.4 CrossSection . . . 213
7.8.5 Evaporation . . . 220
7.8.6 Fermi Breakup . . . 228
7.8.7 Fermi Breakup . . . 230
7.8.8 Gamma Interaction . . . 230
7.8.9 Incl . . . 232
7.8.10 Multifragmentation . . . 236
7.8.11 Parton string . . . 240
7.8.12 Parton string . . . 249
7.8.13 QMD . . . 249
7.8.14 Stopped Absorption . . . 252

8 Photolepton **259**
8.1 Introduction . . . 259
8.2 Gamma-nuclear Interactions . . . 259
8.2.1 Process and Cross Section . . . 259
8.2.2 Final State Generation . . . 259
8.3 Electro-nuclear Interactions . . . 260
8.3.1 Process and Cross Section . . . 260
8.3.2 Final State Generation . . . 260
8.4 Muon-nuclear Interactions . . . 260
8.4.1 Process and Cross Section . . . 260
8.4.2 Final State Generation . . . 260

CHAPTER

ONE

INTRODUCTION

1.1 Introduction

1.1.1 Scope of This Manual

The Physics Reference Manual provides detailed explanations of the physics implemented in the Geant4 toolkit. The manual's purpose is threefold:

- to present the theoretical formulation, model, or parameterization of the physics interactions included in Geant4,
- to describe the probability of the occurrence of an interaction and the sampling mechanisms required to simulate it, and
- to serve as a reference for toolkit users and developers who wish to consult the underlying physics of an interaction.

This manual does not discuss code implementation or how to use the implemented physics interactions in a simulation. These topics are discussed in the User's Guide for Application Developers. Details of the object-oriented design and functionality of the Geant4 toolkit are given in the User's Guide for Toolkit Developers. The Installation Guide for Setting up Geant4 in Your Computing Environment describes how to get the Geant4 code, install it, and run it.

1.1.2 Definition of Terms

Several terms used throughout the Physics Reference Manual have specific meaning within Geant4, but are not well-defined in general usage. The definitions of these terms are given here.

- **process** - a C++ class which describes how and when a specific kind of physical interaction takes place along a particle track. A given particle type typically has several processes assigned to it. Occaisionally "process" refers to the interaction which the process class describes.
- **model** - a C++ class whose methods implement the details of an interaction, such as its kinematics. One or more models may be assigned to each process. In sections discussing the theory of an interaction, "model" may refer to the formulae or parameterization on which the model class is based.
- **Geant3** - a physics simulation tool written in Fortran, and the predecessor of Geant4. Although many references are made to Geant3, no knowledge of it is required to understand this manual.

1.2 Monte Carlo Methods

The Geant4 toolkit uses a combination of the composition and rejection Monte Carlo methods. Only the basic formalism of these methods is outlined here. For a complete account of the Monte Carlo methods, the interested user is referred to the publications of Butcher and Messel, Messel and Crawford, or Ford and Nelson *[3][4][3]*.

Suppose we wish to sample x in the interval $[x_1,\ x_2]$ from the distribution $f(x)$ and the *normalised* probability density function can be written as :

$$f(x) = \sum_{i=1}^{n} N_i f_i(x) g_i(x)$$

where $N_i > 0$, $f_i(x)$ are *normalised* density functions on $[x_1,\ x_2]$, and $0 \leq g_i(x) \leq 1$.

According to this method, x can sampled in the following way:

1. select a random integer $i \in \{1, 2, \cdots n\}$ with probability proportional to N_i
2. select a value x_0 from the distribution $f_i(x)$
3. calculate $g_i(x_0)$ and accept $x = x_0$ with probability $g_i(x_0)$;
4. if x_0 is rejected restart from step 1.

It can be shown that this scheme is correct and the mean number of tries to accept a value is $\sum_i N_i$.

In practice, a good method of sampling from the distribution $f(x)$ has the following properties:

- all the subdistributions $f_i(x)$ can be sampled easily;
- the rejection functions $g_i(x)$ can be evaluated easily/quickly;
- the mean number of tries is not too large.

Thus the different possible decompositions of the distribution $f(x)$ are not equivalent from the practical point of view (e.g. they can be very different in computational speed) and it can be useful to optimise the decomposition.

A remark of practical importance : if our distribution is not normalised

$$\int_{x_1}^{x_2} f(x)dx = C > 0$$

the method can be used in the same manner; the mean number of tries in this case is $\sum_i N_i/C$.

1.3 Particle transport

Particle transport in Geant4 is the result of the combined actions of the Geant4 kernel's Stepping Manager class and the actions of processes which it invokes - physics processes and the Transportation 'process' which identifies the next volume boundary and also the geometrical volume that lies behind it, when the tracks has reached it.

The expected length at which an interaction is expected to occur is determined by polling all processes applicable at each step.

Then it is determined whether the particle will remain within the current volume long enough - otherwise it will cross into a different volume before this potential interaction occurs.

The most important processes for determining the trajectory of a charged particle, including boundary crossing and the effects of external fields are the multiple scattering process and the Transportation process, which is discussed in the second following section.

BIBLIOGRAPHY

[3] J.C. Butcher and H. Messel. *Nucl. Phys.*, 20(15):, 1960.

[4] H. Messel and D. Crawford. *Electron-Photon shower distribution*. Pergamon Press, 1970.

[3] W.R. Nelson, H. Hirayama, and D.W.O. Rogers. *EGS4 code system*. SLAC, Dec 1985. SLAC-265, UC-32.

CHAPTER

TWO

TRANSPORTATION

2.1 Transportation

The transportation process is responsible for determining the geometrical limits of a step. It calculates the length of step with which a track will cross into another volume. When the track actually arrives at a boundary, the transportation process locates the next volume that it enters.

If the particle is charged and there is an electromagnetic (or potentially other) field, it is responsible for propagating the particle in this field. It does this according to an equation of motion. This equation can be provided by Geant4, for the case a magnetic or EM field, or can be provided by the user for other fields.

$$\frac{d\mathbf{p}}{ds} = \frac{1}{v}\mathbf{F} = \frac{q}{v}\big(\mathbf{E} + \mathbf{v} \times \mathbf{B}\big)$$

Extensions are provided for the propagation of the polarisation, and the effect of a gravitational field, of potential interest for cases of slow neutral particles.

Some additional details on motion in fields:

In order to intersect the model Geant4 geometry of a detector or setup, the curved trajectory followed by a charged particle is split into 'chords segments'. A chord is a straight line segment between two trajectory points. Chords are created utilizing a criterion for the maximum estimated value of the sagitta - the distance between the further curve point and the chord.

The equations of motions are solved utilising Runge Kutta methods. For the simplest case of a pure magnetic field, only the position and momentum are integrated. If an electric field is present, the time of flight is also integrated since the velocity changes along the step.

A Runge Kutta integration method for a vector **y** starting at $\mathbf{y}_{start}$ and given its derivative $d\mathbf{y}'(s)$ as a function of y and s. For a given interval h it provides an estimate of the endpoint $\mathbf{y}_{end}$. and of the integration error $\mathbf{y}_{error}$, due to the truncation errors of the RK method and the variability of the derivative.

The position and momentum as used as parts of the vector **y**, and optionally the time of flight in the lab frame and the polarisation.

A proposed step is accepted if the magnitude of the location components of the error is below a tolerated fraction ϵ of the step length s

$$|\Delta\mathbf{x}| = |\mathbf{x}_{error}| < \epsilon * s$$

and the relative momentum error is also below ϵ:

$$|\Delta\mathbf{p}| = |\mathbf{p}_{error}| < \epsilon$$

The transportation also updates the time of flight of a particle. In case of a neutral particle or of a charged particle in a pure magnetic field it utilises the average inverse velocity (average of the initial and final value of the inverse velocity.)

In case of a charged particle in an electric field or other field which does not preserve the energy, an explicit integration of time along the track is used. This is done by integrating the inverse velocity along the track:

$$t_1 = t_0 + \int_{s_0}^{s_1} \frac{1}{v} ds$$

Runge Kutta methods of different order can be utilised for fields depending on the numerical method utilised for approximating the field. Specialised methods for near-constant magnetic fields are also available.

CHAPTER

THREE

DECAY

3.1 Decay

The decay of particles in flight and at rest is simulated by the *G4Decay* class.

3.1.1 Mean Free Path for Decay in Flight

The mean free path λ is calculated for each step using

$$\lambda = \gamma\beta c\tau$$

where τ is the lifetime of the particle and

$$\gamma = \frac{1}{\sqrt{1-\beta^2}}.$$

β and γ are calculated using the momentum at the beginning of the step. The decay time in the rest frame of the particle (proper time) is then sampled and converted to a decay length using β.

3.1.2 Branching Ratios and Decay Channels

G4Decay selects a decay mode for the particle according to branching ratios defined in the *G4DecayTable* class, which is a member of the *G4ParticleDefinition* class. Each mode is implemented as a class derived from *G4VDecayChannel* and is responsible for generating the secondaries and the kinematics of the decay. In a given decay channel the daughter particle momenta are calculated in the rest frame of the parent and then boosted into the laboratory frame. Polarization is not currently taken into account for either the parent or its daughters.

A large number of specific decay channels may be required to simulate an experiment, ranging from two-body to many-body decays and $V - A$ to semi-leptonic decays. Most of these are covered by the five decay channel classes provided by Geant4:

G4PhaseSpaceDecayChannel	: phase space decay
G4DalitzDecayChannel	: dalitz decay
G4MuonDecayChannel	: muon decay
G4TauLeptonicDecayChannel	: tau leptonic decay
G4KL3DecayChannel	: semi-leptonic decays of kaon .

G4PhaseSpaceDecayChannel

The majority of decays in Geant4 are implemented using the *G4PhaseSpaceDecayChannel* class. It simulates phase space decays with isotropic angular distributions in the center-of-mass system. Three private methods of *G4PhaseSpaceDecayChannel* are provided to handle two-, three- and N-body decays:

TwoBodyDecayIt()	
ThreeBodyDecayIt()	
ManyBodyDecayIt()	

Some examples of decays handled by this class are:

$$\pi^0 \rightarrow \gamma\gamma,$$

$$\Lambda \rightarrow p\pi^-$$

and

$$K^0{}_L \rightarrow \pi^0\pi^+\pi^-.$$

G4DalitzDecayChannel

The Dalitz decay

$$\pi^0 \rightarrow \gamma + e^+ + e^-$$

and other Dalitz-like decays, such as

$$K^0{}_L \rightarrow \gamma + e^+ + e^-$$

and

$$K^0{}_L \rightarrow \gamma + \mu^+ + \mu^-$$

are simulated by the *G4DalitzDecayChannel* class. In general, it handles any decay of the form

$$P^0 \rightarrow \gamma + l^+ + l^-,$$

where P^0 is a spin-0 meson of mass M and $l^{\pm}$ are leptons of mass m. The angular distribution of the γ is isotropic in the center-of-mass system of the parent particle and the leptons are generated isotropically and back-to-back in their center-of-mass frame. The magnitude of the leptons' momentum is sampled from the distribution function

$$f(t) = (1 - \frac{t}{M^2})^3 (1 + \frac{2m^2}{t})\sqrt{1 - \frac{4m^2}{t}},$$

where t is the square of the sum of the leptons' energy in their center-of-mass frame.

Muon Decay

G4MuonDecayChannel simulates muon decay according to $V - A$ theory. The electron energy is sampled from the following distribution:

$$d\Gamma = \frac{{G_F}^2 {m_\mu}^5}{192\pi^3} 2\epsilon^2(3 - 2\epsilon)$$

where:

Γ	: decay rate
ϵ	: $= E_e/E_{max}$
E_e	: electron energy
E_{max}	: maximum electron energy $= m_\mu/2$

The magnitudes of the two neutrino momenta are also sampled from the $V-A$ distribution and constrained by energy conservation. The direction of the electron neutrino is sampled using

$$cos(\theta) = 1 - 2/E_e - 2/E_{\nu e} + 2/E_e/E_{\nu e}$$

and the muon anti-neutrino momentum is chosen to conserve momentum. Currently, neither the polarization of the muon nor the electron is considered in this class.

Leptonic Tau Decay

G4TauLeptonicDecayChannel simulates leptonic tau decays according to $V-A$ theory. This class is valid for both

$$\tau^\pm \rightarrow e^\pm + \nu_\tau + \nu_e$$

and

$$\tau^\pm \rightarrow \mu^\pm + \nu_\tau + \nu_\mu$$

modes.

The energy spectrum is calculated without neglecting lepton mass as follows:

$$d\Gamma = \frac{{G_F}^2 {m_\tau}^3}{24\pi^3} p_l E_l (3E_l {m_\tau}^2 - 4{E_l}^2 m_\tau - 2m_\tau {m_l}^2)$$

where:

Γ	: decay rate
E_l	: daughter lepton energy (total energy)
p_l	: daughter lepton momentum
m_l	: daughter lepton mass

As in the case of muon decay, the energies of the two neutrinos are not sampled from their $V-A$ spectra, but are calculated so that energy and momentum are conserved. Polarization of the τ and final state leptons is not taken into account in this class.

Kaon Decay

The class *G4KL3DecayChannel* simulates the following four semi-leptonic decay modes of the kaon:

${K^\pm}_{e3}$	: $K^\pm \rightarrow \pi^0 + e^\pm + \nu$
${K^\pm}_{\mu 3}$	: $K^\pm \rightarrow \pi^0 + \mu^\pm + \nu$
${K^0}_{e3}$	: $K^0_L \rightarrow \pi^\pm + e^\mp + \nu$
${K^0}_{\mu 3}$	: $K^0_L \rightarrow \pi^\pm + \mu^\mp + \nu$

Assuming that only the vector current contributes to $K \to l\pi\nu$ decays, the matrix element can be described by using two dimensionless form factors, f_+ and f_-, which depend only on the momentum transfer $t = (P_K - P_\pi)^2$. The Dalitz plot density used in this class is as follows *[1]*:

$$\rho\left(E_\pi, E_\mu\right) \propto f_+^2\left(t\right)[A + B\xi\left(t\right) + C\xi\left(t\right)^2]$$

where:

$A = m_K(2E_\mu E_\nu - m_K E'_\pi) + {m_\mu}^2(\frac{1}{4}E'_\pi - E_\nu)$	
$B = {m_\mu}^2(E_\nu - \frac{1}{2}E'_\pi)$	
$C = \frac{1}{4}{m_\mu}^2 E'_\pi$	
$E'_\pi = {E_\pi}^{max} - E_\pi$	

Here $\xi\left(t\right)$ is the ratio of the two form factors

$$\xi\left(t\right) = f_-\left(t\right)/f_+\left(t\right).$$

$f_+\left(t\right)$ is assumed to depend linearly on t, i.e.

$$f_+\left(t\right) = f_+\left(0\right)[1 + \lambda_+(t/{m_\pi}^2)]$$

and $f_-\left(t\right)$ is assumed to be constant due to time reversal invariance.

Two parameters, λ_+ and $\xi\left(0\right)$ are then used for describing the Dalitz plot density in this class. The values of these parameters are taken to be the world average values given by the Particle Data Group *[2]*.

BIBLIOGRAPHY

[1] J.M. Gaillard, L.M. Chounet and M.K. Gaillard. The elements of style. *Phys. Reports 4C, 199*, 1972.

[2] D.E. et al. Groom. Review of Particle Physics. *The European Physical Journal*, C15:1+, 2000. URL: http://pdg.lbl.gov.

CHAPTER

FOUR

ELECTROMAGNETIC

4.1 Standard

4.1.1 Positron Annihilation into $\mu^+\mu^-$ Pair in Media

The class G4AnnihiToMuPair simulates the electromagnetic production of muon pairs by the annihilation of high-energy positrons with atomic electrons *[1]*. Details of the implementation are given below and can also be found in Ref. *[2]*.

Total Cross Section

The annihilation of positrons and target electrons producing muon pairs in the final state ($e^+e^- \to \mu^+\mu^-$) may give an appreciable contribution to the total number of muons produced in high-energy electromagnetic cascades. The threshold positron energy in the laboratory system for this process with the target electron at rest is

$$E_{\rm th} = 2m_\mu^2/m_e - m_e \approx 43.69\ {\rm GeV}\,,$$

where m_μ and m_e are the muon and electron masses, respectively. The total cross section for the process on the electron is

$$\sigma = \frac{\pi\, r_\mu^2}{3}\,\xi\left(1+\frac{\xi}{2}\right)\sqrt{1-\xi}\,,$$

where $r_\mu = r_e\, m_e/m_\mu$ is the classical muon radius, $\xi = E_{\rm th}/E$, and E is the total positron energy in the laboratory frame. In Eq.[e1], approximations are made that utilize the inequality $m_e^2 \ll m_\mu^2$.

The cross section as a function of the positron energy E is shown in Fig.[plot:AnnihiToMuPair1]. It has a maximum at $E = 1.396\, E_{\rm th}$ and the value at the maximum is $\sigma_{\rm max} = 0.5426\, r_\mu^2 = 1.008\,\mu{\rm b}$.

Sampling of Energies and Angles

It is convenient to simulate the muon kinematic parameters in the center-of-mass (c.m.) system, and then to convert into the laboratory frame.

The energies of all particles are the same in the c.m. frame and equal to

$$E_{\rm cm} = \sqrt{\frac{1}{2}\, m_e(E+m_e)}\,.$$

The muon momenta in the c.m. frame are $P_{\rm cm} = \sqrt{E_{\rm cm}^2 - m_\mu^2}$. In what follows, let the cosine of the angle between the c.m. momenta of the μ^+ and e^+ be denoted as $x = \cos\theta_{\rm cm}$.

From the differential cross section it is easy to derive that, apart from normalization, the distribution in x is described by

$$f(x)\,dx = (1 + \xi + x^2\,(1 - \xi))\,dx\,, \quad -1 \le x \le 1\,.$$

The value of this function is contained in the interval $(1 + \xi) \le f(x) \le 2$ and the generation of x is straightforward using the rejection technique. Fig.[plot:AnnihiToMuPair2] shows both generated and analytic distributions.

The transverse momenta of the μ^+ and μ^- particles are the same, both in the c.m. and the lab frame, and their absolute values are equal to

$$P_\perp = P_{\rm cm}\,\sin\theta_{\rm cm} = P_{\rm cm}\,\sqrt{1 - x^2}\,.$$

The energies and longitudinal components of the muon momenta in the lab system may be obtained by means of a Lorentz transformation. The velocity and Lorentz factor of the center-of-mass in the lab frame may be written as

$$\beta = \sqrt{\frac{E - m_e}{E + m_e}}\,, \quad \gamma \equiv \frac{1}{\sqrt{1 - \beta^2}} = \sqrt{\frac{E + m_e}{2m_e}} = \frac{E_{\rm cm}}{m_e}\,.$$

The laboratory energies and longitudinal components of the momenta of the positive and negative muons may then be obtained:

$$E_+ = \gamma\,(E_{\rm cm} + x\,\beta\,P_{\rm cm})\,, \quad P_{+_\parallel} = \gamma\,(\beta E_{\rm cm} + x\,P_{\rm cm})\,, \tag{4.1}$$

$$E_- = \gamma\,(E_{\rm cm} - x\,\beta\,P_{\rm cm})\,, \quad P_{-_\parallel} = \gamma\,(\beta E_{\rm cm} - x\,P_{\rm cm})\,. \tag{4.2}$$

Finally, for the vectors of the muon momenta one obtains:

$$\mathbf{P}_+ = (+P_\perp\cos\varphi, +P_\perp\sin\varphi, P_{+_\parallel})\,, \tag{4.3}$$

$$\mathbf{P}_- = (-P_\perp\cos\varphi, -P_\perp\sin\varphi, P_{-_\parallel})\,, \tag{4.4}$$

where φ is a random azimuthal angle chosen between 0 and $2\,\pi$. The z-axis is directed along the momentum of the initial positron in the lab frame.

The maximum and minimum energies of the muons are given by

$$E_{\rm max} \approx \frac{1}{2}\,E\left(1 + \sqrt{1 - \xi}\right)\,,$$

$$E_{\rm min} \approx \frac{1}{2}\,E\left(1 - \sqrt{1 - \xi}\right) = \frac{E_{\rm th}}{2\left(1 + \sqrt{1 - \xi}\right)}\,.$$

The fly-out polar angles of the muons are approximately

$$\theta_+ \approx P_\perp/P_{+_\parallel}, \quad \theta_- \approx P_\perp/P_{-_\parallel}\,;$$

the maximal angle $\theta_{\rm max} \approx \dfrac{m_e}{m_\mu}\,\sqrt{1 - \xi}$ is always small compared to 1.

Validity

The process described is assumed to be purely electromagnetic. It is based on virtual γ exchange, and the Z-boson exchange and $\gamma - Z$ interference processes are neglected. The Z-pole corresponds to a positron energy of $E = M_Z^2/2m_e = 8136\,\text{TeV}$. The validity of the current implementation is therefore restricted to initial positron energies of less than about 1000TeV.

4.1.2 Positron - Electron Annihilation

Introduction

The process G4eplusAnnihilation simulates the in-flight annihilation of a positron with an atomic electron. As is usually done in shower programs [egs4], it is assumed here that the atomic electron is initially free and at rest. Also, annihilation processes producing one, or three or more, photons are ignored because these processes are negligible compared to the annihilation into two photons [egs4][messel].

Cross Section

The annihilation in flight of a positron and electron is described by the cross section formula of Heitler *[1]*[egs4]:

$$\sigma(Z,E) = \frac{Z\pi r_e^2}{\gamma+1}\left[\frac{\gamma^2+4\gamma+1}{\gamma^2-1}\ln\left(\gamma+\sqrt{\gamma^2-1}\right)-\frac{\gamma+3}{\sqrt{\gamma^2-1}}\right] \tag{4.5}$$

where

E = total energy of the incident positron

γ = E/mc^2

r_e = classical electron radius

Sampling the final state

The final state of the $e+e-$ annihilation process

$$e^+\ e^-\ \rightarrow \gamma_a\ \gamma_b$$

is simulated by first determining the kinematic limits of the photon energy and then sampling the photon energy within those limits using the differential cross section. Conservation of energy-momentum is then used to determine the directions of the final state photons.

If the incident e^+ has a kinetic energy T, then the total energy is $E_e = T + mc^2$ and the momentum is $Pc = \sqrt{T(T+2mc^2)}$. The total available energy is $E_{tot} = E_e + mc^2 = E_a + E_b$ and momentum conservation requires $\vec{P} = \vec{P}_{\gamma_a} + \vec{P}_{\gamma_b}$. The fraction of the total energy transferred to one photon (say γ_a) is

$$\epsilon = \frac{E_a}{E_{tot}} \equiv \frac{E_a}{T+2mc^2}.$$

The energy transfered to γ_a is largest when γ_a is emitted in the direction of the incident e^+. In that case $E_{amax} = (E_{tot}+Pc)/2$. The energy transfered to γ_a is smallest when γ_a is emitted in the opposite direction of the incident e^+. Then $E_{amin} = (E_{tot}-Pc)/2$. Hence,

$$\epsilon_{max} = \frac{E_a\mathsf{max}}{E_{tot}} = \frac{1}{2}\left[1+\sqrt{\frac{\gamma-1}{\gamma+1}}\right] \tag{4.6}$$

$$\epsilon_{min} = \frac{E_a\mathsf{min}}{E_{tot}} = \frac{1}{2}\left[1-\sqrt{\frac{\gamma-1}{\gamma+1}}\right] \tag{4.7}$$

where $\gamma = (T+mc^2)/mc^2$. Therefore the range of ϵ is $[\epsilon_{min}\ ;\ \epsilon_{max}]$ $(\equiv [\epsilon_{min}\ ;\ 1-\epsilon_{min}])$.

Sampling the Gamma Energy

A short overview of the sampling method is given in Chapter [secmessel]. The differential cross section of the two-photon positron-electron annihilation can be written as *[1]*[egs4]:

$$\frac{d\sigma(Z,\epsilon)}{d\epsilon} = \frac{Z\pi r_e^2}{\gamma-1}\,\frac{1}{\epsilon}\,\left[1+\frac{2\gamma}{(\gamma+1)^2}-\epsilon-\frac{1}{(\gamma+1)^2}\frac{1}{\epsilon}\right]$$

where Z is the atomic number of the material, r_e the classical electron radius, and $\epsilon \in [\epsilon_{min}\ ;\ \epsilon_{max}]$. The differential cross section can be decomposed as

$$\frac{d\sigma(Z,\epsilon)}{d\epsilon} = \frac{Z\pi r_e^2}{\gamma-1}\alpha f(\epsilon) g(\epsilon)$$

where

$$\begin{aligned} \alpha &= \ln(\epsilon_{max}/\epsilon_{min}) \\ f(\epsilon) &= \frac{1}{\alpha\epsilon} \qquad (4.8) \\ g(\epsilon) &= \left[1+\frac{2\gamma}{(\gamma+1)^2}-\epsilon-\frac{1}{(\gamma+1)^2}\frac{1}{\epsilon}\right] \equiv 1-\epsilon+\frac{2\gamma\epsilon-1}{\epsilon(\gamma+1)^2} \qquad (4.9) \end{aligned}$$

Given two random numbers $r, r' \in [0,1]$, the photon energies are chosen as follows:

1. **sample ϵ from $f(\epsilon)$:** $\epsilon = \epsilon_{min}\left(\frac{\epsilon_{max}}{\epsilon_{min}}\right)^r$
2. test the rejection function: if $g(\epsilon) \geq r'$ accept ϵ, otherwise return to step 1.

Then the photon energies are $E_a = \epsilon E_{tot} \qquad E_b = (1-\epsilon)E_{tot}$.

Computing the Final State Kinematics

If θ is the angle between the incident e^+ and γ_a, then from energy-momentum conservation,

$$\cos\theta = \frac{1}{Pc}\left[T + mc^2\frac{2\epsilon-1}{\epsilon}\right] = \frac{\epsilon(\gamma+1)-1}{\epsilon\sqrt{\gamma^2-1}}.$$

The azimuthal angle, ϕ, is generated isotropically and the photon momentum vectors, $\vec{P_{\gamma_a}}$ and $\vec{P_{\gamma_b}}$, are computed from energy-momentum conservation and transformed into the lab coordinate system.

Annihilation at Rest

The method AtRestDoIt treats the special case when a positron comes to rest before annihilating. It generates two photons, each with energy $k = mc^2$ and an isotropic angular distribution.

4.1.3 Positron Annihilation into Hadrons in Media

Introduction

The process G4eeToHadrons simulates the in-flight annihilation of a positron with an atomic electron into hadrons *[1]*. It is assumed here that the atomic electron is initially free and at rest. Currently accurate cross section is available with a validity range up to 1 TeV.

Cross Section

The annihilation of positrons and target electrons producing pion pairs in the final state ($e^+e^- \to \pi^+\pi^-$) may give an appreciable contribution to electron-jet conversion at the LHC, and for the increasing total number of muons produced in the beam pipe of the linear collider *[1]*. The threshold positron energy in the laboratory system for this process with the target electron at rest is

$$E_{\rm th} = 2m_\pi^2/m_e - m_e \approx 70.35\ {\rm GeV}\,, \tag{4.10}$$

where m_π and m_e are the pion and electron masses, respectively. The total cross section is dominated by the reaction

$$e^+e^- \to \rho\gamma \to \pi^+\pi^-\gamma, \tag{4.11}$$

where γ is a radiative photon and $\rho(770)$ is a well known vector meson. This radiative correction is essential, because it significantly modifies the shape of the resonance. Details of the theory are described in [anniToHad.ben], in which the main term and the leading α^2 corrections are taken into account.

Additional contribution to the hadron production cross section come from $\omega(783)$ and $\phi(1020)$ resonanses with $\pi^+\pi^-\pi^0$, K^+K^-, K_LK_S, $\eta\gamma$, and $\pi^0\gamma$ final states.

Sampling the final state

The final state of the $e + e-$ annihilation process is simulated by first sampling of radiative gamma using a sum of all hadronic cross sections in the center of mass system. Photon energy is used to define new differential cross section. After that, hadronic channel is randomly selected according to it partial cross section. Final state is sampled and final particles transformed to the laboratory system.

4.1.4 Discrete Processes for Charged Particles

Some processes for charged particles following the same interface $G4VEmProcess$ as gamma processes described in section [em_disc]:

- G4CoulombScattering;
- G4eplusAnnihilation (with additional AtRest methods);
- G4eplusPolarizedAnnihilation (with additional AtRest methods);
- G4eeToHadrons;
- G4NuclearStopping;
- G4MicroElecElastic;
- G4MicroElecInelastic.

Corresponding model classes follow the $G4VEmModel$ interface:

- G4DummyModel (zero cross section, no secondaries);
- G4eCoulombScatteringModel;
- G4eSingleCoulombScatteringModel;
- G4IonCoulombScatteringModel;
- G4eeToHadronsModel;
- G4PenelopeAnnihilationModel;
- G4PolarizedAnnihilationModel;

- G4ICRU49NuclearStoppingModel;
- G4MicroElecElasticModel;
- G4MicroElecInelasticModel.

Some processes from do not follow described EM interfaces but provide direct implementations of the basic $G4VDiscreteProcess$ process:

- G4AnnihiToMuPair;
- G4ScreenedNuclearRecoil;
- G4Cerenkov;
- G4Scintillation;
- G4SynchrotronRadiation;

4.1.5 Compton scattering

The Compton scattering is an inelastic gamma scattering on atom with the ejection of an electron. In the standard subpackage two model *G4KleinNishinaCompton* and *G4KleinNishinaModel* are available. The first model is the fastest, in the second model atomic shell effects are taken into account.

Cross Section

When simulating the Compton scattering of a photon from an atomic electron, an empirical cross section formula is used, which reproduces the cross section data down to 10 keV:

$$\sigma(Z, E_\gamma) = \left[P_1(Z)\, \frac{\log(1+2X)}{X} + \frac{P_2(Z) + P_3(Z)X + P_4(Z)X^2}{1 + aX + bX^2 + cX^3} \right].$$

$$\begin{aligned} Z &= \text{atomic number of the medium} && (4.12)\\ E_\gamma &= \text{energy of the photon} && (4.13)\\ X &= E_\gamma / mc^2 && (4.14)\\ m &= \text{electron mass} && (4.15)\\ P_i(Z) &= Z(d_i + e_i Z + f_i Z^2). && (4.16) \end{aligned}$$

The values of the parameters can be found within the method which computes the cross section per atom. A fit of the parameters was made to over 511 data points *[4]*[storm.comp] chosen from the intervals

$$1 \le Z \le 100 \tag{4.17}$$

$$E_\gamma \in [10\ \text{keV}, 100\ \text{GeV}]. \tag{4.18}$$

The accuracy of the fit was estimated to be

$$\frac{\Delta\sigma}{\sigma} = \begin{cases} \approx 10\% & \text{for } E_\gamma \simeq 10\ \text{keV} - 20\ \text{keV} \\ \le 5 - 6\% & \text{for } E_\gamma > 20\ \text{keV} \end{cases}$$

To avoid sampling problems in the Compton process the cross section is set to zero at low-energy limit of cross section table, which is $100eV$ in majority of EM Phyiscs Lists.

Sampling the Final State

The Klein-Nishina differential cross section per atom is [klein.comp]:

$$\frac{d\sigma}{d\epsilon} = \pi r_e^2 \frac{m_e c^2}{E_0} Z \left[\frac{1}{\epsilon} + \epsilon\right] \left[1 - \frac{\epsilon \sin^2\theta}{1+\epsilon^2}\right]$$

where

r_e	classical electron radius
$m_e c^2$	electron mass
E_0	energy of the incident photon
E_1	energy of the scattered photon
ϵ	E_1/E_0 .

Assuming an elastic collision, the scattering angle θ is defined by the Compton formula:

$$E_1 = E_0 \frac{m_e c^2}{m_e c^2 + E_0(1-\cos\theta)}.$$

Sampling the Photon Energy

The value of ϵ corresponding to the minimum photon energy (backward scattering) is given by

$$\epsilon_0 = \frac{m_e c^2}{m_e c^2 + 2E_0},$$

hence $\epsilon \in [\epsilon_0, 1]$. Using the combined composition and rejection Monte Carlo methods described in [butch][messel][egs4] one may set

$$\Phi(\epsilon) \simeq \left[\frac{1}{\epsilon} + \epsilon\right] \left[1 - \frac{\epsilon \sin^2\theta}{1+\epsilon^2}\right] = f(\epsilon) \cdot g(\epsilon) = [\alpha_1 f_1(\epsilon) + \alpha_2 f_2(\epsilon)] \cdot g(\epsilon),$$

$$\begin{array}{lll} \alpha_1 = \ln(1/\epsilon_0) & ; & f_1(\epsilon) = 1/(\alpha_1 \epsilon) \\ \alpha_2 = (1-\epsilon_0^2)/2 & ; & f_2(\epsilon) = \epsilon/\alpha_2. \end{array}$$

f_1 and f_2 are probability density functions defined on the interval $[\epsilon_0, 1]$, and

$$g(\epsilon) = \left[1 - \frac{\epsilon}{1+\epsilon^2} \sin^2\theta\right]$$

is the rejection function $\forall \epsilon \in [\epsilon_0, 1] \Longrightarrow 0 < g(\epsilon) \leq 1$. Given a set of 3 random numbers r, r', r'' uniformly distributed on the interval [0,1], the sampling procedure for ϵ is the following:

1. decide whether to sample from $f_1(\epsilon)$ or $f_2(\epsilon)$: if $r < \alpha_1/(\alpha_1+\alpha_2)$ select $f_1(\epsilon)$, otherwise select $f_2(\epsilon)$
2. sample ϵ from the distributions corresponding to f_1 or f_2: for $f_1 : \epsilon = \epsilon_0^{r'}$ $(\equiv \exp(-r'\alpha_1))$ for $f_2 : \epsilon^2 = \epsilon_0^2 + (1-\epsilon_0^2)r'$
3. calculate $\sin^2\theta = t(2-t)$ where $t \equiv (1-\cos\theta) = m_e c^2(1-\epsilon)/(E_0\epsilon)$
4. test the rejection function: if $g(\epsilon) \geq r''$ accept ϵ, otherwise go to step 1.

Compute the Final State Kinematics

After the successful sampling of ϵ, the polar angles of the scattered photon with respect to the direction of the parent photon are generated. The azimuthal angle, ϕ, is generated isotropically and θ is as defined in the previous section. The momentum vector of the scattered photon, $\overrightarrow{P_{\gamma 1}}$, is then transformed into the World coordinate system. The kinetic energy and momentum of the recoil electron are then

$$T_{el} = E_0 - E_1 \tag{4.19}$$
$$\overrightarrow{P_{el}} = \overrightarrow{P_{\gamma 0}} - \overrightarrow{P_{\gamma 1}}. \tag{4.20}$$

Doppler broading of final electron momentum due to electron motion is implemented only in *G4KleinNishinaModel*. For that emphirical electron density profile function is used.

Atomic shell effects

The differential cross-section described above is valid only for those collisions in which the energy of the recoil electron is large compared to its binding energy (which is ignored). In the alternative model (*G4KleinNishinaModel*) atomic shell effects are taken into account. For that a sampling of a shell is performed with the weight proportional to number of shell electrons. Electron energy distribution function is approximated via simplified form

$$F(T) = \exp\left(-T/E_b\right)/E_b,$$

where E_b is shell bound energy, T - kinetic energy of the electron.

The value T is sampled and scattering is sampled in the rest frame of the electron according the algorithm described in the previous sub-chapter. After sampling an inverse Lorentz transformation to the laboratory frame is performed. Potential energy $(E_b + T)$ is subtracted from the scattered electron kinetic energy. If final electron energy become negative then sampling is repeated. Atomic relaxation are sampled if deexcitation module is enabled. Enabling of atomic relaxation for Compton scattering is performed in the same way as for photoelectric effect [subsec:em.peerelax].

4.1.6 Gamma Conversion into e + e - Pair

In the standard sub-package two models are available. The first model is implemented in the class *G4BetheHeitlerModel*, it was derived from Geant3 and is applicable below $100GeV$. In the second (*G4PairProductionRelModel*) Landau-Pomenrachuk-Migdal (LPM) effect is taken into account and this model can be applied for high energy gammas (above $100MeV$).

Cross Section

According *[4]*, *[1]* the total cross-section per atom for the conversion of a gamma into an (e^+, e^-) pair has been parameterized as

$$\sigma(Z, E_\gamma) = Z(Z+1)\left[F_1(X) + F_2(X)\,Z + \frac{F_3(X)}{Z}\right],$$

where E_γ is the incident gamma energy and $X = \ln(E_\gamma/m_e c^2)$. The functions F_n are given by

$$F_1(X) = a_0 + a_1 X + a_2 X^2 + a_3 X^3 + a_4 X^4 + a_5 X^5 \tag{4.21}$$
$$F_2(X) = b_0 + b_1 X + b_2 X^2 + b_3 X^3 + b_4 X^4 + b_5 X^5$$
$$F_3(X) = c_0 + c_1 X + c_2 X^2 + c_3 X^3 + c_4 X^4 + c_5 X^5,$$

with the parameters a_i, b_i, c_i taken from a least-squares fit to the data *[4]*. Their values can be found in the function which computes formula [conv1]. This parameterization describes the data in the range

$$1 \leq Z \leq 100 \tag{4.22}$$

and

$$E_\gamma \in [1.5 \text{ MeV}, 100 \text{ GeV}]. \tag{4.23}$$

The accuracy of the fit was estimated to be $\frac{\Delta\sigma}{\sigma} \leq 5\%$ with a mean value of $\approx 2.2\%$. Above 100 GeV the cross section is constant. Below $E_{low} = 1.5$ MeV the extrapolation

$$\sigma(E) = \sigma(E_{low}) \cdot \left(\frac{E - 2m_e c^2}{E_{low} - 2m_e c^2} \right)^2$$

is used.

In a given material the mean free path, λ, for a photon to convert into an (e^+, e^-) pair is

$$\lambda(E_\gamma) = \left(\sum_i n_{ati} \cdot \sigma(Z_i, E_\gamma) \right)^{-1}$$

where n_{ati} is the number of atoms per volume of the i^{th} element of the material.

Corrected Bethe-Heitler Cross Section

As written in *[1]*, the Bethe-Heitler formula corrected for various effects is

$$\begin{aligned} \frac{d\sigma(Z,\epsilon)}{d\epsilon} &= \alpha r_e^2 Z[Z + \xi(Z)] \left\{ [\epsilon^2 + (1-\epsilon)^2] \left[\Phi_1(\delta(\epsilon)) - \frac{F(Z)}{2} \right] \right. \\ &\left. + \frac{2}{3}\epsilon(1-\epsilon) \left[\Phi_2(\delta(\epsilon)) - \frac{F(Z)}{2} \right] \right\} \end{aligned} \tag{4.24}$$

where α is the fine-structure constant and r_e the classical electron radius. Here $\epsilon = E/E_\gamma$, E_γ is the energy of the photon and E is the total energy carried by one particle of the (e^+, e^-) pair. The kinematical limits of ϵ are therefore

$$\frac{m_e c^2}{E_\gamma} = \epsilon_0 \leq \epsilon \leq 1 - \epsilon_0.$$

Screening Effect

The *screening variable*, δ, is a function of ϵ

$$\delta(\epsilon) = \frac{136}{Z^{1/3}} \frac{\epsilon_0}{\epsilon(1-\epsilon)},$$

and measures the 'impact parameter' of the projectile. Two screening functions are introduced in the Bethe-Heitler formula :

$$\begin{aligned} \text{for } \delta \leq 1 \quad \Phi_1(\delta) &= 20.867 - 3.242\delta + 0.625\delta^2 \\ \Phi_2(\delta) &= 20.209 - 1.930\delta - 0.086\delta^2 \\ \text{for } \delta > 1 \quad \Phi_1(\delta) &= \Phi_2(\delta) = 21.12 - 4.184 \ln(\delta + 0.952). \end{aligned} \tag{4.25}$$

Because the formula [conv.eq1] is symmetric under the exchange $\epsilon \leftrightarrow (1-\epsilon)$, the range of ϵ can be restricted to

$$\epsilon \in [\epsilon_0, 1/2].$$

Born Approximation

The Bethe-Heitler formula is calculated with plane waves, but Coulomb waves should be used instead. To correct for this, a *Coulomb correction function* is introduced in the Bethe-Heitler formula :

$$\begin{aligned} \text{for } E_\gamma &< 50 \text{ MeV}: \quad F(z) = 8/3 \ln Z \\ \text{for } E_\gamma &\geq 50 \text{ MeV}: \quad F(z) = 8/3 \ln Z + 8 f_c(Z) \end{aligned} \tag{4.26}$$

with

$$\begin{aligned} f_c(Z) &= (\alpha Z)^2 \left[\frac{1}{1+(\alpha Z)^2} \right. \\ &\left. +0.20206 - 0.0369(\alpha Z)^2 + 0.0083(\alpha Z)^4 - 0.0020(\alpha Z)^6 + \cdots \right]. \end{aligned} \tag{4.27}$$

It should be mentioned that, after these additions, the cross section becomes negative if

$$\delta > \delta_{max}(\epsilon_1) = \exp\left[\frac{42.24 - F(Z)}{8.368}\right] - 0.952.$$

This gives an additional constraint on ϵ :

$$\delta \leq \delta_{max} \Longrightarrow \epsilon \geq \epsilon_1 = \frac{1}{2} - \frac{1}{2}\sqrt{1 - \frac{\delta_{min}}{\delta_{max}}}$$

where

$$\delta_{min} = \delta\left(\epsilon = \frac{1}{2}\right) = \frac{136}{Z^{1/3}}\, 4\epsilon_0$$

has been introduced. Finally the range of ϵ becomes

$$\epsilon \in [\epsilon_{min} = \max(\epsilon_0, \epsilon_1),\ 1/2].$$

[width=,height=0.4,draft=false] electromagnetic/standard/conv.eps

Gamma Conversion in the Electron Field

The electron cloud gives an additional contribution to pair creation, proportional to Z (instead of Z^2). This is taken into account through the expression

$$\xi(Z) = \frac{\ln(1440/Z^{2/3})}{\ln(183/Z^{1/3}) - f_c(Z)}.$$

Factorization of the Cross Section

ϵ is sampled using the techniques of 'composition+rejection', as treated in *[6]*[m.butch][messel]. First, two auxiliary screening functions should be introduced:

$$\begin{aligned} F_1(\delta) &= 3\Phi_1(\delta) - \Phi_2(\delta) - F(Z) \\ F_2(\delta) &= \frac{3}{2}\Phi_1(\delta) - \frac{1}{2}\Phi_2(\delta) - F(Z) \end{aligned} \tag{4.28}$$

It can be seen that $F_1(\delta)$ and $F_2(\delta)$ are decreasing functions of δ, $\forall \delta \in [\delta_{min}, \delta_{max}]$. They reach their maximum for $\delta_{min} = \delta(\epsilon = 1/2)$:

$$\begin{aligned} F_{10} &= \max F_1(\delta) = F_1(\delta_{min}) \\ F_{20} &= \max F_2(\delta) = F_2(\delta_{min}). \end{aligned} \tag{4.29}$$

After some algebraic manipulations the formula [conv.eq1] can be written :

$$\begin{aligned}\frac{d\sigma(Z,\epsilon)}{d\epsilon} &= \alpha r_e^2 Z[Z+\xi(Z)]\frac{2}{9}\left[\frac{1}{2}-\epsilon_{min}\right] \\ &\quad \times \left[N_1\, f_1(\epsilon)\, g_1(\epsilon) + N_2\, f_2(\epsilon)\, g_2(\epsilon)\right], \end{aligned} \tag{4.30}$$

where

$$N_1 = \left[\frac{1}{2}-\epsilon_{min}\right]^2 F_{10} \qquad f_1(\epsilon) = \frac{3}{\left[\frac{1}{2}-\epsilon_{min}\right]^3}\left[\frac{1}{2}-\epsilon\right]^2 \qquad g_1(\epsilon) = \frac{F_1(\epsilon)}{F_{10}} \tag{4.31}$$

$$N_2 = \frac{3}{2}F_{20} \qquad f_2(\epsilon) = \text{const} = \frac{1}{\left[\frac{1}{2}-\epsilon_{min}\right]} \qquad g_2(\epsilon) = \frac{F_2(\epsilon)}{F_{20}}. \tag{4.32}$$

$f_1(\epsilon)$ and $f_2(\epsilon)$ are probability density functions on the interval $\epsilon \in [\epsilon_{min}, 1/2]$ such that

$$\int_{\epsilon_{min}}^{1/2} f_i(\epsilon)\, d\epsilon = 1$$

, and $g_1(\epsilon)$ and $g_2(\epsilon)$ are valid rejection functions: $0 < g_i(\epsilon) \leq 1$.

Final State

The differential cross section depends on the atomic number Z of the material in which the interaction occurs. In a compound material the element i in which the interaction occurs is chosen randomly according to the probability

$$Prob(Z_i, E_\gamma) = \frac{n_{ati}\sigma(Z_i, E_\gamma)}{\sum_i [n_{ati}\cdot\sigma_i(E_\gamma)]}.$$

Sampling the Energy

Given a triplet of uniformly distributed random numbers (r_a, r_b, r_c) :

1. use r_a to choose which decomposition term in [conv.eq2] to use:

$$\begin{aligned}\text{if } r_a < N_1/(N_1+N_2) &\rightarrow f_1(\epsilon)\, g_1(\epsilon) \\ \text{otherwise} &\rightarrow f_2(\epsilon)\, g_2(\epsilon)\end{aligned}$$

2. sample ϵ from $f_1(\epsilon)$ or $f_2(\epsilon)$ with r_b :

$$\epsilon = \frac{1}{2} - \left(\frac{1}{2}-\epsilon_{min}\right) r_b^{1/3} \quad \text{or} \quad \epsilon = \epsilon_{min} + \left(\frac{1}{2}-\epsilon_{min}\right) r_b$$

3. reject ϵ if $g_1(\epsilon)$or $g_2(\epsilon) < r_c$

note : below $E_\gamma = 2$ MeV it is enough to sample ϵ uniformly on $[\epsilon_0,\ 1/2]$, without rejection.

Charge

The charge of each particle of the pair is fixed randomly.

Polar Angle of the Electron or Positron

The polar angle of the electron (or positron) is defined with respect to the direction of the parent photon. The energy-angle distribution given by Tsai *[1][2]* is quite complicated to sample and can be approximated by a density function suggested by Urban *[5]* :

$$\forall u \in [0,\ \infty[\quad f(u) = \frac{9a^2}{9+d}\left[u\exp(-au) + d\,u\exp(-3au)\right]$$

with

$$a = \frac{5}{8} \qquad d = 27 \qquad \text{and } \theta_{\pm} = \frac{mc^2}{E_{\pm}}\,u.$$

A sampling of the distribution [conv.eq3] requires a triplet of random numbers such that

$$\text{if } r_1 < \frac{9}{9+d} \rightarrow u = \frac{-\ln(r_2 r_3)}{a} \qquad \text{otherwise } u = \frac{-\ln(r_2 r_3)}{3a}.$$

The azimuthal angle ϕ is generated isotropically. The e^+ and e^- momenta are assumed to be coplanar with the parent photon. This information, together with energy conservation, is used to calculate the momentum vectors of the (e^+, e^-) pair and to rotate them to the global reference system.

Ultra-Relativistic Model

It is implemented in the class *G4PairProductionRelModel* and is configured above $80GeV$ in all reference Physics lists. The cross section is computed using direct integration of differential cross section *[1][2]* and not its parameterisation described in [subsec:xs.conv]. LPM effect is taken into account in the same way as for bremsstrahlung [subsec:lpm.brem]. Secondary generation algorithm is the same as in the standard Bethe-Haitler model.

4.1.7 Bremsstrahlung

The class $G4eBremsstrahlung$ provides the energy loss of electrons and positrons due to the radiation of photons in the field of a nucleus according to the approach described in Section [en_loss]. Above a given threshold energy the energy loss is simulated by the explicit production of photons. Below the threshold the emission of soft photons is treated as a continuous energy loss.

Below electron/positron energies of 1 GeV, the cross section evaluation is based on a dedicated parameterization, above this limit an analytic cross section is used. In GEANT4 the Landau-Pomeranchuk-Migdal effect has also been implemented.

Seltzer-Berger bremsstrahlung model

In order to iprove accuracy of the model described above a new model *G4SeltzerBergerModel* have been design which implementing cross section based on interpolation of published tables *[4][3]*. Single-differential cross section can be written as a sum of a contribution of bremsstrahlung produced in the field of the screened atomic nucleus $d\sigma_n/dk$, and the part $Z\,d\sigma_e/dk$ corresponding to bremsstrahlung produced in the field of the Z atomic electrons,

$$\frac{d\sigma}{dk} = \frac{d\sigma_n}{dk} + Z\frac{d\sigma_e}{dk}\,.$$

The differential cross section depends on the energy k of the emitted photon, the kinetic energy T_1 of the incident electron and the atomic number Z of the target atom.

Seltzer and Berger have published extensive tables for the differential cross section $d\sigma_n/dk$ and $d\sigma_e/dk$ *[4][3]*, covering electron energies from 1keV up to 10GeV, substantially extending previous publications *[5]*. The results are

in good agreement with experimental data, and provided also the basis of bremsstrahlung implementations in many Monte Carlo programs (e.g. Penelope, EGS). The estimated uncertainties for $d\sigma/dk$ are:

- 3% to 5% in the high energy region ($T_1 \geq 50$MeV),
- 5% to 10% in the intermediate energy region ($2 \geq T_1 \leq 50$MeV),
- and 10% at low energies region compared with Pratt results. ($T_1 \leq 2$MeV).

The restricted cross section ([comion.b]) and the energy loss ([comion.c]) are obtained by numerical integration performed at initialisation stage of Geant4. This method guarantees consistent description independent of the energy cutoff. The current version uses an interpolation in tables for 52 available electron energy points versus 31 photon energy points, and for atomic number Z ranging from 1 to 99. It is the default bremsstrahlung model in Geant4 since version 9.5. Figure [fig:brem.cross] shows a comparison of the total bremsstrahlung cross sections with the previous implementation, and with the relativistic model.

After the successful sampling of ϵ, the polar angles of the radiated photon are generated with respect to the parent electron's momentum. It is difficult to find simple formulae for this angle in the literature. For example the double differential cross section reported by Tsai *[1][2]* is

$$\frac{d\sigma}{dkd\Omega} = \frac{2\alpha^2 e^2}{\pi k m^4}\left\{\left[\frac{2\epsilon-2}{(1+u^2)^2}+\frac{12u^2(1-\epsilon)}{(1+u^2)^4}\right]Z(Z+1)\right. \tag{4.33}$$

$$\left.+\left[\frac{2-2\epsilon-\epsilon^2}{(1+u^2)^2}-\frac{4u^2(1-\epsilon)}{(1+u^2)^4}\right]\left[X-2Z^2 f_c((\alpha Z)^2)\right]\right\} \tag{4.34}$$

$$u = \frac{E\theta}{m} \tag{4.35}$$

$$X = \int_{t_{min}}^{m^2(1+u^2)^2}\left[G_Z^{el}(t)+G_Z^{in}(t)\right]\frac{t-t_{min}}{t^2}dt \tag{4.36}$$

$$G_Z^{el,in}(t) \quad \text{atomic form factors} \tag{4.37}$$

$$t_{min} = \left[\frac{km^2(1+u^2)}{2E(E-k)}\right]^2 = \left[\frac{\epsilon m^2(1+u^2)}{2E(1-\epsilon)}\right]^2. \tag{4.38}$$

The sampling of this distribution is complicated. It is also only an approximation to within a few percent, due at least to the presence of the atomic form factors. The angular dependence is contained in the variable $u = E\theta m^{-1}$. For a given value of u the dependence of the shape of the function on Z, E and $\epsilon = k/E$ is very weak. Thus, the distribution can be approximated by a function

$$f(u) = C\left(ue^{-au} + due^{-3au}\right)$$

where

$$C = \frac{9a^2}{9+d} \qquad a = 0.625 \qquad d = 27$$

where E is in GeV. While this approximation is good at high energies, it becomes less accurate around a few MeV. However in that region the ionization losses dominate over the radiative losses. The sampling of the function $f(u)$ can be done with three random numbers r_i, uniformly distributed on the interval [0,1]:

1. choose between ue^{-au} and due^{-3au}:

$$b = \begin{cases} a & \text{if} \quad r_1 < 9/(9+d) \\ 3a & \text{if} \quad r_1 \geq 9/(9+d) \end{cases}$$

2. sample ue^{-bu}:

$$u = -\frac{\log(r_2 r_3)}{b}$$

3. check that:

$$u \leq u_{max} = \frac{E\pi}{m}$$

otherwise go back to 1.

The probability of failing the last test is reported in table [tb:phys341-1].

llll [0.5cm] E (MeV) & P(%) 0.511 & 3.4 0.6 & 2.2 0.8 & 1.2 1.0 & 0.7 2.0 & $<$ 0.1

The function $f(u)$ can also be used to describe the angular distribution of the photon in μ bremsstrahlung and to describe the angular distribution in photon pair production. The azimuthal angle ϕ is generated isotropically. Along with θ, this information is used to calculate the momentum vectors of the radiated photon and parent recoiled electron, and to transform them to the global coordinate system. The momentum transfer to the atomic nucleus is neglected.

Bremsstrahlung of high-energy electrons

Above an electron energy of 1 GeV an analytic differential cross section representation is used *[6]*, which was modified to account for the density effect and the Landau-Pomeranchuk-Migdal (LPM) effect *[7][8]*.

Relativistic Bremsstrahlung cross section

The basis of the implementation is the well known high energy limit of the Bremsstrahlung process *[6]*,

$$\frac{d\sigma}{dk} = \frac{4\alpha r_e^2}{3k}\Big[\{y^2 + 2[1+(1-y)^2]\}[Z^2(F_{el}-f) + ZF_{inel}] + (1-y)\frac{Z^2+Z}{3}\Big]$$

The *elastic from factor* F_{el} and *inelastic form factor* F_{inel}, describe the scattering on the nucleus and on the shell electrons, respectively, and for $Z > 4$ are given by *[9]*

$$F_{el} = \log\left(\frac{184.15}{Z^{\frac{1}{3}}}\right) \tag{4.39}$$

and (4.40)

$$F_{inel} = \log\left(\frac{1194.}{Z^{\frac{2}{3}}}\right). \tag{4.41}$$

This corresponds to the complete screening approximation. The Coulomb correction is defined as *[9]*

$$f = \alpha^2 Z^2 \sum_{n=1}^{\infty} \frac{1}{n(n^2+\alpha^2 Z^2)} \tag{4.42}$$

This approach provides an analytic differential cross section for an efficient evaluation in a Monte Carlo computer code. Note that in this approximation the differential cross section $d\sigma/dk$ is independent of the energy of the initial electron and is also valid for positrons.

The total integrated cross section $\int d\sigma/dk\, dk$ is divergent, but the energy loss integral $\int k d\sigma/dk\, dk$ is finite. This allows the usual separation into continuous enery loss, and discrete photon production according to Eqs. ([comion.c]) and ([comion.b]).

Landau Pomeranchuk Migdal (LPM) effect

At higher energies matter effects become more and more important. In GEANT4 the two leading matter effects, the LPM effect and the dielectric suppresion (or Ter-Mikaelian effect), are considered. The analytic cross section representation, eq., provides the basis for the incorporation of these matter effects. The LPM effect (see for example *[10]*[

ebrem.anthony][ebrem.hansen]) is the suppression of photon production due to the multiple scattering of the electron. If an electron undergoes multiple scattering while traversing the so called "formation zone", the bremsstrahlung amplitudes from before and after the scattering can interfere, reducing the probability of bremsstrahlung photon emission (a similar suppression occurs for pair production). The suppression becomes significant for photon energies below a certain value, given by

$$\frac{k}{E} < \frac{E}{E_{LPM}},$$

where

k	photon energy
E	electron energy
E_{LPM}	characteristic energy for LPM effect (depend on the medium).

The value of the LPM characteristic energy can be written as

$$E_{LPM} = \frac{\alpha m^2 X_0}{4hc},$$

where

α	fine structure constant
m	electron mass
X_0	radiation length in the material
h	Planck constant
c	velocity of light in vacuum.

At high energies (approximately above 1 GeV) the differential cross section including the Landau-Pomeranchuk-Migdal effect, can be expressed using an evaluation based on *[11][8][7]*

$$\frac{d\sigma}{dk} = \frac{4\alpha r_e^2}{3k}\Big[\xi(s)\{y^2 G(s) + 2[1+(1-y)^2]\phi(s)\} \times [Z^2(F_{el}-f) + ZF_{inel}] + (1-y)\frac{Z^2+Z}{3}\Big]$$

where LPM suppression functions are defined by *[11]*

$$G(s) \quad = 24s^2\left(\tfrac{\pi}{2} - \int_0^\infty e^{-st}\tfrac{\sin(st)}{\sinh(\frac{t}{2})}dt\right) \tag{4.43}$$

and

$$\phi(s) \quad = 12s^2\left(-\tfrac{\pi}{2} + \int_0^\infty e^{-st}\sin(st)\sinh\left(\tfrac{t}{2}\right)dt\right) \tag{4.44}$$

They can be piecewise approximated with simple analytic functions, see e.g. *[8]*. The suppression function $\xi(s)$ is recursively defined via

$$s = \sqrt{\frac{k\,E_{\mathrm{LPM}}}{8E(E-k)\xi(s)}} \tag{4.45}$$

but can be well approximated using an algorithm introduced by *[8]*. The material dependent characteristic energy E_{LPM} is defined in Eq. ([eq:ebrem.elpm]) according to *[12]*. Note that this definition differs from other definition (e.g. *[7]*) by a factor $\frac{1}{2}$.

An additional multiplicative factor governs the dielectric suppression effect (Ter-Mikaelian effect) *[13]*.

$$S(k) = \frac{k^2}{k^2 + k_p^2} \tag{4.46}$$

The characteristic photon energy scale k_p is given by the plasma frequency of the media, defined as

$$k_p = \hbar\omega_p \frac{E_e}{m_e c^2} = \frac{\hbar E_e}{m_e c^2} \cdot \sqrt{\frac{n_e e^2}{\epsilon_0 m_e}} \; . \tag{4.47}$$

Both suppression effects, dielectric suppresion and LPM effect, reduce the effective formation length of the photon, so the suppressions *do not simply multiply.* A consistent treatment of the overlap region, where both suppression mechanism, was suggested by *[14]*. The algorithm garanties that the LPM suppression is turned off as the density effect becomes important. This is achieved by defining a modified suppression variable $\hat{s}$ via

$$\hat{s} \quad = s \cdot \left(1 + \tfrac{k_p^2}{k^2}\right) \tag{4.48}$$

and using $\hat{s}$ in the LPM suppression functions $G(s)$ and $\phi(s)$ instead of s in Eq. ([eq:ebrem.lpm]).

4.1.8 Ionization

Method

The $G4eIonisation$ class provides the continuous and discrete energy losses of electrons and positrons due to ionization in a material according to the approach described in Section [en_loss]. The value of the maximum energy transferable to a free electron T_{max} is given by the following relation:

$$T_{max} = \begin{cases} E - mc^2 & for \;\; e^+ \\ (E - mc^2)/2 & for \;\; e^- \end{cases}$$

where mc^2 is the electron mass. Above a given threshold energy the energy loss is simulated by the explicit production of delta rays by Möller scattering ($e^- e^-$), or Bhabha scattering ($e^+ e^-$). Below the threshold the soft electrons ejected are simulated as continuous energy loss by the incident $e^{\pm}$.

Continuous Energy Loss

The integration of [comion.a] leads to the Berger-Seltzer formula [m.messel]:

$$\left.\frac{dE}{dx}\right]_{T<T_{cut}} = 2\pi r_e^2 mc^2 n_{el} \frac{1}{\beta^2} \left[\ln \frac{2(\gamma+1)}{(I/mc^2)^2} + F^{\pm}(\tau, \tau_{up}) - \delta\right]$$

with

r_e	classical electron radius: $e^2/(4\pi\epsilon_0 mc^2)$
mc^2	mass energy of the electron
n_{el}	electron density in the material
I	mean excitation energy in the material
γ	E/mc^2
β^2	$1 - (1/\gamma^2)$
τ	$\gamma - 1$
T_{cut}	minimum energy cut for δ -ray production
τ_c	T_{cut}/mc^2
τ_{max}	maximum energy transfer: τ for e^+, $\tau/2$ for e^-
τ_{up}	$\min(\tau_c, \tau_{max})$
δ	density effect function.

In an elemental material the electron density is

$$n_{el} = Z\, n_{at} = Z\, \frac{\mathcal{N}_{av}\rho}{A}.$$

$\mathcal{N}_{av}$ is Avogadro's number, ρ is the material density, and A is the mass of a mole. In a compound material

$$n_{el} = \sum_i Z_i \, n_{ati} = \sum_i Z_i \, \frac{\mathcal{N}_{av} w_i \rho}{A_i},$$

where w_i is the proportion by mass of the i^{th} element, with molar mass A_i .

The mean excitation energies I for all elements are taken from *[1]*.

The functions $F^{\pm}$ are given by :

$$\begin{aligned} F^+(\tau, \tau_{up}) &= \ln(\tau\tau_{up}) \\ &\quad -\frac{\tau_{up}^2}{\tau}\left[\tau + 2\tau_{up} - \frac{3\tau_{up}^2 y}{2} - \left(\tau_{up} - \frac{\tau_{up}^3}{3}\right) y^2 - \left(\frac{\tau_{up}^2}{2} - \tau\frac{\tau_{up}^3}{3} + \frac{\tau_{up}^4}{4}\right) y^3\right] \end{aligned} \tag{4.49}$$

$$\begin{aligned} F^-(\tau, \tau_{up}) &= -1 - \beta^2 \\ &\quad + \ln\left[(\tau - \tau_{up})\tau_{up}\right] + \frac{\tau}{\tau - \tau_{up}} + \frac{1}{\gamma^2}\left[\frac{\tau_{up}^2}{2} + (2\tau + 1)\ln\left(1 - \frac{\tau_{up}}{\tau}\right)\right] \end{aligned} \tag{4.50}$$

where $y = 1/(\gamma + 1)$.

The density effect correction is calculated according to the formalism of Sternheimer *[2]*:

Total Cross Section per Atom and Mean Free Path

The total cross section per atom for Möller scattering (e^-e^-) and Bhabha scattering (e^+e^-) is obtained by integrating Eq. [comion.b]. In Geant4 T_{cut} is always 1 keV or larger. For delta ray energies much larger than the excitation energy of the material ($T \gg I$), the total cross section becomes [m.messel] for Möller scattering,

$$\begin{aligned} \sigma(Z, E, T_{cut}) &= \frac{2\pi r_e^2 Z}{\beta^2(\gamma - 1)} \times \\ &\quad \left[\frac{(\gamma - 1)^2}{\gamma^2}\left(\frac{1}{2} - x\right) + \frac{1}{x} - \frac{1}{1 - x} - \frac{2\gamma - 1}{\gamma^2}\ln\frac{1 - x}{x}\right], \end{aligned} \tag{4.51}$$

and for Bhabha scattering (e^+e^-),

$$\begin{aligned} \sigma(Z, E, T_{cut}) &= \frac{2\pi r_e^2 Z}{(\gamma - 1)} \times \\ &\quad \left[\frac{1}{\beta^2}\left(\frac{1}{x} - 1\right) + B_1 \ln x + B_2(1 - x) - \frac{B_3}{2}(1 - x^2) + \frac{B_4}{3}(1 - x^3)\right]. \end{aligned} \tag{4.52}$$

Here

$$\begin{array}{llll} \gamma = E/mc^2 & & B_1 = 2 - y^2 \\ \beta^2 = 1 - (1/\gamma^2) & & B_2 = (1 - 2y)(3 + y^2) \\ x = T_{cut}/(E - mc^2) & & B_3 = (1 - 2y)^2 + (1 - 2y)^3 \\ y = 1/(\gamma + 1) & & B_4 = (1 - 2y)^3. \end{array}$$

The above formulas give the total cross section for scattering above the threshold energies

$$T^{\rm thr}_{\rm Moller} = 2T_{cut} \qquad \text{and} \qquad T^{\rm thr}_{\rm Bhabha} = T_{cut}.$$

In a given material the mean free path is then

$$\lambda = (n_{at} \cdot \sigma)^{-1} \quad or \quad \lambda = \left(\textstyle\sum_i n_{ati} \cdot \sigma_i\right)^{-1}.$$

Simulation of Delta-ray Production

Differential Cross Section

For $T \gg I$ the differential cross section per atom becomes [m.messel] for Möller scattering,

$$\begin{aligned} \frac{d\sigma}{d\epsilon} &= \frac{2\pi r_e^2 Z}{\beta^2(\gamma-1)} \times \\ &\left[\frac{(\gamma-1)^2}{\gamma^2} + \frac{1}{\epsilon}\left(\frac{1}{\epsilon} - \frac{2\gamma-1}{\gamma^2}\right) + \frac{1}{1-\epsilon}\left(\frac{1}{1-\epsilon} - \frac{2\gamma-1}{\gamma^2}\right)\right] \end{aligned} \tag{4.53}$$

and for Bhabha scattering,

$$\frac{d\sigma}{d\epsilon} = \frac{2\pi r_e^2 Z}{(\gamma-1)}\left[\frac{1}{\beta^2\epsilon^2} - \frac{B_1}{\epsilon} + B_2 - B_3\epsilon + B_4\epsilon^2\right].$$

Here $\epsilon = T/(E - mc^2)$. The kinematical limits of ϵ are

$$\epsilon_0 = \frac{T_{cut}}{E - mc^2} \leq \epsilon \leq \frac{1}{2} \quad \text{for } e^-e^- \qquad\qquad \epsilon_0 = \frac{T_{cut}}{E - mc^2} \leq \epsilon \leq 1 \quad \text{for } e^+e^-.$$

Sampling

The delta ray energy is sampled according to methods discussed in Chapter [secmessel]. Apart from normalization, the cross section can be factorized as

$$\frac{d\sigma}{d\epsilon} = f(\epsilon)g(\epsilon).$$

For e^-e^- scattering

$$f(\epsilon) = \frac{1}{\epsilon^2}\frac{\epsilon_0}{1-2\epsilon_0} \tag{4.54}$$

$$g(\epsilon) = \frac{4}{9\gamma^2 - 10\gamma + 5}\left[(\gamma-1)^2\epsilon^2 - (2\gamma^2+2\gamma-1)\frac{\epsilon}{1-\epsilon} + \frac{\gamma^2}{(1-\epsilon)^2}\right] \tag{4.55}$$

and for e^+e^- scattering

$$f(\epsilon) = \frac{1}{\epsilon^2}\frac{\epsilon_0}{1-\epsilon_0} \tag{4.56}$$

$$g(\epsilon) = \frac{B_0 - B_1\epsilon + B_2\epsilon^2 - B_3\epsilon^3 + B_4\epsilon^4}{B_0 - B_1\epsilon_0 + B_2\epsilon_0^2 - B_3\epsilon_0^3 + B_4\epsilon_0^4}. \tag{4.57}$$

Here $B_0 = \gamma^2/(\gamma^2-1)$ and all other quantities have been defined above.

To choose ϵ, and hence the delta ray energy,

1. ϵ is sampled from $f(\epsilon)$
2. the rejection function $g(\epsilon)$ is calculated using the sampled value of ϵ
3. ϵ is accepted with probability $g(\epsilon)$.

After the successful sampling of ϵ, the direction of the ejected electron is generated with respect to the direction of the incident particle. The azimuthal angle ϕ is generated isotropically and the polar angle θ is calculated from energy-momentum conservation. This information is used to calculate the energy and momentum of both the scattered incident particle and the ejected electron, and to transform them to the global coordinate system.

4.1.9 Hadron and Ion Ionization

Method

The class *G4hIonisation* provides the continuous energy loss due to ionization and simulates the 'discrete' part of the ionization, that is, delta rays produced by charged hadrons. The class *G4ionIonisation* is intended for the simulation of energy loss by positive ions with change greater than unit. Inside these classes the following models are used:

- *G4BetherBlochModel* (valid for protons with $T > 2\ MeV$)
- *G4BraggModel* (valid for protons with $T < 2\ MeV$)
- *G4BraggIonModel* (valid for protons with $T < 2\ MeV$)
- *G4ICRU73QOModel* (valid for anti-protons with $T < 2\ MeV$)

The scaling relation ([enloss.sc]) is a basic conception for the description of ionization of heavy charged particles. It is used both in energy loss calculation and in determination of the validity range of models. Namely the $T_p = 2MeV$ limit for protons is scaled for a particle with mass M_i by the ratio of the particle mass to the proton mass $T_i = T_p M_p / M_i$.

For all ionization models the value of the maximum energy transferable to a free electron T_{max} is given by the following relation *[4]*:

$$T_{max} = \frac{2m_e c^2(\gamma^2 - 1)}{1 + 2\gamma(m_e/M) + (m_e/M)^2},$$

where m_e is the electron mass and M is the mass of the incident particle. The method of calculation of the continuous energy loss and the total cross-section are explained below.

Continuous Energy Loss

The integration of [comion.a] leads to the Bethe-Bloch restricted energy loss ($T < T_{cut}$ formula *[4]*, which is modified taken into account various corrections *[5]*:

$$\frac{dE}{dx} = 2\pi r_e^2 mc^2 n_{el} \frac{z^2}{\beta^2} \left[\ln\left(\frac{2mc^2\beta^2\gamma^2 T_{up}}{I^2} \right) - \beta^2 \left(1 + \frac{T_{up}}{T_{max}} \right) - \delta - \frac{2C_e}{Z} + F \right]$$

where

r_e	classical electron radius: $e^2/(4\pi\epsilon_0 mc^2)$
mc^2	mass-energy of the electron
n_{el}	electrons density in the material
I	mean excitation energy in the material
Z	atomic number of the material
z	charge of the hadron in units of the electron change
γ	E/mc^2
β^2	$1 - (1/\gamma^2)$
T_{up}	$\min(T_{cut}, T_{max})$
δ	density effect function
C_e	shell correction function
F	high order corrections

In a single element the electron density is

$$n_{el} = Z\, n_{at} = Z\, \frac{\mathcal{N}_{av}\rho}{A}$$

($\mathcal{N}_{av}$: Avogadro number, ρ: density of the material, A: mass of a mole). In a compound material

$$n_{el} = \sum_i Z_i \, n_{ati} = \sum_i Z_i \, \frac{\mathcal{N}_{av} w_i \rho}{A_i}.$$

w_i is the proportion by mass of the i^{th} element, with molar mass A_i.

The mean excitation energy I for all elements is tabulated according to the ICRU recommended values *[1]*.

Shell Correction

$2C_e/Z$ is the so-called *shell correction term* which accounts for the fact of interaction of atomic electrons with atomic nucleus. This term more visible at low energies and for heavy atoms. The classical expression for the term *[3]* is used

$$C = \sum C_\nu(\theta_\nu, \eta_\nu), \;\; \nu = K, L, M, ..., \; \theta = \frac{J_\nu}{\epsilon_\nu}, \;\; \eta_\nu = \frac{\beta^2}{\alpha^2 Z_\nu^2},$$

where α is the fine structure constant, β is the hadron velocity, J_ν is the ionisation energy of the shell ν, ϵ_ν is Bohr ionisation energy of the shell ν, Z_ν is the effective charge of the shell ν. First terms C_K and C_L can be analytically computed in using an assumption non-relativistic hydrogenic wave functions *[6][7]*. The results *[8]* of tabulation of these computations in the interval of parameters $\eta_\nu = 0.005 \div 10$ and $\theta_\nu = 0.25 \div 0.95$ are used directly. For higher values of η_ν the parameterization *[8]* is applied:

$$C_\nu = \frac{K_1}{\eta} + \frac{K_2}{\eta^2} + \frac{K_3}{\eta^3},$$

where coefficients K_i provide smooth shape of the function. The effective nuclear charge for the L-shell can be reproduced as $Z_L = Z - d$, d is a parameter shown in Table [hion.t].

Z	3	4	5	6	7	8	9	>9
d	1.72	2.09	2.48	2.82	3.16	3.53	3.84	4.15

Table: Effective nuclear charge for the L-shell *[3]*.

For outer shells the calculations are not available, so L-shell parameterization is used and the following scaling relation *[3][9]* is applied:

$$C_\nu = V_\nu C_L(\theta_L, H_\nu \eta_L), \;\; V_\nu = \frac{n_\nu}{n_L}, \;\; H_\nu = \frac{J_\nu}{J_L},$$

where V_ν is a vertical scaling factor proportional to number of electrons at the shell n_ν. The contribution of the shell correction term is about 10% for protons at $T = 2MeV$.

Density Correction

δ is a correction term which takes into account the reduction in energy loss due to the so-called *density effect*. This becomes important at high energies because media have a tendency to become polarized as the incident particle velocity increases. As a consequence, the atoms in a medium can no longer be considered as isolated. To correct for this effect the formulation of Sternheimer *[2]* is used:

High Order Corrections

High order corrections term to Bethe-Bloch formula ([hion.d]) can be expressed as

$$F = G - S + 2(zL_1 + z^2 L_2),$$

where G is the Mott correction term, S is the finite size correction term, L_1 is the Barkas correction, L_2 is the Bloch correction. The Mott term *[5]* describes the close-collision corrections tend to become more important at large velocities and higher charge of projectile. The Fermi result is used:

$$G = \pi\alpha z\beta.$$

The Barkas correction term describes distant collisions. The parameterization of Ref. is expressed in the form:

$$L_1 = \frac{1.29F_A(b/x^{1/2})}{Z^{1/2}x^{3/2}}, \quad x = \frac{\beta^2}{Z\alpha^2},$$

where F_A is tabulated function *[10]*, b is scaled minimum impact parameter shown in Table [hion.t1]. This and other corrections depending on atomic properties are assumed to be additive for mixtures and compounds.

Table: Scaled minimum impact parameter b *[3]*.

For the Bloch correction term the classical expression *[3]* is following:

$$z^2L_2 = -y^2\sum_{n=1}^{\infty}\frac{1}{n(n^2+y^2)}, \quad y = \frac{z\alpha}{\beta}.$$

The finite size correction term takes into account the space distribution of charge of the projectile particle. For muon it is zero, for hadrons this term become visible at energies above few hundred GeV and the following parameterization *[5]* is used:

$$S = ln(1+q), \quad q = \frac{2m_eT_{max}}{\varepsilon^2},$$

where T_{max} is given in relation ([hion.c]), ε is proportional to the inverse effective radius of the projectile (Table [hion.t2]).

Table: The values of the ε parameter for different particle types.

All these terms break scaling relation ([enloss.sc]) if the projectile particle charge differs from ± 1. To take this circumstance into account in *G4ionIonisation* process at initialisation time the term F is ignored for the computation of the dE/dx table. At run time this term is taken into account by adding to the mean energy loss a value

$$\Delta T' = 2\pi r_e^2 mc^2 n_{el}\frac{z^2}{\beta^2}F\Delta s,$$

where Δs is the *true step length* and F is the high order correction term ([hion.cor]).

Parameterizations at Low Energies

For scaled energies below $T_{lim} = 2\ MeV$ shell correction becomes very large and precision of the Bethe-Bloch formula degrades, so parameterisation of evaluated data for stopping powers at low energies is required. These parameterisations for all atoms is available from ICRU'49 report *[3]*. The proton parametrisation is used in *G4BraggModel*, which is included by default in the process *G4hIonisation*. The alpha particle parameterisation is used in the *G4BraggIonModel*, which is included by default in the process *G4ionIonisation*. To provide a smooth transition between low-energy and high-energy models the modified energy loss expression is used for high energy

$$S(T) = S_H(T) + (S_L(T_{lim}) - S_H(T_{lim}))\frac{T_{lim}}{T}, \quad T > T_{lim},$$

where S is smoothed stopping power, S_H is stopping power from formula ([hion.d]) and S_L is the low-energy parameterisation.

The precision of Bethe-Bloch formula for $T > 10MeV$ is within 2%, below the precision degrades and at $1keV$ only 20% may be garanteed. In the energy interval $1-10MeV$ the quality of description of the stopping power varied from

atom to atom. To provide more stable and precise parameterisation the data from the NIST databases are included inside the standard package. These data are provided for 74 materials of the NIST material database [hion.nist]. The data from the PSTAR database are included into *G4BraggModel*. The data from the ASTAR database are included into *G4BraggIonModel*. So, if Geant4 material is defined as a NIST material, than NIST data are used for low-energy parameterisation of stopping power. If material is not from the NIST database, then the ICRU'49 parameterisation is used.

Nuclear Stopping

Nuclear stopping due to elastic ion-ion scattering since Geant4 v9.3 can be simulated with the continuous process *G4NuclearStopping*. By default this correction is active and the ICRU'49 parameterisation *[3]* is used, which is implemented in the model class *G4ICRU49NuclearStoppingModel*.

Total Cross Section per Atom

For $T \gg I$ the differential cross section can be written as

$$\frac{d\sigma}{dT} = 2\pi r_e^2 mc^2 Z \frac{z_p^2}{\beta^2}\frac{1}{T^2}\left[1 - \beta^2\frac{T}{T_{max}} + \frac{T^2}{2E^2}\right]$$

[4]. In Geant4 $T_{cut} \geq 1$ keV. Integrating from T_{cut} to T_{max} gives the total cross section per atom :

$$\begin{aligned}\sigma(Z,E,T_{cut}) &= \frac{2\pi r_e^2 Z z_p^2}{\beta^2}mc^2 \times \\ &\left[\left(\frac{1}{T_{cut}} - \frac{1}{T_{max}}\right) - \frac{\beta^2}{T_{max}}\ln\frac{T_{max}}{T_{cut}} + \frac{T_{max}-T_{cut}}{2E^2}\right]\end{aligned} \tag{4.58}$$

The last term is for spin $1/2$ only. In a given material the mean free path is:

$$\lambda = (n_{at}\cdot\sigma)^{-1} \quad or \quad \lambda = \left(\textstyle\sum_i n_{ati}\cdot\sigma_i\right)^{-1}$$

The mean free path is tabulated during initialization as a function of the material and of the energy for all kinds of charged particles.

Simulating Delta-ray Production

A short overview of the sampling method is given in Chapter [secmessel]. Apart from the normalization, the cross section [hion.i] can be factorized :

$$\frac{d\sigma}{dT} = f(T)g(T) \quad with \quad T \in [T_{cut},\, T_{max}] \tag{4.59}$$

where

$$f(T) = \left(\frac{1}{T_{cut}} - \frac{1}{T_{max}}\right)\frac{1}{T^2} \tag{4.60}$$

$$g(T) = 1 - \beta^2\frac{T}{T_{max}} + \frac{T^2}{2E^2}. \tag{4.61}$$

The last term in $g(T)$ is for spin $1/2$ only. The energy T is chosen by

1. sampling T from $f(T)$
2. calculating the rejection function $g(T)$ and accepting the sampled T with a probability of $g(T)$.

After the successful sampling of the energy, the direction of the scattered electron is generated with respect to the direction of the incident particle. The azimuthal angle ϕ is generated isotropically. The polar angle θ is calculated from energy-momentum conservation. This information is used to calculate the energy and momentum of both scattered particles and to transform them into the *global* coordinate system.

Ion Effective Charge

As ions penetrate matter they exchange electrons with the medium. In the implementation of *G4ionIonisation* the effective charge approach is used [hion.Ziegler85]. A state of equilibrium between the ion and the medium is assumed, so that the ion's effective charge can be calculated as a function of its kinetic energy in a given material. Before and after each step the dynamic charge of the ion is recalculated and saved in $G4DynamicParticle$, where it can be used not only for energy loss calculations but also for the sampling of transportation in an electromagnetic field.

The ion effective charge is expressed via the ion charge z_i and the fractional effective charge of ion γ_i:

$$z_{eff} = \gamma_i z_i.$$

For helium ions fractional effective charge is parameterized for all elements

$$\begin{aligned} (\gamma_{He})^2 &= \left(1 - \exp\left[-\sum_{j=0}^{5} C_j Q^j\right]\right)\left(1 + \frac{7 + 0.05Z}{1000}\exp(-(7.6 - Q)^2)\right)^2, \\ Q &= \max(0, \ln T), \end{aligned} \tag{4.62}$$

where the coefficients C_j are the same for all elements, and the helium ion kinetic energy T is in keV/amu.

The following expression is used for heavy ions [hion.BK]:

$$\gamma_i = \left(q + \frac{1-q}{2}\left(\frac{v_0}{v_F}\right)^2 \ln\left(1 + \Lambda^2\right)\right)\left(1 + \frac{(0.18 + 0.0015Z)\exp(-(7.6 - Q)^2)}{Z_i^2}\right),$$

where q is the fractional average charge of the ion, v_0 is the Bohr velocity, v_F is the Fermi velocity of the electrons in the target medium, and Λ is the term taking into account the screening effect:

$$\Lambda = 10\frac{v_F}{v_0}\frac{(1-q)^{2/3}}{Z_i^{1/3}(6+q)}.$$

The Fermi velocity of the medium is of the same order as the Bohr velocity, and its exact value depends on the detailed electronic structure of the medium. The expression for the fractional average charge of the ion is the following:

$$q = [1 - \exp(0.803y^{0.3} - 1.3167y^{0.6} - 0.38157y - 0.008983y^2)],$$

where y is a parameter that depends on the ion velocity v_i

$$y = \frac{v_i}{v_0 Z^{2/3}}\left(1 + \frac{v_F^2}{5v_i^2}\right).$$

The parametrisation of the effective charge of the ion applied if the kinetic energy is below limit value

$$T < 10 z_i \frac{M_i}{M_p}\ MeV,$$

where M_i is the ion mass and M_p is the proton mass.

4.1.10 Single Scattering, Screened Coulomb Potential and NIEL

Alternative model of Coulomb scattering of ions have been developed based on *[2]* and references therein. The advantage of this model is the wide applicability range in energy from 50 keV to 100 TeV per nucleon.

Nucleus–Nucleus Interactions

As discussed in Ref. *[2]*, at small distances from the nucleus, the potential energy is a Coulomb potential, while - at distances larger than the Bohr radius - the nuclear field is screened by the fields of atomic electrons. The interaction between two nuclei is usually described in terms of an interatomic Coulomb potential (e.g., see Section 2.1.4.1 of Ref. *[3]* and Section 4.1 of Ref. *[3]*), which is a function of the radial distance r between the two nuclei

$$V(r) = \frac{zZe^2}{r}\ \Psi_{\rm I}(r_{\rm r}),$$

where ez (projectile) and eZ (target) are the charges of the bare nuclei and $\Psi_{\rm I}$ is the *interatomic screening function* and $r_{\rm r}$ is given by

$$r_{\rm r} = \frac{r}{{\rm a}_{\rm I}},$$

with ${\rm a}_{\rm I}$ the so-called *screening length* (also termed *screening radius*). In the framework of the Thomas–Fermi model of the atom (e.g., see Ref. *[2]* and references therein) - thus, following the approach of ICRU Report 49 (1993) -, a commonly used screening length for $z = 1$ incoming particles is that from Thomas–Fermi

$${\rm a}_{\rm TF} = \frac{C_{\rm TF}\,{\rm a}_0}{Z^{1/3}},$$

and - for incoming particles with $z \geq 2$ - that introduced by Ziegler, Biersack and Littmark (1985) (and termed *universal screening length*):

$${\rm a}_{\rm U} = \frac{C_{\rm TF}\,{\rm a}_0}{z^{0.23} + Z^{0.23}},$$

where

$${\rm a}_0 = \frac{\hbar^2}{me^2}$$

is the Bohr radius, m is the electron rest mass and

$$C_{\rm TF} = \frac{1}{2}\left(\frac{3\,\pi}{4}\right)^{2/3} \simeq 0.88534$$

is a constant introduced in the Thomas–Fermi model.

The simple scattering model due to Wentzel *[4]* - with a single exponential screening-function $\Psi_{\rm I}(r_{\rm r})$ {e.g., see Ref. *[2]* and references therein} - was repeatedly employed in treating single and multiple Coulomb-scattering with screened potentials. The resulting elastic differential cross section differs from the Rutherford differential cross section by an additional term - the so-called *screening parameter* - which prevents the divergence of the cross section when the angle θ of scattered particles approaches 0°. The screening parameter $A_{\rm s}$ [e.g., see Equation (21) of Bethe (1953)] - as derived by Molière (1947, 1948) for the single Coulomb scattering using a Thomas–Fermi potential - is expressed as

$$A_{\rm s} = \left(\frac{\hbar}{2\,p\,a_{\rm I}}\right)^2 \left[1.13 + 3.76 \times \left(\frac{\alpha z Z}{\beta}\right)^2\right]$$

where $a_{\rm I}$ is the screening length - from Eqs. ([T_F_sc_rad], [Universal_sc_rad]) for particles with $z = 1$ and $z \geq 2$, respectively; α is the fine-structure constant; p (βc) is the momentum (velocity) of the incoming particle undergoing the scattering onto a target supposed to be initially at rest; c and $\hbar$ are the speed of light and the reduced Planck constant, respectively. When the (relativistic) mass - with corresponding rest mass m - of the incoming particle is much lower than the rest mass (M) of the target nucleus, the differential cross section - obtained from the Wentzel–Molière treatment of the single scattering - is:

$$\frac{d\sigma^{\rm WM}(\theta)}{d\Omega} = \left(\frac{zZe^2}{2\,p\,\beta c}\right)^2 \frac{1}{\left[A_{\rm s} + \sin^2(\theta/2)\right]^2}.$$

Equation ([eq:diff_cross_W_M_model_sin]) differs from Rutherford's formula - as already mentioned - for the additional term $A_{\rm s}$ to $\sin^2(\theta/2)$. As discussed in Ref. *[2]*, for $\beta \simeq 1$ (i.e., at very large p) and with $A_{\rm s} \ll 1$, one finds that the cross section approaches a constant:

$$\sigma_{\rm c}^{\rm WM} \simeq \left(\frac{2\,zZe^2 a_{\rm I}}{\hbar c}\right)^2 \frac{\pi}{1.13 + 3.76 \times (\alpha z Z)^2}.$$

As discussed in Ref. *[2]* and references therein, for a scattering under the action of a central potential (for instance that due to a screened Coulomb field), when the rest mass of the target particle is no longer much larger than the relativistic mass of the incoming particle, the expression of the differential cross section must properly be re-written - in the center of mass system - in terms of an "effective particle" with momentum equal to that of the incoming particle (p'_{in}) and rest mass equal to the relativistic reduced mass

$$\mu_{\rm rel} = \frac{mM}{M_{1,2}},$$

where $M_{1,2}$ is the invariant mass; m and M are the rest masses of the incoming and target particles, respectively. The "effective particle" velocity is given by:

$$\beta_{\rm r} c = c\sqrt{\left[1 + \left(\frac{\mu_{\rm rel} c}{p'_{in}}\right)^2\right]^{-1}}.$$

Thus, one finds (e.g, see Ref. *[2]*):

$$\frac{d\sigma^{\rm WM}(\theta')}{d\Omega'} = \left(\frac{zZe^2}{2\,p'_{in}\,\beta_{\rm r} c}\right)^2 \frac{1}{\left[A_{\rm s} + \sin^2(\theta'/2)\right]^2},$$

with

$$A_{\rm s} = \left(\frac{\hbar}{2\,p'_{in}\,a_{\rm I}}\right)^2 \left[1.13 + 3.76 \times \left(\frac{\alpha z Z}{\beta_{\rm r}}\right)^2\right]$$

and θ' the scattering angle in the center of mass system.

The energy T transferred to the recoil target is related to the scattering angle as $T = T_{max} \sin^2(\theta'/2)$ - where T_{max} is the maximum energy which can be transferred in the scattering (e.g., see Section 1.5 of Ref. *[3]*) -, thus, assuming an isotropic azimuthal distribution one can re-write Eq. ([eq:diff_cross_W_M_model_r]) in terms of the kinetic recoil energy T of the target

$$\frac{d\sigma^{\rm WM}(T)}{dT} = \pi \left(\frac{zZe^2}{p'_{in}\,\beta_{\rm r} c}\right)^2 \frac{T_{max}}{\left[T_{max}\,A_{\rm s} + T\right]^2}.$$

Furthermore, one can demonstrates that Eq. ([eq:diff_cross_W_M_model_T]) can be re-written as (e.g, see Ref. *[2]*);

$$\frac{d\sigma^{\rm WM}(T)}{dT} = 2\,\pi \left(zZe^2\right)^2 \frac{E^2}{p^2 M c^4} \frac{1}{\left[T_{max}\,A_{\rm s} + T\right]^2}$$

with p and E the momentum and total energy of the incoming particle in the laboratory. Equation ([eq:diff_cross_W_M_model_T_1]) expresses - as already mentioned - the differential cross section as a function of the (kinetic) energy T achieved by the recoil target.

Nuclear Stopping Power

Using Eq. ([eq:diff_cross_W_M_model_T_1]) the nuclear stopping power - in MeVcm^{-1} - is obtained as

$$-\left(\frac{dE}{dx}\right)_{\rm nucl} = 2\,n_A \pi \left(zZe^2\right)^2 \frac{E^2}{p^2 M c^4} \left[\frac{A_{\rm s}}{A_{\rm s}+1} - 1 + \ln\left(\frac{A_{\rm s}+1}{A_{\rm s}}\right)\right]$$

with n_A the number of nuclei (atoms) per unit of volume and, finally, the negative sign indicates that the energy is lost by the incoming particle (thus, achieved by recoil targets). As discussed in Ref. *[2]*, a slight increase of the nuclear stopping power with energy is expected because of the decrease of the screening parameter with energy.

For instance, in Fig. [fig:dEdx] the nuclear stopping power in silicon - in MeVcm^{2}g^{-1} - is shown as a function of the kinetic energy per nucleon - from 50keV/nucleon up 100TeV/nucleon - for protons, α-particles and ^{11}B-, ^{12}C-, ^{28}Si-, ^{56}Fe-, ^{115}In-, ^{208}Pb-nuclei.

A comparison of the present treatment with that obtained from Ziegler, Biersack and Littmark (1985) - available in SRIM (2008) *[5]* - using the so-called *universal screening potential* (see also Ref. *[6]*) is discussed in Ref. *[2]*: a good agreement is achieved down to about 150keV/nucleon. At large energies, the non-relativistic approach due to Ziegler, Biersack and Littmark (1985) becomes less appropriate and deviations from stopping powers calculated by means of the universal screening potential are expected and observed.

The non-relativistic approach - based on the universal screening potential - of Ziegler, Biersack and Littmark (1985) was also used by ICRU (1993) to calculate nuclear stopping powers due to protons and α-particles in materials. ICRU (1993) used as screening lengths those from Eqs. ([T_F_sc_rad], [Universal_sc_rad]) for protons and α-particles, respectively. As discussed in Ref. *[2]*, the stopping powers for protons (α-particles) from Eq. ([de/dx_nuclear_T]) are less than $\approx 5\%$ larger than those reported by ICRU (1993) from 50keV/nucleon up to ≈ 8MeV (19MeV/nucleon). At larger energies the stopping powers from Eq. ([de/dx_nuclear_T]) differ from those from ICRU - as expected - due to the complete relativistic treatment of the present approach (see Ref. *[2]*).

The simple screening parameter used so far [Eq. ([eq:As_r])] - derived by Molière (1947) - can be modified by means of a *practical correction*, i.e.,

$$A'_{\rm s} = \left(\frac{\hbar}{2\,p'_{in}\,a_{\rm I}}\right)^2 \left[1.13 + 3.76 \times C \left(\frac{\alpha z Z}{\beta_{\rm r}}\right)^2\right] ,$$

to achieve a better agreement with low energy calculations of Ziegler, Biersack and Littmark (1985). For instance - as discussed in Ref. *[2]* -, for α-particles and heavier ions, with

$$C = (10\pi z Z \alpha)^{0.12}$$

the stopping powers obtained from Eq. ([de/dx_nuclear_T]) - in which $A'_{\rm s}$ replaces $A_{\rm s}$ - differ from the values of SRIM (2008) by less than ≈ 4.7 (3.6)% for α-particles (lead ions) in silicon down to about 50keV/nucleon. With respect to the tabulated values of ICRU (1993), the agreement for α-particles is usually better than 4% at low energy down to 50keV/nucleon - a 5% agreement is achieved at about 50keV/nucleon in case of a lead medium. At very high energy, the stopping power is slightly affected when $A'_{\rm s}$ replaces $A_{\rm s}$ (a further disvussion is found in Ref. *[2]*).

Non-Ionizing Energy Loss due to Coulomb Scattering

A relevant process - which causes permanent damage to the silicon bulk structure - is the so-called *displacement damage* (e.g., see Chapter 4 of Ref. *[3]*, Ref. *[7]* and references therein). Displacement damage may be inflicted when a *primary knocked-on atom* (PKA) is generated. The interstitial atom and relative vacancy are termed Frenkel-pair (FP). In turn, the displaced atom may have sufficient energy to migrate inside the lattice and - by further collisions - can displace other atoms as in a collision cascade. This displacement process modifies the bulk characteristics of the device and causes its degradation. The total number of FPs can be estimated calculating the energy density deposited from displacement processes. In turn, this energy density is related to the *Non-Ionizing Energy Loss* (NIEL), i.e., the energy per unit path lost by the incident particle due to displacement processes.

In case of Coulomb scattering on nuclei, the non-ionizing energy-loss can be calculated using the Wentzel–Molière differential cross section [Eq. ([eq:diff_cross_W_M_model_T_1])] discussed in Sect. [Nucleus_Nucleus_Potentials], i.e.,

$$-\left(\frac{dE}{dx}\right)^{\rm NIEL}_{\rm nucl} = n_A \int_{T_d}^{T_{max}} T\,L(T)\,\frac{d\sigma^{\rm WM}(T)}{dT}\,dT ,$$

where E is the kinetic energy of the incoming particle, T is the kinetic energy transferred to the target atom, $L(T)$ is the fraction of T deposited by means of displacement processes. The expression of $L(T)$ - the so-called *Lindhard partition function* - can be found, for instance, in Equations (4.94, 4.96) of Section 4.2.1.1 in Ref. *[3]* (see also references therein). $T_{\rm de} = T\,L(T)$ is the so-called *damage energy*, i.e., the energy deposited by a recoil nucleus with kinetic energy T via displacement damages inside the medium. The integral in Eq. ([eq:NIEL]) is computed from the minimum energy T_d - the so-called *threshold energy for displacement*, i.e., that energy necessary to displace the atom from its lattice position - up to the maximum energy T_{max} that can be transferred during a single collision process. T_d is about 21eV in silicon. For instance, in Fig. [fig:NIELdEdx] the non-ionizing energy loss - in MeVcm^{2}g^{-1} - in silicon is shown as a function of the kinetic energy per nucleon - from 50keV/nucleon up 100TeV/nucleon - for protons, α-particles and ^{11}B-, ^{12}C-, ^{28}Si-, ^{56}Fe-, ^{115}In-, ^{208}Pb-nuclei.

A further discussion on the agreement with the results obtained by Jun and collaborators (2003) - using a relativistic treatment of Coulomb scattering of protons with kinetic energies above 50MeV and up to 1GeV upon silicon - can be found in Ref. *[2]*.

G4IonCoulombScatteringModel

As discussed sofar, high energetic particles may inflict permanent damage to the electronic devices employed in a radiation environment. In particular the *nuclear energy loss* is important for the formation of defects in semiconductor devices. Nuclear energy loss is also responsible for the displacement damage which is the typical cause of degradation for silicon devices. The electromagnetic model *G4IonCoulombScatteringModel* was created in order to simulate the single scattering of protons, alpha particles and all heavier nuclei incident on all target materials in the energy range from 50–100 keV/nucleon to 10 TeV.

The Method

The differential cross section previously described is calculated by means of the class *G4IonCoulombCrossSection* where a modified version of the Wentzel's cross section is used. To solve the scattering problem of heavy ions it is necessary to introduce an effective particle whose mass is equal to the relativistic reduced mass of the system defined as

$$\mu_r \equiv \frac{m_1 m_2 c^2}{E_{cm}}.$$

where m_1 and m_2 are incident and target rest masses respectively and E_{cm} (in Eq. ([eq:mu]) $M_{1,2} = E_{cm}/c^2$) is the total center of mass energy of the two particles system. The effective particle interacts with a fixed scattering center with interacting potential expressed by Eq. ([eq:VcoulombScreen]) . The momentum of the effective particle is equal to the momentum of the incoming particle calculated in the center of mass system ($\mathbf{p}_r \equiv \mathbf{p}_{1cm}$). Since the target particle is inside the material it can be considered at rest in the laboratory as a consequence the magnitude of $\mathbf{p}_r$ is calculated as

$$p_r \equiv p_{1cm} = p_{1lab}\frac{m_2 c^2}{E_{cm}},$$

with E_{cm} given by

$$E_{cm} = \sqrt{(m_1 c^2)^2 + (m_2 c^2)^2 + 2E_{1lab} m_2 c^2},$$

where p_{1lab} and E_{1lab} are the momentum and the total energy of the incoming particle in the laboratory system respectively. The velocity (β_r) of the effective particle is obtained by the relation

$$\frac{1}{\beta_r^2} = 1 + \left(\frac{\mu_r c^2}{p_r c}\right)^2.$$

The modified Wentzel's cross section is then equal to:

$$\frac{d\sigma(\theta_r)}{d\Omega} = \left(\frac{Z_1 Z_2 e^2}{p_r c\,\beta_r}\right)^2 \frac{1}{(2A_s + 1 - \cos\theta_r)^2}$$

(in Eq. ([eq:diff_cross_W_M_model_r]) $p'_{in} \equiv p_r$) where Z_1 and Z_2 are the nuclear proton numbers of projectile and of target respectively; A_s is the screening coefficient [see Eq. ([eq:As_r])] and θ_r is the scattering angle of the effective particle which is equal the one in the center of mass system ($\theta_r \equiv \theta_{1cm}$). Knowing the scattering angle the recoil kinetic energy of the target particle after scattering is calculated by

$$T = m_2 c^2 \left(\frac{p_{1lab} c}{E_{cm}}\right)^2 (1 - \cos\theta_r).$$

The momentum and the total energy of the incident particle after scattering in the laboratory system are obtained by the usual Lorentz's transformations.

Implementation Details

In the *G4IonCoulombScatteringModel* the scattering off electrons is not considered: only scattering off nuclei is simulated. Secondary particles are generated when T [Eq. ([eq:T])] is greater then a given threshold for displacement T_d; it is not cut in range. The user can set this energy threshold T_d by the method *SetRecoilThreshold(G4double :math:'(T_d)')*. The default screening coefficient A_s is given by Eq. ([eq:As_r]). If the user wants to use the one given by Eq. ([eq:As_r_mod]) the condition *SetHeavyIonCorr(1)* must be set. When $Z_1 = 1$ the Thomas-Fermi screening length [a_{TF} see Eq. ([T_F_sc_rad])] is used in the calculation of A_s. For $Z_1 \geq 2$ the screening length is the universal one [a_U see Eq. ([Universal_sc_rad])]. In the *G4IonCoulombCrossSection* the total differential cross section is obtained by the method *NuclearCrossSection()* where the Eq. ([eq:cross]) is integrated in the interval (0, π):

$$\sigma = \pi \left(\frac{Z_1 Z_2 e^2}{p_r c\,\beta_r}\right)^2 \frac{1}{A_s(A_s + 1)}$$

The cosine of the scattering angle is chosen randomly in the interval (-1, 1) according to the distribution of the total cross section and it is given by the method *SampleCosineTheta()* which returns $(1 - \cos\theta_r)$.

4.1.11 Multiple Scattering

Elastic scattering of electrons and other charged particles is an important component of any transport code. Elastic cross section is huge when particle energy decreases, so multiple scattering (MSC) approach should be introduced in order to have acceptable CPU performance of the simulation. A universal interface *G4VMultipleScattering* is used by all Geant4 MSC processes *[1]*:

- *G4eMultipleScattering;*
- *G4hMultipleScattering;*
- *G4MuMultipleScattering.*

For concrete simulation the *G4VMscModel* interface is used, which is an extension of the base *G4VEmModel* interface. The following models are available:

- *G4UrbanMscModel* - since Geant4 10.0 only one *Urban* model is available and it is applicable to all types of particles;
- *G4GoudsmitSaundersonModel* - for electrons and positrons *[5]*;
- *G4LowEWentzelVIModel* - for all particles with low-energy limit 10 eV;
- *G4WentzelVIModel* - for muons and hadrons, for muons should be included in Physics List together with *G4CoulombScattering* process, for hadrons large angle scattering is simulated by hadron elastic process.

The discussion on Geant4 MSC models is available in Ref.:cite:*msc.all*. Below we will describe models developed by L. Urban *[6]*, because these models are used in many Geant4 applications and have general components reused by other models.

Introduction

MSC simulation algorithms can be classified as either *detailed* or *condensed*. In the detailed algorithms, all the collisions/interactions experienced by the particle are simulated. This simulation can be considered as exact, it gives the same results as the solution of the transport equation. However, it can be used only if the number of collisions is not too large, a condition fulfilled only for special geometries (such as thin foils, or low density gas). In solid or liquid media the average number of collisions is very large and the detailed simulation becomes very inefficient. High energy simulation codes use condensed simulation algorithms, in which the global effects of the collisions are simulated at the end of a track segment. The global effects generally computed in these codes are the net energy loss, displacement, and change of direction of the charged particle. The last two quantities are computed from MSC theories used in the codes and the accuracy of the condensed simulations is limited by accuracy of MSC approximation.

Most particle physics simulation codes use the multiple scattering theories of Molière *[2]*, Goudsmit and Saunderson *[4]* and Lewis *[7]*. The theories of Molière and Goudsmit-Saunderson give only the angular distribution after a step, while the Lewis theory computes the moments of the spatial distribution as well. None of these MSC theories gives the probability distribution of the spatial displacement. Each of the MSC simulation codes incorporates its own algorithm to determine the angular deflection, true path length correction, and spatial displacement of the charged particle after a given step. These algorithms are not exact, of course, and are responsible for most of the uncertainties of the transport codes. Also due to inaccuracy of MSC the simulation results can depend on the value of the step length and generally user has to select the value of the step length carefully.

A new class of MSC simulation, the *mixed* simulation algorithms (see e.g.:cite:*msc.fernandez*), appeared in the literature recently. The mixed algorithm simulates the *hard* collisions one by one and uses a MSC theory to treat the effects of the *soft* collisions at the end of a given step. Such algorithms can prevent the number of steps from becoming too large and also reduce the dependence on the step length. Geant4 original implementation of a similar approach is realized in *G4WentzelVIModel [8]*.

The Urban MSC models used in Geant4 belongs to the class of condensed simulations. Urban uses model functions to determine the angular and spatial distributions after a step. The functions have been chosen in such a way as to give the same moments of the (angular and spatial) distributions as are given by the Lewis theory [msc.lewis].

Definition of Terms

In simulation, a particle is transported by steps through the detector geometry. The shortest distance between the endpoints of a step is called the *geometrical path length*, z. In the absence of a magnetic field, this is a straight line. For non-zero fields, z is the length along a curved trajectory. Constraints on z are imposed when particle tracks cross volume boundaries. The path length of an actual particle, however, is usually longer than the *geometrical path length*, due to multiple scattering. This distance is called the *true path length*, t. Constraints on t are imposed by the physical processes acting on the particle.

The properties of the MSC process are determined by the *transport mean free paths*, λ_k, which are functions of the energy in a given material. The k-th transport mean free path is defined as

$$\frac{1}{\lambda_k} = 2\pi n_a \int_{-1}^{1} [1 - P_k(cos\chi)] \frac{d\sigma(\chi)}{d\Omega} d(cos\chi)$$

where $d\sigma(\chi)/d\Omega$ is the differential cross section of the scattering, $P_k(cos\chi)$ is the k-th Legendre polynomial, and n_a is the number of atoms per volume.

Most of the mean properties of MSC computed in the simulation codes depend only on the first and second transport mean free paths. The mean value of the geometrical path length (first moment) corresponding to a given true path

length t is given by

$$\langle z \rangle = \lambda_1 \left[1 - \exp\left(-\frac{t}{\lambda_1} \right) \right]$$

Eq. [msc.a] is an exact result for the mean value of z if the differential cross section has axial symmetry and the energy loss can be neglected. The transformation between true and geometrical path lengths is called the *path length correction*. This formula and other expressions for the first moments of the spatial distribution were taken from either *[3]* or *[9]*, but were originally calculated by Goudsmit and Saunderson *[4]* and Lewis [msc.lewis].

At the end of the true step length, t, the scattering angle is θ. The mean value of $cos\theta$ is

$$\langle cos\theta \rangle = \exp\left[-\frac{t}{\lambda_1} \right]$$

The variance of $cos\theta$ can be written as

$$\sigma^2 = \langle cos^2\theta \rangle - \langle cos\theta \rangle^2 = \frac{1 + 2e^{-2\kappa\tau}}{3} - e^{-2\tau}$$

where $\tau = t/\lambda_1$ and $\kappa = \lambda_1/\lambda_2$. The mean lateral displacement is given by a more complicated formula *[3]*, but this quantity can also be calculated relatively easily and accurately. The square of the *mean lateral displacement* is

$$\langle x^2 + y^2 \rangle = \frac{4\lambda_1^2}{3} \left[\tau - \frac{\kappa + 1}{\kappa} + \frac{\kappa}{\kappa - 1} e^{-\tau} - \frac{1}{\kappa(\kappa - 1)} e^{-\kappa\tau} \right]$$

Here it is assumed that the initial particle direction is parallel to the the z axis. The lateral correlation is determined by the equation

$$\langle x v_x + y v_y \rangle = \frac{2\lambda_1}{3} \left[1 - \frac{\kappa}{\kappa - 1} e^{-\tau} + \frac{1}{\kappa - 1} e^{-\kappa\tau} \right]$$

where v_x and v_y are the x and y components of the direction unit vector. This equation gives the correlation strength between the final lateral position and final direction.

The transport mean free path values have been calculated in Refs.:cite:*msc.liljequist0*,:cite:*msc.liljequist2* for electrons and positrons in the kinetic energy range in 15 materials. The Urban MSC model in Geant4 uses these values for kinetic energies below 10 MeV. For high energy particles (above 10 MeV) the transport mean free path values have been taken from a paper of R. Mayol and F. Salvat *[10]*. When necessary, the model linearly interpolates or extrapolates the transport cross section, $\sigma_1 = 1/\lambda_1$, in atomic number Z and in the square of the particle velocity, β^2. The ratio κ is a very slowly varying function of the energy: $\kappa > 2$ for $T >$ a few keV, and $\kappa \to 3$ for very high energies (see *[9]*). Hence, a constant value of 2.5 is used in the model.

Nuclear size effects are negligible for low energy particles and they are accounted for in the Born approximation in *[10]*, so there is no need for extra corrections of this kind in the Urban model.

Path Length Correction

As mentioned above, the path length correction refers to the transformation $t \longrightarrow g$ and its inverse. The $t \longrightarrow g$ transformation is given by Eq. [msc.a] if the step is small and the energy loss can be neglected. If the step is not small the energy dependence makes the transformation more complicated. For this case Eqs. [msc.c],[msc.a] should be modified as

$$\langle cos\theta \rangle = \exp\left[-\int_0^t \frac{du}{\lambda_1(u)} \right]$$

$$\langle z \rangle = \int_0^t \langle cos\theta \rangle_u \, du$$

where θ is the scattering angle, t and z are the true and geometrical path lengths, and λ_1 is the transport mean free path.

In order to compute Eqs. [msc.ax],[msc.bx] the t dependence of the transport mean free path must be known. λ_1 depends on the kinetic energy of the particle which decreases along the step. All computations in the model use a linear approximation for this t dependence:

$$\lambda_1(t) = \lambda_{10}(1 - \alpha t)$$

Here λ_{10} denotes the value of λ_1 at the start of the step, and α is a constant. It is worth noting that Eq. [msc.cx] is *not* a crude approximation. It is rather good at low (< 1 MeV) energy. At higher energies the step is generally much smaller than the range of the particle, so the change in energy is small and so is the change in λ_1. Using Eqs. [msc.ax] - [msc.cx] the explicit formula for $\langle cos\theta \rangle$ and $\langle z \rangle$ are:

$$\langle cos\theta \rangle = (1 - \alpha t)^{\frac{1}{\alpha \lambda_{10}}}$$

$$\langle z \rangle = \frac{1}{\alpha(1 + \frac{1}{\alpha \lambda_{10}})} \left[1 - (1 - \alpha t)^{1 + \frac{1}{\alpha \lambda_{10}}}\right]$$

The value of the constant α can be expressed using λ_{10} and λ_{11} where λ_{11} is the value of the transport mean free path at the end of the step

$$\alpha = \frac{\lambda_{10} - \lambda_{11}}{t \lambda_{10}}$$

At low energies ($T_{kin} < M$, M - particle mass) α has a simpler form:

$$\alpha = \frac{1}{r_0}$$

where r_0 denotes the range of the particle at the start of the step. It can easily be seen that for a small step (i.e. for a step with small relative energy loss) the formula of $\langle z \rangle$ is

$$\langle z \rangle = \lambda_{10} \left[1 - \exp\left(-\frac{t}{\lambda_{10}}\right)\right]$$

Eq. [msc.dx] or [msc.gx] gives the mean value of the geometrical step length for a given true step length. The actual geometrical path length is sampled in the model according to the simple probability density function defined for $v = z/t \in [0, 1]$:

$$f(v) = (k + 1)(k + 2)v^k(1 - v)$$

The value of the exponent k is computed from the requirement that $f(v)$ must give the same mean value for $z = vt$ as Eq. [msc.dx] or [msc.gx]. Hence

$$k = \frac{3\langle z \rangle - t}{t - \langle z \rangle}$$

The value of $z = vt$ is sampled using $f(v)$ if $k > 0$, otherwise $z = \langle z \rangle$ is used. The $g \longrightarrow t$ transformation is performed using the mean values. The transformation can be written as

$$t(z) = \langle t \rangle = -\lambda_1 \log\left(1 - \frac{z}{\lambda_1}\right)$$

if the geometrical step is small and

$$t(z) = \frac{1}{\alpha}\left[1 - (1 - \alpha w z)^{\frac{1}{w}}\right]$$

where

$$w = 1 + \frac{1}{\alpha \lambda_{10}}$$

if the step is not small, i.e. the energy loss should be taken into account.

Angular Distribution

The quantity $u = cos\theta$ is sampled according to a model function $g(u)$. The shape of this function has been chosen such that Eqs. [msc.c] and [msc.c1] are satisfied. The functional form of g is

$$g(u) = q[pg_1(u) + (1-p)g_2(u)] + (1-q)g_3(u)$$

where $0 \leq p, q \leq 1$, and the g_i are simple functions of $u = cos\theta$, normalized over the range $u \in [-1,\ 1]$. The functions g_i have been chosen as

$$g_1(u) = C_1 \quad e^{-a(1-u)} \qquad -1 \leq u_0 \leq u \leq 1$$

$$g_2(u) = C_2 \quad \frac{1}{(b-u)^d} \qquad -1 \leq u \leq u_0 \leq 1$$

$$g_3(u) = C_3 \qquad -1 \leq u \leq 1$$

where $a > 0$, $b > 0$, $d > 0$ and u_0 are model parameters, and the C_i are normalization constants. It is worth noting that for small scattering angles, θ, $g_1(u)$ is nearly Gaussian ($exp(-\theta^2/2\theta_0^2)$) if $\theta_0^2 \approx 1/a$, while $g_2(u)$ has a Rutherford-like tail for large θ, if $b \approx 1$ and d is not far from 2 .

Determination of the Model Parameters

The parameters a, b, d, u_0 and p, q are not independent. The requirement that the angular distribution function $g(u)$ and its first derivative be continuous at $u = u_0$ imposes two constraints on the parameters:

$$p\ g_1(u_0) = (1-p)\ g_2(u_0)$$

$$p\ a\ g_1(u_0) = (1-p)\ \frac{d}{b-u_0}\ g_2(u_0)$$

A third constraint comes from Eq. [msc.ax] : $g(u)$ must give the same mean value for u as the theory. It follows from Eqs. [msc.ff] and [msc.d] that

$$q\{p\langle u\rangle_1 + (1-p)\langle u\rangle_2\} = [1 - \alpha\ t]^{\ \frac{1}{\alpha\lambda_{10}}}$$

where $\langle u\rangle_i$ denotes the mean value of u computed from the distribution $g_i(u)$. The parameter a was chosen according to a modified Highland-Lynch-Dahl formula for the width of the angular distribution *[11]*, *[12]*.

$$a = \frac{0.5}{1 - cos(\theta_0)}$$

where θ_0 is

$$\theta_0 = \frac{13.6MeV}{\beta cp} z_{ch} \sqrt{\frac{t}{X_0}} \left[1 + h_c \ln\left(\frac{t}{X_0}\right)\right]$$

when the original Highland-Lynch-Dahl formula is used. Here $\theta_0 = \theta_{plane}^{rms}$ is the width of the approximate Gaussian projected angle distribution, p, βc and z_{ch} are the momentum, velocity and charge number of the incident particle, and t/X_0 is the true path length in radiation length unit. The correction term h_c = 0.038 in the formula. This value of θ_0 is from a fit to the Molière distribution for singly charged particles with $\beta = 1$ for all Z, and is accurate to 11 % or better for $10^{-3} \leq t/X_0 \leq 100$ (see e.g. Rev. of Particle Properties, section 23.3).

The model uses a slightly modified Highland-Lynch-Dahl formula to compute θ_0. For electrons/positrons the modified θ_0 formula is

$$\theta_0 = \frac{13.6MeV}{\beta cp} z_{ch} \sqrt{y} c$$

where

$$y = \ln\left(\frac{t}{X_0}\right)$$

The correction term c and coeffitients c_i are

$$c = c_0\dot{(}c_1 + c_2 y),$$

$$c_0 = 0.990395 - 0.168386Z^{1/6} + 0.093286Z^{1/3},$$

$$c_1 = 1 - \frac{0.08778}{Z},$$

$$c_2 = 0.04078 + 0.00017315Z.$$

This formula gives a much smaller step dependence in the angular distribution than the Highland form. The value of the parameter u_0 has been chosen as

$$u_0 \quad = \quad 1 - \frac{\xi}{a}$$

where

$$\xi = d_1 + d_2 v + d_3 v^2 + d_4 v^3$$

with

$$v = \ln\left(\frac{t}{\lambda_1}\right)$$

The parameters d_i-s have the form

$$d_i = d_{i0} + d_{i1} Z^{\frac{1}{3}} + d_{i2} Z^{\frac{2}{3}}$$

The numerical values of the d_{ij} constants can be found in the code.

The tail parameter d is the same as the parameter ξ .

This (empirical) expression is obtained comparing the simulation results to the data of the MuScat experiment *[13]*. The remaining three parameters can be computed from Eqs. [msc.p1] - [msc.par1]. The numerical value of the parameters can be found in the code.

In the case of heavy charged particles (μ, π, p, etc.) the mean transport free path is calculated from the electron or positron λ_1 values with a 'scaling' applied. This is possible because the transport mean free path λ_1 depends only on the variable $P\beta c$, where P is the momentum, and βc is the velocity of the particle.

In its present form the model samples the path length correction and angular distribution from model functions, while for the lateral displacement and the lateral correlation only the mean values are used and all the other correlations are neglected. However, the model is general enough to incorporate other random quantities and correlations in the future.

Step Limitation Algorithm

In Geant4 the boundary crossing is treated by the transportation process. The transportation ensures that the particle does not penetrate in a new volume without stopping at the boundary, it restricts the step size when the particle leaves a volume. However, this step restriction can be rather weak in big volumes and this fact can result a not very good angular distribution after the volume. At the same time, there is no similar step limitation when a particle enters a volume and this fact does not allow a good backscattering simulation for low energy particles. Low energy particles penetrate too deeply into the volume in the first step and then - because of energy loss - they are not able to reach again the boundary in backward direction.

MSC step limitation algorithm has been developed *[6]* in order to achieve optimal balance between simulation precision and CPU performance of simulation for different applications. At the start of a track or after entering in a new volume, the algorithm restricts the step size to a value

$$f_r \cdot max\{r, \lambda_1\}$$

where r is the range of the particle, f_r is a parameter $\in [0, 1]$, taking the max of r and λ_1 is an empirical choice.The value of f_r is constant for low energy particles while for particles with $\lambda_1 > \lambda_{lim}$ an effective value is used given by the scaling equation

$$f_{reff} = f_r \cdot \left[1 - sc + sc * \frac{\lambda_1}{\lambda_{lim}}\right]$$

(The numerical values $sc = 0.25$ and $\lambda_{lim} = 1\ \ mm$ are used in the equation.) In order not to use very small - unphysical - step sizes a lower limit is given for the step size as

$$tlimitmin = max\left[\frac{\lambda_1}{nstepmax}, \lambda_{elastic}\right]$$

with $nstepmax = 25$ and $\lambda_{elastic}$ is the elastic mean free path of the particle (see later). It can be easily seen that this kind of step limitation poses a real constraint only for low energy particles. In order to prevent a particle from crossing a volume in just one step, an additional limitation is imposed: after entering a volume the step size cannot be bigger than

$$\frac{d_{geom}}{f_g}$$

where d_{geom} is the distance to the next boundary (in the direction of the particle) and f_g is a constant parameter. A similar restriction at the start of a track is

$$\frac{2d_{geom}}{f_g}$$

At this point the program also checks whether the particle has entered a new volume. If it has, the particle steps cannot be bigger than $t_{lim} = f_r\ \ max(r, \lambda)$. This step limitation is governed by the physics, because t_{lim} depends on the particle energy and the material.

The choice of the parameters f_r and f_g is also related to performance. By default $f_r = 0.02$ and $f_g = 2.5$ are used, but these may be set to any other value in a simple way. One can get an approximate simulation of the backscattering with the default value, while if a better backscattering simulation is needed it is possible to get it using a smaller value for f_r. However, this model is very simple and it can only approximately reproduce the backscattering data.

Boundary Crossing Algorithm

A special stepping algorithm has been implemented in order to improve the simulation around interfaces. This algorithm does not allow 'big' last steps in a volume and 'big' first steps in the next volume. The step length of these steps around a boundary crossing can not be bigger than the mean free path of the elastic scattering of the particle in the given volume (material). After these small steps the particle scattered according to a single scattering law (i.e. there is no multiple scattering very close to the boundary or at the boundary).

The key parameter of the algorithm is the variable called $skin$. The algorithm is not active for $skin \leq 0$, while for $skin > 0$ it is active in layers of thickness $skin \cdot \lambda_{elastic}$ before boundary crossing and of thickness $(skin-1) \cdot \lambda_{elastic}$ after boundary crossing (for $skin = 1$ there is only one small step just before the boundary). In this active area the particle performs steps of length $\lambda_{elastic}$ (or smaller if the particle reaches the boundary traversing a smaller distance than this value).

The scattering at the end of a small step is single or plural and for these small steps there are no path length correction and lateral displacement computation. In other words the program works in this thin layer in 'microscopic mode'. The elastic mean free path can be estimated as

$$\lambda_{elastic} = \lambda_1 \cdot rat\,(T_{kin})$$

where $rat(T_{kin})$ a simple empirical function computed from the elastic and first transport cross section values of Mayol and Salvat *[10]*

$$rat\,(T_{kin}) = \frac{0.001(MeV)^2}{T_{kin}\,(T_{kin} + 10MeV)}$$

T_{kin} is the kinetic energy of the particle.

At the end of a small step the number of scatterings is sampled according to the Poisson's distribution with a mean value $t/\lambda_{elastic}$ and in the case of plural scattering the final scattering angle is computed by summing the contributions of the individual scatterings. The single scattering is determined by the distribution

$$g(u) = C\frac{1}{(2a + 1 - u)^2}$$

where $u = \cos(\theta)$, a is the screening parameter, C is a normalization constant. The form of the screening parameter is the same as in the single scattering (see there).

Implementation Details

The step length of a particles is determined by the physics processes or the geometry of the detectors. The tracking/stepping algorithm checks all the step lengths demanded by the (continuous or discrete) physics processes and determines the minimum of these step lengths (see [tsl]). The MSC model should be called to compute step limit after all processes except the transportation process. The following sequence of computations are performed to make the step:

- the minimum of all processes *true step length* limit t including one of the MSC process is selected;
- The conversion $t \longrightarrow g$ (*geometrical step limit*) is performed;
- the minimum of obtained value g and the transportation step limit is selected;
- The final conversion $g \longrightarrow t$ is performed.

The reason for this ordering is that the physics processes 'feel' the true path length t traveled by the particle, while the transportation process (geometry) uses the z step length.

A new optional mechanis was recently introduced allowing sample displacemnt in vicinity of geometry boundary. If it is enabled and the transportation limit the step due to geometry boundary then after initial sampling of the displacenet an additional 'push' of track is applied forcing end point be at the boundary. Corresponding correction to the true step length is applied according to the value of the 'push'.

After the actual step of the particle is done, the MSC model is responsible for sampling of scattering angle and relocation of the end-point of the step. The scattering angle θ of the particle after the step of length 't' is sampled according to the model function given in Eq. [msc.d] . The azimuthal angle ϕ is generated uniformly in the range $[0, 2\pi]$.

After the simulation of the scattering angle, the lateral displacement is computed using Eq. [msc.e1]. Then the correlation given by Eq. [msc.e2] is used to determine the direction of the lateral displacement. Before 'moving' the particle according to the displacement a check is performed to ensure that the relocation of the particle with the lateral displacement does not take the particle beyond the volume boundary.

Default MSC parameter values optimized per particle type are shown in Table [msc.t]. Note, that there is three types of step limitation by multiple scattering process:

- Minimal - only f_r parameter and range are used;
- UseSafety - f_r parameter, range and geometrical safety are used;
- UseSafetyPlus - f_r parameter, range and geometrical safety are used;
- UseDistanceToBoundary - uses particle range, geometrical safety and linear distance to geometrical boundary.

particle	e^+, e^-	*muons, hadrons*	*ions*
StepLimitType	*fUseSafety*	*fMinimal*	*fMinimal*
skin	0	0	0
f_r	0.04	0.2	0.2
f_g	2.5	0.1	0.1
LateralDisplacement	*true*	*true*	*false*

Table: The default values of parameters for different particle type.

The parameters of the model can be changed via public functions of the base class *G4VMultipleSacttering*. They can be changed for all multiple scattering processes simultaneously via *G4EmParameters* class, *G4EmProcessOptions* class, or via Geant4 UI commands. The following commands are available:

- /process/msc/StepLimit UseDistanceToBoundary
- /process/msc/LateralDisplacement false
- /process/msc/MuHadLateralDisplacement false
- /process/msc/DisplacementBeyondSafety true
- /process/msc/RangeFactor 0.02
- /process/msc/GeomFactor 2.5
- /process/msc/Skin 2*

4.1.12 Ion Scattering

The necessity of accurately computing the characteristics of interatomic scattering arises in many disciplines in which energetic ions pass through materials. Traditionally, solutions to this problem not involving hadronic interactions have been dominated by the multiple scattering, which is reasonably successful, but not very flexible. In particular, it is relatively difficult to introduce into such a system a particular screening function which has been measured for a specific atomic pair, rather than the universal functions which are applied. In many problems of current interest, such as the behavior of semiconductor device physics in a space environment, nuclear reactions, particle showers, and other effects are critically important in modeling the full details of ion transport. The process *G4ScreenedNuclearRecoil* provides simulation of ion elastic scattering *[1]*. This process is available with extended electromagnetic example *TestEm7*.

Method

The method used in this computation is a variant of a subset of the method described in Ref.:cite:*MendenhallWellerXSection*. A very short recap of the basic material is included here. The scattering of two atoms from each other is assumed to be a completely classical process, subject to an interatomic potential described by a potential function

$$V(r) = \frac{Z_1 Z_2 e^2}{r} \phi\left(\frac{r}{a}\right)$$

where Z_1 and Z_2 are the nuclear proton numbers, e^2 is the electromagnetic coupling constant ($q_e^2/4\pi\epsilon_0$ in SI units), r is the inter-nuclear separation, ϕ is the screening function describing the effect of electronic screening of the bare nuclear charges, and a is a characteristic length scale for this screening. In most cases, ϕ is a universal function used for all ion pairs, and the value of a is an appropriately adjusted length to give reasonably accurate scattering behavior. In the method described here, there is no particular need for a universal function ϕ, since the method is capable of directly solving the problem for most physically plausible screening functions. It is still useful to define a typical screening length a in the calculation described below, to keep the equations in a form directly comparable with our previous work even though, in the end, the actual value is irrelevant as long as the final function $\phi(r)$ is correct. From this potential $V(r)$ one can then compute the classical scattering angle from the reduced center-of-mass energy $\varepsilon \equiv E_c a/Z_1 Z_2 e^2$ (where E_c is the kinetic energy in the center-of-mass frame) and reduced impact parameter $\beta \equiv b/a$

$$\theta_c = \pi - 2\beta \int_{x_0}^{\infty} f(z)\, dz/z^2$$

where

$$f(z) = \left(1 - \frac{\phi(z)}{z\,\varepsilon} - \frac{\beta^2}{z^2}\right)^{-1/2}$$

and x_0 is the reduced classical turning radius for the given ε and β.

The problem, then, is reduced to the efficient computation of this scattering integral. In our previous work, a great deal of analytical effort was included to proceed from the scattering integral to a full differential cross section calculation, but for application in a Monte-Carlo code, the scattering integral $\theta_c(Z_1,\, Z_2,\, E_c,\, b)$ and an estimated total cross section $\sigma_0(Z_1,\, Z_2,\, E_c)$ are all that is needed. Thus, we can skip algorithmically forward in the original paper to equations 15-18 and the surrounding discussion to compute the reduced distance of closest approach x_0. This computation follows that in the previous work exactly, and will not be reintroduced here.

For the sake of ultimate accuracy in this algorithm, and due to the relatively low computational cost of so doing, we compute the actual scattering integral (as described in equations 19-21 of *[2]*) using a Lobatto quadrature of order 6, instead of the 4th order method previously described. This results in the integration accuracy exceeding that of any available interatomic potentials in the range of energies above those at which molecular structure effects dominate, and should allow for future improvements in that area. The integral α then becomes (following the notation of the previous paper)

$$\alpha \approx \frac{1+\lambda_0}{30} + \sum_{i=1}^{4} w_i'\, f\left(\frac{x_0}{q_i}\right)$$

where

$$\lambda_0 = \left(\frac{1}{2} + \frac{\beta^2}{2\,x_0^2} - \frac{\phi'(x_0)}{2\,\varepsilon}\right)^{-1/2}$$

$w_i' \in$[0.03472124, 0.1476903, 0.23485003, 0.1860249] $q_i \in$[0.9830235, 0.8465224, 0.5323531, 0.18347974] Then

$$\theta_c = \pi - \frac{\pi\beta\alpha}{x_0}$$

The other quantity required to implement a scattering process is the total scattering cross section σ_0 for a given incident ion and a material through which the ion is propagating. This value requires special consideration for a process such as screened scattering. In the limiting case that the screening function is unity, which corresponds to Rutherford scattering, the total cross section is infinite. For various screening functions, the total cross section may or may not be finite. However, one must ask what the intent of defining a total cross section is, and determine from that how to define it.

In Geant4, the total cross section is used to determine a mean-free-path l_μ which is used in turn to generate random transport distances between discrete scattering events for a particle. In reality, where an ion is propagating through,

for example, a solid material, scattering is not a discrete process but is continuous. However, it is a useful, and highly accurate, simplification to reduce such scattering to a series of discrete events, by defining some minimum energy transfer of interest, and setting the mean free path to be the path over which statistically one such minimal transfer has occurred. This approach is identical to the approach developed for the original TRIM code *[3]*. As long as the minimal interesting energy transfer is set small enough that the cumulative effect of all transfers smaller than that is negligible, the approximation is valid. As long as the impact parameter selection is adjusted to be consistent with the selected value of l_μ, the physical result isn't particularly sensitive to the value chosen.

Noting, then, that the actual physical result isn't very sensitive to the selection of l_μ, one can be relatively free about defining the cross section σ_0 from which l_μ is computed. The choice used for this implementation is fairly simple. Define a physical cutoff energy E_{min} which is the smallest energy transfer to be included in the calculation. Then, for a given incident particle with atomic number Z_1, mass m_1, and lab energy E_{inc}, and a target atom with atomic number Z_2 and mass m_2, compute the scattering angle θ_c which will transfer this much energy to the target from the solution of

$$E_{min} = E_{inc} \frac{4\, m_1\, m_2}{(m_1 + m_2)^2} \sin^2 \frac{\theta_c}{2}$$

. Then, noting that α from eq. [alpha_eq] is a number very close to unity, one can solve for an approximate impact parameter b with a single root-finding operation to find the classical turning point. Then, define the total cross section to be $\sigma_0 = \pi b^2$, the area of the disk inside of which the passage of an ion will cause at least the minimum interesting energy transfer. Because this process is relatively expensive, and the result is needed extremely frequently, the values of $\sigma_0(E_{inc})$ are precomputed for each pairing of incident ion and target atom, and the results cached in a cubic-spline interpolation table. However, since the actual result isn't very critical, the cached results can be stored in a very coarsely sampled table without degrading the calculation at all, as long as the values of the l_μ used in the impact parameter selection are rigorously consistent with this table.

The final necessary piece of the scattering integral calculation is the statistical selection of the impact parameter b to be used in each scattering event. This selection is done following the original algorithm from TRIM, where the cumulative probability distribution for impact parameters is

$$P(b) = 1 - \exp\left(\frac{-\pi\, b^2}{\sigma_0}\right)$$

where $N\, \sigma_0 \equiv 1/l_\mu$ where N is the total number density of scattering centers in the target material and l_μ is the mean free path computed in the conventional way. To produce this distribution from a uniform random variate r on (0,1], the necessary function is

$$b = \sqrt{\frac{-\log r}{\pi\, N\, l_\mu}}$$

This choice of sampling function does have the one peculiarity that it can produce values of the impact parameter which are larger than the impact parameter which results in the cutoff energy transfer, as discussed above in the section on the total cross section, with probability $1/e$. When this occurs, the scattering event is not processed further, since the energy transfer is below threshold. For this reason, impact parameter selection is carried out very early in the algorithm, so the effort spent on uninteresting events is minimized.

The above choice of impact sampling is modified when the mean-free-path is very short. If $\sigma_0 > \pi \left(\frac{l}{2}\right)^2$ where l is the approximate lattice constant of the material, as defined by $l = N^{-1/3}$, the sampling is replaced by uniform sampling on a disk of radius $l/2$, so that

$$b = \frac{l}{2}\sqrt{r}$$

This takes into account that impact parameters larger than half the lattice spacing do not occur, since then one is closer to the adjacent atom. This also derives from TRIM.

One extra feature is included in our model, to accelerate the production of relatively rare events such as high-angle scattering. This feature is a cross-section scaling algorithm, which allows the user access to an unphysical control of

the algorithm which arbitrarily scales the cross-sections for a selected fraction of interactions. This is implemented as a two-parameter adjustment to the central algorithm. The first parameter is a selection frequency f_h which sets what fraction of the interactions will be modified. The second parameter is the scaling factor for the cross-section. This is implemented by, for a fraction f_h of interactions, scaling the impact parameter by $b' = b/\sqrt{scale}$. This feature, if used with care so that it does not provide excess multiple-scattering, can provide between 10 and 100-fold improvements to event rates. If used without checking the validity by comparing to un-adjusted scattering computations, it can also provide utter nonsense.

Implementation Details

The coefficients for the summation to approximate the integral for α in eq.([alpha_eq]) are derived from the values in Abramowitz & Stegun *[4]*, altered to make the change-of-variable used for this integral. There are two basic steps to the transformation. First, since the provided abscissas x_i and weights w_i are for integration on [-1,1], with only one half of the values provided, and in this work the integration is being carried out on [0,1], the abscissas are transformed as:

$$y_i \in \left\{ \frac{1 \mp x_i}{2} \right\}$$

Then, the primary change-of-variable is applied resulting in:

$$q_i = \cos \frac{\pi\, y_i}{2} \tag{4.63}$$

$$w_i' = \frac{w_i}{2} \sin \frac{\pi\, y_i}{2} \tag{4.64}$$

except for the first coefficient $w_1'$where the $\sin()$ part of the weight is taken into the limit of λ_0 as described in eq.([lambda_eqn]). This value is just $w_1' = w_1/2$.

4.1.13 Photoabsorption Ionization Model

Cross Section for Ionizing Collisions

The Photoabsorption Ionization (PAI) model describes the ionization energy loss of a relativistic charged particle in matter. For such a particle, the differential cross section $d\sigma_i/d\omega$ for ionizing collisions with energy transfer ω can be expressed most generally by the following equations [pai.asosk]:

$$\frac{d\sigma_i}{d\omega} = \frac{2\pi Z e^4}{mv^2} \left\{ \frac{f(\omega)}{\omega \left|\varepsilon(\omega)\right|^2} \left[\ln \frac{2mv^2}{\omega \left|1-\beta^2\varepsilon\right|} - \right.\right.$$
$$\left.\left. - \frac{\varepsilon_1 - \beta^2 \left|\varepsilon\right|^2}{\varepsilon_2} \arg(1-\beta^2\varepsilon^*) \right] + \frac{\tilde{F}(\omega)}{\omega^2} \right\}, \tag{4.65}$$

$$\tilde{F}(\omega) = \int_0^\omega \frac{f(\omega')}{\left|\varepsilon(\omega')\right|^2} d\omega',$$

$$f(\omega) = \frac{m\omega\varepsilon_2(\omega)}{2\pi^2 Z N \hbar^2}.$$

Here m and e are the electron mass and charge, $\hbar$ is Planck's constant, $\beta = v/c$ is the ratio of the particle's velocity v to the speed of light c, Z is the effective atomic number, N is the number of atoms (or molecules) per unit volume, and $\varepsilon = \varepsilon_1 + i\varepsilon_2$ is the complex dielectric constant of the medium. In an isotropic non-magnetic medium the dielectric constant can be expressed in terms of a complex index of refraction, $n(\omega) = n_1 + in_2$, $\varepsilon(\omega) = n^2(\omega)$. In the energy range above the first ionization potential I_1 for all cases of practical interest, and in particular for all gases, $n_1 \sim 1$.

Therefore the imaginary part of the dielectric constant can be expressed in terms of the photoabsorption cross section $\sigma_\gamma(\omega)$:

$$\varepsilon_2(\omega) = 2n_1 n_2 \sim 2n_2 = \frac{N\hbar c}{\omega}\sigma_\gamma(\omega).$$

The real part of the dielectric constant is calculated in turn from the dispersion relation

$$\varepsilon_1(\omega) - 1 = \frac{2N\hbar c}{\pi} V.p. \int_0^\infty \frac{\sigma_\gamma(\omega')}{\omega'^2 - \omega^2} d\omega',$$

where the integral of the pole expression is considered in terms of the principal value. In practice it is convenient to calculate the contribution from the continuous part of the spectrum only. In this case the normalized photoabsorption cross section

$$\tilde{\sigma}_\gamma(\omega) = \frac{2\pi^2\hbar e^2 Z}{mc}\sigma_\gamma(\omega)\left[\int_{I_1}^{\omega_{max}} \sigma_\gamma(\omega')d\omega'\right]^{-1},\ \omega_{max} \sim 100\ keV$$

is used, which satisfies the quantum mechanical sum rule [pai.fano]:

$$\int_{I_1}^{\omega_{max}} \tilde{\sigma}_\gamma(\omega')d\omega' = \frac{2\pi^2\hbar e^2 Z}{mc}.$$

The differential cross section for ionizing collisions is expressed by the photoabsorption cross section in the continuous spectrum region:

$$\begin{aligned}\frac{d\sigma_i}{d\omega} &= \frac{\alpha}{\pi\beta^2}\left\{\frac{\tilde{\sigma}_\gamma(\omega)}{\omega\left|\varepsilon(\omega)\right|^2}\left[\ln\frac{2mv^2}{\omega\left|1-\beta^2\varepsilon\right|} - \right.\right. \\ &\left.\left. -\frac{\varepsilon_1 - \beta^2\left|\varepsilon\right|^2}{\varepsilon_2}\arg(1-\beta^2\varepsilon^*)\right] + \frac{1}{\omega^2}\int_{I_1}^{\omega}\frac{\tilde{\sigma}_\gamma(\omega')}{\left|\varepsilon(\omega')\right|^2}d\omega'\right\}, \qquad (4.66)\end{aligned}$$

$$\varepsilon_2(\omega) = \frac{N\hbar c}{\omega}\tilde{\sigma}_\gamma(\omega),$$

$$\varepsilon_1(\omega) - 1 = \frac{2N\hbar c}{\pi} V.p. \int_{I_1}^{\omega_{max}} \frac{\tilde{\sigma}_\gamma(\omega')}{\omega'^2 - \omega^2} d\omega'.$$

For practical calculations using Eq. [PAI1] it is convenient to represent the photoabsorption cross section as a polynomial in ω^{-1} as was proposed in [sandia]:

$$\sigma_\gamma(\omega) = \sum_{k=1}^{4} a_k^{(i)}\omega^{-k},$$

where the coefficients, $a_k^{(i)}$ result from a separate least-squares fit to experimental data in each energy interval i. As a rule the interval borders are equal to the corresponding photoabsorption edges. The dielectric constant can now be calculated analytically with elementary functions for all ω, except near the photoabsorption edges where there are breaks in the photoabsorption cross section and the integral for the real part is not defined in the sense of the principal value. The third term in Eq. ([PAI1]), which can only be integrated numerically, results in a complex calculation of $d\sigma_i/d\omega$. However, this term is dominant for energy transfers $\omega > 10\ keV$, where the function $|\varepsilon(\omega)|^2 \sim 1$. This is clear from physical reasons, because the third term represents the Rutherford cross section on atomic electrons which can be considered as quasifree for a given energy transfer [allis]. In addition, for high energy transfers, $\varepsilon(\omega) = 1 - \omega_p^2/\omega^2 \sim 1$, where ω_p is the plasma energy of the material. Therefore the factor $|\varepsilon(\omega)|^{-2}$ can be removed from under the integral and the differential cross section of ionizing collisions can be expressed as:

$$\begin{aligned}\frac{d\sigma_i}{d\omega} &= \frac{\alpha}{\pi\beta^2\left|\varepsilon(\omega)\right|^2}\left\{\frac{\tilde{\sigma}_\gamma(\omega)}{\omega}\left[\ln\frac{2mv^2}{\omega\left|1-\beta^2\varepsilon\right|} - \right.\right. \\ &\left.\left. -\frac{\varepsilon_1 - \beta^2\left|\varepsilon\right|^2}{\varepsilon_2}\arg(1-\beta^2\varepsilon^*)\right] + \frac{1}{\omega^2}\int_{I_1}^{\omega}\tilde{\sigma}_\gamma(\omega')d\omega'\right\}. \qquad (4.67)\end{aligned}$$

This is especially simple in gases when $|\varepsilon(\omega)|^{-2} \sim 1$ for all $\omega > I_1$ [allis].

Energy Loss Simulation

For a given track length the number of ionizing collisions is simulated by a Poisson distribution whose mean is proportional to the total cross section of ionizing collisions:

$$\sigma_i = \int_{I_1}^{\omega_{max}} \frac{d\sigma(\omega')}{d\omega'} d\omega'.$$

The energy transfer in each collision is simulated according to a distribution proportional to

$$\sigma_i(>\omega) = \int_{\omega}^{\omega_{max}} \frac{d\sigma(\omega')}{d\omega'} d\omega'.$$

The sum of the energy transfers is equal to the energy loss. PAI ionisation is implemented according to the model approach (class G4PAIModel) allowing a user to select specific models in different regions. Here is an example physics list:

```
const G4RegionStore* theRegionStore = G4RegionStore::GetInstance();
G4Region* gas = theRegionStore->GetRegion("VertexDetector");
...
if (particleName == "e-")
{
  ...
  G4eIonisation* eion = new G4eIonisation();
  G4PAIModel*     pai = new G4PAIModel(particle,"PAIModel");

  // here 0 is the highest priority in region 'gas'
  eion->AddEmModel(0,pai,pai,gas);
  ...
}
...
```

It shows how to select the G4PAIModel to be the preferred ionisation model for electrons in a *G4Region* named *VertexDetector*. The first argument in *AddEmModel* is 0 which means highest priority.

The class *G4PAIPhotonModel* generates both δ-electrons and photons as secondaries and can be used for more detailed descriptions of ionisation space distribution around the particle trajectory.

Photoabsorption Cross Section at Low Energies

The photoabsorption cross section, $\sigma_\gamma(\omega)$, where ω is the photon energy, is used in Geant4 for the description of the photo-electric effect, X-ray transportation and ionization effects in very thin absorbers. As mentioned in the discussion of photoabsorption ionization (see section [secpai]), it is convenient to represent the cross section as a polynomial in ω^{-1} [sandia.bigg] :

$$\sigma_\gamma(\omega) = \sum_{k=1}^{4} a_k^{(i)} \omega^{-k}.$$

Using cross sections from the original Sandia data tables, calculations of primary ionization and energy loss distributions produced by relativistic charged particles in gaseous detectors show clear disagreement with experimental data, especially for gas mixtures which include xenon. Therefore a special investigation was performed [sandia.grich] by fitting the coefficients $a_k^{(i)}$ to modern data from synchrotron radiation experiments in the energy range of $10 - 50\ eV$. The fits were performed for elements typically used in detector gas mixtures: hydrogen, fluorine, carbon, nitrogen and oxygen. Parameters for these elements were extracted from data on molecular gases such as N_2, O_2, CO_2, CH_4, and CF_4 [sandia.lee73][sandia.lee77]. Parameters for the noble gases were found using data given in the tables [sandia.marr][sandia.west].

4.1.14 PhotoElectric effect

The photoelectric effect is the ejection of an electron from a material after a photon has been absorbed by that material. In the standard model *G4PEEffectFluoModel* it is simulated by using a parameterized photon absorption cross section to determine the mean free path, atomic shell data to determine the energy of the ejected electron, and the K-shell angular distribution to sample the direction of the electron.

Cross Section

The parameterization of the photoabsorption cross section proposed by Biggs et al. *[1]* was used :

$$\sigma(Z, E_\gamma) = \frac{a(Z, E_\gamma)}{E_\gamma} + \frac{b(Z, E_\gamma)}{E_\gamma^2} + \frac{c(Z, E_\gamma)}{E_\gamma^3} + \frac{d(Z, E_\gamma)}{E_\gamma^4} \tag{4.68}$$

Using the least-squares method, a separate fit of each of the coefficients a, b, c, d to the experimental data was performed in several energy intervals [ph.sandia.grich]. As a rule, the boundaries of these intervals were equal to the corresponding photoabsorption edges. The cross section (and correspondingly mean free path) are discontinuous and must be computed 'on the fly' from the formula [(4.68)]. Coefficients are defined to each Sandia table energy interval.

If photon energy is below the lowest Sandia energy for the material the cross section is computed for this lowest energy, so gamma is absorbed by photoabsorption at any energy. This approach is implemented coherently for models of photoelectric effect of Geant4. As a result, any media become not transparant for low-energy gammas.

Final State

Choosing an Element

The binding energies of the shells depend on the atomic number Z of the material. In compound materials the i^{th} element is chosen randomly according to the probability:

$$Prob(Z_i, E_\gamma) = \frac{n_{ati}\sigma(Z_i, E_\gamma)}{\sum_i [n_{ati} \cdot \sigma_i(E_\gamma)]}.$$

Shell

A quantum can be absorbed if $E_\gamma > B_{shell}$ where the shell energies are taken from G4AtomicShells data: the closest available atomic shell is chosen. The photoelectron is emitted with kinetic energy :

$$T_{photoelectron} = E_\gamma - B_{shell}(Z_i)$$

Theta Distribution of the Photoelectron

The polar angle of the photoelectron is sampled from the Sauter-Gavrila distribution (for K-shell) *[2]*, which is correct only to zero order in αZ :

$$\frac{d\sigma}{d(\cos\theta)} \sim \frac{\sin^2\theta}{(1-\beta\cos\theta)^4}\left\{1 + \frac{1}{2}\gamma(\gamma-1)(\gamma-2)(1-\beta\cos\theta)\right\}$$

where β and γ are the Lorentz factors of the photoelectron.

$\cos\theta$ is sampled from the probability density function :

$$f(\cos\theta) = \frac{1-\beta^2}{2\beta}\frac{1}{(1-\beta\cos\theta)^2} \quad \Longrightarrow \quad \cos\theta = \frac{(1-2r)+\beta}{(1-2r)\beta+1}$$

The rejection function is :

$$g(\cos\theta) = \frac{1-\cos^2\theta}{(1-\beta\cos\theta)^2}\left[1+b(1-\beta\cos\theta)\right]$$

with $b = \gamma(\gamma-1)(\gamma-2)/2$ It can be shown that $g(\cos\theta)$ is positive $\forall\cos\theta \in [-1,\ +1]$, and can be majored by :

$$\begin{aligned} gsup &= \gamma^2\left[1+b(1-\beta)\right] \text{ if } \gamma \in]1,2] \\ &= \gamma^2\left[1+b(1+\beta)\right] \text{ if } \gamma > 2 \end{aligned} \tag{4.69}$$

The efficiency of this method is $\sim 50\%$ if $\gamma < 2$, $\sim 25\%$ if $\gamma \in [2,\ 3]$.

Relaxation

Atomic relaxations can be sampled using the de-excitation module of the low-energy sub-package [relax]. For that atomic de-excitation option should be activated. In the *physics_list* sub-library this activation is done automatically for *G4EmLivermorePhysics*, *G4EmPenelopePhysics*, *G4EmStandardPhysics_option3* and *G4EmStandardPhysics_option4*. For other standard physics constructors the de-excitation module is already added but is disabled. The simulation of fluorescence and Auger electron emmision may be enabled for all geometry via UI commands: */process/em/fluo true /process/em/auger true* There is a possiblity to enable atomic deexcitation only for *G4Region* by its name: */process/em/deexcitation myregion true true false* where three boolean arguments enable/disable fluorescence, Auger electron production and PIXE (deexcitation induced by ionisation).

4.1.15 Introduction

With the EM polarization extension it is possible to track polarized particles (leptons and photons). Special emphasis will be put in the proper treatment of polarized matter and its interaction with longitudinal polarized electrons/positrons or circularly polarized photons, which is for instance essential for the simulation of positron polarimetry. The implementation is base on Stokes vectors [polIntro:McMaster:1961]. Further details can be found in [polIntro:Laihem:thesis].

In its current state, the following polarization dependent processes are considered

- Bhabha/Møller scattering,
- Positron Annihilation,
- Compton scattering,
- Pair creation,
- Bremsstrahlung.

Several simulation packages for the realistic description of the development of electromagnetic showers in matter have been developed. A prominent example of such codes is EGS (Electron Gamma Shower):cite:*egs4*. For this simulation framework extensions with the treatment of polarized particles exist [polIntro:Floettmann:thesis][polIntro:Namito:1993sv][polIntro:Liu:2000ey]; the most complete has been developed by K. Flöttmann [polIntro:Floettmann:thesis]. It is based on the matrix formalism [polIntro:McMaster:1961], which enables a very general treatment of polarization. However, the Flöttmann extension concentrates on evaluation of polarization transfer, i.e. the effects of polarization induced asymmetries are neglected, and interactions with polarized media are not considered.

Another important simulation tool for detector studies is Geant3 [polIntro:Brun:1985ps]. Here also some effort has been made to include polarization [polIntro:Alexander:2003fh][polIntro:Hoogduin:thesis], but these extensions are not publicly available.

In general the implementation of polarization in this EM polarization library follows very closely the approach by K. Flöttmann [polIntro:Floettmann:thesis]. The basic principle is to associate a *Stokes vector* to each particle and

track the mean polarization from one interaction to another. The basics for this approach is the matrix formalism as introduced in [polIntro:McMaster:1961].

Stokes vector

The *Stokes vector* [polIntro:Stokes:1852][polIntro:McMaster:1961] is a rather simple object (in comparison to e.g. the spin density matrix), three real numbers are sufficient for the characterization of the polarization state of any single electron, positron or photon. Using *Stokes vectors* **all** possible polarization states can be described, i.e. circular and linear polarized photons can be handled with the same formalism as longitudinal and transverse polarized electron/positrons.

The *Stokes vector* can be used also for beams, in the sense that it defines a mean polarization.

In the EM polarization library the Stokes vector is defined as follows:

	Photons	Electrons
ξ_1	linear polarization	polarization in x direction
ξ_2	linear polarization but $\pi/4$ to right	polarization in y direction
ξ_3	circular polarization	polarization in z direction

This definition is assumed in the *particle reference frame*, i.e. with the momentum of the particle pointing to the z direction, cf. also next section about coordinate transformations. Correspondingly a 100% longitudinally polarized electron or positron is characterized by

$$\boldsymbol{\xi} = \begin{pmatrix} 0 \\ 0 \\ \pm 1 \end{pmatrix},$$

where ± 1 corresponds to spin parallel (anti parallel) to particle's momentum. Note that this definition is similar, but not identical to the definition used in McMaster [polIntro:McMaster:1961].

Many scattering cross sections of polarized processes using Stokes vectors for the characterization of initial and final states are available in [polIntro:McMaster:1961]. In general a differential cross section has the form

$$\frac{d\sigma(\boldsymbol{\zeta}^{(1)}, \boldsymbol{\zeta}^{(2)}, \boldsymbol{\xi}^{(1)}, \boldsymbol{\xi}^{(2)})}{d\Omega} ,$$

i.e. it is a function of the polarization states of the initial particles $\boldsymbol{\zeta}^{(1)}$ and $\boldsymbol{\zeta}^{(2)}$, as well as of the polarization states of the final state particles $\boldsymbol{\xi}^{(1)}$ and $\boldsymbol{\xi}^{(2)}$ (in addition to the kinematic variables E, θ, and ϕ).

Consequently, in a simulation we have to account for

- Asymmetries:
- Polarization of beam ($\boldsymbol{\zeta}^{(1)}$) and target ($\boldsymbol{\zeta}^{(2)}$) can induce azimuthal and polar asymmetries, and may also influence on the total cross section (Geant4: GetMeanFreePath()).
- Polarization transfer / depolarization effects
- The dependence on the final state polarizations defines a possible transfer from initial polarization to final state particles.

Transfer matrix

Using the formalism of McMaster, differential cross section and polarization transfer from the initial state ($\boldsymbol{\zeta}^{(1)}$) to one final state particle ($\boldsymbol{\xi}^{(1)}$) are combined in an interaction matrix T:

$$\begin{pmatrix} O \\ \boldsymbol{\xi}^{(1)} \end{pmatrix} = T \begin{pmatrix} I \\ \boldsymbol{\zeta}^{(1)} \end{pmatrix} ,$$

where I and O are the incoming and outgoing currents, respectively. In general the 4×4 matrix T depends on the target polarization $\boldsymbol{\zeta}^{(2)}$ (and of course on the kinematic variables E, θ, ϕ). Similarly one can define a matrix defining the polarization transfer to second final state particle like

$$\begin{pmatrix} O \\ \boldsymbol{\xi}^{(2)} \end{pmatrix} = T' \begin{pmatrix} I \\ \boldsymbol{\zeta}^{(1)} \end{pmatrix} .$$

In this framework the transfer matrix T is of the form

$$T = \begin{pmatrix} S & A_1 & A_2 & A_3 \\ P_1 & M_{11} & M_{21} & M_{31} \\ P_2 & M_{12} & M_{22} & M_{32} \\ P_3 & M_{13} & M_{23} & M_{33} \end{pmatrix} .$$

The matrix elements T_{ij} can be identified as (unpolarized) differential cross section (S), polarized differential cross section (A_j), polarization transfer (M_{ij}), and (de)polarization (P_i). In the Flöttmann extension the elements A_j and P_i have been neglected, thus concentrating on polarization transfer only. Using the full matrix takes now all polarization effects into account.

The transformation matrix, i.e. the dependence of the mean polarization of final state particles, can be derived from the asymmetry of the differential cross section w.r.t. this particular polarization. Where the asymmetry is defined as usual by

$$A = \frac{\sigma(+1) - \sigma(-1)}{\sigma(+1) + \sigma(-1)} .$$

The mean final state polarizations can be determined coefficient by coefficient. In general, the differential cross section is a linear function of the polarizations, i.e.

$$\begin{aligned} \frac{d\sigma(\boldsymbol{\zeta}^{(1)}, \boldsymbol{\zeta}^{(2)}, \boldsymbol{\xi}^{(1)}, \boldsymbol{\xi}^{(2)})}{d\Omega} &= \Phi_{(\zeta^{(1)},\zeta^{(2)})} + \boldsymbol{A}_{(\zeta^{(1)},\zeta^{(2)})} \cdot \boldsymbol{\xi}^{(1)} + \boldsymbol{B}_{(\zeta^{(1)},\zeta^{(2)})} \cdot \boldsymbol{\xi}^{(2)} \\ &\quad + {\boldsymbol{\xi}^{(1)}}^T M_{(\zeta^{(1)},\zeta^{(2)})} \boldsymbol{\xi}^{(2)} \end{aligned} \tag{4.70}$$

In this form, the mean polarization of the final state can be read off easily, and one obtains

$$\langle \boldsymbol{\xi}^{(1)} \rangle = \frac{1}{\Phi_{(\zeta^{(1)},\zeta^{(2)})}} \boldsymbol{A}_{(\zeta^{(1)},\zeta^{(2)})} \quad \text{and} \tag{4.71}$$

$$\langle \boldsymbol{\xi}^{(2)} \rangle = \frac{1}{\Phi_{(\zeta^{(1)},\zeta^{(2)})}} \boldsymbol{B}_{(\zeta^{(1)},\zeta^{(2)})} . \tag{4.72}$$

Note, that the *mean* polarization states do not depend on the correlation matrix $M_{(\zeta^{(1)},\zeta^{(2)})}$. In order to account for correlation one has to generate *single* particle Stokes vector explicitly, i.e. on an event by event basis. However, this implementation generates *mean* polarization states, and neglects correlation effects.

Coordinate transformations

Three different coordinate systems are used in the evaluation of polarization states:

- **World frame** The geometry of the target, and the momenta of all particles in Geant4 are noted in the world frame X, Y, Z (the *global reference frame*, GRF). It is the basis of the calculation of any other coordinate system.
- **Particle frame** Each particle is carrying its own coordinate system. In this system the direction of motion coincides with the z-direction. Geant4 provides a transformation from any particle frame to the World frame by the method G4ThreeMomemtum::rotateUz(). Thus, the y-axis of the *particle reference frame* (PRF) lies in the X-Y-plane of the world frame.

  The Stokes vector of any moving particle is defined w.r.t. the corresponding particle frame. Particles at rest (e.g. electrons of a media) use the world frame as particle frame.

- **Interaction frame** For the evaluation of the polarization transfer another coordinate system is used, defined by the scattering plane, cf.fig. [pol.interframe]. There the z-axis is defined by the direction of motion of the incoming particle. The scattering plane is spanned by the z-axis and the x-axis, in a way, that the direction of *particle 1* has a positive x component. The definition of *particle 1* depends on the process, for instance in Compton scattering, the outgoing photon is referred as *particle 1* [1].

All frames are right handed.

Polarized beam and material

Polarization of beam particles is well established. It can be used for simulating low-energy Compton scattering of linear polarized photons. The interpretation as Stokes vector allows now the usage in a more general framework. The polarization state of a (initial) beam particle can be fixed using standard the ParticleGunMessenger class. For example, the class G4ParticleGun provides the method SetParticlePolarization(), which is usually accessable via

```
/gun/polarization <Sx> <Sy> <Sz>
```

in a macro file.

In addition for the simulation of polarized media, a possibility to assign Stokes vectors to physical volumes is provided by a new class, the so-called *G4PolarizationManager*. The procedure to assign a polarization vector to a media, is done during the *detector construction*. There the *logical volumes* with certain polarization are made known to *polarization manager*. One example DetectorConstruction might look like follows:

```
G4double Targetthickness = .010*mm;
G4double Targetradius    = 2.5*mm;

G4Tubs *solidTarget =
  new G4Tubs("solidTarget",
             0.0,
             Targetradius,
             Targetthickness/2,
             0.0*deg,
             360.0*deg );

G4LogicalVolume * logicalTarget =
  new G4LogicalVolume(solidTarget,
                      iron,
                      "logicalTarget",
                      0,0,0);

G4VPhysicalVolume *  physicalTarget =
  new G4PVPlacement(0,G4ThreeVector(0.*mm, 0.*mm, 0.*mm),
                    logicalTarget,
                    "physicalTarget",
                    worldLogical,
                    false,
                    0);

G4PolarizationManager * polMgr = G4PolarizationManager::GetInstance();
polMgr->SetVolumePolarization(logicalTarget,G4ThreeVector(0.,0.,0.08));
```

Once a logical volume is known to the G4PolarizationManager, its polarization vector can be accessed from a macro file by its name, e.g. the polarization of the logical volume called “logicalTarget” can be changed via

```
/polarization/volume/set logicalTarget 0. 0. -0.08
```

Note, the polarization of a material is stated in the world frame.

4.1.16 Ionization

Method

The class *G4ePolarizedIonization* provides continuous and discrete energy losses of polarized electrons and positrons in a material. It evaluates polarization transfer and – if the material is polarized – asymmetries in the explicit delta rays production. The implementation baseline follows the approach derived for the class *G4eIonization* described in sections [en_loss] and [sec:em.eion]. For continuous energy losses the effects of a polarized beam or target are negligible provided the separation cut $T_{\rm cut}$ is small, and are therefore not considered separately. On the other hand, in the explicit production of delta rays by Møller or Bhabha scattering, the effects of polarization on total cross section and mean free path, on distribution of final state particles and the average polarization of final state particles are taken into account.

Total cross section and mean free path

Kinematics of Bhabha and Møller scattering is fixed by initial energy

$$\gamma = \frac{E_{k_1}}{mc^2}$$

and variable

$$\epsilon = \frac{E_{p_2} - mc^2}{E_{k_1} - mc^2},$$

which is the part of kinetic energy of initial particle carried out by scatter. Lower kinematic limit for ϵ is 0, but in order to avoid divergencies in both total and differential cross sections one sets

$$\epsilon_{min} = x = \frac{T_{min}}{E_{k_1} - mc^2},$$

where T_{min} has meaning of minimal kinetic energy of secondary electron. And, $\epsilon_{\max} = 1(1/2)$ for Bhabha(Møller) scatterings.

Total Møller cross section

The total cross section of the polarized Møller scattering can be expressed as follows

$$\sigma^M_{pol} = \frac{2\pi\gamma^2 r_e^2}{(\gamma-1)^2(\gamma+1)}\left[\sigma^M_0 + \zeta^{(1)}_3\zeta^{(2)}_3\sigma^M_L + \left(\zeta^{(1)}_1\zeta^{(2)}_1 + \zeta^{(1)}_2\zeta^{(2)}_2\right)\sigma^M_T\right],$$

where the r_e is classical electron radius, and

$$\begin{aligned}
\sigma^M_0 &= -\frac{1}{1-x} + \frac{1}{x} - \frac{(\gamma-1)^2}{\gamma^2}\left(\frac{1}{2} - x\right) + \frac{2-4\,\gamma}{2\,\gamma^2}\,\ln\left(\frac{1-x}{x}\right) \\
\sigma^M_L &= \frac{\left(-3+2\,\gamma+\gamma^2\right)\,(1-2\,x)}{2\,\gamma^2} + \frac{2\,\gamma\,(-1+2\,\gamma)}{2\,\gamma^2}\,\ln\left(\frac{1-x}{x}\right) \\
\sigma^M_T &= \frac{2\,(\gamma-1)\,(2\,x-1)}{2\,\gamma^2} + \frac{(1-3\,\gamma)}{2\,\gamma^2}\,\ln\left(\frac{1-x}{x}\right)
\end{aligned} \tag{4.73}$$

Total Bhabha cross section

The total cross section of the polarized Bhabha scattering can be expressed as follows

$$\sigma^B_{pol} = \frac{2\pi r_e^2}{\gamma - 1}\left[\sigma^B_0 + \zeta^{(1)}_3\zeta^{(2)}_3\sigma^B_L + \left(\zeta^{(1)}_1\zeta^{(2)}_1 + \zeta^{(1)}_2\zeta^{(2)}_2\right)\sigma^B_T\right],$$

where

$$\begin{aligned}
\sigma^B_0 &= \frac{1-x}{2\,(\gamma-1)\,x} + \frac{2\left(-1+3\,x-6\,x^2+4\,x^3\right)}{3\,(1+\gamma)^3} \\
&+ \frac{-1-5\,x+12\,x^2-10\,x^3+4\,x^4}{2\,(1+\gamma)\,x} + \frac{-3-x+8\,x^2-4\,x^3-\ln(x)}{(1+\gamma)^2} \\
&+ \frac{3+4\,x-9\,x^2+3\,x^3-x^4+6\,x\,\ln(x)}{3\,x} \\
\sigma^B_L &= \frac{2\left(1-3\,x+6\,x^2-4\,x^3\right)}{3\,(1+\gamma)^3} + \frac{-14+15\,x-3\,x^2+2\,x^3-9\,\ln(x)}{3\,(1+\gamma)} \\
&+ \frac{5+3\,x-12\,x^2+4\,x^3+3\,\ln(x)}{3\,(1+\gamma)^2} + \frac{7-9\,x+3\,x^2-x^3+6\,\ln(x)}{3} \\
\sigma^B_T &= \frac{2\left(-1+3\,x-6\,x^2+4\,x^3\right)}{3\,(1+\gamma)^3} + \frac{-7-3\,x+18\,x^2-8\,x^3-3\,\ln(x)}{3\,(1+\gamma)^2} \\
&+ \frac{5+3\,x-12\,x^2+4\,x^3+9\,\ln(x)}{6\,(1+\gamma)}
\end{aligned} \tag{4.74}$$

Mean free path

With the help of the total polarized Møller cross section one can define a longitudinal asymmetry A^M_L and the transverse asymmetry A^M_T, by

Similarly, using the polarized Bhabha cross section one can introduce a longitudinal asymmetry A^B_L and the transverse asymmetry A^B_T via

These asymmetries are depicted in figures [pol.moller1] and [pol.bhabha1] respectively.

If both beam and target are polarized the mean free path as defined in section [sec:em.eion] has to be modified. In the class *G4ePolarizedIonization* the polarized mean free path :math:)‘(lambda^{rm pol}‘ is derived from the unpolarized mean free path :math:)‘(lambda^{rm unpol}‘ via

$$\lambda^{\rm pol} = \frac{\lambda^{\rm unpol}}{1 + \zeta^{(1)}_3\zeta^{(2)}_3\,A_L + \left(\zeta^{(1)}_1\zeta^{(2)}_1 + \zeta^{(1)}_2\zeta^{(2)}_2\right)\,A_T}$$

|[pol.bhabha1]Bhabha total cross section asymmetries depending on the total energy of the incoming positron, with a cut-off :math:‘\(T_{\rm cut}= 1 {\rm keV}\)‘. Transverse asymmetry is plotted in blue, longitudinal asymmetry in red. Left part, between 0.5 MeV and 2 MeV, right part up to 10 MeV.| |[pol.bhabha1]Bhabha total cross section asymmetries depending on the total energy of the incoming positron, with a cut-off :math:‘\(T_{\rm cut}= 1 {\rm keV}\)‘. Transverse asymmetry is plotted in blue, longitudinal asymmetry in red. Left part, between 0.5 MeV and 2 MeV, right part up to 10 MeV.|

|[pol.bhabha1]Bhabha total cross section asymmetries depending on the total energy of the incoming positron, with a cut-off :math:‘\(T_{\rm cut}= 1 {\rm keV}\)‘. Transverse asymmetry is plotted in blue, longitudinal asymmetry in red. Left part, between 0.5 MeV and 2 MeV, right part up to 10 MeV.| |[pol.bhabha1]Bhabha total cross section asymmetries depending on the total energy of the incoming positron, with a cut-off :math:‘\(T_{\rm cut}= 1 {\rm keV}\)‘. Transverse asymmetry is plotted in blue, longitudinal asymmetry in red. Left part, between 0.5 MeV and 2 MeV, right part up to 10 MeV.|

Sampling the final state

Differential cross section

The polarized differential cross section is rather complicated, the full result can be found in [polIoni:Star:2006][polIoni:Ford:1957][polIoni:Stehle:1957]. In *G4PolarizedMollerCrossSection* the complete result is available taking all mass effects into account, only binding effects are neglected. Here we state only the ultra-relativistic approximation (URA), to show the general dependencies.

$$\frac{d\sigma^M_{URA}}{d\epsilon d\varphi} = \frac{{r_\epsilon}^2}{\gamma+1} \times \left[\frac{\left(1-\epsilon+\epsilon^2\right)^2}{4\left(\epsilon-1\right)^2\epsilon^2} + \zeta_3^{(1)}\zeta_3^{(2)}\frac{2-\epsilon+\epsilon^2}{-4\,\epsilon(1-\epsilon)} + \left(\zeta_2^{(1)}\zeta_2^{(2)} - \zeta_1^{(1)}\zeta_1^{(2)}\right)\frac{1}{4} + \left(\xi_3^{(1)}\zeta_3^{(1)} - \xi_3^{(2)}\zeta_3^{(2)}\right)\frac{1-\epsilon+2\,\epsilon^2}{4\,(1-\epsilon)\,\epsilon^2} + \left(\xi_3^{(2)}\zeta_3^{(1)} - \xi_3^{(1)}\zeta_3^{(2)}\right)\frac{2-3\,\epsilon+2\,\epsilon^2}{4\,(1-\epsilon)^2\,\epsilon}\right] \tag{4.75}$$

The corresponding cross section for Bhabha cross section is implemented in *G4PolarizedBhabhaCrossSection*. In the ultra-relativistic approximation it reads

$$\frac{d\sigma^B_{URA}}{d\epsilon d\varphi} = \frac{{r_\epsilon}^2}{\gamma-1} \times \left[\frac{\left(1-\epsilon+\epsilon^2\right)^2}{4\,\epsilon^2} + \zeta_3^{(1)}\zeta_3^{(2)}\frac{(\epsilon-1)\,\left(2-\epsilon+\epsilon^2\right)}{4\,\epsilon} + \left(\zeta_2^{(1)}\zeta_2^{(2)} - \zeta_1^{(1)}\zeta_1^{(2)}\right)\frac{(1-\epsilon)^2}{4} + \left(\xi_3^{(1)}\zeta_3^{(1)} - \xi_3^{(2)}\zeta_3^{(2)}\right)\frac{1-2\,\epsilon+3\,\epsilon^2-2\,\epsilon^3}{4\,\epsilon^2} + \left(\xi_3^{(2)}\zeta_3^{(1)} - \xi_3^{(1)}\zeta_3^{(2)}\right)\frac{2-3\,\epsilon+2\,\epsilon^2}{4\epsilon}\right] \tag{4.76}$$

where

Sampling

The delta ray is sampled according to methods discussed in Chapter 2. After exploitation of the symmetry in the Møller cross section under exchanging ϵ versus $(1-\epsilon)$, the differential cross section can be approximated by a simple function $f^M(\epsilon)$:

$$f^M(\epsilon) = \frac{1}{\epsilon^2}\frac{\epsilon_0}{1-2\epsilon_0}$$

with the kinematic limits given by

$$\epsilon_0 = \frac{T_{\rm cut}}{E_{k_1} - m_e c^2} \le \epsilon \le \frac{1}{2}$$

A similar function $f^B(\epsilon)$ can be found for Bhabha scattering:

$$f^B(\epsilon) = \frac{1}{\epsilon^2}\frac{\epsilon_0}{1-\epsilon_0}$$

with the kinematic limits given by

$$\epsilon_0 = \frac{T_{\rm cut}}{E_{k_1} - m_e c^2} \le \epsilon \le 1$$

The kinematic of the delta ray production is constructed by the following steps:

1. ϵ is sampled from $f(\epsilon)$
2. calculate the differential cross section, depending on the initial polarizations $\zeta^{(1)}$ and $\zeta^{(2)}$.
3. ϵ is accepted with the probability defined by ratio of the differential cross section over the approximation function.
4. The φ is diced uniformly.
5. φ is determined from the differential cross section, depending on the initial polarizations $\zeta^{(1)}$ and $\zeta^{(2)}$

Note, for initial states without transverse polarization components, the φ distribution is always uniform. In figure [pol.moller2] the asymmetries indicate the influence of polarization. In general the effect is largest around $\epsilon = \frac{1}{2}$.

|[pol.moller2]Differential cross section asymmetries in% for Møller (left) and Bhabha (right) scattering (red - :math:‘\(A_{ZZ}(\epsilon)\)‘, green - :math:‘\(A_{XX}(\epsilon)\)‘, blue - :math:‘\(A_{YY}(\epsilon)\)‘, lightblue - :math:‘\(A_{ZX}(\epsilon)\)‘)| |[pol.moller2]Differential cross section asymmetries in% for Møller (left) and Bhabha (right) scattering (red - :math:‘\(A_{ZZ}(\epsilon)\)‘, green - :math:‘\(A_{XX}(\epsilon)\)‘, blue - :math:‘\(A_{YY}(\epsilon)\)‘, lightblue - :math:‘\(A_{ZX}(\epsilon)\)‘)|

After both ϕ and ϵ are known, the kinematic can be constructed fully. Using momentum conservation the momenta of the scattered incident particle and the ejected electron are constructed in global coordinate system.

Polarization transfer

After the kinematics is fixed the polarization properties of the outgoing particles are determined. Using the dependence of the differential cross section on the final state polarization a mean polarization is calculated according to method described in section [sec:pol.intro].

The resulting polarization transfer functions $\xi_3^{(1,2)}(\epsilon)$ are depicted in figures [pol.moller3] and [pol.bhabha3].

|[pol.moller3]Polarization transfer functions in Møller scattering. Longitudinal polarization :math:‘\(\xi^{(2)}_3\)‘ of electron with energy :math:‘\(E_{p_2}\)‘ in blue; longitudinal polarization :math:‘\(\xi^{(1)}_3\)‘ of second electron in red. Kinetic energy of incoming electron :math:‘\(T_{k_1} = 10 {\rm MeV}\)‘| |[pol.moller3]Polarization transfer functions in Møller scattering. Longitudinal polarization :math:‘\(\xi^{(2)}_3\)‘ of electron with energy :math:‘\(E_{p_2}\)‘ in blue; longitudinal polarization :math:‘\(\xi^{(1)}_3\)‘ of second electron in red. Kinetic energy of incoming electron :math:‘\(T_{k_1} = 10 {\rm MeV}\)‘|

.

|[pol.bhabha3]Polarization Transfer in Bhabha scattering. Longitudinal polarization :math:‘\(\xi^{(2)}_3\)‘ of electron with energy :math:‘\(E_{p_2}\)‘ in blue; longitudinal polarization :math:‘\(\xi^{(1)}_3\)‘ of scattered positron. Kinetic energy of incoming positron :math:‘\(T_{k_1} = 10 {\rm MeV}\)‘| |[pol.bhabha3]Polarization Transfer in Bhabha scattering. Longitudinal polarization :math:‘\(\xi^{(2)}_3\)‘ of electron with energy :math:‘\(E_{p_2}\)‘ in blue; longitudinal polarization :math:‘\(\xi^{(1)}_3\)‘ of scattered positron. Kinetic energy of incoming positron :math:‘\(T_{k_1} = 10 {\rm MeV}\)‘|

.

4.1.17 Positron - Electron Annihilation

Method

The class *G4eplusPolarizedAnnihilation* simulates annihilation of polarized positrons with electrons in a material. The implementation baseline follows the approach derived for the class *G4eplusAnnihilation* described in section [sec:em.annil]. It evaluates polarization transfer and – if the material is polarized – asymmetries in the produced photons. Thus, it takes the effects of polarization on total cross section and mean free path, on distribution of final

state photons into account. And calculates the average polarization of these generated photons. The material electrons are assumed to be free and at rest.

Total cross section and mean free path

Kinematics of annihilation process is fixed by initial energy

$$\gamma = \frac{E_{k_1}}{mc^2}$$

and variable

$$\epsilon = \frac{E_{p_1}}{E_{k_1} + mc^2},$$

which is the part of total energy available in initial state carried out by first photon. This variable has the following kinematical limits

$$\frac{1}{2}\left(1 - \sqrt{\frac{\gamma-1}{\gamma+1}}\right) \;<\; \epsilon \;<\; \frac{1}{2}\left(1 + \sqrt{\frac{\gamma-1}{\gamma+1}}\right) .$$

Total Cross Section

The total cross section of the annihilation of a polarized e^+e^- pair into two photons could be expressed as follows

$$\sigma^A_{pol} = \frac{\pi r_e^2}{\gamma+1}\left[\sigma^A_0 + \zeta_3^{(1)}\zeta_3^{(2)}\sigma^A_L + \left(\zeta_1^{(1)}\zeta_1^{(2)} + \zeta_2^{(1)}\zeta_2^{(2)}\right)\sigma^A_T\right],$$

where

$$\sigma^A_0 = \frac{-(3+\gamma)\,\sqrt{-1+\gamma^2} + (1+\gamma\,(4+\gamma))\,\ln(\gamma+\sqrt{-1+\gamma^2})}{4\,(\gamma^2-1)}$$

$$\sigma^A_L = \frac{-\sqrt{-1+\gamma^2}\,(5+\gamma\,(4+3\,\gamma)) + \left(3+\gamma\,\left(7+\gamma+\gamma^2\right)\right)\,\ln(\gamma+\sqrt{\gamma^2-1})}{4\,(\gamma-1)^2\,(1+\gamma)}$$

$$\sigma^A_T = \frac{(5+\gamma)\,\sqrt{-1+\gamma^2} - (1+5\,\gamma)\,\ln(\gamma+\sqrt{-1+\gamma^2})}{4\,(-1+\gamma)^2\,(1+\gamma)}$$

Mean free path

With the help of the total polarized annihilation cross section one can define a longitudinal asymmetry A^A_L and the transverse asymmetry A^A_T, by

These asymmetries are depicted in figure [pol.annihi1].

If both incident positron and target electron are polarized the mean free path as defined in section [sec:em.annil] has to be modified. The polarized mean free path $\lambda^{\rm pol}$ is derived from the unpolarized mean free path $\lambda^{\rm unpol}$ via

$$\lambda^{\rm pol} = \frac{\lambda^{\rm unpol}}{1 + \zeta_3^{(1)}\zeta_3^{(2)}\,A_L + \left(\zeta_1^{(1)}\zeta_1^{(2)} + \zeta_2^{(1)}\zeta_2^{(2)}\right)\,A_T}$$

I[pol.annihi1]Annihilation total cross section asymmetries depending on the total energy of the incoming positron E_{k_1}. The transverse asymmetry is shown in blue, the longitudinal asymmetry in red. I I[pol.annihi1]Annihilation total cross section asymmetries depending on the total energy of the incoming positron E_{k_1}. The transverse asymmetry is shown in blue, the longitudinal asymmetry in red. I

Sampling the final state

Differential Cross Section

The fully polarized differential cross section is implemented in the class *G4PolarizedAnnihilationCrossSection*, which takes all mass effects into account, but binding effects are neglected [polAnnihi:Star:2006][polAnnihi:Page:1957]. In the ultra-relativistic approximation (URA) and concentrating on longitudinal polarization states only the cross section is rather simple:

$$\begin{aligned}\frac{d\sigma^A_{URA}}{d\epsilon d\varphi} &= \frac{{r_e}^2}{\gamma-1}\times\left(\frac{1-2\,\epsilon+2\,\epsilon^2}{8\,\epsilon-8\,\epsilon^2}\left(1+\zeta_3^{(1)}\zeta_3^{(2)}\right)\right.\\ &\left.+\frac{(1-2\,\epsilon)\left(\zeta_3^{(1)}+\zeta_3^{(2)}\right)\left(\xi_3^{(1)}-\xi_3^{(2)}\right)}{8\,(\epsilon-1)\,\epsilon}\right)\end{aligned} \tag{4.77}$$

where

r_e	classical electron radius
γ	E_{k_1}/m_ec^2
E_{k_1}	energy of the incident positron
m_ec^2	electron mass
$\boldsymbol{\zeta}^{(1)}$	Stokes vector of the incoming positron
$\boldsymbol{\zeta}^{(2)}$	Stokes vector of the target electron
$\boldsymbol{\xi}^{(1)}$	Stokes vector of the 1st photon
$\boldsymbol{\xi}^{(2)}$	Stokes vector of the 2nd photon .

Sampling

The photon energy is sampled according to methods discussed in Chapter 2. After exploitation of the symmetry in the Annihilation cross section under exchanging ϵ versus $(1-\epsilon)$, the differential cross section can be approximated by a simple function $f(\epsilon)$:

$$f(\epsilon)=\frac{1}{\epsilon}\ln^{-1}\left(\frac{\epsilon_{\max}}{\epsilon_{\min}}\right)$$

with the kinematic limits given by

$$\begin{aligned}\epsilon_{\min} &= \frac{1}{2}\left(1-\sqrt{\frac{\gamma-1}{\gamma+1}}\right)\,,\\ \epsilon_{\max} &= \frac{1}{2}\left(1+\sqrt{\frac{\gamma-1}{\gamma+1}}\right)\,.\end{aligned} \tag{4.78}$$

The kinematic of the two photon final state is constructed by the following steps:

1. ϵ is sampled from $f(\epsilon)$
2. calculate the differential cross section, depending on the initial polarizations $\boldsymbol{\zeta}^{(1)}$ and $\boldsymbol{\zeta}^{(2)}$.
3. ϵ is accepted with the probability defined by the ratio of the differential cross section over the approximation function $f(\epsilon)$.
4. The φ is diced uniformly.
5. φ is determined from the differential cross section, depending on the initial polarizations $\boldsymbol{\zeta}^{(1)}$ and $\boldsymbol{\zeta}^{(2)}$.

A short overview over the sampling method is given in Chapter 2. In figure [pol.annihi2] the asymmetries indicate the influence of polarization for an 10MeV incoming positron. The actual behavior is very sensitive to the energy of the incoming positron.

Polarization transfer

After the kinematics is fixed the polarization of the outgoing photon is determined. Using the dependence of the differential cross section on the final state polarizations a mean polarization is calculated for each photon according to method described in section [sec:pol.intro].

The resulting polarization transfer functions $\xi^{(1,2)}(\epsilon)$ are depicted in figure [pol.annihi3].

|[pol.annihi3] Polarization Transfer in annihilation process. Blue line corresponds to the circular polarization :math:‘\(\xi_3^{(1)}\)‘ of the photon with energy :math:‘\(m(\gamma + 1)\epsilon\)‘; red line – circular polarization :math:‘\(\xi_3^{(2)}\)‘ of the photon photon with energy :math:‘\(m(\gamma + 1)(1-\epsilon)\)‘.|
|[pol.annihi3] Polarization Transfer in annihilation process. Blue line corresponds to the circular polarization :math:‘\(\xi_3^{(1)}\)‘ of the photon with energy :math:‘\(m(\gamma + 1)\epsilon\)‘; red line – circular polarization :math:‘\(\xi_3^{(2)}\)‘ of the photon photon with energy :math:‘\(m(\gamma + 1)(1-\epsilon)\)‘.|

Annihilation at Rest

The method `AtRestDoIt` treats the special case where a positron comes to rest before annihilating. It generates two photons, each with energy $E_{p_{1/2}} = mc^2$ and an isotropic angular distribution. Starting with the differential cross section for annihilation with positron and electron spins opposed and parallel, respectively,:cite:*polAnnihi:Page:1957*

$$d\sigma_1 = \sim \frac{(1-\beta^2)+\beta^2(1-\beta^2)(1-\cos^2\theta)^2}{(1-\beta^2\cos^2\theta)^2} d\cos\theta \tag{4.79}$$

$$d\sigma_2 = \sim \frac{\beta^2(1-\cos^4\theta)}{(1-\beta^2\cos^2\theta)^2} d\cos\theta \tag{4.80}$$

In the limit $\beta \to 0$ the cross section $d\sigma_1$ becomes one, and the cross section $d\sigma_2$ vanishes. For the opposed spin state, the total angular momentum is zero and we have a uniform photon distribution. For the parallel case the total angular momentum is 1. Here the two photon final state is forbidden by angular momentum conservation, and it can be assumed that higher order processes (e.g. three photon final state) play a dominant role. However, in reality 100% polarized electron targets do not exist, consequently there are always electrons with opposite spin, where the positron can annihilate with. Final state polarization does not play a role for the decay products of a spin zero state, and can be safely neglected. (Is set to zero)

4.1.18 Polarized Compton scattering

Method

The class *G4PolarizedCompton* simulates Compton scattering of polarized photons with (possibly polarized) electrons in a material. The implementation follows the approach described for the class *G4ComptonScattering* introduced in section [sec:em.compton]. Here the explicit production of a Compton scattered photon and the ejected electron is considered taking the effects of polarization on total cross section and mean free path as well as on the distribution of final state particles into account. Further the average polarizations of the scattered photon and electron are calculated. The material electrons are assumed to be free and at rest.

Total cross section and mean free path

Kinematics of the Compton process is fixed by the initial energy

$$X = \frac{E_{k_1}}{mc^2}$$

and the variable

$$\epsilon = \frac{E_{p_1}}{E_{k_1}},$$

which is the part of total energy avaible in initial state carried out by scattered photon, and the scattering angle

$$\cos\theta = 1 - \frac{1}{X}\left(\frac{1}{\epsilon} - 1\right)$$

The variable ϵ has the following limits:

$$\frac{1}{1+2X} \;<\; \epsilon \;<\; 1$$

Total Cross Section

The total cross section of Compton scattering reads

$$\sigma^C_{pol} = \frac{\pi\, {r_e}^2}{X^2\,(1+2\,X)^2}\left[\sigma^C_0 + \zeta^{(1)}_3\zeta^{(2)}_3\sigma^C_L\right]$$

where

$$\sigma^C_0 = \frac{2\,X\;(2+X\;(1+X)\;(8+X)) - (1+2\,X)^2\;(2+(2-X)\;X)\;\ln(1+2\,X)}{X}$$

and

$$\sigma^C_L = 2\,X\;(1+X\;(4+5\,X)) - (1+X)\;(1+2\,X)^2\;\ln(1+2\,X)$$

I[pol.compton1]Compton total cross section asymmetry depending on the energy of incoming photon. Left part, between 0 and $\sim$ 1 MeV, right part – up to 10MeV. I I[pol.compton1]Compton total cross section asymmetry depending on the energy of incoming photon. Left part, between 0 and $\sim$ 1 MeV, right part – up to 10MeV. I

Mean free path

When simulating the Compton scattering of a photon with an atomic electron, an empirical cross section formula is used, which reproduces the cross section data down to 10 keV (see section [sec:em.compton]). If both, beam and target, are polarized this mean free path has to be corrected.

In the class *G4ComptonScattering* the polarized mean free path $\lambda^{\rm pol}$ is defined on the basis of the the unpolarized mean free path $\lambda^{\rm unpol}$ via

$$\lambda^{\rm pol} = \frac{\lambda^{\rm unpol}}{1+\zeta^{(1)}_3\zeta^{(2)}_3\,A^C_L}$$

where

$$A^C_L = \frac{\sigma^A_L}{\sigma^A_0}$$

$$is the expected asymmetry from the the total polarized Compton cross$$

section given above. This asymmetry is depicted in figure [pol.compton1].

Sampling the final state

Differential Compton Cross Section

In the ultra-relativistic approximation the dependence of the differential cross section on the longitudinal/circular degree of polarization is very simple. It reads

$$\frac{d\sigma^C_{URA}}{ded\varphi} = \frac{{r_e}^2}{X}\left(\frac{\epsilon^2+1}{2\,\epsilon} + \frac{\epsilon^2-1}{2\,\epsilon}\left(\zeta_3^{(1)}\zeta_3^{(2)} + \zeta_3^{(2)}\,\xi_3^{(1)} - \zeta_3^{(1)}\,\xi_3^{(2)}\right)\right.$$
$$\left. + \frac{\epsilon^2+1}{2\,\epsilon}\left(\zeta_3^{(1)}\,\xi_3^{(1)} - \zeta_3^{(2)}\,\xi_3^{(2)}\right)\right) \tag{4.81}$$

where

r_e	classical electron radius
X	E_{k_1}/m_ec^2
E_{k_1}	energy of the incident photon
m_ec^2	electron mass

The fully polarized differential cross section is available in the class *G4PolarizedComptonCrossSection*. It takes all mass effects into account, but binding effects are neglected [polCompt:Star:2006][polCompt:Lipps:1954]. The cross section dependence on ϵ for right handed circularly polarized photons and longitudinally polarized electrons is plotted in figure [pol.compton2a]

Sampling

The photon energy is sampled according to methods discussed in Chapter 2. The differential cross section can be approximated by a simple function $\Phi(\epsilon)$:

$$\Phi(\epsilon) = \frac{1}{\epsilon} + \epsilon$$

with the kinematic limits given by

$$\epsilon_{\min} = \frac{1}{1+2X} \tag{4.82}$$
$$\epsilon_{\max} = 1 \tag{4.83}$$

The kinematic of the scattered photon is constructed by the following steps:

1. ϵ is sampled from $\Phi(\epsilon)$
2. calculate the differential cross section, depending on the initial polarizations $\boldsymbol{\zeta}^{(1)}$ and $\boldsymbol{\zeta}^{(2)}$, which the correct normalization.
3. ϵ is accepted with the probability defined by ratio of the differential cross section over the approximation function.
4. The φ is diced uniformly.
5. φ is determined from the differential cross section, depending on the initial polarizations $\boldsymbol{\zeta}^{(1)}$ and $\boldsymbol{\zeta}^{(2)}$.

In figure [pol.compton2] the asymmetries indicate the influence of polarization for an 10MeV incoming positron. The actual behavior is very sensitive to energy of the incoming positron.

Polarization transfer

After the kinematics is fixed the polarization of the outgoing photon is determined. Using the dependence of the differential cross section on the final state polarizations a mean polarization is calculated for each photon according to the method described in section [sec:pol.intro].

The resulting polarization transfer functions $\xi^{(1,2)}(\epsilon)$ are depicted in figure [pol.compton3].

|[pol.compton3] Polarization Transfer in Compton scattering. Blue line corresponds to the longitudinal polarization :math:‘\(\xi_3^{(2)}\)‘ of the electron, red line – circular polarization :math:‘\(\xi_3^{(1)}\)‘ of the photon.| |[pol.compton3] Polarization Transfer in Compton scattering. Blue line corresponds to the longitudinal polarization :math:‘\(\xi_3^{(2)}\)‘ of the electron, red line – circular polarization :math:‘\(\xi_3^{(1)}\)‘ of the photon.|

4.1.19 Polarized Bremsstrahlung for electron and positron

Method

The polarized version of Bremsstrahlung is based on the unpolarized cross section. Energy loss, mean free path, and distribution of explicitly generated final state particles are treated by the unpolarized version *G4eBremsstrahlung*. For details consult section [sec:em.ebrem].

The remaining task is to attribute polarization vectors to the generated final state particles, which is discussed in the following.

Polarization in gamma conversion and bremsstrahlung

Gamma conversion and bremsstrahlung are cross-symmetric processes (i.e. the Feynman diagram for electron bremsstrahlung can be obtained from the gamma conversion diagram by flipping the incoming photon and outgoing positron lines) and their cross sections closely related. For both processes, the interaction occurs in the field of the nucleus and the total and differential cross section are polarization independent. Therefore, only the polarization transfer from the polarized incoming particle to the outgoing particles is taken into account.

For both processes, the scattering can be formulated by:

$$\mathcal{K}_1(k_1, \boldsymbol{\zeta}^{(1)}) + \mathcal{N}_1(k_{\mathcal{N}_1}, \boldsymbol{\zeta}^{(\mathcal{N}_1)}) \longrightarrow \mathcal{P}_1(p_1, \boldsymbol{\xi}^{(1)}) + \mathcal{P}_2(p_2, \boldsymbol{\xi}^{(2)}) + \mathcal{N}_2(p_{\mathcal{N}_2}, \boldsymbol{\xi}^{(\mathcal{N}_2)})$$

Where :math:)‘(mathcal{N}_{1}(k_{mathcal {N}_{1}}, {{boldsymbol{zeta}}}^{(mathcal {N}_{1})})‘ and :math:)‘(mathcal{N}_{2}(p_{mathcal{N}_{2}}, {{boldsymbol{xi}}}^{(mathcal{N}_{2})})‘ are the initial and final state of the field of the nucleus respectively assumed to be unchanged, at rest and unpolarized. This leads to :math:)‘(k_{mathcal {N}_{1}} = k_{mathcal {N}_{2}} = 0‘ and :math:)‘({{boldsymbol{zeta}}}^{(mathcal {N}_{1})} = {{boldsymbol{xi}}}^{(mathcal{N}_{2})} = 0‘

In the case of gamma conversion process: $\mathcal{K}_1(k_1, \boldsymbol{\zeta}^{(1)})$ is the incoming photon initial state with momentum k_1 and polarization state $\boldsymbol{\zeta}^{(1)}$. $\mathcal{P}_1(p_1, \boldsymbol{\xi}^{(1)})$ and $\mathcal{P}_2(p_2, \boldsymbol{\xi}^{(2)})$ are the two photons final states with momenta p_1 and p_2 and polarization states $\boldsymbol{\xi}^{(1)}$ and $\boldsymbol{\xi}^{(2)}$.

In the case of bremsstrahlung process: $\mathcal{K}_1(k_1, \boldsymbol{\zeta}^{(1)})$ is the incoming lepton $e^-(e^+)$ initial state with momentum k_1 and polarization state $\boldsymbol{\zeta}^{(1)}$. $\mathcal{P}_1(p_1, \boldsymbol{\xi}^{(1)})$ is the lepton $e^-(e^+)$ final state with momentum p_1 and polarization state $\boldsymbol{\xi}^{(1)}$. $\mathcal{P}_2(p_2, \boldsymbol{\xi}^{(2)})$ is the bremsstrahlung photon in final state with momentum p_2 and polarization state $\boldsymbol{\xi}^{(2)}$.

Polarization transfer from the lepton $e^-(e^+)$ to a photon

The polarization transfer from an electron (positron) to a photon in a bremsstrahlung process was first calculated by Olsen and Maximon [polBrems:Olsen_Maximon] taking into account both Coulomb and screening effects. In the

Stokes vector formalism, the $e^-(e^+)$ polarization state can be transformed to a photon polarization finale state by means of interaction matrix T^b_γ. It defined via

$$\begin{pmatrix} O \\ \boldsymbol{\xi}^{(2)} \end{pmatrix} = T^b_\gamma \begin{pmatrix} 1 \\ \boldsymbol{\zeta}^{(1)} \end{pmatrix} ,$$

and

$$T^b_\gamma \approx \begin{pmatrix} 1 & 0 & 0 & 0 \\ D & 0 & 0 & 0 \\ 0 & 0 & 0 & 0 \\ 0 & T & 0 & L \end{pmatrix} ,$$

where

$$I = (\epsilon_1^2 + \epsilon_2^2)(3 + 2\Gamma) - 2\epsilon_1\epsilon_2(1 + 4u^2\hat{\xi}^2\Gamma) \tag{4.84}$$

$$D = \left\{8\epsilon_1\epsilon_2 u^2\hat{\xi}^2\Gamma\right\}/I \tag{4.85}$$

$$T = \left\{-4k\epsilon_2\hat{\xi}(1 - 2\hat{\xi})u\Gamma\right\}/I \tag{4.86}$$

$$L = k\{(\epsilon_1 + \epsilon_2)(3 + 2\Gamma) - 2\epsilon_2(1 + 4u^2\hat{\xi}^2\Gamma)\}/I \tag{4.87}$$

and

Coulomb and screening effects are contained in Γ, defined as follows

$$\Gamma = \ln\left(\frac{1}{\delta}\right) - 2 - f(Z) + \mathcal{F}\left(\frac{\hat{\xi}}{\delta}\right) \quad \text{for } \Delta \leq 120 \tag{4.88}$$

$$\Gamma = \ln\left(\frac{111}{\hat{\xi}Z^{\frac{1}{3}}}\right) - 2 - f(z) \quad \text{for } \Delta \geq 120 \tag{4.89}$$

with

$$\Delta = \frac{12Z^{\frac{1}{3}}\epsilon_1\epsilon_2\hat{\xi}}{121k} \quad \text{with } Z \text{ the atomic number and } \delta = \frac{k}{2\epsilon_1\epsilon 2} \tag{4.90}$$

$f(Z)$ is the coulomb correction term derived by Davies, Bethe and Maximon *[2]*. $\mathcal{F}(\hat{\xi}/\delta)$ contains the screening effects and is zero for $\Delta \leq 0.5$ (No screening effects). For :math:)‘(0.5 le Delta le 120 ‘ (intermediate screening) it is a slowly decreasing function. The $\mathcal{F}(\hat{\xi}/\delta)$ values versus Δ are given in table [koch] and used with a linear interpolation in between.

The polarization vector of the incoming $e^-(e^+)$ must be rotated into the frame defined by the scattering plane (x-z-plane) and the direction of the outgoing photon (z-axis). The resulting polarization vector of the bremsstrahlung photon is also given in this frame.

Table: $\mathcal{F}(\hat{\xi}/\delta)$ for intermediate values of the screening factor *[1]*.

Using Eq. ([eq:brem_gamma]) and the transfer matrix given by Eq. ([eq:matrix_brem_g]) the bremsstrahlung photon polarization state in the Stokes formalism [polBrems:McMaster1][polBrems:McMaster2] is given by

$$\xi^{(2)} = \begin{pmatrix} \xi_1^{(2)} \\ \xi_2^{(2)} \\ \xi_3^{(2)} \end{pmatrix} \approx \begin{pmatrix} D \\ 0 \\ \zeta_1^{(1)}L + \zeta_2^{(1)}T \end{pmatrix}$$

Remaining polarization of the lepton after emitting a bremsstrahlung photon

The $e^-(e^+)$ polarization final state after emitting a bremsstrahlung photon can be calculated using the interaction matrix T^b_l which describes the lepton depolarization. The polarization vector for the outgoing $e^-(e^+)$ is not

given by Olsen and Maximon. However, their results can be used to calculate the following transfer matrix [polBrems:klausFl][polBrems:hoogduin].

$$\begin{pmatrix} O \\ \boldsymbol{\xi}^{(1)} \end{pmatrix} = T_l^b \begin{pmatrix} 1 \\ \boldsymbol{\zeta}^{(1)} \end{pmatrix}$$

$$T_l^b \approx \begin{pmatrix} 1 & 0 & 0 & 0 \\ D & M & 0 & E \\ 0 & 0 & M & 0 \\ 0 & F & 0 & M+P \end{pmatrix}$$

where

$$I = (\epsilon_1^2+\epsilon_2^2)(3+2\Gamma) - 2\epsilon_1\epsilon_2(1+4u^2\hat{\xi}^2\Gamma) \quad (4.91)$$

$$F = \epsilon_2\left\{4k\hat{\xi}u(1-2\hat{\xi})\Gamma\right\}/I \quad (4.92)$$

$$E = \epsilon_1\left\{4k\hat{\xi}u(2\hat{\xi}-1)\Gamma\right\}/I \quad (4.93)$$

$$M = \left\{4k\epsilon_1\epsilon_2(1+\Gamma-2u^2\hat{\xi}^2\Gamma)\right\}/I \quad (4.94)$$

$$P = \left\{k^2(1+8\Gamma(\hat{\xi}-0.5)^2\right\}/I \quad (4.95)$$

and

Using Eq. ([eq:brem_lepton]) and the transfer matrix given by Eq. ([eq:matrix_brem_l]) the $e^-(e^+)$ polarization state after emitting a bremsstrahlung photon is given in the Stokes formalism by

$$\xi^{(1)} = \begin{pmatrix} \xi_1^{(1)} \\ \xi_2^{(1)} \\ \xi_3^{(1)} \end{pmatrix} \approx \begin{pmatrix} \zeta_1^{(1)}M + \zeta_3^{(1)}E \\ \zeta_2^{(1)}M \\ \zeta_3^{(1)}(M+P) + \zeta_1^{(1)}F \end{pmatrix} .$$

4.1.20 Polarized Gamma conversion into an electron–positron pair

Method

The polarized version of gamma conversion is based on the EM standard process *G4GammaConversion*. Mean free path and the distribution of explicitly generated final state particles are treated by this version. For details consult section [sec:em.conv].

The remaining task is to attribute polarization vectors to the generated final state leptons, which is discussed in the following.

Polarization transfer from the photon to the two leptons

Gamma conversion process is essentially the inverse process of Bremsstrahlung and the interaction matrix is obtained by inverting the rows and columns of the bremsstrahlung matrix and changing the sign of ϵ_2, cf. section [sec:pol.bremsstrahlung]. It follows from the work by Olsen and Maximon [polPair:Olsen_Maximon] that the polarization state $\xi^{(1)}$ of an electron or positron after pair production is obtained by

$$\begin{pmatrix} O \\ \boldsymbol{\xi}^{(1)} \end{pmatrix} = T_l^p \begin{pmatrix} 1 \\ \boldsymbol{\zeta}^{(1)} \end{pmatrix}$$

and

$$T_l^p \approx \begin{pmatrix} 1 & D & 0 & 0 \\ 0 & 0 & 0 & T \\ 0 & 0 & 0 & 0 \\ 0 & 0 & 0 & L \end{pmatrix} ,$$

where

$$I = (\epsilon_1^2 + \epsilon_2^2)(3 + 2\Gamma) + 2\epsilon_1\epsilon_2(1 + 4u^2\hat{\xi}^2\Gamma) \quad (4.96)$$

$$D = \left\{-8\epsilon_1\epsilon_2 u^2\hat{\xi}^2\Gamma\right\}/I \quad (4.97)$$

$$T = \left\{-4k\epsilon_2\hat{\xi}(1 - 2\hat{\xi})u\Gamma\right\}/I \quad (4.98)$$

$$L = k\{(\epsilon_1 - \epsilon_2)(3 + 2\Gamma) + 2\epsilon_2(1 + 4u^2\hat{\xi}^2\Gamma)\}/I \quad (4.99)$$

and

Coulomb and screening effects are contained in Γ, defined in section [sec:pol.bremsstrahlung].

Using Eq. ([eq:conv_lepton]) and the transfer matrix given by Eq. ([eq:matrix_conv]) the polarization state of the produced $e^-(e^+)$ is given in the Stokes formalism by:

$$\xi^{(1)} = \begin{pmatrix} \xi_1^{(1)} \\ \xi_2^{(1)} \\ \xi_3^{(1)} \end{pmatrix} \approx \begin{pmatrix} \zeta_3^{(1)} T \\ 0 \\ \zeta_3^{(1)} L \end{pmatrix}$$

4.1.21 Polarized Photoelectric Effect

Method

This section describes the basic formulas of polarization transfer in the photoelectric effect class (*G4PolarizedPhotoElectricEffect*). The photoelectric effect is the emission of electrons from matter upon the absorption of electromagnetic radiation, such as ultraviolet radiation or x-rays. The energy of the photon is completely absorbed by the electron and, if sufficient, the electron can escape from the material with a finite kinetic energy. A single photon can only eject a single electron, as the energy of one photon is only absorbed by one electron. The electrons that are emitted are often called photoelectrons. If the photon energy is higher than the binding energy the remaining energy is transferred to the electron as a kinetic energy

$$E_{kin}^{e^-} = k - B_{shell}$$

In Geant4 the photoelectric effect process is taken into account if:

$$k > B_{shell}$$

Where k is the incoming photon energy and B_{shell} the electron binding energy provided by the class *G4AtomicShells*.

The polarized version of the photoelectric effect is based on the EM standard process *G4PhotoElectricEffect*. Mean free path and the distribution of explicitly generated final state particles are treated by this version. For details consult section [sec:em.pee].

The remaining task is to attribute polarization vectors to the generated final state electron, which is discussed in the following.

Polarization transfer

The polarization state of an incoming polarized photon is described by the Stokes vector $\vec{\zeta}^{(1)}$. The polarization transfer to the photoelectron can be described in the Stokes formalism using the same approach as for the Bremsstrahlung and gamma conversion processes, cf. [sec:pol.bremsstrahlung] and [sec:pol.conv]. The relation between the photoelectron's Stokes parameters and the incoming photon's Stokes parameters is described by the interaction matrix T_l^p derived from H. Olsen [polPEE:H.Olsen.Kgl] and reviewed by H.W McMaster [polPEE:McMaster2]:

$$\begin{pmatrix} I' \\ \vec{\xi}^{(1)} \end{pmatrix} = T_l^p \begin{pmatrix} I_0 \\ \vec{\zeta}^{(1)} \end{pmatrix}$$

In general, for the photoelectric effect as a two-body scattering, the cross section should be correlated with the spin states of the incoming photon and the target electron. In our implementation the target electron is not polarized and only the polarization transfer from the photon to the photoelectron is taken into account. In this case the cross section of the process remains polarization independent. To compute the matrix elements we take advantage of the available kinematic variables provided by the generic *G4PhotoelectricEffect* class. To compute the photoelectron spin state (Stokes parameters), four main parameters are needed:

- The incoming photon Stokes vector $\vec{\zeta}^{(1)}$
- The incoming photon's energy k.
- the photoelectron's kinetic energy $E^{e^-}_{kin}$ or the Lorentz factors β and γ.
- The photoelectron's polar angle θ or $\cos\theta$.

The interaction matrix derived by H. Olsen [polPEE:H.Olsen.Kgl] is given by:

$$T^P_l = \begin{pmatrix} 1+D & -D & 0 & 0 \\ 0 & 0 & 0 & B \\ 0 & 0 & 0 & 0 \\ 0 & 0 & 0 & A \end{pmatrix}$$

Where

$$D = \frac{1}{k}\left[\frac{2}{k\epsilon(1-\beta\cos\theta)} - 1\right] \tag{4.100}$$

$$A = \frac{\epsilon}{\epsilon+1}\left[\frac{2}{k\epsilon} + \beta\cos\theta + \frac{2}{k\epsilon^2(1-\beta\cos\theta)}\right] \tag{4.101}$$

$$B = \frac{\epsilon}{\epsilon+1}\beta\sin\theta\left[\frac{2}{k\epsilon(1-\beta\cos\theta)} - 1\right] \tag{4.102}$$

Using Eq. ([eq:photo_lepton]) and the transfer matrix given by Eq. ([eq:matrix_photo]) the polarization state of the produced e^- is given in the Stokes formalism by:

$$\vec{\xi}^{(1)} = \begin{pmatrix} \xi^{(1)}_1 \\ \xi^{(1)}_2 \\ \xi^{(1)}_3 \end{pmatrix} = \begin{pmatrix} \zeta^{(1)}_3 B \\ 0 \\ \zeta^{(1)}_3 A \end{pmatrix}$$

From equation ([eq:final_stat]) one can see that a longitudinally (transversally) polarized photoelectron can only be produced if the incoming photon is circularly polarized.

4.1.22 Photoabsorption Cross Section at Low Energies

The photoabsorption cross section, $\sigma_\gamma(\omega)$, where ω is the photon energy, is used in Geant4 for the description of the photo-electric effect, X-ray transportation and ionization effects in very thin absorbers. As mentioned in the discussion of photoabsorption ionization (see section [secpai]), it is convenient to represent the cross section as a polynomial in ω^{-1} [sandia.bigg] :

$$\sigma_\gamma(\omega) = \sum_{k=1}^{4} a^{(i)}_k \omega^{-k}.$$

Using cross sections from the original Sandia data tables, calculations of primary ionization and energy loss distributions produced by relativistic charged particles in gaseous detectors show clear disagreement with experimental data, especially for gas mixtures which include xenon. Therefore a special investigation was performed [sandia.grich] by fitting the coefficients $a^{(i)}_k$ to modern data from synchrotron radiation experiments in the energy range of $10 - 50\,eV$. The fits were performed for elements typically used in detector gas mixtures: hydrogen, fluorine, carbon, nitrogen and oxygen. Parameters for these elements were extracted from data on molecular gases such as N_2, O_2, CO_2, CH_4, and CF_4 [sandia.lee73][sandia.lee77]. Parameters for the noble gases were found using data given in the tables [sandia.marr][sandia.west].

4.1.23 Single Scattering

Single elastic scattering process is an alternative to the multiple scattering process. The advantage of the single scattering process is in possibility of usage of theory based cross sections, in contrary to the Geant4 multiple scattering model [singscat.urban], which uses a number of phenomenological approximations on top of Lewis theory. The process $G4CoulombScattering$ was created for simulation of single scattering of muons, it also applicable with some physical limitations to electrons, muons and ions. Because each of elastic collisions are simulated the number of steps of charged particles significantly increasing in comparison with the multiple scattering approach, correspondingly its CPU performance is pure. However, in low-density media (vacuum, low-density gas) multiple scattering may provide wrong results and single scattering processes is more adequate.

Coulomb Scattering

The single scattering model of Wentzel [singscat.wentzel] is used in many multiple scattering models including the Penelope code *[3]*. The Wentzel model for describing elastic scattering of particles with charge ze ($z = -1$ for electron) by atomic nucleus with atomic number Z is based on simplified scattering potential

$$V(r) = \frac{zZe^2}{r} exp(-r/R),$$

where the exponential factor tries to reproduce the effect of screening. The parameter R is a screening radius [singscat.bethe]

$$R = 0.885 Z^{-1/3} r_B,$$

where r_B is the Bohr radius. In the first Born approximation the elastic scattering cross section $\sigma^(W)$ can be obtained as

$$\frac{d\sigma^{(W)}(\theta)}{d\Omega} = \frac{(ze^2)^2}{(p\beta c)^2} \frac{Z(Z+1)}{(2A+1-cos\theta)^2},$$

where p is the momentum and β is the velocity of the projectile particle. The screening parameter A according to Moliere and Bethe [singscat.bethe]

$$A = \left(\frac{\hbar}{2pR}\right)^2 (1.13 + 3.76(\alpha Z/\beta)^2),$$

where α is a fine structure constant and the factor in brackets is used to take into account second order corrections to the first Born approximation. The total elastic cross section σ can be expressed via Wentzel cross section ([singscat.a2])

$$\frac{d\sigma(\theta)}{d\Omega} = \frac{d\sigma^{(W)}(\theta)}{d\Omega} \left(\frac{Z}{(1+\frac{(qR_N)^2}{12})^2} + 1\right) \frac{1}{Z+1},$$

where q is momentum transfer to the nucleus, R_N is nuclear radius. This term takes into account nuclear size effect [singscat.kokoulin], the second term takes into account scattering off electrons. The results of simulation with the single scattering model (Fig.[plot:Alumin]) are competitive with the results of the multiple scattering.

Implementation Details

The total cross section of the process is obtained as a result of integration of the differential cross section ([singscat.a4]). The first term of this cross section is integrated in the interval $(0, \pi)$. The second term in the smaller interval $(0, \theta_m)$, where θ_m is the maximum scattering angle off electrons, which is determined using the cut value for the delta electron production. Before sampling of angular distribution the random choice is performed between scattering off the nucleus and off electrons.

4.1.24 Synchrotron Radiation

Synchrotron radiation photons are produced when ultra-relativistic electrons travel along an approximately circular path. In the following treatment, the magnetic field is assumed to be constant and uniform, and the radius of curvature of the electron is assumed to be constant over its trajectory.

Spectral and Angular Distributions of Synchrotron Radiation

The spectral distribution of the mean number of synchrotron radiation photons, $d\bar{N}/d\omega$, produced by an ultra-relativistic electron along a circular trajectory of length L, can be expressed in terms of the mean energy loss spectrum $d\bar{\Delta}/d\omega$ [synch.maier]:

$$\frac{d\bar{N}}{d\omega} = \frac{1}{\omega}\frac{d\bar{\Delta}}{d\omega} = \frac{\sqrt{3}}{2\pi}\alpha\left(\frac{L\gamma}{R}\right)\frac{1}{\omega_c}\int_{\omega/\omega_c}^{\infty} K_{5/3}(\eta)d\eta.$$

Here,

ω	photon energy	(4.103)
α	fine structure constant	(4.104)
R	instantaneous radius of curvature of the trajectory	(4.105)
K	Macdonald function	(4.106)
$\omega_c = 1.5\beta(\hbar c/R)\gamma^3$	characteristic energy of synchrotron radiation.	(4.107)
		(4.108)

β is the ratio of the electron velocity v to c, $\gamma = 1/\sqrt{1-\beta^2}$, and η is an arbitrary integration variable. In the SI system of units: $R(m) = P(GeV/c)/0.3B_{\perp}(T)$, where $B_{\perp}$ is the component of magnetic flux density perpendicular to the electron velocity, and P is the electron momentum.

In order to simulate the energy spectrum of synchrotron radiation using the Monte Carlo method, $\bar{N}_{>\omega}$, the mean number of photons above a given energy ω, must be determined. This is done by integrating Eq. [synch.a] over energy, after first transforming $d\bar{N}/d\omega$ by using the integral representation of the Macdonald function [synch.abram]:

$$\begin{aligned}\bar{N}_{>\omega} &= \int_{\omega}^{\infty}\frac{d\bar{N}}{d\omega'}d\omega' \\ &= \frac{\sqrt{3}}{2\pi}\alpha\left(\frac{L\gamma}{R}\right)\int_0^{\infty}\frac{\cosh\left(\frac{5}{3}t\right)}{\cosh^2(t)}\exp\left[-\frac{\omega}{\omega_c}\cosh(t)\right]dt.\end{aligned} \tag{4.109}$$

Here, t is also an arbitrary integration variable. The latter integral is calculated numerically by the quadrature Laguerre formula *[1]*. Calculations indicate that about 50 roots of the Laguerre polynomials are required in order for the accuracy of the integral estimation to be better than 10^{-4} [synch.bag].

The Monte Carlo method also requires the mean number of synchrotron radiation photons at all energies, $\bar{N}$ (= $\bar{N}_{>0}$), in order to determine the next occurrence of synchrotron radiation along a trajectory, and to normalize the spectral distribution of the radiation. Setting $\omega = 0$ in Eq. [synch.b] yields

$$\begin{aligned}\bar{N} = \bar{N}_{>0} &= \frac{\sqrt{3}}{2\pi}\alpha\left(\frac{L\gamma}{R}\right)\int_0^{\infty}\frac{\cosh\left(\frac{5}{3}t\right)}{\cosh^2(t)}dt \\ &= \frac{5}{2\sqrt{3}}\alpha\left(\frac{L\gamma}{R}\right) \approx 10^{-2}\left(\frac{L\gamma}{R}\right).\end{aligned} \tag{4.110}$$

Qualitatively this result can be manipulated using the fact that the mean number of photons produced along the formation zone length $z \approx R/\gamma$ is proportional to α. Then for length L, $\bar{N} \approx \alpha L/(R/\gamma)$. Note that when $\gamma \gg 1$, and $R \sim \gamma$, $\bar{N}$ does not depend on the electron energy but is defined by the values of L and $B_{\perp}$ only. Instead, it is the mean

energy loss due to synchrotron radiation $\bar{\Delta}$, corresponding to a trajectory of length L, that displays the characteristic relativistic rise:

$$\bar{\Delta} = \int_0^\infty \omega \frac{d\bar{N}}{d\omega} d\omega = \frac{2}{3}\alpha\hbar c \left(\frac{L\gamma^2}{R^2}\right)\beta\gamma^2 = \frac{8\bar{N}}{15\sqrt{3}}\omega_c \approx 0.31\bar{N}\omega_c \sim \gamma^2.$$

The angular distribution of synchrotron radiation produced by ultra-relativistic electrons shows a clear 'searchlight' effect. Most of the photons are radiated within an angular range of order $1/\gamma$ centered on the electron trajectory direction. In the interesting region of $\gamma > 10^3$ the angular resolution of X-ray and gamma detectors usually does not allow the details of the angular distribution to be measured. Therefore, the angular distribution is set to be flat in the range $0 - 1/\gamma$.

Simulating Synchrotron Radiation

The distance x along the electron/positron trajectory to the next occurrence of a synchrotron radiation photon is simulated according to the exponential distribution, $exp(-x\bar{N}/L)$. The energy ω of the photon is simulated according to the distribution $\bar{N}_{>\omega}/\bar{N}$. The direction of the photon (θ, φ) is generated relative to the local z-axis which is taken to be along the instantaneous direction of the electron. θ and φ are distributed randomly in the ranges [0, $1/\gamma$] and [0, 2π], respectively.

4.1.25 MuPGen

Gamma Conversion into $\mu^+\mu^-$ Pair

The class *G4GammaConversionToMuons* simulates the process of gamma conversion into muon pairs. Given the photon energy and Z and A of the material in which the photon converts, the probability for the conversions to take place is calculated according to a parameterized total cross section. Next, the sharing of the photon energy between the μ^+ and μ^- is determined. Finally, the directions of the muons are generated. Details of the implementation are given below and can be also found in:cite:*MuPgen*.

Cross Section and Energy Sharing

Muon pair production on atomic electrons, $\gamma + e \to e + \mu^+ + \mu^-$, has a threshold of $2m_\mu(m_\mu + m_e)/m_e \approx 43.9$ GeV . Up to several hundred GeV this process has a much lower cross section than the corresponding process on the nucleus. At higher energies, the cross section on atomic electrons represents a correction of $\sim 1/Z$ to the total cross section.

For the approximately elastic scattering considered here, momentum, but no energy, is transferred to the nucleon. The photon energy is fully shared by the two muons according to

$$E_\gamma = E_\mu^+ + E_\mu^-$$

or in terms of energy fractions

$$x_+ = \frac{E_\mu^+}{E_\gamma}, \qquad x_- = \frac{E_\mu^-}{E_\gamma}, \qquad x_+ + x_- = 1\ .$$

The differential cross section for electromagnetic pair creation of muons in terms of the energy fractions of the muons is

$$\frac{d\sigma}{dx_+} = 4\,\alpha\,Z^2\,r_c^2\left(1 - \frac{4}{3}\,x_+x_-\right)\log(W)\ ,$$

where Z is the charge of the nucleus, r_c is the classical radius of the particles which are pair produced (here muons) and

$$W = W_\infty \, \frac{1 + (D_n\sqrt{e} - 2)\,\delta\,/m_\mu}{1 + B\,Z^{-1/3}\,\sqrt{e}\,\delta\,/m_e}$$

where

$$W_\infty = \frac{B\,Z^{-1/3}}{D_n}\,\frac{m_\mu}{m_e} \qquad \delta = \frac{m_\mu^2}{2\,E_\gamma\,x_+x_-} \qquad \sqrt{e} = 1.6487\ldots.$$

$$\begin{array}{rrr} \text{For hydrogen} & B = 202.4 & D_n = 1.49 \\ \text{and for all other nuclei} & B = 183 & D_n = 1.54\,A^{0.27}. \end{array}$$

These formulae are obtained from the differential cross section for muon bremsstrahlung *[1]* by means of crossing relations. The formulae take into account the screening of the field of the nucleus by the atomic electrons in the Thomas-Fermi model, as well as the finite size of the nucleus, which is essential for the problem under consideration. The above parameterization gives good results for $E_\gamma \gg m_\mu$. The fact that it is approximate close to threshold is of little practical importance. Close to threshold, the cross section is small and the few low energy muons produced will not travel very far. The cross section calculated from Eq.([eq:dSigxPlus]) is positive for $E_\gamma > 4m_\mu$ and

$$x_{\min} \le x \le x_{\max} \quad \text{with} \quad x_{\min} = \frac{1}{2} - \sqrt{\frac{1}{4} - \frac{m_\mu}{E_\gamma}} \qquad x_{\max} = \frac{1}{2} + \sqrt{\frac{1}{4} - \frac{m_\mu}{E_\gamma}}\,,$$

except for very asymmetric pair-production, close to threshold, which can easily be taken care of by explicitly setting $\sigma = 0$ whenever $\sigma < 0$.

Note that the differential cross section is symmetric in x_+ and x_- and that

$$x_+x_- = x - x^2$$

where x stands for either x_+ or x_-. By defining a constant

$$\sigma_0 = 4\,\alpha\,Z^2\,r_c^2\log(W_\infty)$$

the differential cross section Eq.([eq:dSigxPlus]) can be rewritten as a normalized and symmetric as function of x:

$$\frac{1}{\sigma_0}\,\frac{d\sigma}{dx} = \left[1 - \frac{4}{3}\,(x - x^2)\right]\,\frac{\log W}{\log W_\infty}\,.$$

This is shown in Fig.[plot:dsigdx] for several elements and a wide range of photon energies. The asymptotic differential cross section for $E_\gamma \to \infty$

$$\frac{1}{\sigma_0}\,\frac{d\sigma_\infty}{dx} = 1 - \frac{4}{3}\,(x - x^2)$$

is also shown.

Parameterization of the Total Cross Section

The total cross section is obtained by integration of the differential cross section Eq.([eq:dSigxPlus]), that is

$$\sigma_{\rm tot}(E_\gamma) = \int_{x_{\min}}^{x_{\max}} \frac{d\sigma}{dx_+}\,dx_+ = 4\,\alpha\,Z^2\,r_c^2\,\int_{x_{\min}}^{x_{\max}} \left(1 - \frac{4}{3}\,x_+x_-\right)\log(W)\,dx_+\,.$$

W is a function of (x_+, E_γ) and (Z, A) of the element (see Eq.([eq:W])). Numerical values of W are given in Table[tab:W].

E_γ	W for H	W for Be	W for Cu	W for Pb
GeV				
1	2.11	1.594	1.3505	5.212
10	19.4	10.85	6.803	43.53
100	191.5	102.3	60.10	332.7
1000	1803	919.3	493.3	1476.1
10000	11427	4671	1824	1028.1
∞	28087	8549	2607	1339.8

Table: Numerical values of W for $x_+ = 0.5$ for different elements.

Values of the total cross section obtained by numerical integration are listed in Table[tab:sigmatot] for four different elements. Units are in μbarn , where $1\,\mu\text{barn} = 10^{-34}\,\text{m}^2$.

E_γ	σ_{tot}, H	σ_{tot}, Be	σ_{tot}, Cu	σ_{tot}, Pb
GeV	μbarn	μbarn	μbarn	μbarn
1	0.01559	0.1515	5.047	30.22
10	0.09720	1.209	49.56	334.6
100	0.1921	2.660	121.7	886.4
1000	0.2873	4.155	197.6	1476
10000	0.3715	5.392	253.7	1880
∞	0.4319	6.108	279.0	2042

Table: Numerical values for the total cross section

Well above threshold, the total cross section rises about linearly in $\log(E_\gamma)$ with the slope

$$W_M = \frac{1}{4\,D_n\,\sqrt{e}\,m_\mu}$$

until it saturates due to screening at σ_∞. Fig.[plot:SigTot] shows the normalized cross section where

$$\sigma_\infty = \frac{7}{9}\,\sigma_0 \qquad \text{and} \qquad \sigma_0 = 4\,\alpha\,Z^2\,r_c^2\,\log(W_\infty)\ .$$

Numerical values of W_M are listed in Table[tab:WM].

Table: Numerical values of W_M.

The total cross section can be parameterized as

$$\sigma_{\text{par}} = \frac{28\,\alpha\,Z^2\,r_c^2}{9}\ \log(1 + W_M C_f E_g)\ ,$$

with

$$E_g = \left(1 - \frac{4m_\mu}{E_\gamma}\right)^t \left(W_{\text{sat}}^s + E_\gamma^s\right)^{1/s}\ .$$

and

$$W_{\text{sat}} = \frac{W_\infty}{W_M} = B\,Z^{-1/3}\,\frac{4\,\sqrt{e}\,m_\mu^2}{m_e}\ .$$

The threshold behavior in the cross section was found to be well approximated by $t = 1.479 + 0.00799 D_n$ and the saturation by $s = -0.88$. The agreement at lower energies is improved using an empirical correction factor, applied to the slope W_M, of the form

$$C_f = \left[1 + 0.04\log\left(1 + \frac{E_c}{E_\gamma}\right)\right]\ ,$$

where

$$E_c = \left[-18. + \frac{4347.}{B\,Z^{-1/3}}\right]\ \mathrm{GeV}\ .$$

A comparison of the parameterized cross section with the numerical integration of the exact cross section shows that the accuracy of the parametrization is better than 2%, as seen in Fig.[plot:SigApRat].

Multi-differential Cross Section and Angular Variables

The angular distributions are based on the multi-differential cross section for lepton pair production in the field of the Coulomb center

$$\frac{d\sigma}{dx_+\,du_+\,du_-\,d\varphi} = \frac{4\,Z^2\alpha^3}{\pi}\,\frac{m_\mu^2}{q^4}\,u_+\,u_-$$
$$\left\{\frac{u_+^2+u_-^2}{(1+u_+^2)\,(1+u_-^2)} - 2x_+x_-\right.$$
$$\left.\left[\frac{u_+^2}{(1+u_+^2)^2}+\frac{u_-^2}{(1+u_-^2)^2}\right] - \frac{2u_+u_-(1-2x_+x_-)\,\cos\varphi}{(1+u_+^2)\,(1+u_-^2)}\right\}\ .$$

Here

$$u_\pm = \gamma_\pm\theta_\pm \quad , \qquad \gamma_\pm = \frac{E_\mu^\pm}{m_\mu} \quad , \qquad q^2 = q_\parallel^2 + q_\perp^2 \quad ,$$

where

$$q_\parallel^2 = q_{\min}^2\,(1 + x_-u_+^2 + x_+u_-^2)^2\,,$$
$$q_\perp^2 = m_\mu^2\left[(u_+-u_-)^2 + 2\,u_+u_-(1-\cos\varphi)\right]\ .$$

q^2 is the square of the momentum $\mathbf{q}$ transferred to the target and $q_\parallel^2$ and $q_\perp^2$ are the squares of the components of the vector $\mathbf{q}$, which are parallel and perpendicular to the initial photon momentum, respectively. The minimum momentum transfer is $q_{\min} = m_\mu^2/(2E_\gamma\,x_+x_-)$. The muon vectors have the components

$$\begin{aligned}\mathbf{p}_+ &= p_+\,(\ \sin\theta_+\cos(\varphi_0+\varphi/2)\,,\quad \sin\theta_+\sin(\varphi_0+\varphi/2)\,,\ \cos\theta_+)\,,\\ \mathbf{p}_- &= p_-\,(-\sin\theta_-\cos(\varphi_0-\varphi/2)\,,\ -\sin\theta_-\sin(\varphi_0-\varphi/2)\,,\ \cos\theta_-)\,,\end{aligned}$$

where $p_\pm = \sqrt{E_\pm^2 - m_\mu^2}$. The initial photon direction is taken as the z-axis. The cross section of Eq.([eq:MultiDiff]) does not depend on φ_0. Because of azimuthal symmetry, φ_0 can simply be sampled at random in the interval $(0,\,2\,\pi)$.

Eq.([eq:MultiDiff]) is too complicated for efficient Monte Carlo generation. To simplify, the cross section is rewritten to be symmetric in u_+, u_- using a new variable u and small parameters ξ, β, where $u_\pm = u \pm \xi/2$ and $\beta = u\,\varphi$. When higher powers in small parameters are dropped, the differential cross section in terms of u, ξ, β becomes

$$\frac{d\sigma}{dx_+\,d\xi\,d\beta\,u du} = \frac{4\,Z^2\alpha^3}{\pi}\,\frac{m_\mu^2}{\left(q_\parallel^2 + m_\mu^2(\xi^2+\beta^2)\right)^2}$$
$$\left\{\xi^2\left[\frac{1}{(1+u^2)^2} - 2\,x_+x_-\,\frac{(1-u^2)^2}{(1+u^2)^4}\right] + \frac{\beta^2(1-2x_+x_-)}{(1+u^2)^2}\right\}\,,$$

where, in this approximation,

$$q_\parallel^2 = q_{\min}^2\,(1+u^2)^2\,.$$

For Monte Carlo generation, it is convenient to replace (ξ, β) by the polar coordinates (ρ, ψ) with $\xi = \rho \cos\psi$ and $\beta = \rho \sin\psi$. Integrating Eq. [eq:MultiDiff2] over ψ and using symbolically du^2 where $du^2 = 2u\,du$ yields

$$\frac{d\sigma}{dx_+\,d\rho\,du^2} = \frac{4Z^2\alpha^3}{m_\mu^2}\,\frac{\rho^3}{(q_\parallel^2/m_\mu^2+\rho^2)^2}\,\left\{\frac{1-x_+x_-}{(1+u^2)^2} - \frac{x_+x_-(1-u^2)^2}{(1+u^2)^4}\right\}.$$

Integration with logarithmic accuracy over ρ gives

$$\int \frac{\rho^3\,d\rho}{(q_\parallel^2/m_\mu^2+\rho^2)^2} \approx \int\limits_{q_\parallel/m_\mu}^{1} \frac{d\rho}{\rho} = \log\left(\frac{m_\mu}{q_\parallel}\right).$$

Within the logarithmic accuracy, $\log(m_\mu/q_\parallel)$ can be replaced by $\log(m_\mu/q_{\min})$, so that

$$\frac{d\sigma}{dx_+\,du^2} = \frac{4\,Z^2\alpha^3}{m_\mu^2}\,\left\{\frac{1-x_+x_-}{(1+u^2)^2} - \frac{x_+x_-(1-u^2)^2}{(1+u^2)^4}\right\}\,\log\left(\frac{m_\mu}{q_{\min}}\right).$$

Making the substitution $u^2 = 1/t - 1$, $du^2 = -dt\,/t^2$ gives

$$\frac{d\sigma}{dx_+\,dt} = \frac{4\,Z^2\alpha^3}{m_\mu^2}\,\left[1 - 2\,x_+x_- + 4\,x_+x_-t\,(1-t)\right]\,\log\left(\frac{m_\mu}{q_{\min}}\right).$$

Atomic screening and the finite nuclear radius may be taken into account by multiplying the differential cross section determined by Eq.([eq:MultiDiff2]) with the factor

$$\left(F_a(q) - F_n(q)\right)^2,$$

where F_a and F_n are atomic and nuclear form factors. Please note that after integrating Eq. [mupgen.b] over ρ, the q-dependence is lost.

Procedure for the Generation of $\mu^+\mu^-$ Pairs

Given the photon energy E_γ and Z and A of the material in which the γ converts, the probability for the conversions to take place is calculated according to the parametrized total cross section Eq.([eq:sigpar]). The next step, determining how the photon energy is shared between the μ^+ and μ^-, is done by generating x_+ according to Eq.([eq:dSigxPlus]). The directions of the muons are then generated via the auxilliary variables t, ρ, ψ. In more detail, the final state is generated by the following five steps, in which $R_{1,2,3,4,\ldots}$ are random numbers with a flat distribution in the interval [0,1]. The generation proceeds as follows. **1)** Sampling of the positive muon energy $E_\mu^+ = x_+\,E_\gamma$. This is done using the rejection technique. x_+ is first sampled from a flat distribution within kinematic limits using

$$x_+ = x_{\min} + R_1(x_{\max} - x_{\min})$$

and then brought to the shape of Eq.([eq:dSigxPlus]) by keeping all x_+ which satisfy

$$\left(1 - \frac{4}{3}\,x_+x_-\right)\,\frac{\log(W)}{\log(W_{\max})} < R_2\,.$$

Here $W_{\max} = W(x_+ = 1/2)$ is the maximum value of W, obtained for symmetric pair production at $x_+ = 1/2$. About 60% of the events are kept in this step. Results of a Monte Carlo generation of x_+ are illustrated in Fig.[plot:xPlusGen]. The shape of the histograms agrees with the differential cross section illustrated in Fig.[plot:dsigdx].

2) Generate $t(=\frac{1}{\gamma^2\theta^2+1})$. The distribution in t is obtained from Eq.([eq:sigmadxdt]) as

$$f_1(t)\,dt = \frac{1 - 2\,x_+x_- + 4\,x_+x_-t\,(1-t)}{1 + C_1/t^2}\,dt\,, \quad 0 < t \le 1\,.$$

with form factors taken into account by

$$C_1 = \frac{(0.35\,A^{0.27})^2}{x_+x_-\,E_\gamma/m_\mu}\,.$$

In the interval considered, the function $f_1(t)$ will always be bounded from above by

$$\max[f_1(t)] = \frac{1 - x_+x_-}{1 + C_1}\ .$$

For small x_+ and large E_γ, $f_1(t)$ approaches unity, as shown in Fig.[f1t.eps].

The function $f_1(t)$ at $E_\gamma = 10\,\mathrm{GeV}$ (left) and $E_\gamma = 1\,\mathrm{TeV}$ (right) in beryllium for different values of x_+.**||The function :math:‘\(f_1(t)\)‘ at :math:‘\(E_\gamma = 10\,{\rm GeV}\)‘ (left) and :math:‘\(E_\gamma = 1\,{\rm TeV}\)‘ (right) in beryllium for different values of :math:‘\(x_+\)‘.|**

The Monte Carlo generation is done using the rejection technique. About 70% of the generated numbers are kept in this step. Generated t-distributions are shown in Fig.[f1t_gen.eps]. **3)** Generate ψ by the rejection technique using t generated in the previous step for the frequency distribution

$$f_2(\psi) = \Big[1 - 2\,x_+x_- + 4\,x_+x_-t\,(1-t)\,(1+\cos(2\psi))\Big]\ , \qquad 0 \le \psi \le 2\pi\,.$$

The maximum of $f_2(\psi)$ is

$$\max[f_2(\psi)] = 1 - 2\,x_+x_-\,[1 - 4\,t\,(1-t)]\ .$$

Generated distributions in ψ are shown in Fig.[plot:PsiGen.eps]. **4)** Generate ρ. The distribution in ρ has the form

$$f_3(\rho)\,d\rho = \frac{\rho^3\,d\rho}{\rho^4 + C_2}\,, \quad 0 \le \rho \le \rho_{\max}\,,$$

where

$$\rho^2_{\max} = \frac{1.9}{A^{0.27}}\,\left(\frac{1}{t} - 1\right),$$

and

$$C_2 = \frac{4}{\sqrt{x_+x_-}}\left[\left(\frac{m_\mu}{2E_\gamma x_+x_-\,t}\right)^2 + \left(\frac{m_e}{183\,Z^{-1/3}\,m_\mu}\right)^2\right]^2\ .$$

The ρ distribution is obtained by a direct transformation applied to uniform random numbers R_i according to

$$\rho = [C_2(\exp(\beta\,R_i) - 1)]^{1/4}\ ,$$

where

$$\beta = \log\left(\frac{C_2 + \rho^4_{\max}}{C_2}\right)\ .$$

Generated distributions of ρ are shown in Fig.[plot:rho.eps]

5) Calculate θ_+, θ_- and φ from t, ρ, ψ with

$$\gamma_\pm = \frac{E^\pm_\mu}{m_\mu} \qquad \text{and} \qquad u = \sqrt{\frac{1}{t} - 1}\,.$$

according to

$$\theta_+ = \frac{1}{\gamma_+}\left(u + \frac{\rho}{2}\,\cos\psi\right)\,, \quad \theta_- = \frac{1}{\gamma_-}\left(u - \frac{\rho}{2}\,\cos\psi\right) \quad \text{and} \quad \varphi = \frac{\rho}{u}\,\sin\psi\,.$$

The muon vectors can now be constructed from Eq.([eq:pvec]), where φ_0 is chosen randomly between 0 and 2π. Fig.[plot:thetaPlus] shows distributions of θ_+ at different photon energies (in beryllium). The spectra peak around $1/\gamma$ as expected.

The most probable values are $\theta_+ \sim m_\mu/E_\mu^+ = 1/\gamma_+$. In the small angle approximation used here, the values of θ_+ and θ_- can in principle be any positive value from 0 to ∞. In the simulation, this may lead (with a very small probability, of the order of m_μ/E_γ) to unphysical events in which θ_+ or θ_- is greater than π. To avoid this, a limiting angle $\theta_{\rm cut} = \pi$ is introduced, and the angular sampling repeated, whenever $\max(\theta_+, \theta_-) > \theta_{\rm cut}$.

Figs.[plot:Fig1],[plot:Fig2] and [plot:Fig3] show distributions of the simulated angular characteristics of muon pairs in comparison with results of exact calculations. The latter were obtained by means of numerical integration of the squared matrix elements with respective nuclear and atomic form factors. All these calculations were made for iron, with $E_\gamma = 10\,\mathrm{GeV}$ and $x_+ = 0.3$. As seen from Fig.[plot:Fig1], wide angle pairs (at low values of the argument in the figure) are suppressed in comparison with the Coulomb center approximation. This is due to the influence of the finite nuclear size which is comparable to the inverse mass of the muon. Typical angles of particle emission are of the order of $1/\gamma_\pm = m_\mu/E_\mu^\pm$ (Fig.[plot:Fig2]). Fig.[plot:Fig3] illustrates the influence of the momentum transferred to the target on the angular characteristics of the produced pair. In the frame of the often used model which neglects target recoil, the pair particles would be symmetric in transverse momenta, and coplanar with the initial photon.

4.2 Low Energy

4.2.1 Bremsstrahlung

The class G4LivermoreBremsstrahlungModel calculates the continuous energy loss due to low energy gamma emission and simulates the gamma production by electrons. The gamma production threshold for a given material ω_c is used to separate the continuous and the discrete parts of the process. The energy loss of an electron with the incident energy T are expressed via the integrand over energy of the gammas:

$$\frac{dE}{dx} = \sigma(T)\frac{\int_{0.1eV}^{\omega_c} t\frac{d\sigma}{d\omega}d\omega}{\int_{0.1eV}^{T}\frac{d\sigma}{d\omega}d\omega},$$

where $\sigma(T)$ is the total cross-section at a given incident kinetic energy, T, $0.1eV$ is the low energy limit of the EEDL data. The production cross-section is a complimentary function:

$$\sigma = \sigma(T)\frac{\int_{\omega_c}^{T}\frac{d\sigma}{d\omega}d\omega}{\int_{0.1eV}^{T}\frac{d\sigma}{d\omega}d\omega}.$$

The total cross-section, σ_s, is obtained from an interpolation of the evaluated cross-section data in the EEDL library *[1]*, according to the formula ([eqloglog]) in Section [subsubsigmatot].

The EEDL data *[2]* of total cross-sections are parametrised *[1]* according to ([eqloglog]). The probability of the emission of a photon with energy, ω, considering an electron of incident kinetic energy, T, is generated according to the formula:

$$\frac{d\sigma}{d\omega} = \frac{F(x)}{x}, \quad \text{with} x = \frac{\omega}{T}.$$

The function, $F(x)$, describing energy spectra of the outcoming photons is taken from the EEDL library. For each element 15 points in x from 0.01 to 1 are used for the linear interpolation of this function. The function F is normalised by the condition $F(0.01) = 1$. The energy distributions of the emitted photons available in the EEDL library are for only a few incident electron energies (about 10 energy points between 10 eV and 100 GeV). For other energies a logarithmic interpolation formula ([eqloglog]) is used to obtain values for the function, $F(x)$. For high energies, the spectral function is very close to:

$$F(x) = 1 - x + 0.75x^2.$$

Bremsstrahlung angular distributions

The angular distribution of the emitted photons with respect to the incident electron can be sampled according to three alternative generators described below. The direction of the outcoming electron is determined from the energy-momentum balance. This generators are currently implemented in G4ModifiedTsai, G4Generator2BS and G4Generator2BN classes.

G4ModifiedTsai

The angular distribution of the emitted photons is obtained from a simplified *[1]* formula based on the Tsai cross-section *[1][2]*, which is expected to become isotropic in the low energy limit.

G4Generator2BS

In G4Generator2BS generator, the angular distribution of the emitted photons is obtained from the 2BS Koch and Motz bremsstrahlung double differential cross-section *[1]*:

$$d\sigma_{k,\theta} = \frac{4Z^2 r_0^2}{137}\frac{dk}{k} y dy \left\{ \frac{16y^2 E}{(y^2+1)^4 E_0} - \frac{(E_0+E)^2}{(y^2+1)^2 E_0^2} + \left[\frac{E_0^2+E^2}{(y^2+1)^2 E_0^2} - \frac{4y^2 E}{(y^2+1)^4 E_0} \right] lnM(y) \right\}$$

where k the photon energy, θ the emission angle, E_0 and E are the initial and final electron energy in units of $m_e c^2$, r_0 is the classical electron radius and Z the atomic number of the material. y and $M(y)$ are defined as:

$$y = \frac{E_0 \theta}{}$$

$$\frac{1}{M(y)} = \left(\frac{k}{2E_0 E}\right)^2 + \left(\frac{Z^{1/3}}{111(y^2+1)}\right)^2$$

The adopted sampling algorithm is based on the sampling scheme developed by A. F. Bielajew et al. *[7]*, and latter implemented in EGS4. In this sampling algorithm only the angular part of 2BS is used, with the emitted photon energy, k, determined by GEANT4 $\left(\frac{d\sigma}{dk}\right)$ differential cross-section.

G4Generator2BN

The angular distribution of the emitted photons is obtained from the 2BN Koch and Motz bremsstrahlung double differential cross-section *[1]* that can be written as:

$$d\sigma_{k,\theta} = \frac{Z^2 r_0^2}{8\pi 137}\frac{dk}{k}\frac{p}{p_0} d\Omega_k \left\{ \frac{8\sin^2\theta(2E_0^2+1)}{p_0^2\Delta_0^4} - \frac{2(5E_0^2+2EE_0+3)}{p_0^2\Delta_0^2} - \frac{2(p_0^2-k^2)}{Q^2\Delta_0} + \frac{4E}{p_2^2\Delta_0} + \frac{L}{pp_0} \left[\frac{4E_0\sin^2\theta(3k-p_0^2E)}{p_0^2\Delta^4} + \frac{4E_0^2(E_0^2+E^2)}{p_0^2\Delta_0^2} + \frac{2-2(7E_0^2-3EE_0+E^2)}{p_0^2\Delta_0^2} + \frac{2k(E_0^2+EE_0-1)}{p_0^2\Delta_0} \right] - \left(\frac{4\epsilon}{p\Delta 0}\right) + \left(\frac{\epsilon^Q}{pQ}\right)\left[\frac{4}{\Delta_0^2} - \frac{6k}{\Delta_0} - \frac{2k(p_0^2-k^2)}{Q^2\Delta_0}\right] \right\}$$

in which:

$$\begin{aligned} L = & \quad \ln\left[\frac{EE_0 - 1 + pp_0}{EE_0 - 1 - pp_0}\right] \\ \Delta_0 = & \quad E_0 - p_0\cos\theta \\ Q^2 = & \quad p_0^2 + k^2 - 2p_0 k\cos\theta \\ \epsilon = & \quad \ln\left[\frac{E+p}{E-p}\right] \qquad \epsilon^Q = \ln\left[\frac{Q+p}{Q-p}\right] \end{aligned}$$

where k is the photon energy, θ the emission angle and (E_0, p_0) and (E, p) are the total (energy, momentum) of the electron before and after the radiative emission, all in units of $m_e c^2$.
Since the 2BN cross–section is a 2-dimensional non-factorized distribution an acceptance-rejection technique was the adopted. For the 2BN distribution, two functions $g_1(k)$ and $g_2(\theta)$ were defined:

$$g_1(k) = k^{-b} \qquad g_2(\theta) = \frac{\theta}{1 + c\theta^2}$$

such that:

$$Ag_1(k)g_2(\theta) \geq \frac{d\sigma}{dkd\theta}$$

where A is a global constant to be completed. Both functions have an analytical integral G and an analytical inverse G^{-1}. The b parameter of $g_1(k)$ was empirically tuned and set to 1.2. For positive θ values, $g_2(\theta)$ has a maximum at $\frac{1}{\sqrt{(c)}}$. c parameter controls the function global shape and it was used to tune $g_2(\theta)$ according to the electron kinetic energy.
To generate photon energy k according to g_1 and θ according to g_2 the inverse-transform method was used. The integration of these functions gives

$$G_1 = C_1 \int_{k_{min}}^{k_{max}} k'^{-b} dk' = C_1 \frac{k^{1-b} - k_{min}^{1-b}}{1-b}$$

$$G_2 = C_2 \int_0^{\theta} \frac{\theta'}{1 + c\theta'^2} d\theta' = C_2 \frac{\log(1 + c\theta^2)}{2c}$$

where C_1 and C_2 are two global constants chosen to normalize the integral in the overall range to the unit. The photon momentum k will range from a minimum cut value k_{min} (required to avoid infrared divergence) to a maximum value equal to the electron kinetic energy E_k, while the polar angle ranges from 0 to π, resulting for C_1 and C_2:

$$C_1 = \frac{1-b}{E_k^{1-b}} \qquad C_2 = \frac{2c}{\log(1 + c\pi^2)}$$

k and θ are then sampled according to:

$$k = \left[\frac{1-b}{C_1}\xi_1 + k_{min}^{1-b}\right] \qquad \theta = \sqrt{\frac{\exp\left(\frac{2c\xi_2}{C_1}\right)}{2c}}$$

where ξ_1 and ξ_2 are uniformly sampled in the interval (0,1). The event is accepted if:

$$uAg_1(k)g_2(\theta) \leq \frac{d\sigma}{dkd\theta}$$

where u is a random number with uniform distribution in (0,1). The A and c parameters were computed in a logarithmic grid, ranging from 1 keV to 1.5 MeV with 100 points per decade. Since the $g_2(\theta)$ function has a maximum at $\theta = \frac{1}{\sqrt{c}}$, the c parameter was computed using the relation $c = \frac{1}{\theta_{max}}$. At the point (k_{min}, θ_{max}) where k_{min} is the k cut value,

the double differential cross-section has its maximum value, since it is monotonically decreasing in k and thus the global normalization parameter A is estimated from the relation:

$$Ag_1(k_{min})g_2(\theta_{max}) = \left(\frac{d^2\sigma}{dkd\theta}\right)_{max}$$

where $g_1(k_{min})g_2(\theta_{max}) = \frac{k_{min}^{-b}}{2\sqrt{c}}$. Since A and c can only be retrieved for a fixed number of electron kinetic energies there exists the possibility that $Ag_1(k_{min})g_2(\theta_{max}) \leq \left(\frac{d^2\sigma}{dkd\theta}\right)_{max}$ for a given E_k. This is a small violation that can be corrected introducing an additional multiplicative factor to the A parameter, which was empirically determined to be 1.04 for the entire energy range.

Comparisons between Tsai, 2BS and 2BN generators

The currently available generators can be used according to the user required precision and timing requirements. Regarding the energy range, validation results indicate that for lower energies ($\leq$ 100 keV) there is a significant deviation on the most probable emission angle between Tsai/2BS generators and the 2BN generator - Figure [br-dist]. The 2BN generator maintains however a good agreement with Kissel data *[8]*, derived from the work of Tseng and co-workers *[9]*, and it should be used for energies between 1 keV and 100 keV *[10]*. As the electron kinetic energy increases, the different distributions tend to overlap and all generators present a good agreement with Kissel data.

|Comparison of polar angle distribution of bremsstrahlung photons (:math:‘\(k/T=0.5\)‘) for 10 keV (*left*) and 100 keV (*middle*) and 500 keV (*right*) electrons in silver, obtained with Tsai, 2BS and 2BN generator||Comparison of polar angle distribution of bremsstrahlung photons (:math:‘\(k/T=0.5\)‘) for 10 keV (*left*) and 100 keV (*middle*) and 500 keV (*right*) electrons in silver, obtained with Tsai, 2BS and 2BN generator||Comparison of polar angle distribution of bremsstrahlung photons (:math:‘\(k/T=0.5\)‘) for 10 keV (*left*) and 100 keV (*middle*) and 500 keV (*right*) electrons in silver, obtained with Tsai, 2BS and 2BN generator|

In figure [br-eff] the sampling efficiency for the different generators are presented. The sampling generation efficiency was defined as the ratio between the number of generated events and the total number of trials. As energies increases the sampling efficiency of the 2BN algorithm decreases from 0.65 at 1 keV electron kinetic energy down to almost 0.35 at 1 MeV. For energies up to 10 keV the 2BN sampling efficiency is superior or equivalent to the one of the 2BS generator. These results are an indication that precision simulation of low energy bremsstrahlung can be obtained with little performance degradation. For energies above 500 keV, Tsai generator can be used, retaining a good physics accuracy and a sampling efficiency superior to the 2BS generator.

4.2.2 Compton Scattering

Total Cross Section

The total cross section for the Compton scattering process is determined from the data as described in section [sub-subsigmatot]. To avoid sampling problems in the Compton process the cross section is set to zero at low-energy limit of cross section table, which is $100eV$ in majority of EM Phyiscs Lists.

Sampling of the Final State

For low energy incident photons, the simulation of the Compton scattering process is performed according to the same procedure used for the “standard” Compton scattering simulation, with the addition that Hubbel’s atomic form factor *[1]* or scattering function, SF, is taken into account. The angular and energy distribution of the incoherently scattered photon is then given by the product of the Klein-Nishina formula $\Phi(\epsilon)$ and the scattering function, $SF(q)$ *[2]*

$$P(\epsilon, q) = \Phi(\epsilon) \times SF(q).$$

ϵ is the ratio of the scattered photon energy E', and the incident photon energy E. The momentum transfer is given by $q = E \times \sin^2(\theta/2)$, where θ is the polar angle of the scattered photon with respect to the direction of the parent photon. $\Phi(\epsilon)$ is given by

$$\Phi(\epsilon) \cong [\frac{1}{\epsilon} + \epsilon][1 - \frac{\epsilon}{1+\epsilon^2} sin^2\theta].$$

The effect of the scattering function becomes significant at low energies, especially in suppressing forward scattering *[2]*.

The sampling method of the final state is based on composition and rejection Monte Carlo methods [butch][messel][egs4], with the SF function included in the rejection function

$$g(\epsilon) = \left[1 - \frac{\epsilon}{1+\epsilon^2} \sin^2\theta\right] \times SF(q),$$

with $0 < g(\epsilon) < Z$. Values of the scattering functions at each momentum transfer, q, are obtained by interpolating the evaluated data for the corresponding atomic number, Z.

The polar angle θ is deduced from the sampled ϵ value. In the azimuthal direction, the angular distributions of both the scattered photon and the recoil electron are considered to be isotropic *[6]*.

Since the incoherent scattering occurs mainly on the outermost electronic subshells, the binding energies can be neglected, as stated in reference *[6]*. The momentum vector of the scattered photon, $\overrightarrow{P'_\gamma}$, is transformed into the World coordinate system. The kinetic energy and momentum of the recoil electron are then

$$\begin{aligned} T_{el} &= E - E' \\ \overrightarrow{P_{el}} &= \overrightarrow{P_\gamma} - \overrightarrow{P'_\gamma}. \end{aligned}$$

4.2.3 Geant4-DNA processes and models

The Geant4-DNA processes and models (theoretical, semi-empirical) are adapted for track structure simulations in liquid water down to the eV scale. They are described on a dedicated web site: http://geant4-dna.org, which includes a full list of publications.

Any report or published results obtained using the Geant4-DNA software shall cite the following publication : Comparison of Geant4 very low energy cross section models with experimental data in water, S. Incerti et al., Med. Phys. 37 (2010) 4692-4708

4.2.4 Gamma Conversion

Total cross-section

The total cross-section of the Gamma Conversion process is determined from the data as described in section [subsubsigmatot].

Sampling of the final state

For low energy incident photons, the simulation of the Gamma Conversion final state is performed according to *[5]*.

The secondary $e^\pm$ energies are sampled using the Bethe-Heitler cross-sections with Coulomb correction.

The Bethe-Heitler differential cross-section with the Coulomb correction for a photon of energy E to produce a pair with one of the particles having energy ϵE (ϵ is the fraction of the photon energy carried by one particle of the pair) is

given by [6]:

$$\frac{d\sigma(Z,E,\epsilon)}{d\epsilon} = \frac{r_0^2 \alpha Z(Z+\xi(Z))}{E^2}\left[(\epsilon^2+(1-\epsilon)^2)\left(\Phi_1(\delta)-\frac{F(Z)}{2}\right)+\right.$$
$$\left.+\frac{2}{3}\epsilon(1-\epsilon)\left(\Phi_2(\delta)-\frac{F(Z)}{2}\right)\right]$$

where $\Phi_i(\delta)$ are the screening functions depending on the screening variable δ [5].

The value of ϵ is sampled using composition and rejection Monte Carlo methods [5][butch][messel].

After the successful sampling of ϵ, the process generates the polar angles of the electron with respect to an axis defined along the direction of the parent photon. The electron and the positron are assumed to have a symmetric angular distribution. The energy-angle distribution is given by [1][2]:

$$\frac{d\sigma}{dpd\Omega} = \frac{2\alpha^2 e^2}{\pi k m^4}\left[\left(\frac{2x(1-x)}{(1+l)}^2 - \frac{12lx(1-x)}{(1+l)^4}\right)(Z^2+Z)+\right.$$
$$\left.+\left(\frac{2x^2-2x+1}{(1+l)^2}+\frac{4lx(1-x)}{(1+l)^4}\right)(X-2Z^2 f((\alpha Z)^2))\right]$$

where k is the photon energy, p the momentum and E the energy of the electron of the $e^{\pm}$ pair $x = E/k$ and $l = E^2\theta^2/m^2$. The sampling of this cross-section is obtained according to [5].

The azimuthal angle ϕ is generated isotropically.

This information together with the momentum conservation is used to calculate the momentum vectors of both decay products and to transform them to the GEANT coordinate system. The choice of which particle in the pair is the electron/positron is made randomly.

4.2.5 Low energy extentions

Energy losses of slow negative particles

At low energies, e.g. below a few MeV for protons/antiprotons, the Bethe-Bloch formula is no longer accurate in describing the energy loss of charged hadrons and higher Z terms should be taken in account. Odd terms in Z lead to a significant difference between energy loss of positively and negatively charged particles. The energy loss of negative hadrons is scaled from that of antiprotons. The antiproton energy loss is calculated according to the quantum harmonic oscillator model is used, as described in [1] and references therein. The lower limit of applicability of the model is chosen for all materials at $10\ keV$. Below this value stopping power is set to constant equal to the dE/dx at $10\ keV$.

Energy losses of hadrons in compounds

To obtain energy losses in a mixture or compound, the absorber can be thought of as made up of thin layers of pure elements with weights proportional to the electron density of the element in the absorber (Bragg's rule):

$$\frac{dE}{dx} = \sum_i \left(\frac{dE}{dx}\right)_i,$$

where the sum is taken over all elements of the absorber, i is the number of the element, $(\frac{dE}{dx})_i$ is energy loss in the pure i-th element.

Bragg's rule is very accurate for relativistic particles when the interaction of electrons with a nucleus is negligible. But at low energies the accuracy of Bragg's rule is limited because the energy loss to the electrons in any material depends on the detailed orbital and excitation structure of the material. In the description of Geant4 materials there is a special attribute: the chemical formula. It is used in the following way:

- if the data on the stopping power for a compound as a function of the proton kinetic energy is available (Table [hlei.tab1]), then the direct parametrisation of the data for this material is performed;
- if the data on the stopping power for a compound is available for only one incident energy (Table [hlei.tab2]), then the computation is performed based on Bragg's rule and the chemical factor for the compound is taken into account;
- if there are no data for the compound, the computation is performed based on Bragg's rule.

In the review *[2]* the parametrisation stopping power data are presented as

$$S_e(T_p) = S_{Bragg}(T_p)\left[1 + \frac{f(T_p)}{f(125\ keV)}\left(\frac{S_{exp}(125\ keV)}{S_{Bragg}(125\ keV)} - 1\right)\right],$$

where $S_{exp}(125\ keV)$ is the experimental value of the energy loss for the compound for $125\ keV$ protons or the reduced experimental value for He ions, $S_{Bragg}(T_p)$ is a value of energy loss calculated according to Bragg's rule, and $f(T_p)$ is a universal function, which describes the disappearance of deviations from Bragg's rule for higher kinetic energies according to:

$$f(T_p) = \frac{1}{1 + \exp\left[1.48(\frac{\beta(T_p)}{\beta(25\ keV)} - 7.0)\right]},$$

where $\beta(T_p)$ is the relative velocity of the proton with kinetic energy T_p.

Number	Chemical formula
1.	AlO
2.	C_2O
3.	CH_4
4.	(C_2H_4)_N-Polyethylene
5.	(C_2H_4)_N-Polypropylene
6.	(C_8H_8)_N
7.	C_3H_8
8.	SiO_2
9.	H_2O
10.	H_2O-Gas
11.	Graphite

Number	Chemical formula	Number	Chemical formula
1.	H_2O	28.	C_2H_6
2.	C_2H_4O	29.	C_2F_6
3.	C_3H_6O	30.	C_2H_6O
4.	C_2H_2	31.	C_3H_6O
5.	C_H_3OH	32.	C_4H_10O
6.	C_2H_5OH	33.	C_2H_4
7.	C_3H_7OH	34.	C_2H_4O
8.	C_3H_4	35.	C_2H_4S
9.	NH_3	36.	SH_2
10.	C_14H_10	37.	CH_4
11.	C_6H_6	38.	CCLF_3
12.	C_4H_10	39.	CCl_2F_2
13.	C_4H_6	40.	CHCl_2F
14.	C_4H_8O	41.	(CH_3)_2S
15.	CCl_4	42.	N_2O
16.	CF_4	43.	C_5H_10O
17.	C_6H_8	44.	C_8H_6
18.	C_6H_12	45.	(CH_2)_N
19.	C_6H_10O	46.	(C_3H_6)_N
20.	C_6H_10	47.	(C_8H_8)_N
21.	C_8H_16	48.	C_3H_8
22.	C_5H_10	49.	C_3H_6-Propylene
23.	C_5H_8	50.	C_3H_6O

Fluctuations of energy losses of hadrons

The total continuous energy loss of charged particles is a stochastic quantity with a distribution described in terms of a straggling function. The straggling is partially taken into account by the simulation of energy loss by the production of δ-electrons with energy $T > T_c$. However, continuous energy loss also has fluctuations. Hence in the current GEANT4 implementation two different models of fluctuations are applied depending on the value of the parameter κ which is the lower limit of the number of interactions of the particle in the step. The default value chosen is $\kappa = 10$. To select a model for thick absorbers the following boundary conditions are used:

$$\Delta E > T_c\kappa) \;\; or \;\; T_c < I\kappa,$$

where ΔE is the mean continuous energy loss in a track segment of length s, T_c is the cut kinetic energy of δ-electrons, and I is the average ionisation potential of the atom.

For long path lengths the straggling function approaches the Gaussian distribution with Bohr's variance *[3]*:

$$\Omega^2 = KN_{el}\frac{Z_h^2}{\beta^2}T_c s f\left(1 - \frac{\beta^2}{2}\right),$$

where f is a screening factor, which is equal to unity for fast particles, whereas for slow positively charged ions with $\beta^2 < 3Z(v_0/c)^2$ $f = a + b/Z_{eff}^2$, where parameters a and b are parametrised for all atoms *[4][5]*.

For short path lengths, when the condition [le_cond] is not satisfied, the model described in the charter [gen_fluctuations] is applied.

ICRU 73-based energy loss model

The ICRU 73 *[1]* report contains stopping power tables for ions with atomic numbers 3–18 and 26, covering a range of different elemental and compound target materials. The stopping powers derive from calculations with the PASS code *[6]*, which implements the binary stopping theory described in *[6][7]*. Tables in ICRU 73 extend over an energy range up to 1 GeV/nucleon. All stopping powers were incorporated into Geant4 and are available through a parameterisation model (G4IonParametrisedLossModel). For a few materials revised stopping powers were included (water, water vapor, nylon type 6 and 6/6 from P. Sigmund et al *[8]* and copper from P. Sigmund *[9]*), which replace the corresponding tables of the original ICRU 73 report.

To account for secondary electron production above T_c, the continuous energy loss per unit path length is calculated according to

$$\left.\frac{dE}{dx}\right|_{T<T_C} = \left(\frac{dE}{dx}\right)_{ICRU73} - \left(\frac{dE}{dx}\right)_{\delta}$$

where $(dE/dx)_{ICRU73}$ refers to stopping powers obtained by interpolating ICRU 73 tables and $(dE/dx)_\delta$ is the mean energy transferred to δ-electrons per path length given by

$$\left(\frac{dE}{dx}\right)_{\delta} = \sum_i n_{at,i}\int_{T_c}^{T_{max}}\frac{d\sigma_i(T)}{dT}TdT$$

where the index i runs over all elements composing the material, $n_{at,i}$ is the number of atoms of the element i per volume, T_{max} is the maximum energy transferable to an electron according to formula and $d\sigma_i/dT$ specifies the differential cross section per atom for producing an δ-electron following equation For compound targets not considered in the ICRU 73 report, the first term on the rightern side in equation ([hlei.rstp]) is computed by applying Bragg's additivity rule *[3]* if tables for all elemental components are available in ICRU 73.

4.2.6 Electron ionisation

The class *G4LivermoreIonisationModel* calculates the continuous energy loss due to electron ionisation and simulates δ-ray production by electrons. The $delta$-electron production threshold for a given material, T_c, is used to separate the continuous and the discrete parts of the process. The energy loss of an electron with the incident energy, T, is expressed via the sum over all atomic shells, s, and the integral over the energy, t, of $delta$-electrons:

$$\frac{dE}{dx} = \sum_s \left(\sigma_s(T) \frac{\int_{0.1eV}^{T_c} t \frac{d\sigma}{dt} dt}{\int_{0.1eV}^{T_{max}} \frac{d\sigma}{dt} dt} \right),$$

where $T_{max} = 0.5T$ is the maximum energy transfered to a δ-electron, $\sigma_s(T)$ is the total cross-section for the shell, s, at a given incident kinetic energy, T, and $0.1eV$ is the low energy limit of the EEDL data. The δ-electron production cross-section is a complimentary function:

$$\sigma(T) = \sum_s \left(\sigma_s(T) \frac{\int_{T_c}^{T_{max}} \frac{d\sigma}{dt} dt}{\int_{0.1eV}^{T_{max}} \frac{d\sigma}{dt} dt} \right).$$

The partial sub-shell cross-sections, σ_s, are obtained from an interpolation of the evaluated cross-section data in the EEDL library [io-EEDL], according to the formula ([eqloglog]) in Section [subsubsigmatot].

The probability of emission of a δ-electron with kinetic energy, t, from a sub-shell, s, of binding energy, B_s, as the result of the interaction of an incoming electron with kinetic energy, T, is described by:

$$\frac{d\sigma}{dt} = \frac{P(x)}{x^2}, \quad \text{with} x = \frac{t + B_s}{T + B_s},$$

where the parameter x is varied from $x_{min} = (0.1eV + B_s)/(T + B_s)$ to 0.5. The function, $P(x)$, is parametrised differently in 3 regions of x: from x_{min} to x_1 the linear interpolation with linear scale of 4 points is used; from x_1 to x_2 the linear interpolation with logarithmic scale of 16 points is used; from x_2 to 0.5 the following interpolation is applied:

$$P(x) = 1 - gx + (1 - g)x^2 + \frac{x^2}{1 - x}\left(\frac{1}{1 - x} - g\right) + A * (0.5 - x)/x,$$

where A is a fit coefficient, g is expressed via the gamma factor of the incoming electron:

$$g = (2\gamma - 1)/\gamma^2.$$

For the high energy case ($x >> 1$) the formula ([io-ff]) is transformed to the Möller electron-electron scattering formula *[1]*[messel].

The value of the coefficient, A, for each element is obtained as a result of the fit on the spectrum from the EEDL data for those energies which are available in the database. The values of x_1 and x_2 are chosen for each atomic shell according to the spectrum of δ-electrons in this shell. Note that x_1 corresponds to the maximum of the spectrum, if the maximum does not coincide with x_{min}. The dependence of all 24 parameters on the incident energy, T, is evaluated from a logarithmic interpolation ([eqloglog]).

The sampling of the final state proceeds in three steps. First a shell is randomly selected, then the energy of the $delta$-electron is sampled, finally the angle of emission of the scattered electron and of the δ-ray is determined by energy-momentum conservation taken into account electron motion on the atomic orbit.

The interaction leaves the atom in an excited state. The deexcitation of the atom is simulated as described in section [relax]. Sampling of the excitations is carried out for both the continuous and the discrete parts of the process.

4.2.7 Ionisation

The total cross section at a given incident kinetic energy T is calculated by summing the partial cross sections at such energy for all the subshells of an element. The partial subshell cross sections at incident energy T are obtained from an interpolation of the evaluated cross section data in the EEDL library, according to the formula [eqloglog].

The subshell from which the electron is emitted is randomly selected according to the cross sections of the subshells, determined at the energy T by interpolating the evaluated cross section data from the EEDL data library.

The probability of emission of an electron (δ ray) with kinetic energy t from a subshell of binding energy B_i as the result of the interaction of an incoming electron of kinetic energy T is described by:

$$Prob(T, t, B_i) = \sum_{j=2}^{7} \frac{a_j(T)}{(t + b_i)^j}$$

for $t < t_0$ and

$$Prob(T, t, B_i) = \frac{c(T)}{t^2}$$

for $t > t_0$, where t_0 is a parameter. Both formulas result from empirical fits to the EEDL data and are normalized to 1. The a, b and c coefficients are determined by fitting the data; their energy dependence is evaluated from a semilogarithmic interpolation of the fitted data.

The sampling of the final state proceeds through two steps: first the range of the energy ($t < t_0$ or $t > t_0$) is determined by a random number extraction, taking into account the relative area determined by the two functions [eqionihigh] and [eqionilow], then the energy of the δ ray is generated according to the corresponding probability distribution.

The angle of emission of the scattered electron and of the δ ray is determined by energy-momentum conservation.

The interaction leaves the atom in an excited state, with excitation energy equal to the binding energy of the subshell from which the electron has been emitted. The deexcitation of the atom proceeds via the emission of fluorescence photons, as described in section [secphoto].

4.2.8 The MicroElec [1] extension for microelectronics applications

The Geant4-MicroElec extension *[1]*, developed by CEA, aims at modeling the effect of ionizing radiation in highly integrated microelectronic components. It describes the transport and generation of very low energy electrons by incident electrons, protons and heavy ions in silicon.

All Geant4-MicroElec physics processes and models simulate step-by-step interactions of particles in silicon down to the eV scale; they are pure discrete processes. Table [muelec:proc] summarizes the list of physical interactions per particle type that can be modeled using the Geant4-MicroElec extension, along with the corresponding process classes, model classes, low energy limit applicability of models, high energy applicability of models and energy threshold below which the incident particle is killed (stopped and the kinetic energy is locally deposited). All models are interpolated. For now, they are valid for silicon only (use the **G4_Si** Geant4-NIST material).

Particle & **Interaction & **Process, Model, Range & **Kill Electron & Elastic scattering & G4MicroElastic & 16.7 eV (*) && G4MicroElecElasticModel & && 5 eV :math:‘(lt E lt)‘ 100 MeV & Electron & Ionisation & G4MicroElecInelastic & — && G4MicroElecInelasticModel & && 16.7 eV :math:‘(lt E lt)‘ 100 MeV & Protons, ions & Ionisation & G4MicroElecInelastic & — && G4MicroElecInelasticModel & && 50 keV/:math:‘(u)‘ :math:‘(E <)‘ 23 MeV/u & ******			

Table: List of G4MicroElec physical interactions

(*) because of the low energy limit applicability of the inelastic model.

All details regarding the physics and formula used for these processes and models and available in *[2]* for incident electrons and in *[3]* for incident protons and heavy ions.

4.2.9 Monash Low Energy Photon Processes

Introduction

The Monash Compton Scattering models, for polarised (G4LowEPPolarizedComptonModel) and non-polarised (G4LowEPComptonModel) photons, are an alternative set of Compton scattering models to those of Livermore and Penelope that were constructed using Ribberfors' theoretical framework *[1][2][3]*. The limitation of the Livermore and Penelope models is that only the components of the pre-collision momentum of the target electron contained within the photon plane, two-dimensional plane defined by the incident and scattered photon, is incorporated into their scattering frameworks *[4]*. Both models are forced to constrain the ejected direction of the Compton electron into the photon plane as a result. The Monash Compton scattering models avoid this limitation through the use of a two-body fully relativistic three-dimensional scattering framework to ensure the conservation of energy and momentum in the Relativistic Impulse Approximation (RIA) *[5][6]*.

Physics and Simulation

Total Cross Section

The Monash Compton scattering models were built using the Livermore and Polarised Livermore Compton scattering models as templates. As a result the total cross section for the Compton scattering process and handling of polarisation effects mimic those outlined in Section 9.

Sampling of the Final State

The scattering diagram seen in Figure [fig:figure1] outlines the basic principles of Compton scattering with an electron of non-zero pre-collision momentum in the RIA.

The process of sampling the target atom, atomic shell and target electron pre-collision momentum mimic that outlined in Section 9. After the sampling of these parameters the following four equations are utilised to model the scattered photon energy E', recoil electron energy T_{el} and recoil electron polar and azimuthal angles (ϕ and ψ) with respect to the incident photon direction and out-going plane of polarisation:

$$E' = \frac{\gamma mc\left(c - u\cos\alpha\right)}{1 - \cos\theta + \frac{\gamma mc(c - u\cos\theta\cos\alpha - u\sin\theta\sin\alpha\cos\beta)}{E}},$$

$$T_{el} = E - E' - E_B,$$

$$\cos\phi = \frac{-Y \pm \sqrt{Y^2 - 4WZ}}{2W},$$

$$\cos\psi = \frac{C - B\cos\phi}{A\sin\phi},$$

where:

$$A = E'u'\sin\theta,$$

$$B = E'u'\cos\theta - Eu',$$

$$C = c\left(E' - E\right) - \frac{EE'}{\gamma' mc}\left(1 - \cos\theta\right),$$

$$D = \frac{\gamma mE'}{c}\left(c - u\cos\theta\cos\alpha - u\sin\theta\cos\beta\sin\alpha\right) + m^2c^2\left(\gamma\gamma' - 1\right) - \gamma' mE',$$

$$F = (\gamma\gamma' m^2 uu'\cos\beta\sin\alpha - \frac{\gamma' mE'u'}{c}\sin\theta),$$

$$G = \gamma\gamma' m^2 uu' \sin\beta \sin\alpha,$$

$$H = (\gamma\gamma' m^2 uu' \cos\alpha - \frac{\gamma' mE'}{c} u' \cos\theta),$$

$$W = (FB - HA)^2 + G^2A^2 + G^2B^2,$$

$$Y = 2\left((AD - FC)(FB - HA) - G^2BC\right),$$

$$Z = (AD - FC)^2 + G^2\left(C^2 - A^2\right),$$

and c is the speed of light, m is the rest mass of an electron, u is the speed of the target electron, u' is the speed of the recoil electron, $\gamma = \left(1 - \left(u^2/c^2\right)\right)^{-1/2}$ and $\gamma' = \left(1 - \left(u'^2/c^2\right)\right)^{-1/2}$. Further information regarding the Monash Compton scattering models can be found in *[6]*.

4.2.10 Introduction

Additional electromagnetic physics processes for photons, electrons, hadrons and ions have been implemented in Geant4 in order to extend the validity range of particle interactions to lower energies than those available in the standard Geant4 electromagnetic processes *[2]* Because atomic shell structure is more important in most cases at low energies than it is at higher energies, the low energy processes make direct use of shell cross section data. The standard processes, which are optimized for high energy physics applications, rely on parameterizations of these data.

The low energy processes include the photo-electric effect, Compton scattering, Rayleigh scattering, gamma conversion, bremsstrahlung and ionization. Fluorescence and Auger electron emission of excited atoms is also considered.

Some features common to all low energy processes currently implemented in Geant4 are summarized in this section. Subsequent sections provide more detailed information for each process.

Physics

The low energy processes of Geant4 represent electromagnetic interactions at lower energies than those covered by the equivalent Geant4 standard electromagnetic processes.

The current implementation of low energy processes is valid for energies down to $10eV$ and can be used up to approximately $100GeV$ for gamma processes. For electron processes upper limit is significantly below. It covers elements with atomic number between 1 and 99.

All processes involve two distinct phases:

- the calculation and use of total cross sections, and
- the generation of the final state.

Both phases are based on the theoretical models and on exploitation of evaluated data.

Data Sources

The data used for the determination of cross-sections and for sampling of the final state are extracted from a set of publicly distributed evaluated data libraries:

- EPDL97 (Evaluated Photons Data Library) *[1]*;
- EEDL (Evaluated Electrons Data Library) *[1]*;
- EADL (Evaluated Atomic Data Library) *[1]*;
- binding energy values based on data of Scofield *[5]*.

Evaluated data sets are produced through the process of critical comparison, selection, renormalization and averaging of the available experimental data, normally complemented by model calculations. These libraries provide the following data relevant for the simulation of Geant4 low energy processes:

- total cross-sections for photoelectric effect, Compton scattering, Rayleigh scattering, pair production and bremsstrahlung;
- subshell integrated cross sections for photo-electric effect and ionization;
- energy spectra of the secondaries for electron processes;
- scattering functions for the Compton effect;
- binding energies for electrons for all subshells;
- transition probabilities between subshells for fluorescence and the Auger effect.

The energy range covered by the data libraries extends from 100 GeV down to 1 eV for Rayleigh and Compton effects, down to the lowest binding energy for each element for photo-electric effect and ionization, and down to 10 eV for bremsstrahlung.

Distribution of the Data Sets

The author of EPDL97 *[1]*, who is also responsible for the EEDL *[1]* and EADL *[1]* data libraries, Dr. Red Cullen, has kindly permitted the libraries and their related documentation to be distributed with the Geant4 toolkit. The data are reformatted for Geant4 input. They can be downloaded from the source code section of the Geant4 page: http://cern.ch/geant4/geant4.html.

The EADL, EEDL and EPDL97 data-sets are also available from several public distribution centres in a format different from the one used by Geant4 *[6]*.

Calculation of Total Cross Sections

The energy dependence of the total cross section is derived for each process from the evaluated data libraries. For ionisation, bremsstrahlung and Compton scattering the total cross is obtained by interpolation according to the formula *[7]*:

$$\log(\sigma(E)) = \frac{log(\sigma_1)log(E_2/E) + log(\sigma_2)log(E/E_1)}{log(E_2/E_1)}$$

where E is actial energy, E_1 and E_2 are respectively the closest lower and higher energy points for which data (σ_1 and σ_2) are available. For other processes interpolation method is chosen depending on cross section shape.

4.2.11 Penelope physics

Introduction

A new set of physics processes for photons, electrons and positrons is implemented in Geant4: it includes Compton scattering, photoelectric effect, Rayleigh scattering, gamma conversion, bremsstrahlung, ionization (to be released) and positron annihilation (to be released). These processes are the Geant4 implementation of the physics models developed for the PENELOPE code (PENetration and Energy LOss of Positrons and Electrons), version 2001, that are described in detail in Ref. *[3]*. The Penelope models have been specifically developed for Monte Carlo simulation and great care was given to the low energy description (i.e. atomic effects, etc.). Hence, these implementations provide reliable results for energies down to a few hundred eV and can be used up to $\sim$1 GeV *[3][4]*. For this reason, they may be used in Geant4 as an alternative to the Low Energy processes. For the same physics processes, the user now has more alternative descriptions from which to choose, including the cross section calculation and the final state sampling.

Compton scattering

Total cross section

The total cross section of the Compton scattering process is determined from an analytical parameterization. For γ energy E greater than 5 MeV, the usual Klein-Nishina formula is used for $\sigma(E)$. For a more accurate parameterization is used, which takes into account atomic binding effects and Doppler broadening *[5]*:

$$\sigma(E) = 2\pi \int_{-1}^{1} \frac{r_e^2}{2} \frac{E_C^2}{E^2} \left(\frac{E_C}{E} + \frac{E}{E_C} - \sin^2\theta\right) \cdot \sum_{shells} f_i \Theta(E - U_i) n_i(p_z^{max})\, d(\cos\theta)$$

where: r_e = classical radius of the electron; m_e = mass of the electron; θ = scattering angle; E_C = Compton energy

$$= \frac{E}{1 + \frac{E}{m_e c^2}(1 - \cos\theta)}$$

f_i = number of electrons in the i-th atomic shell; U_i = ionisation energy of the i-th atomic shell; Θ = Heaviside step function; p_z^{max} = highest possible value of p_z (projection of the initial momentum of the electron in the direction of the scattering angle)

$$= \frac{E(E - U_i)(1 - \cos\theta) - m_e c^2 U_i}{c\sqrt{2E(E - U_i)(1 - \cos\theta) + U_i^2}}.$$

Finally,

$$n_i(x) = \begin{cases} \frac{1}{2} e^{\left[\frac{1}{2} - \left(\frac{1}{2} - \sqrt{2} J_{i0} x\right)^2\right]} & \text{if} \quad x < 0 \\ 1 - \frac{1}{2} e^{\left[\frac{1}{2} - \left(\frac{1}{2} + \sqrt{2} J_{i0} x\right)^2\right]} & \text{if} \quad x > 0 \end{cases}$$

where J_{i0} is the value of the p_z-distribution profile $J_i(p_z)$ for the i-th atomic shell calculated in $p_z = 0$. The values of J_{i0} for the different shells of the different elements are tabulated from the Hartree-Fock atomic orbitals of Ref. *[6]*. The integration of Eq.([equno]) is performed numerically using the 20-point Gaussian method. For this reason, the initialization of the Penelope Compton process is somewhat slower than the Low Energy process.

Sampling of the final state

The polar deflection $\cos\theta$ is sampled from the probability density function

$$P(\cos\theta) = \frac{r_e^2}{2} \frac{E_C^2}{E^2} \left(\frac{E_C}{E} + \frac{E}{E_C} - \sin^2\theta\right) \sum_{shells} f_i \Theta(E - U_i) n_i(p_z^{max})$$

(see Ref. *[3]* for details on the sampling algorithm). Once the direction of the emerging photon has been set, the active electron shell i is selected with relative probability equal to $Z_i \Theta(E - U_i) n_i[p_z^{max}(E, \theta)]$.

A random value of p_z is generated from the analytical Compton profile *[6]*. The energy of the emerging photon is

$$E' = \frac{E\tau}{1 - \tau t} \left[(1 - \tau t \cos\theta) + \frac{p_z}{|p_z|} \sqrt{(1 - \tau t \cos\theta)^2 - (1 - t\tau^2)(1 - t)}\right],$$

where

$$t = \left(\frac{p_z}{m_e c}\right)^2 \quad \text{and} \quad \tau = \frac{E_C}{E}.$$

The azimuthal scattering angle ϕ of the photon is sampled uniformly in the interval (0,2 π). It is assumed that the Compton electron is emitted with energy $E_e = E - E' - U_i$, with polar angle θ_e and azimuthal angle $\phi_e = \phi + \pi$, relative to the direction of the incident photon. In this case $\cos\theta_e$ is given by

$$\cos\theta_e \;=\; \frac{E - E'\cos\theta}{\sqrt{E^2 + E'^2 - 2EE'\cos\theta}}.$$

Since the active electron shell is known, characteristic x-rays and electrons emitted in the de-excitation of the ionized atom can also be followed. The de-excitation is simulated as described in section [relax]. For further details see *[3]*.

Rayleigh scattering

Total cross section

The total cross section of the Rayleigh scattering process is determined from an analytical parameterization. The atomic cross section for coherent scattering is given approximately by *[7]*

$$\sigma(E) \;=\; \pi r_e^2 \int_{-1}^{1} \frac{1+\cos^2\theta}{2}[F(q,Z)]^2 \, d\cos\theta,$$

where $F(q,Z)$ is the atomic form factor, Z is the atomic number and q is the magnitude of the momentum transfer, i.e.

$$q \;=\; 2\,\frac{E}{c}\,\sin\Big(\frac{\theta}{2}\Big).$$

In the numerical calculation the following analytical approximations are used for the form factor:

$$F(q,Z) = f(x,Z) = \begin{array}{ll} Z\,\frac{1+a_1x^2+a_2x^3+a_3x^4}{(1+a_4x^2+a_5x^4)^2} & \text{or} \\ \max[f(x,Z), F_K(x,Z)] & \text{if } Z>10 \text{ and } f(x,Z)<2 \end{array}$$

where

$$F_K(x,Z) \;=\; \frac{\sin(2b\arctan Q)}{bQ(1+Q^2)^b},$$

with

$$x = 20.6074\frac{q}{m_e c}, \quad Q = \frac{q}{2m_e c a}, \quad b = \sqrt{1-a^2}, \quad a = \alpha\Big(Z - \frac{5}{16}\Big),$$

where α is the fine-structure constant. The function $F_K(x,Z)$ is the contribution to the atomic form factor due to the two K-shell electrons (see *[8]*). The parameters of expression $f(x,Z)$ have been determined in Ref. *[8]* for Z=1 to 92 by numerically fitting the atomic form factors tabulated in Ref. *[9]*. The integration of Eq.([eqtre]) is performed numerically using the 20-point Gaussian method. For this reason the initialization of the Penelope Rayleigh process is somewhat slower than the Low Energy process.

Sampling of the final state

The angular deflection $\cos\theta$ of the scattered photon is sampled from the probability distribution function

$$P(\cos\theta) \;=\; \frac{1+\cos^2\theta}{2}[F(q,Z)]^2.$$

For details on the sampling algorithm (which is quite heavy from the computational point of view) see Ref. *[3]*. The azimuthal scattering angle ϕ of the photon is sampled uniformly in the interval (0, 2π).

Gamma conversion

Total cross section

The total cross section of the γ conversion process is determined from the data *[10]*, as described in section [subsub-sigmatot].

Sampling of the final state

The energies E_- and E_+ of the secondary electron and positron are sampled using the Bethe-Heitler cross section with the Coulomb correction, using the semiempirical model of Ref. *[8]*. If

$$\epsilon \;=\; \frac{E_- + m_e c^2}{E}$$

is the fraction of the γ energy E which is taken away from the electron,

$$\kappa \;=\; \frac{E}{m_e c^2} \quad \text{and} \quad a = \alpha Z,$$

the differential cross section, which includes a low-energy correction and a high-energy radiative correction, is

$$\frac{d\sigma}{d\epsilon} \;=\; r_e^2 a (Z+\eta) C_r \frac{2}{3}\Big[2\Big(\frac{1}{2}-\epsilon\Big)^2 \phi_1(\epsilon) + \phi_2(\epsilon)\Big],$$

where:

$$\begin{aligned}\phi_1(\epsilon) \;=\; & \frac{7}{3} - 2\ln(1+b^2) - 6b\arctan(b^{-1}) \\ & -b^2[4 - 4b\arctan(b^{-1}) - 3\ln(1+b^{-2})] \\ & +4\ln(Rm_e c/\hbar) - 4f_C(Z) + F_0(\kappa, Z)\end{aligned}$$

and

$$\begin{aligned}\phi_2(\epsilon) \;=\; & \frac{11}{6} - 2\ln(1+b^2) - 3b\arctan(b^{-1}) \\ & +\frac{1}{2}b^2[4 - 4b\arctan(b^{-1}) - 3\ln(1+b^{-2})] \\ & +4\ln(Rm_e c/\hbar) - 4f_C(Z) + F_0(\kappa, Z),\end{aligned}$$

with

$$b \;=\; \frac{Rm_e c}{\hbar}\frac{1}{2\kappa}\frac{1}{\epsilon(1-\epsilon)}.$$

In this case R is the screening radius for the atom Z (tabulated in *[4]* for Z=1 to 92) and η is the contribution of pair production in the electron field (rather than in the nuclear field). The parameter η is approximated as

$$\eta \;=\; \eta_\infty(1 - e^{-v}),$$

where

$$\begin{aligned}v \;=\; & (0.2840 - 0.1909a)\ln(4/\kappa) + (0.1095 + 0.2206a)\ln^2(4/\kappa) \\ & +(0.02888 - 0.04269a)\ln^3(4/\kappa) \\ & +(0.002527 + 0.002623)\ln^4(4/\kappa)\end{aligned}$$

and η_∞ is the contribution for the atom Z in the high-energy limit and is tabulated for Z=1 to 92 in Ref. *[4]*. In the Eq.([eqquattro]), the function $f_C(Z)$ is the high-energy Coulomb correction of Ref. *[2]*, given by

$$\begin{aligned} f_C(Z) &= a^2[(1+a^2)^{-1} + 0.202059 - 0.03693a^2 + 0.00835a^4 \\ &\quad -0.00201a^6 + 0.00049a^8 - 0.00012a^{10} + 0.00003a^{12}]; \end{aligned}$$

$C_r = 1.0093$ is the high-energy limit of Mork and Olsen's radiative correction (see Ref. *[4]*); $F_0(\kappa, Z)$ is a Coulomb-like correction function, which has been analytically approximated as *[3]*

$$\begin{aligned} F_0(\kappa, Z) &= (-0.1774 - 12.10a + 11.18a^2)(2/\kappa)^{1/2} \\ &\quad +(8.523 + 73.26a - 44.41a^2)(2/\kappa) \\ &\quad -(13.52 + 121.1a - 96.41a^2)(2/\kappa)^{3/2} \\ &\quad +(8.946 + 62.05a - 63.41a^2)(2/\kappa)^2. \end{aligned}$$

The kinetic energy E_+ of the secondary positron is obtained as

$$E_+ = E - E_- - 2m_e c^2.$$

The polar angles θ_- and θ_+ of the directions of movement of the electron and the positron, relative to the direction of the incident photon, are sampled from the leading term of the expression obtained from high-energy theory (see Ref. *[13]*)

$$p(\cos\theta_\pm) = a(1 - \beta_\pm \cos\theta_\pm)^{-2},$$

where a is the a normalization constant and $\beta_\pm$ is the particle velocity in units of the speed of light. As the directions of the produced particles and of the incident photon are not necessarily coplanar, the azimuthal angles ϕ_- and ϕ_+ of the electron and of the positron are sampled independently and uniformly in the interval (0, 2π).

Photoelectric effect

Total cross section

The total photoelectric cross section at a given photon energy E is calculated from the data *[1]*, as described in section [subsubsigmatot].

Sampling of the final state

The incident photon is absorbed and one electron is emitted. The direction of the electron is sampled according to the Sauter distribution *[2]*. Introducing the variable $\nu = 1 - \cos\theta_e$, the angular distribution can be expressed as

$$p(\nu) = (2-\nu)\Big[\frac{1}{A+\nu} + \frac{1}{2}\beta\gamma(\gamma-1)(\gamma-2)\Big]\frac{\nu}{(A+\nu)^3},$$

where

$$\gamma = 1 + \frac{E_e}{m_e c^2}, \quad A = \frac{1}{\beta} - 1,$$

E_e is the electron energy, m_e its rest mass and β its velocity in units of the speed of light c. Though the Sauter distribution, strictly speaking, is adequate only for ionisation of the K-shell by high-energy photons, in many practical simulations it does not introduce appreciable errors in the description of any photoionisation event, irrespective of the atomic shell or of the photon energy. The subshell from which the electron is emitted is randomly selected according to the relative cross sections of subshells, determined at the energy E by interpolation of the data of Ref. *[13]*. The electron kinetic energy is the difference between the incident photon energy and the binding energy of the electron before the interaction in the sampled shell. The interaction leaves the atom in an excited state; the subsequent de-excitation is simulated as described in section [relax].

Bremsstrahlung

Introduction

The class G4PenelopeBremsstrahlung calculates the continuous energy loss due to soft γ emission and simulates the photon production by electrons and positrons. As usual, the gamma production threshold T_c for a given material is used to separate the continuous and the discrete parts of the process.

Electrons

The total cross sections are calculated from the data *[1]*, as described in sections [subsubsigmatot] and [lowebrems]. The energy distribution $\frac{d\sigma}{dW}(E)$, i.e. the probability of the emission of a photon with energy W given an incident electron of kinetic energy E, is generated according to the formula

$$\frac{d\sigma}{dW}(E) \;=\; \frac{F(\kappa)}{\kappa}, \quad \kappa \;=\; \frac{W}{E}.$$

The functions $F(\kappa)$ describing the energy spectra of the outgoing photons are taken from Ref. *[3]*. For each element Z from 1 to 92, 32 points in κ, ranging from 10^{-12} to 1, are used for the linear interpolation of this function. $F(\kappa)$ is normalized using the condition $F(10^{-12}) = 1$. The energy distribution of the emitted photons is available in the library *[3]* for 57 energies of the incident electron between 1 keV and 100 GeV. For other primary energies, logarithmic interpolation is used to obtain the values of the function $F(\kappa)$. The direction of the emitted bremsstrahlung photon is determined by the polar angle θ and the azimuthal angle ϕ. For isotropic media, with randomly oriented atoms, the bremsstrahlung differential cross section is independent of ϕ and can be expressed as

$$\frac{d^2\sigma}{dW\, d\cos\theta} \;=\; \frac{d\sigma}{dW} p(Z, E, \kappa; \cos\theta).$$

Numerical values of the "shape function" $p(Z, E, \kappa; \cos\theta)$, calculated by partial-wave methods, have been published in Ref. *[16]* for the following benchmark cases: Z= 2, 8, 13, 47, 79 and 92; E= 1, 5, 10, 50, 100 and 500 keV; κ= 0, 0.6, 0.8 and 0.95. It was found in Ref. *[3]* that the benchmark partial-wave shape function of Ref. *[16]* can be closely approximated by the analytical form (obtained in the Lorentz-dipole approximation)

$$p(\cos\theta) = A\frac{3}{8}\Big[1 + \Big(\frac{\cos\theta - \beta'}{1 - \beta'\cos\theta}\Big)^2\Big]\frac{1 - \beta'^2}{(1 - \beta'\cos\theta)^2}$$
$$+(1 - A)\frac{3}{4}\Big[1 - \Big(\frac{\cos\theta - \beta'}{1 - \beta'\cos\theta} m\Big)^2\Big]\frac{1 - \beta'^2}{(1 - \beta'\cos\theta)^2},$$

with $\beta' = \beta(1 + B)$, if one considers A and B as adjustable parameters. The parameters A and B have been determined, by least squares fitting, for the 144 combinations of atomic numbers, electron energies and reduced photon energies corresponding to the benchmark shape functions tabulated in *[16]*. The quantities $\ln(AZ\beta)$ and $B\beta$ vary smoothly with Z, β and κ and can be obtained by cubic spline interpolation of their values for the benchmark cases. This permits the fast evaluation of the shape function $p(Z, E, \kappa; \cos\theta)$ for any combination of Z, β and κ. The stopping power $\frac{dE}{dx}$ due to soft bremsstrahlung is calculated by interpolating in E and κ the numerical data of scaled cross sections of Ref. *[17]*. The energy and the direction of the outgoing electron are determined by using energy-momentum balance.

Positrons

The radiative differential cross section $\frac{d\sigma^+}{dW}(E)$ for positrons reduces to that for electrons in the high-energy limit, but is smaller for intermediate and low energies. Owing to the lack of more accurate calculations, the differential

cross section for positrons is obtained by multiplying the electron differential cross section $\frac{d\sigma^-}{dW}(E)$ by a $\kappa-$indendent factor, i.e.

$$\frac{d\sigma^+}{dW} \;=\; F_p(Z,E)\frac{d\sigma^-}{dW}.$$

The factor $F_p(Z,E)$ is set equal to the ratio of the radiative stopping powers for positrons and electrons, which has been calculated in Ref. *[18]*. For the actual calculation, the following analytical approximation is used:

$$\begin{aligned} F_p(Z,E) \;=\; 1-\exp(&-1.2359\cdot 10^{-1}t + 6.1274\cdot 10^{-2}t^2 - 3.1516\cdot 10^{-2}t^3 \\ &+7.7446\cdot 10^{-3}t^4 - 1.0595\cdot 10^{-3}t^5 + 7.0568\cdot 10^{-5}t^6 \\ &-1.8080\cdot 10^{-6}t^7), \end{aligned}$$

where

$$t \;=\; \ln\Big(1+\frac{10^6}{Z^2}\frac{E}{m_ec^2}\Big).$$

Because the factor $F_p(Z,E)$ is independent on κ, the energy distribution of the secondary γ's has the same shape as electron bremsstrahlung. Similarly, owing to the lack of numerical data for positrons, it is assumed that the shape of the angular distribution $p(Z,E,\kappa;\cos\theta)$ of the bremsstrahlung photons for positrons is the same as for the electrons. The energy and direction of the outgoing positron are determined from energy-momentum balance.

Ionisation

The G4PenelopeIonisation class calculates the continuous energy loss due to electron and positron ionisation and simulates the δ-ray production by electrons and positrons. The electron production threshold T_c for a given material is used to separate the continuous and the discrete parts of the process. The simulation of inelastic collisions of electrons and positrons is performed on the basis of a Generalized Oscillation Strength (GOS) model (see Ref. *[3]* for a complete description). It is assumed that GOS splits into contributions from the different atomic electron shells.

Electrons

The total cross section $\sigma^-(E)$ for the inelastic collision of electrons of energy E is calculated analytically. It can be split into contributions from distant longitudinal, distant transverse and close interactions,

$$\sigma^-(E) \;=\; \sigma_{dis,l} + \sigma_{dis,t} + \sigma^-_{clo}.$$

The contributions from distant longitudinal and transverse interactions are

$$\sigma_{dis,l} \;=\; \frac{2\pi e^4}{m_ev^2}\sum_{shells} f_k\frac{1}{W_k}\ln\Big(\frac{W_k}{Q_k^{min}}\,\frac{Q_k^{min}+2m_ec^2}{W_k+2m_ec^2}\Big)\Theta(E-W_k)$$

and

$$\sigma_{dis,t} \;=\; \frac{2\pi e^4}{m_ev^2}\sum_{shells} f_k\frac{1}{W_k}\Big[\ln\Big(\frac{1}{1-\beta^2}\Big)-\beta^2-\delta_F\Big]\Theta(E-W_k)$$

respectively, where: m_e = mass of the electron; v = velocity of the electron; β = velocity of the electron in units of c; f_k = number of electrons in the k-th atomic shell; Θ = Heaviside step function; W_k = resonance energy of the k-th atomic shell oscillator; Q_k^{min} = minimum kinematically allowed recoil energy for energy transfer W_k

$$= \sqrt{\Big[\sqrt{E(E+2m_ec^2)}-\sqrt{(E-W_k)(E-W_k+2m_ec^2)}\Big]^2+m_e^2c^4}-m_ec^2;$$

δ_F = Fermi density effect correction, computed as described in Ref. *[19]*. The value of W_k is calculated from the ionisation energy U_k of the k-th shell as . This relation is derived from the hydrogenic model, which is valid for the innermost shells. In this model, the shell ionisation cross sections are only roughly approximated; nevertheless the ionisation of inner shells is a low-probability process and the approximation has a weak effect on the global transport properties [1]. The integrated cross section for close collisions is the Møller cross section

$$\sigma^-_{clo} \;=\; \frac{2\pi e^4}{m_e v^2}\sum_{shells} f_k \int_{W_k}^{\frac{E}{2}} \frac{1}{W^2} F^-(E,W)dW,$$

where

$$F^-(E,W) \;=\; 1+\Big(\frac{W}{E-W}\Big)^2 - \frac{W}{E-W} + \Big(\frac{E}{E+m_e c^2}\Big)^2\Big(\frac{W}{E-W}+\frac{W^2}{E^2}\Big).$$

The integral of Eq.([close]) can be evaluated analytically. In the final state there are two indistinguishable free electrons and the fastest one is considered as the "primary"; accordingly, the maximum allowed energy transfer in close collisions is $\frac{E}{2}$. The GOS model also allows evaluation of the spectrum $\frac{d\sigma^-}{dW}$ of the energy W lost by the primary electron as the sum of distant longitudinal, distant transverse and close interaction contributions,

$$\frac{d\sigma^-}{dW} \;=\; \frac{d\sigma^-_{clo}}{dW} + \frac{d\sigma_{dis,l}}{dW} + \frac{d\sigma_{dis,t}}{dW}.$$

In particular,

$$\frac{d\sigma_{dis,l}}{dW} \;=\; \frac{2\pi e^4}{m_e v^2}\sum_{shells} f_k \frac{1}{W_k}\ln\Big(\frac{W_k}{Q_-}\,\frac{Q_-+2m_e c^2}{W_k+2m_e c^2}\Big)\delta(W-W_k)\Theta(E-W_k),$$

where

$$Q_- \;=\; \sqrt{\Big[\sqrt{E(E+2m_e c^2)}-\sqrt{(E-W)(E-W+2m_e c^2)}\Big]^2 + m_e^2 c^4} - m_e c^2,$$

$$\frac{d\sigma_{dis,t}}{dW} \;=\; \frac{2\pi e^4}{m_e v^2}\sum_{shells} f_k \frac{1}{W_k}\Big[\ln\Big(\frac{1}{1-\beta^2}\Big)-\beta^2-\delta_F\Big] \Theta(E-W_k)\delta(W-W_k)$$

and

$$\frac{d\sigma^-_{clo}}{dW} \;=\; \frac{2\pi e^4}{m_e v^2}\sum_{shells} f_k \frac{1}{W^2} F^-(E,W)\Theta(W-W_k).$$

Eqs. ([dist1]), ([dist2]) and ([close]) derive respectively from the integration in dW of Eqs. ([ddist1]), ([ddist2]) and ([dclose]) in the interval [0,:math:*(W_{max})*], where $W_{max} = E$ for distant interactions and $W_{max} = \frac{E}{2}$ for close. The analytical GOS model provides an accurate *average* description of inelastic collisions. However, the continuous energy loss spectrum associated with single distant excitations of a given atomic shell is approximated as a single resonance (a δ distribution). As a consequence, the simulated energy loss spectra show unphysical narrow peaks at energy losses that are multiples of the resonance energies. These spurious peaks are automatically smoothed out after multiple inelastic collisions. The explicit expression of $\frac{d\sigma^-}{dW}$, Eq. ([aaa]), allows the analytic calculation of the partial cross sections for soft and hard ionisation events, i.e.

$$\sigma^-_{soft} \;=\; \int_0^{T_c} \frac{d\sigma^-}{dW}dW \quad \text{and} \quad \sigma^-_{hard} \;=\; \int_{T_c}^{W_{max}} \frac{d\sigma^-}{dW}dW.$$

The first stage of the simulation is the selection of the active oscillator k and the oscillator branch (distant or close). In distant interactions with the k-th oscillator, the energy loss W of the primary electron corresponds to the excitation

energy W_k, i.e. W=W_k. If the interaction is transverse, the angular deflection of the projectile is neglected, i.e. $\cos\theta$=1. For longitudinal collisions, the distribution of the recoil energy Q is given by

$$P_k(Q) = \begin{cases} \frac{1}{Q[1+Q/(2m_ec^2)]} & \text{if } Q_- < Q < W_{max} \\ 0 & \text{otherwise} \end{cases}$$

Once the energy loss W and the recoil energy Q have been sampled, the polar scattering angle is determined as

$$\cos\theta \;=\; \frac{E(E+2m_ec^2)+(E-W)(E-W+2m_ec^2)-Q(Q+2m_ec^2)}{2\sqrt{E(E+2m_ec^2)(E-W)(E-W+2m_ec^2)}}.$$

The azimuthal scattering angle ϕ is sampled uniformly in the interval (0,2:math:*(pi)*). For close interactions, the distributions for the reduced energy loss $\kappa \equiv W/E$ for electrons are

$$P_k^-(\kappa) \;=\; \Big[\frac{1}{\kappa^2}+\frac{1}{(1-\kappa)^2}-\frac{1}{\kappa(1-\kappa)}+\Big(\frac{E}{E+m_ec^2}\Big)^2\Big(1+\frac{1}{\kappa(1-\kappa)}\Big)\Big] \\ \Theta(\kappa-\kappa_c)\Theta(\frac{1}{2}-\kappa)$$

with $\kappa_c = \max(W_k, T_c)/E$. The maximum allowed value of κ is 1/2, consistent with the indistinguishability of the electrons in the final state. After the sampling of the energy loss $W = \kappa E$, the polar scattering angle θ is obtained as

$$\cos^2\theta \;=\; \frac{E-W}{E}\,\frac{E+2m_ec^2}{E-W+2m_ec^2}.$$

The azimuthal scattering angle ϕ is sampled uniformly in the interval (0,2:math:*(pi)*). According to the GOS model, each oscillator W_k corresponds to an atomic shell with f_k electrons and ionisation energy U_k. In the case of ionisation of an inner shell i (K or L), a secondary electron (δ-ray) is emitted with energy $E_s = W - U_i$ and the residual ion is left with a vacancy in the shell (which is then filled with the emission of fluorescence x-rays and/or Auger electrons). In the case of ionisation of outer shells, the simulated δ-ray is emitted with kinetic energy $E_s = W$ and the target atom is assumed to remain in its ground state. The polar angle of emission of the secondary electron is calculated as

$$\cos^2\theta_s \;=\; \frac{W^2/\beta^2}{Q(Q+2m_ec^2)}\Big[1+\frac{Q(Q+2m_ec^2)-W^2}{2W(E+m_ec^2)}\Big]^2$$

(for close collisions $Q = W$), while the azimuthal angle is $\phi_s = \phi + \pi$. In this model, the Doppler effects on the angular distribution of the δ rays are neglected. The stopping power due to soft interactions of electrons, which is used for the computation of the continuous part of the process, is analytically calculated as

$$S_{in}^- \;=\; N\int_0^{T_c} W\frac{d\sigma^-}{dW}dW$$

from the expression ([aaa]), where N is the number of scattering centers (atoms or molecules) per unit volume.

Positrons

The total cross section $\sigma^+(E)$ for the inelastic collision of positrons of energy E is calculated analytically. As in the case of electrons, it can be split into contributions from distant longitudinal, distant transverse and close interactions,

$$\sigma^+(E) \;=\; \sigma_{dis,l} + \sigma_{dis,t} + \sigma_{clo}^+.$$

The contributions from distant longitudinal and transverse interactions are the same as for electrons, Eq. ([dist1]) and ([dist2]), while the integrated cross section for close collisions is the Bhabha cross section

$$\sigma_{clo}^+ \;=\; \frac{2\pi e^4}{m_ev^2}\sum_{shells} f_k\int_{W_k}^{E}\frac{1}{W^2}F^+(E,W)dW,$$

where

$$F^+(E,W) = 1 - b_1\frac{W}{E} + b_2\frac{W^2}{E^2} - b_3\frac{W^3}{E^3} + b_4\frac{W^4}{E^4};$$

the Bhabha factors are

$$b_1 = \left(\frac{\gamma-1}{\gamma}\right)^2 \frac{2(\gamma+1)^2-1}{\gamma^2-1} \quad b_2 = \left(\frac{\gamma-1}{\gamma}\right)^2 \frac{3(\gamma+1)^2+1}{(\gamma+1)^2},$$
$$b_3 = \left(\frac{\gamma-1}{\gamma}\right)^2 \frac{2(\gamma-1)\gamma}{(\gamma+1)^2}, \qquad b_4 = \left(\frac{\gamma-1}{\gamma}\right)^2 \frac{(\gamma-1)^2}{(\gamma+1)^2},$$

and γ is the Lorentz factor of the positron. The integral of Eq. ([closepos]) can be evaluated analytically. The particles in the final state are not undistinguishable so the maximum energy transfer W_{max} in close collisions is E. As for electrons, the GOS model allows the evaluation of the spectrum $\frac{d\sigma^+}{dW}$ of the energy W lost by the primary positron as the sum of distant longitudinal, distant transverse and close interaction contributions,

$$\frac{d\sigma^+}{dW} = \frac{d\sigma^+_{clo}}{dW} + \frac{d\sigma_{dis,l}}{dW} + \frac{d\sigma_{dis,t}}{dW},$$

where the distant terms $\frac{d\sigma_{dis,l}}{dW}$ and $\frac{d\sigma_{dis,t}}{dW}$ are those from Eqs. ([ddist1]) and ([ddist2]), while the close contribution is

$$\frac{d\sigma^+_{clo}}{dW} = \frac{2\pi e^4}{m_e v^2}\sum_{shells} f_k \frac{1}{W^2} F^+(E,W)\Theta(W-W_k).$$

Also in this case, the explicit expression of $\frac{d\sigma^+}{dW}$, Eq. ([bbb]), allows an analytic calculation of the partial cross sections for soft and hard ionisation events, i.e.

$$\sigma^+_{soft} = \int_0^{T_c} \frac{d\sigma^+}{dW} dW \quad \text{and} \quad \sigma^+_{hard} = \int_{T_c}^{E} \frac{d\sigma^+}{dW} dW.$$

The sampling of the final state in the case of distant interactions (transverse or longitudinal) is performed in the same way as for primary electrons, see section [ionelect]. For close positron interactions with the k-th oscillator, the distribution for the reduced energy loss $\kappa \equiv W/E$ is

$$P^+_k(\kappa) = \left[\frac{1}{\kappa^2} - \frac{b_1}{\kappa} + b_2 - b_3\kappa + b_4\kappa^2\right]\Theta(\kappa-\kappa_c)\Theta(1-\kappa)$$

with $\kappa_c = \max(W_k, T_c)/E$. In this case, the maximum allowed reduced energy loss κ is 1. After sampling the energy loss $W = \kappa E$, the polar angle θ and the azimuthal angle ϕ are obtained using the equations introduced for electrons in section [ionelect]. Similarly, the generation of δ rays is performed in the same way as for electrons. Finally, the stopping power due to soft interactions of positrons, which is used for the computation of the continuous part of the process, is analytically calculated as

$$S^+_{in} = N\int_0^{T_c} W\frac{d\sigma^+}{dW} dW$$

from the expression ([bbb]), where N is the number of scattering centers per unit volume.

Positron Annihilation

Total Cross Section

The total cross section (per target electron) for the annihilation of a positron of energy E into two photons is evaluated from the analytical formula *[1]*[egs]

$$\sigma(E) = \frac{\pi r_e^2}{(\gamma+1)(\gamma^2-1)} \times$$
$$\left\{(\gamma^2+4\gamma+1)\ln\left[\gamma+\sqrt{\gamma^2-1}\right] - (3+\gamma)\sqrt{\gamma^2-1}\right\}.$$

where r_e = classical radius of the electron, and γ = Lorentz factor of the positron.

Sampling of the Final State

The target electrons are assumed to be free and at rest: binding effects, that enable one-photon annihilation *[1]*, are neglected. When the annihilation occurs in flight, the two photons may have different energies, say E_- and E_+ (the photon with lower energy is denoted by the superscript "$-$"), whose sum is $E + 2m_ec^2$. Each annihilation event is completely characterized by the quantity

$$\zeta = \frac{E_-}{E + 2m_ec^2},$$

which is in the interval $\zeta_{min} \leq \zeta \leq \frac{1}{2}$, with

$$\zeta_{min} = \frac{1}{\gamma + 1 + \sqrt{\gamma^2 - 1}}.$$

The parameter ζ is sampled from the differential distribution

$$P(\zeta) = \frac{\pi r_e^2}{(\gamma + 1)(\gamma^2 - 1)}[S(\zeta) + S(1 - \zeta)],$$

where γ is the Lorentz factor and

$$S(\zeta) = -(\gamma + 1)^2 + (\gamma^2 + 4\gamma + 1)\frac{1}{\zeta} - \frac{1}{\zeta^2}.$$

From conservation of energy and momentum, it follows that the two photons are emitted in directions with polar angles

$$\cos\theta_- = \frac{1}{\sqrt{\gamma^2 - 1}}\left(\gamma + 1 - \frac{1}{\zeta}\right)$$

and

$$\cos\theta_+ = \frac{1}{\sqrt{\gamma^2 - 1}}\left(\gamma + 1 - \frac{1}{1 - \zeta}\right)$$

that are completely determined by ζ; in particuar, when $\zeta = \zeta_{min}$, $\cos\theta_- = -1$. The azimuthal angles are ϕ_- and $\phi_+ = \phi_- + \pi$; owing to the axial symmetry of the process, the angle ϕ_- is uniformly distributed in $(0, 2\pi)$.

4.2.12 Photoelectric effect

Three model classes are available *G4LivermorePhotoElectricModel G4LivermorePolarizedPhotoElectricModel*, and *G4LivermorePolarizedPhotelectricGDModel*.

Cross sections

The total photoelectric and single shell cross-sections are tabulated from threshold to $600keV$. Above $600keV$ EPDL97 cross sections *[1]* are parameterized as following:

$$\sigma(E) = \frac{a_1}{E} + \frac{a_2}{E^2} + \frac{a_3}{E^3} + \frac{a_4}{E^4} + \frac{a_5}{E^5}.$$

The accuracy of such parameterisation is better than 1%. To avoid tracking problems for very low-energy gamma the photoelectric cross section is not zero below first ionisation potential but stay constant, so all types of media are not transparant for gamma.

Sampling of the final state

The incident photon is absorbed and an electron is emitted.

The electron kinetic energy is the difference between the incident photon energy and the binding energy of the electron before the interaction. The sub-shell, from which the electron is emitted, is randomly selected according to the relative cross-sections of all subshells, determined at the given energy. The interaction leaves the atom in an excited state. The deexcitation of the atom is simulated as described in section [relax].

Angular distribution of the emitted photoelectron

For sampling of the direction of the emitted photoelectron by default the angular generator *G4SauterGavrilaAngularDistribution* is used. The algorithm is described in [sec:em.pee].

For polarized models alternative angular generators are applied.

G4LivermorePolarizedPhotoElectricModel uses the *G4PhotoElectricAngularGeneratorPolarized* angular generator.

This model models the double differential cross section (for angles θ and ϕ) and thus it is capable of account for polarization of the incident photon. The developed generator was based in the research of Sauter in 1931 *[2][3]*. Sauter's formula was recalculated by Gavrila in 1959 for the K-shell *[4]* and in 1961 for the L-shells *[5]*. These new double differential formulas have some limitations, αZ<<1 and have a range between 0.1< β <0.99 c.

The double differential photoeffect for K–shell can be written as *[4]*:

$$\frac{d\sigma}{d\omega}(\theta,\phi) = \frac{4}{m^2}\alpha^6 Z^5 \frac{\beta^3(1-\beta^2)^3}{\left[1-(1-\beta^2)^{1/2}\right]}\left(F\left(1-\frac{\pi\alpha Z}{\beta}\right)+\pi\alpha Z G\right)$$

where

$$\begin{aligned} F = & \frac{\sin^2\theta\cos^2\phi}{(1-\beta\cos\theta)^4} - \frac{1-(1-\beta^2)^{1/2}}{2(1-\beta^2)}\frac{\sin^2\theta\cos^2\phi}{(1-\beta\cos\theta)^3} \\ & + \frac{\left[1-(1-\beta^2)^{1/2}\right]^2}{4(1-\beta^2)^{3/2}}\frac{\sin^2\theta}{(1-\beta\cos\theta)^3} \end{aligned}$$

$$\begin{aligned} G = & \frac{[1-(1-\beta^2)^{1/2}]^{1/2}}{2^{7/2}\beta^2(1-\beta\cos\theta)^{5/2}}\left[\frac{4\beta^2}{(1-\beta^2)^{1/2}}\frac{\sin^2\theta\cos^2\phi}{1-\beta\cos\theta}+\frac{4\beta}{1-\beta^2}\cos\theta\cos^2\phi-\right. \\ & - 4\,\frac{1-(1-\beta^2)^{1/2}}{1-\beta^2}(1-\cos^2\phi) - \beta^2\,\frac{1-(1-\beta^2)^{1/2}}{1-\beta^2}\frac{\sin^2\theta}{1-\beta\cos\theta}- \\ & \left. + 4\beta^2\frac{1-(1-\beta^2)^{1/2}}{(1-\beta^2)^{3/2}} - 4\beta\frac{\left[1-(1-\beta^2)^{1/2}\right]^2}{(1-\beta^2)^{3/2}}\right] \\ & + \frac{1-(1-\beta^2)^{1/2}}{4\beta^2(1-\beta\cos\theta)^2}\left[\frac{\beta}{1-\beta^2} - \frac{2}{1-\beta^2}\cos\theta\cos^2\phi + \frac{1-(1-\beta^2)^{1/2}}{(1-\beta^2)^{3/2}}\cos\theta\right. \\ & \left. - \beta\frac{1-(1-\beta^2)^{1/2}}{(1-\beta^2)^{3/2}}\right] \end{aligned}$$

where β is the electron velocity, α is the fine–structure constant, Z is the atomic number of the material and θ, ϕ are the emission angles with respect to the electron initial direction.

The double differential photoeffect distribution for L1–shell is the same as for K–shell despising a constant *[5]*:

$$B = \xi\frac{1}{8}$$

where ξ is equal to 1 when working with unscreened Coulomb wave functions as it is done in this development.

Since the polarized Gavrila cross–section is a 2–dimensional non–factorized distribution an acceptance–rejection technique was the adopted *[6]*. For the Gravrila distribution, two functions were defined $g_1(\phi)$ and $g_2(\theta)$:

$$g_1(\phi) = a$$
$$g_2(\theta) = \frac{\theta}{1 + c\theta^2}$$

such that:

$$Ag_1(\phi)g_2(\theta) \geq \frac{d^2\sigma}{d\phi d\theta}$$

where A is a global constant. The method used to calculate the distribution is the same as the one used in Low Energy 2BN Bremsstrahlung Generator, being the difference $g_1(\phi) = a$.

G4LivermorePolarizedPhotoElectricGDModel uses its own methods to produce the angular distribution of the photoelectron. The method to sample the azimuthal angle ϕ is described in *[7]*.

4.2.13 PIXE

PIXE data

4.2.14 Compton Scattering by Linearly Polarized Gamma Rays

The Cross Section

The quantum mechanical Klein - Nishina differential cross section for polarized photons is *[1]*:

$$\frac{d\sigma}{d\Omega} = \frac{1}{2} r_0^2 \frac{h\nu^2}{h\nu_o^2} \left[\frac{h\nu_o}{h\nu} + \frac{h\nu}{h\nu_o} - sin^2\Theta \right]$$

where Θ is the angle between the two polarization vectors. In terms of the polar and azimuthal angles (θ, ϕ) this cross section can be written as

$$\frac{d\sigma}{d\Omega} = \frac{1}{2} r_0^2 \frac{h\nu^2}{h\nu_o^2} \left[\frac{h\nu_o}{h\nu} + \frac{h\nu}{h\nu_o} - 2cos^2\phi sin^2\theta \right]$$

.

Angular Distribution

The integration of this cross section over the azimuthal angle produces the standard cross section. The angular and energy distribution are then obtained in the same way as for the standard process. Using these values for the polar angle and the energy, the azimuthal angle is sampled from the following distribution:cite:*Depaola*:

$$P(\phi) = 1 - 2\frac{a}{b} cos^2\phi$$

where $a = sin^2\theta$ and $b = \epsilon + 1/\epsilon$. ϵ is the ratio between the scattered photon energy and the incident photon energy.

Polarization Vector

The components of the vector polarization of the scattered photon are calculated from (*[2]*):

$$\vec{\epsilon_\perp'} = \frac{1}{N} \left(\hat{j} cos\theta - \hat{k} sin\theta sin\phi \right) sin\beta$$

$$\vec{\epsilon_{\parallel}} = \left[N\hat{i} - \frac{1}{N}\hat{j}sin^2\theta sin\phi cos\phi - \frac{1}{N}\hat{k}sin\theta cos\theta cos\phi\right] cos\beta$$

where

$$N = \sqrt{1 - sin^2\theta cos^2\phi}.$$

$cos\beta$ is calculated from $cos\Theta = Ncos\beta$, while $cos\Theta$ is sampled from the Klein - Nishina distribution.

The binding effects and the Compton profile are neglected. The kinetic energy and momentum of the recoil electron are then

$$T_{el} = E - E'$$

$$\vec{P_{el}} = \vec{P_{\gamma}} - \vec{P'_{\gamma}}.$$

The momentum vector of the scattered photon $\vec{P_{\gamma}}$ and its polarization vector are transformed into the World coordinate system. The polarization and the direction of the scattered gamma in the final state are calculated in the reference frame in which the incoming photon is along the z-axis and has its polarization vector along the x-axis. The transformation to the World coordinate system performs a linear combination of the initial direction, the initial poalrization and the cross product between them, using the projections of the calculated quantities along these axes.

Unpolarized Photons

A special treatment is devoted to unpolarized photons. In this case a random polarization in the plane perpendicular to the incident photon is selected.

4.2.15 Pair production by Linearly Polarized Gamma Rays

A method to study the pair production interaction of linearly polarized gamma rays at energies > 50 MeV was discussed in *[1]*. The study of the differential cross section for pair production shows that the polarization information is coded in the azimuthal distribution of the electron - positron pair created by polarized photons (Fig.[fig1]).

Relativistic cross section for linearly polarized gamma ray

The cross section for pair production by linearly polarized gamma rays in the high energy limit using natural units with $h/2\pi = c = 1$ is

$$\begin{aligned} d\sigma = \quad & \frac{-2\alpha Z^2 r_0 m^2}{(2\pi)^2\omega^3} dE d\Omega_+ d\Omega_- \frac{E(\omega - E)}{|\vec{q}|^4} \left\{ 4\left[E\frac{\sin\theta_- \cos\Psi}{1-\cos\theta_-} + (\omega - E)\frac{\sin\theta_+ \cos(\Psi+\phi)}{1-\cos\theta_+}\right]^2 \right. \\ & -|\vec{q}|^2 \left[\frac{\sin\theta_- \cos\Psi}{1-\cos\theta_-} - \frac{\sin\theta_+ \cos(\Psi+\phi)}{1-\cos\theta_+}\right]^2 \\ & \left. -\omega^2 \frac{\sin\theta_- \sin\theta_+}{(1-\cos\theta_-)(1-\cos\theta_+)} \left[\frac{E\sin\theta_+}{(\omega_E)\sin\theta_-} + \frac{(\omega - E)\sin\theta_-}{E\sin\theta_+} + 2\cos\phi\right]\right\} , \end{aligned}$$

with

$$\begin{aligned} |\vec{q}|^2 = \quad & -2\left[E(\omega - E)(1 - \sin\theta_+ \sin\theta_- \cos\phi - \cos\theta_+ \cos\theta_-)\right. \\ & \left. +\omega E(\cos\theta_+ - 1) + \omega(\omega - E)(cos\theta_- - 1) + m^2\right] . \end{aligned}$$

E is the positron energy and we have assumed that the polarization direction is along the x axis (see Fig.[fig1]).

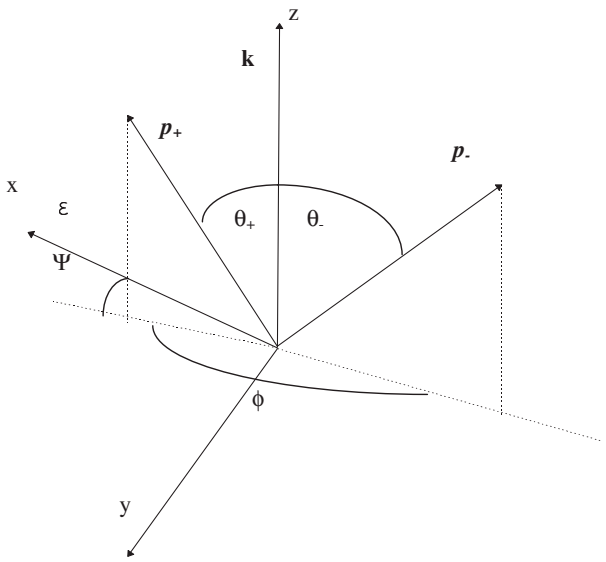

Fig. 4.1: Angles occurring in the pair creation

Spatial azimuthal distribution

Integrating this cross section over energy and polar angles yields the spatial azimuthal distribution, that was calculated in *[1]* using a Monte Carlo procedure.

Fig. [fig2] shows an example of this distribution for 100 MeV gamma - ray. In this figure the range of the ϕ axis is restricted between 3.0 and π since it gives the most interesting part of the distribution. For angles smaller than 3.0 this distribution monotonically decreases to zero.

In Geant4 the azimuthal distribution surface is parametrized in terms of smooth functions of (ϕ, ψ) .

$$f(\phi, \psi) = f_{\pi/2}(\phi) \sin^2 \psi + f_0(\phi) \cos^2 \psi \ .$$

Since both $f_0(\phi)$ and $f_{\pi/2}(\phi)$ are functions that rapidly vary when ϕ approaches π, it was necessary to adjust the functions in two ranges of ϕ: (I) $0 \leq \phi \leq 3.05$ rad. (II) 3.06 rad $\leq \phi \leq \pi$, whereas in the small range $3.05 \leq \phi \leq 3.06$ we extrapolate the two fitting functions until the intersection point is reached.

In region II we used Lorentzian functions of the form

$$f(\phi) = y_0 + \frac{2A\omega}{\pi[\omega^2 + 4(\phi - x_c)^2]} \ ,$$

whereas for region I the best fitting function was found to adopt the form:

$$f(\phi) = a + d \tan{(b\phi + c)} \ .$$

The paper *[1]* reports the coefficients obtained in different energy regions to fit the angular distribution and their function form as function of gamma-ray as energy reported in the tables[tabla2] and [tabla3] below.

Table: Fit for the parameter of $f_0(\phi)$ function.

[tabla2]

Table: Fit for the parameter of $f_{\pi/2}(\phi)$ function.

[tabla3]

Unpolarized Photons

A special treatment is devoted to unpolarized photons. In this case a random polarization in the plane perpendicular to the incident photon is selected.

4.2.16 Rayleigh Scattering

Total Cross Section

The total cross section for the Rayleigh scattering process is determined from the data as described in section [subsub-sigmatot].

Sampling of the Final State

The coherent scattered photon angle θ is sampled according to the distribution obtained from the product of the Rayleigh formula $(1 + \cos^2 \theta) \sin \theta$ and the square of Hubbel's form factor $FF^2(q)$ *[1] [2]*

$$\Phi(E, \theta) = [1 + \cos^2 \theta] \sin \theta \times FF^2(q),$$

where $q = 2E \sin(\theta/2)$ is the momentum transfer.

Form factors introduce a dependency on the initial energy E of the photon that is not taken into account in the Rayleigh formula. At low energies, form factors are isotropic and do not affect angular distribution, while at high energies they are forward peaked. For effective sampling of final state a method proposed by D.E. Cullen *[2]* has been implemented: form factor data were fitted and fitted parameters included in the *G4LivermoreRayleighModel*.

The sampling procedure is following:

1. atom is selected randomly according to cross section;
2. $cos\theta$ is sampled as proposed in *[2]*;
3. azimuthal angle is sampled uniformly.

4.2.17 Atomic relaxation

Atomic relaxation processes can be induced by any ionisation process that leaves the interested atom in an excited state (i.e. with a vacancy in its electronic structure). Processes inducing atomic relaxation in Geant4 are photoelectric effect, Compton and ionization (both Standard and Lowenergy).

Geant4 uses the Livermore Evaluation Atomic Data Library EADL *[1]*, that contains data to describe the relaxation of atoms back to neutrality after they are ionised. It is assumed that the binding energy of all subshells (from now on shells are the same for neutral ground state atoms as for ionised atoms *[1]*).

Data in EADL includes the radiative and non-radiative transition probabilities for each sub-shell of each element, for Z=1 to 100. The atom has been ionised by a process that has caused an electron to be ejected from an atom, leaving a vacancy or "hole" in a given subshell. The EADL data are then used to calculate the complete radiative and non-radiative spectrum of X-rays and electrons emitted as the atom relaxes back to neutrality.

Non-radiative de-excitation can occur via the Auger effect (the initial and secondary vacancies are in different shells) or Coster-Kronig effect (transitions within the same shell).

Fluorescence

The simulation procedure for the fluorescence process is the following:

1. If the vacancy shell is not included in the data, energy equal to the binding energy of the shell is deposited locally
2. If the vacancy subshell is included in the data, an outer subshell is randomly selected taking into account the relative transition probabilities for all possible outer subshells.
3. In the case where the energy corresponding to the selected transition is larger than a user defined cut value (equal to zero by default), a photon particle is created and emitted in a random direction in 4π, with an energy equal to the transition energy, provided by EADL.
4. the procedure is repeated from step 1, for the new vacancy subshell.

The final local energy deposit is the difference between the binding energy of the initial vacancy subshell and the sum of all transition energies which were taken by fluorescence photons. The atom is assumed to be initially ionised with an electric charge of $+1e$.

Sub-shell data are provided in the EADL data bank *[1]* for Z=1 through 100. However, transition probabilities are only explicitly included for Z=6 through 100, from the subshells of the K, L, M, N shells and some O subshells. For subshells O,P,Q: transition probabilities are negligible (of the order of 0.1%) and smaller than the precision with which they are known. Therefore, for the time being, for Z=1 through 5, only a local energy deposit corresponding to the binding energy B of an electron in the ionised subshell is simulated. For subshells of the O, P, and Q shells, a photon is emitted with that energy B.

Auger process

The Auger effect is complimentary to fluorescence, hence the simulation process is the same as for the fluorescence, with the exception that two random shells are selected, one for the transition electron that fills the original vacancy, and the other for selecting the shell generating the Auger electron.

Subshell data are provided in the EADL data bank *[1]* for $Z = 6$ through 100. Since in EADL no data for elements with $Z < 5$ are provided, Auger effects are only considered for $5 < Z < 100$ and always due to the EADL data tables, only for those transitions which have a probabiliy to occur $> 0.1\%$ of the total non-radiative transition probability. EADL probability data used are, however, normalized to one for Fluorescence + Auger.

PIXE

PIXE (Particle Induced X-Ray Emission) can be simulated for ionisation continuous processes perfomed by ions. Ionised shells are selected randomly according the ionisation cross section of each shell once known the (continuous) energy loss along the step [en_loss].

Different shell ionisation cross sections models are available in different energy ranges:

- ECPSSR:cite:*ecpssrK*,:cite:*ecpssrL* internal Geant4 calculation for K and L shells.
- ECPSSR calculations from Factor Form according to Reis:cite:*reis* for K and L shells from 0.1 to 100 MeV and for M shells from 0.1 to 10 MeV.
- empirical "reference" K-shell values from Paul for protons:cite:*PaulP* and for for alphas:cite:*PaulAlpha*. Energies ranges are 0.1 - 10 MeV/amu circa, depending on the atomic number that varies between 4 and 32.
- semi-empirical L-subshell values from Orlic:cite:*orlic_semiemp*. Energy Range 0.1-10 MeV for Z between 41 and 92.

Otside Z and energy of limited shell ionisation cross sections, the ECPSSR internal calculation method is applied.

Please refer to ref.:cite:*mantero* and original papers to have detailed information of every model.

4.2.18 Triple Gamma Conversion

The class *G4BoldyshevTripletModel* was developed to simulate the pair production by linearly polarized gamma rays on electrons For the angular distribution of electron recoil we used the cross section by Vinokurov and Kuraev *[1][2]* using the Borsellino diagrams in the high energy For energy distribution for the pair, we used Boldyshev *[3]* formula that differs only in the normalization from Wheeler-Lamb. The cross sections include a cut off for momentum detections *[4]*.

Method

The first step is sample the probability to have an electron recoil with momentum greater than a threshold define by the user (by default, this value is $p_0 = 1$ in units of mc). This probability is

$$\sigma(p \geq p_0) = \alpha r_0^2 \left(\frac{82}{27} - \frac{14}{9} ln X_0 + \frac{4}{15} X_0 - 0.0348 X_0^2 + 0.008 X_0^3 - ... \right)$$

$$X_0 = 2 \left(\sqrt{p_0^2 +} - 1 \right).$$

Since that total cross section is $\sigma = \alpha r_0^2 \left(\frac{28}{4} ln 2E_\gamma - \frac{218}{27} \right)$, if a random number is $\xi \geq \sigma(p \geq p_0)/\sigma$ we create the electron recoil, otherwise we deposited the energy in the local point.

[le:rayl]

Azimuthal Distribution for Electron Recoil

The expression for the differential cross section is composed of two terms which express the azimuthal dependence as follows:

$$d\sigma = d\sigma^{(t)} - Pd\sigma^{(l)}cos(2\varphi)$$

Where, both $d\sigma_{(t)}$ and $d\sigma_{(l)}$, are independent of the azimuthal angle, φ, referred to an origin chosen in the direction of the polarization vector $\vec{P}$ of the incoming photons.

Monte Carlo Simulation of the Asymptotic Expression

In this section we present an algorithm for Monte Carlo simulation of the asymptotic expressions calculate by Vinokurov et.al. *[1][2]*.

We must generate random values of θ and φ distributed with probability proportional to the following function $f(\theta, \varphi)$, for θ restricted inside of its allowed interval value *[3]* (0, or $\theta_{max}(p_0)$):

$$f\left(\theta,\varphi\right) = \frac{\sin\theta}{\cos^3\theta}\left(F_1\left(\theta\right) - \mathrm{P}\cos\left(2\varphi\right)F_P\left(\theta\right)\right)$$

$$F_1\left(\theta\right) = 1 - \frac{1-5\cos^2\theta}{\cos\theta}\ln\left(\cot\left(\theta/2\right)\right)$$

$$F_P\left(\theta\right) = 1 - \frac{\sin^2\theta}{\cos\theta}\ln\left(\cot\left(\theta/2\right)\right)$$

As we will see, for $\theta < \pi/2$, F_1 is several times greater than F_P, and since both are positive, it follows that f is positive for any possible value of P ($0 \leq P \leq 1$).

Since F_1 is the dominant term in expression , it is more convenient to begin developing the algorithm of this term, belonging to the unpolarized radiation.

Algorithm for Non Polarized Radiation

The algorithm was described in Ref.:cite:*dep*. We must generate random values of θ between 0 and $\theta_{max} = arccos\left(\frac{E_1-mc^2}{p_0} + mc^2\frac{E_1+mc^2}{E_\gamma p_0}\right)$, $E_1 = \sqrt{p_0^2 + (mc^2)^2}$ distributed with probability proportional to the following function $f_1(\theta)$:

$$\begin{aligned} f_1(\theta) &= \frac{\sin(\theta)}{\cos^3(\theta)}\left(1 - \frac{1-5\cos^2(\theta)}{\cos(\theta)}\ln(\cot(\theta/2))\right) \\ &= \frac{\sin(\theta)}{\cos^3(\theta)} \times F_1\left(\theta\right) \end{aligned}$$

By substitution $\cos(\theta/2) = \sqrt{\frac{1+cos\theta}{2}}$ and $\sin(\theta/2) = \sqrt{\frac{1-cos\theta}{2}}$, We can write:

$$\ln\left(\cot\left(\theta/2\right)\right) = \frac{1}{2}\ln\left(\frac{1+\cos\theta}{1-\cos\theta}\right)$$

In order to simulate the f_1 function, it may be decomposed in two factors: the first, $sin(\theta)/cos^3(\theta)$, easy to integrate, and the other, $F_1(\theta)$, which may constitute a reject function, on despite of its $\theta = 0$ divergence. This is possible because they have very low probability. On other hand, θ values near to zero are not useful to measure polarization because for those angles it is very difficult to determine the azimuthal distribution (due to multiple scattering).

Then, it is possible to choose some value of θ_0, small enough that it is not important that the sample is fitted rigorously for $\theta < \theta_0$, and at the same time $F_1(\theta_0)$ is not too big.

Modifying F_1 so that it is constant for $\theta \leq \theta_0$, we may obtain an adequate reject function. Doing this, we introduce only a very few missed points, all of which lie totally outside of the interesting region.

Expanding F_1 for great values of θ, we see it is proportional to $cos^2\theta$:

$$F_1(\theta) \to \frac{14}{3}\cos^2\theta\left(1+\frac{33}{35}\cos^2\theta+\ldots\right), \quad \text{if } \theta \to \pi/2$$

Thus, it is evident that F_1 divided by $cos^2(\theta)$ will be a better reject function, because it tends softly to a some constant value $(14/3 = 4,6666...)$ for large θs, whereas its behavior is not affected in the region of small θs, where $cos(\theta) \to 1$.

It seems adequate to choose θ_0 near 5^0, and, after some manipulation looking for round numbers we obtain:

$$\frac{F_1\left(4.47^0\right)}{\cos^2\left(4.47^0\right)} \cong 14.00$$

Finally we define a reject function:

$$\begin{array}{rcll} r(\theta) & = & \frac{1}{14}\frac{F_1(\theta)}{\cos^2(\theta)} = \frac{1}{14\cos^2(\theta)} & \\ & & \left(1-\frac{1-5\cos^2(\theta)}{2\cos(\theta)}\ln\left(\frac{1+\cos\theta}{1-\cos\theta}\right)\right) & ; \quad \text{for } \theta \geq 4.47^0 \\ r(\theta) & = & 1 & ; \quad \text{for} \theta \leq 4.47^0 \end{array}$$

Now we have a probability distribution function (PDF) for θ, $p(\theta) = Cf_1(\theta)$, expressed as a product of another PDF, $\pi(\theta)$, by the reject function:

$$p(\theta) = Cf_1(\theta) \cong C^{'}\pi(\theta)\, r(\theta)$$

where C is the normalization constant belonging to the function $p(\theta)$.

One must note that the equality between $C \sim f_1(\theta)$ and $C^{'}\pi(\theta)r(\theta)$ is not exact for small values of θ, where we have truncated the infinity of $F_1(\theta)$; but this can not affect appreciably the distribution because $f_1 \to 0$ there. Now the PDF $\pi(\theta)$ is:

$$\pi(\theta) = C_\pi\,\frac{14sin(\theta)}{cos(\theta)}$$

From the normalization, the constant C_π results:

$$C_\pi = \frac{1}{14\int_0^{\theta_{max}}\frac{sin(\theta)}{cos(\theta)}d\theta} = \frac{-1}{14\ln\left(cos(\theta_{max})\right)} = \frac{1}{7}\ln\left(\frac{\omega}{4m}\right)$$

And the relation with C is given by:

$$C = \frac{1}{\int_0^{\theta_{max}} f_1(\theta)d\theta} \cong C'C_\pi$$

Then we obtain the cumulative probability by integrating the PDF $\pi(\theta)$:

$$P_\pi = \int_0^\theta \pi(\theta')d\theta' = \frac{-14\ln(\cos(\theta))}{7\ln\left(\frac{\omega}{4m}\right)} = \frac{2\ln(\cos(\theta))}{\ln\left(4m/\omega\right)}$$

Finally for the Monte Carlo method we sample a random number ξ_1 (between 0 and 1), which is defined as equal to P_π , and obtain the corresponding θ value:

$$\xi_1 = \frac{2\,\ln(\cos\theta)}{\ln\left(4\mathrm{m}/\omega\right)} = \frac{\ln(\cos\theta)}{\ln\left(\cos(\theta_{\max})\right)}$$

Then,

$$\theta = \arccos\left(\left(\frac{4m}{\omega}\right)^{\frac{\xi_1}{2}}\right)$$

Another random number ξ_2 is sampled for the reject process: the θ value is accepted if $\xi_2 \leq r(\theta)$, and reject in the contrary.

For $\theta \leq 4,47^0$ all values are accepted. It happens automatically without any modification in the algorithm previously defined (it is not necessary to define the truncated reject function for $\theta < \theta_0$).

Algorithm for Polarized Radiation

The algorithm was also described in Ref.:cite:*dep*. As we have seen, the azimuthal dependence of the differential cross section is given by the expressions and :

$$f(\theta,\varphi) = \frac{\sin\theta}{\cos^3\theta}\left(F_1(\theta) - \mathrm{P}\cos(2\varphi)\,F_P(\theta)\right)$$

$$F_P(\theta) = 1 - \frac{\sin^2\theta}{\cos\theta}\ln\left(\cot(\theta/2)\right)$$

We see that F_P tends to 1 at $\theta = 0$, decreases monotonically to 0 as θ goes to $\pi/2$.

Furthermore, the expansion of F_P for θ near $\pi/2$ shows that it is proportional to $cos^2(\theta)$, in virtue of which $F_P/cos^2(\theta)$ tends to a non null value, $2/3$. This value is exactly 7 times the value of $F_1/cos^2(\theta)$.

This suggests applying the combination method, rearranging the whole function as follows:

$$f(\theta,\varphi) = \tan(\theta)\frac{F_1(\theta)}{cos^2(\theta)}\left(1 - cos(2\varphi)P\frac{F_P(\theta)}{F_1(\theta)}\right)$$

and the normalized PDF $p(\theta,\varphi)$:

$$p(\theta,\varphi) = Cf(\theta,\varphi)$$

where is C the normalization constant

$$\frac{1}{C} = \int_0^{\theta_{\max}}\int_0^{2\pi} f(\theta,\varphi)\,d\varphi d\theta$$

Taking account that $\int_0^{2\,\pi}\cos(2\varphi)\,d\varphi = 0$, then:

$$\frac{1}{C} = 2\pi\int_0^{\theta_{\max}}\tan(\theta)\frac{F_1(\theta)}{\cos^2(\theta)}d\theta$$

On the other hand the integration over the azimuthal angle is straightforward and gives:

$$q(\theta) = \int_0^{2\pi} p(\theta,\varphi)d\varphi = 2\pi C\tan(\theta)\frac{F_1(\theta)}{cos^2(\theta)}$$

and $p(\varphi/\theta)$ is the conditional probability of φ given θ:

$$\begin{aligned} p(\varphi/\theta) &= \frac{p(\theta,\varphi)}{q(\theta)} = \frac{1}{2\pi C\tan(\theta)\frac{F_1(\theta)}{cos^2(\theta)}}C\frac{sin(\theta)}{cos^3(\theta)}F_1(\theta)\left(1 - cos(2\varphi)P\frac{F_P(\theta)}{F_1(\theta)}\right) \\ &= \frac{1}{2\pi}\left(1 - \cos(2\varphi)P\frac{F_P(\theta)}{F_1(\theta)}\right) \end{aligned}$$

Now the procedure consists of sampling θ according the PDF $q(\theta)$; then, for each value of θ we must sample φ according to the conditional PDF $p(\varphi/\theta)$.

Knowing that F_1 is several times greater than F_P, we can see that P $F_1/F_P << 1$, and thus $p(\varphi/\theta)$ maintains a nearly constant value slightly diminished in some regions of φ. Consequently the φ sample can be done directly by the rejecting method with high efficiency.

On the other hand, $q(\theta)$ is the same function $p(\theta)$ given by , that is the PDF for unpolarized radiation, $q(\theta) \cong C'\pi(\theta)r(\theta)$, so we can sample θ with exactly the same procedure, specified as follows: **1.-** We begin sampling a random number ξ_1 and obtain θ from :

$$\theta = \arccos\left(\left(\frac{4m}{\omega}\right)^{\frac{\xi_1}{2}}\right)$$

2.- Then we sample a second random number $\xi 2$ and accept the values of θ if $\xi_2 \leq r(\theta)$, where $r(\theta)$ is the same expression defined before:

$$\mathrm{r}\,(\theta) = \frac{1}{14\cos^2\theta}\left(1 - \frac{1 - 5\cos^2\theta}{2\cos\theta}\ln\left(\frac{1+\cos\theta}{1-\cos\theta}\right)\right)$$

For $\theta \geq 4,47^0$ and for $\theta \leq 4,47^0$ all values are accepted.

3.- Now we sample φ. According to the reject method, we sample a third random number ξ_3 (which is defined as $\varphi/2\pi$) and evaluate the reject function (which is essentially):

$$r_\theta(\xi_3) = \frac{1}{2\pi}\left(1 - \cos\left(4\pi\xi_3\right)P\frac{F_P\left(\theta\right)}{F_1\left(\theta\right)}\right)$$

$$= \frac{1}{2\pi}\left(1 - \cos(4\pi\xi_3)P\frac{\cos\theta - \sin^2\theta\ln\left(\cot\left(\frac{\theta}{2}\right)\right)}{cos\theta - (1 - 5cos^2\theta)\ln\left(\cot\left(\frac{\theta}{2}\right)\right)}\right)$$

4.- Finally, with a fourth random number ξ_4 , we accept the values of $\varphi = 2\pi\xi_4$ if $\xi_4 \leq r_\theta(\xi_3)$.

Sampling of Energy

For the electron recoil we calculate the energy from the maximum momentum that can take according with the θ angle

$$E_r = mc^2\frac{\left(S + (mc^2)^2\right)}{D2}$$

Where

$$\begin{aligned} S &= mc^2\left(2E_{gamma} + mc^2\right) \\ D2 &= 4Smc^2 + \left(S - (mc^2)^2\right)^2\sin^2(\theta) \end{aligned}$$

The remnant energy is distributed to the pair according to the Boldyshev formula *[3]* (x is the fraction of the positron energy):

$$2\pi\frac{d^2\sigma}{dxd\phi} = 2\alpha r_0^2\left\{\left[1 - 2x\left(1-x\right)\right]J_1(p_0) + 2x\left(1-x\right)\left[1 - P\cos(\phi)\right]J_2(p_0)\right\}$$

$$J_1(p_0) = 2\left(t\frac{\cosh(t)}{\sinh(t)} - ln(2\sinh(t))\right)$$

$$J_2(p_0) = -\frac{2}{3}\ln(2\sinh(t)) + t\frac{\cosh(t)}{\sinh(t)} + \frac{\sinh(t) - t\cosh^3(t)}{3\sinh^3(t)}, \qquad \sinh(2t) = p_0$$

This distribution can by write like a PDF for x:

$$P(x) = N\left(1 - Jx(1-x)\right)$$

where N is a normalization constant and $J = (J_1 - J_2)/J_1$. Solving for x (ξ is a random number):

$$x = \frac{c_1^{1/3}}{2J} + \frac{J-4}{2c_1^{1/3}} + \frac{1}{2}$$

$$\begin{aligned} c_1 &= \left(-6 + 12r_n + J + 2a\right) J^2 \\ a &= \left(\frac{16 - 3J - 36r_n + 36Jr_n^2 + 6r_n J^2}{J}\right) \\ r_n &= \xi\left(1 - \frac{J}{6}\right) \end{aligned}$$

4.3 Miscellaneous

4.3.1 True Step Length

Geant4 simulation of particle transport is performed step by step *[1]*. A *true step length* for a next physics interaction is randomly sampled using the *mean free path* of the interaction or by various *step limitations* established by different Geant4 components. The smallest step limit defines the new true step length.

The Interaction Length or Mean Free Path

Computation of mean free path of a particle in a media is performed in Geant4 using cross section of a particular physics process and density of atoms. In a simple material the number of atoms per volume is:

$$n = \frac{\mathcal{N}\rho}{A}$$

where:

$\mathcal{N}$	Avogadro's number
ρ	density of the medium
A	mass of a mole

In a compound material the number of atoms per volume of the i^{th} element is:

$$n_i = \frac{\mathcal{N}\rho w_i}{A_i}$$

where:

w_i	proportion by mass of the i^{th} element
A_i	mass of a mole of the i^{th} element

The **mean free path** of a process, λ, also called the **interaction length**, can be given in terms of the total cross section:

$$\lambda(E) = \left(\sum_i [n_i \cdot \sigma(Z_i, E)]\right)^{-1}$$

where $\sigma(Z, E)$ is the total cross section per atom of the process and $\sum_i$ runs over all elements composing the material. $\sum_i [n_i\sigma(Z_i, E)]$ is also called the *macroscopic cross section*. The mean free path is the inverse of the macroscopic cross section.

Cross sections per atom and mean free path values may be tabulated during initialisation.

Determination of the Interaction Point

The mean free path, λ, of a particle for a given process depends on the medium and cannot be used directly to sample the probability of an interaction in a heterogeneous detector. The number of mean free paths which a particle travels is:

$$n_\lambda = \int_{x_1}^{x_2} \frac{dx}{\lambda(x)},$$

which is independent of the material traversed. If n_r is a random variable denoting the number of mean free paths from a given point to the point of interaction, it can be shown that n_r has the distribution function:

$$P(n_r < n_\lambda) = 1 - e^{-n_\lambda}$$

The total number of mean free paths the particle travels before reaching the interaction point, n_λ, is sampled at the beginning of the trajectory as:

$$n_\lambda = -\log(\eta)$$

where η is a random number uniformly distributed in the range $(0, 1)$. n_λ is updated after each step Δx according the formula:

$$n'_\lambda = n_\lambda - \frac{\Delta x}{\lambda(x)}$$

until the step originating from $s(x) = n_\lambda \cdot \lambda(x)$ is the shortest and this triggers the specific process.

Step Limitations

The short description given above is the *differential approach* to particle transport, which is used in the most popular simulation codes EGS and Geant3. In this approach besides the other (*discrete*) processes the continuous energy loss imposes a limit on the step-size too *[1]*, because the cross section of different processes depend of the energy of the particle. Then it is assumed that the step is small enough so that the particle cross sections remain approximately constant during the step. In principle one must use very small steps in order to insure an accurate simulation, but computing time increases as the step-size decreases. A good compromise depends on required accuracy of a concrete simulation. For electromagnetic physics the problem is reduced using integral approach, which is described below in sub-chapter [integral]. However, this only provides effectively correct cross sections but step limitation is needed also for more precise tracking. Thus, in Geant4 any process may establish additional step limitation, the most important limits see below in sub-chapters [drover_range] and [msc_step]).

Updating the Particle Time

The laboratory time of a particle should be updated after each step:

$$\Delta t_{lab} = 0.5\Delta x(\frac{1}{v_1} + \frac{1}{v_2}),$$

where Δx is a true step length traveled by the particle, v_1 and v_2 are particle velocities at the beginning and at the end of the step correspondingly.

4.3.2 Conversion from Cut in Range to Energy Threshold

In Geant4 charged particles are tracked to the end of their range. The differential cross section of δ-electron productions and bremsstrahlung grow rapidly when secondary energy decrease. If all secondary particles will be tracked the CPU

performance of any Monte Carlo code will be pure. The traditional solution is to use cuts. The specific of Geant4 *[1]* is that user provides value of cut in term of *cut in range*, which is unique for defined *G4Region* or for the complete geometry *[2]*.

Range is used, rather than energy, as a more natural concept for designing a coherent policy for different particles and materials. Definition of the certain value of the *cut in range* means the requirement for precision of spatial radioactive dose deposition. This conception is more strict for a simulation code and provides less handles for user to modify final results. At the same time, it ensures that simulation validated in one geometry is valid also for the other geometries.

The value of cut is defined for electrons, positrons, gamma and protons. At the beginning of initialization of Geant4 physics the conversion is performed from unique *cut in range* to cuts (production thresholds) in kinetic energy for each *G4MaterialCutsCouple [2]*. At that moment no energy loss or range table is created, so computation should be performed using original formulas. For electrons and positrons ionization above $10keV$ a simplified Berger-Seltzer energy loss formula ([eion.de]) is used, in which the density correction term is omitted. The contribution of the bremsstrahlung is added using empirical parameterized formula. For $T < 10keV$ the linear dependence of ionization losses on electron velocity is assumed, bremsstrahlung contribution is neglected. The stopping range is defined as

$$R(T) = \int_0^T \frac{1}{(dE/dx)}\, dE.$$

The integration has been done analytically for the low energy part and numerically above an energy limit $1\ keV$. For each *cut in range* the corresponding kinetic energy can be found out. If obtained production threshold in kinetic energy cannot be below the parameter $lowlimit$ (default $1\ keV$) and above $highlimit$ (default $10\ GeV$). If in specific application lower threshold is required, then the allowed energy cut needs to be extended: *G4ProductionCutsTable::GetProductionCutsTable():math:'(to)'SetEnergyRange(lowlimit,highlimit);* or via UI commands $/cuts/setMinCutEnergy\ \ 100\ \ eV\ /cuts/setMaxCutEnergy\ \ 100\ \ TeV$ In contrary to electrons, gammas has no range, so some approximation should be used for range to energy conversion. An approximate empirical formula is used to compute the *absorption cross section* of a photon in an element σ_{abs}. Here, the *absorption cross section* means the sum of the cross sections of the gamma conversion, Compton scattering and photoelectric effect. These processes are the "destructive" processes for photons: they destroy the photon or decrease its energy. The coherent or Rayleigh scattering changes the direction of the gamma only; its cross section is not included in the *absorption cross section*. The AbsorptionLength L_{abs} vector is calculated for every material as

$$L_{abs} = 5/\sigma_{abs}.$$

The factor 5 comes from the requirement that the probability of having no 'destructive' interaction should be small, hence

$$\exp(-L_{abs}\sigma_{abs}) = \exp(-5) = 6.7 \times 10^{-3}.$$

The photon cross section for a material has a minimum at a certain energy E_{min}. Correspondingly L_{abs} has a maximum at $E = E_{min}$, the value of the maximal L_{abs} is the biggest "meaningful" cut in absorption length. If the cut given by the user is bigger than this maximum, a warning is printed and the cut in kinetic energy is set to the *highlimit*.

The cut for proton is introduced with Geant4 v9.3. The main goal of this cut is to limit production of all recoil ions including protons in elastic scattering processes. A simple linear conversion formula is used to compute energy threshold from the value of cut in range, in particular, the cut in range $1\ mm$ corresponds to the production threshold $100keV$.

The conversion from range to energy can be studied using *G4EmCalculator* class. This class allows access or recalculation of energy loss, ranges and other values. It can be instantiated and at any place of user code and can be used after initialisation of Physics Lists: *G4EmCalculator calc; calc.ComputeEnergyCutFromRangeCut(range, particle, material);* here particle and material may be string names or corresponding const pointers to *G4ParticleDefinition* and *G4Material*.

4.4 Muons

4.4.1 Multiple scattering

The G4MultipleScattering class simulates the multiple scattering of charged particles in material. It uses a new multiple scattering (MSC) model which does not use the Moliere formalism *[2]*. This MSC model simulates the scattering of the particle after a given step , computes the mean path length correction and the mean lateral displacement as well.

Let us define a few notation first.

The true path length ('t' path length) is the total length travelled by the particle. All the physical processes restrict this 't' step.

The geometrical (or 'z') path length is the straight distance between the starting and endpoint of the step , if there is no magnetic field. The geometry gives a constraint for this 'z' step. It should be noted, that the geometrical step length is meaningful in the case of magnetic field, too, but in this case it is a distance along a curved trajectory.

The mean properties of the multiple scattering process are determined by the transport mean free path , λ , which is a function of the energy in a given material.Some of the mean properties - the mean lateral displacement and the second moment of cos(theta) - depend on the second transport mean free path, too. (The transport mean free path is called first transport mean free path as well.)

The 't'⇒'z' (true path length – geometrical path length) transformation is given by the simple equation

$$z = \lambda * (1. - exp(-t/\lambda)) \tag{4.111}$$

which is an exact result for the mean values of z , if the differential cross section has an axial symmetry and the energy loss can be neglected . This formula and some other expressions for the first moments of the spatial distribution after a given 'true' path length t have been taken from the excellent paper of Fernandez-Varea et al. *[3]*, but the expressions have been calculated originally by Goudsmit and Saunderson *[4]* and Lewis [msc.lewis]. Inverting eq. (4.111) the 'z'⇒'t' transformation can be written as

$$t = -\lambda * ln(1. - z/\lambda) \tag{4.112}$$

where $z < \lambda$ should be required (this condition is fulfilled if z has been computed from eq. (4.111)).

The mean value of $cos(\theta)$ - θ is the scattering angle after a true step length t - is

$$< cos(\theta) >= exp(-t/\lambda) \tag{4.113}$$

The transport mean free path values have been calculated by Liljequist et al. *[4]*[msc.liljequist1] for electrons and positrons in the kinetic energy range $0.1keV - 20MeV$ in 15 materials. The MSC model uses these values with an appropriate interpolation or extrapolation in the atomic number Z and in the velocity of the particle β , when it is necessary.

The quantity $cos(\theta)$ is sampled in the MSC model according to a model function $f(cos(\theta))$. The shape of this function has been choosen in such a way, that $f(cos(\theta))$ reproduces the results of the direct simulation ot the particle transport rather well and eq. [msc.c] is satisfied. The functional form of this model function is

$$f(x) = p\frac{(a+1)^2(a-1)^2}{2a}\frac{1}{(a-x)^3} + (1-p)\frac{1}{2} : label : eq : msc.dsdfsf$$

where $x = cos(\theta)$, $0 \leq p \leq 1$ and $a > 1$. The model parameters p and a depend on the path length t , the energy of the particle and the material.They are not independent parameters , they should satisfy the constraint

$$\frac{p}{a} = exp(-\frac{t}{\lambda}) \tag{4.114}$$

which follows from eq. (4.113) .

The mean lateral displacement is given by a more complicated formula (see the paper *[3]*), but this quantity also can be calculated relatively easily and accurately.

It is worth to note that in this MSC model there is no step limitation originated from the multiple scattering process. Another important feature of this model that the total 'true' path length of the particle does not depend the length of the steps . Most of the algorithms used in simulations do not have these properties.

In the case of heavy charged particles ($\mu, \pi, proton, etc.$) the mean transport free path is calculated from the $e+/e-$ λ values with a 'scaling'.

In its present form the model computes and uses *mean* path length corrections and lateral displacements, the only *random* quantity is the scattering angle θ which is sampled according to the model function f.

The G4MultipleScattering process has 'AlongStep' and 'PostStep' parts.

The AlongStepGetPhysicalInteractionLength function performs the transformation . It should be called after the other physics GetPhysicalInteractionLength functions but before the GetPhysicalInteractionLength of the transportation process.The reason for this restriction is the following: The physics processes 'feel' the true path length travelled by the particle , the geometry (transport) uses the 'z' step length.If we want to compare the minimum step size coming from the physics with the constraint of the geometry, we have make the transformation.

The AlongStepDoIt function of the process performs the inverse, 'z'⇒'t' transformation.This function should be called after the AlongStepDoIt of the transportation process , i.e. after the particle relocation determined by the geometrical step length, but before applying any other (physics) AlongStepDoIt.

The PostStepGetPhysicalInteractionLength part of the multiple scattering process is very simple , it sets the force flag to 'Forced' in order to ensure the call of the PostStepDoIt in every step and returns a big value as interaction length (that means that the multiple scattering process does not restrict the step size).

4.4.2 Bremsstrahlung

Bremsstrahlung dominates other muon interaction processes in the region of catastrophic collisions ($v \geq 0.1$), that is at "moderate" muon energies above the kinematic limit for knock–on electron production. At high energies ($E \geq 1$ TeV) this process contributes about 40% of the average muon energy loss.

Differential Cross Section

The differential cross section for muon bremsstrahlung (in units of $\mathrm{cm}^2/(\mathrm{g\ GeV})$) can be written as

$$\begin{aligned}\frac{d\sigma(E,\epsilon,Z,A)}{d\epsilon} &= \frac{16}{3}\alpha N_A(\frac{m}{\mu}r_e)^2\frac{1}{\epsilon A}Z(Z\Phi_n+\Phi_e)(1-v+\frac{3}{4}v^2)\\ &= 0 \quad \text{if} \quad \epsilon \geq \epsilon_{\max} = E-\mu,\end{aligned}$$

where μ and m are the muon and electron masses, Z and A are the atomic number and atomic weight of the material, and N_A is Avogadro's number. If E and T are the initial total and kinetic energy of the muon, and ϵ is the emitted photon energy, then $\epsilon = E - E'$ and the relative energy transfer $v = \epsilon/E$.

Φ_n represents the contribution of the nucleus and can be expressed as

$$\begin{aligned}\Phi_n &= \ln\frac{BZ^{-1/3}(\mu+\delta(D'_n\sqrt{e}-2))}{D'_n(m+\delta\sqrt{e}BZ^{-1/3})};\\ &= 0 \quad \text{if} \quad \text{negative}.\end{aligned}$$

Φ_e represents the contribution of the electrons and can be expressed as

$$\begin{aligned}\Phi_e = & \ln \frac{B' Z^{-2/3} \mu}{\left(1+\frac{\delta\mu}{m^2\sqrt{e}}\right)(m+\delta\sqrt{e}B'Z^{-2/3})}; \\ = & \ 0 \quad \text{if} \quad \epsilon \geq \epsilon'_{\max} = E/(1+\mu^2/2mE); \\ = & \ 0 \quad \text{if} \quad \text{negative}.\end{aligned}$$

In Φ_n and Φ_e, for all nuclei except hydrogen,

$$\begin{aligned}\delta = & \ \mu^2\epsilon/2EE' = \mu^2 v/2(E-\epsilon); \\ D'_n = & \ D_n^{(1-1/Z)}, \quad D_n = 1.54A^{0.27}; \\ B = & \ 183, \quad B' = 1429, \quad \sqrt{e} = 1.648(721271).\end{aligned}$$

For hydrogen (Z=1) $B = 202.4,\ B' = 446,\ D'_n = D_n$.

These formulae are taken mostly from Refs. *[1]* and *[2]*. They include improved nuclear size corrections in comparison with Ref. *[3]* in the region $v \sim 1$ and low Z. Bremsstrahlung on atomic electrons (taking into account target recoil and atomic binding) is introduced instead of a rough substitution $Z(Z+1)$. A correction for processes with nucleus excitation is also included *[4]*.

Applicability and Restrictions of the Method

The above formulae assume that: 1. $E \gg \mu$, hence the ultrarelativistic approximation is used; 2. $E \leq 10^{20}$ eV; above this energy, LPM suppression can be expected; 3. $v \geq 10^{-6}$; below 10^{-6} Ter-Mikaelyan suppression takes place. However, in the latter region the cross section of muon bremsstrahlung is several orders of magnitude less than that of other processes. The Coulomb correction (for high Z) is not included. However, existing calculations *[5]* show that for muon bremsstrahlung this correction is small.

Continuous Energy Loss

The restricted energy loss for muon bremsstrahlung $(dE/dx)_{\rm rest}$ with relative transfers $v = \epsilon/(T+\mu) \leq v_{\rm cut}$ can be calculated as follows :

$$\left(\frac{dE}{dx}\right)_{\rm rest} = \int_0^{\epsilon_{\rm cut}} \epsilon\,\sigma(E,\epsilon)\,d\epsilon = (T+\mu)\int_0^{v_{\rm cut}} \epsilon\,\sigma(E,\epsilon)\,dv\,.$$

If the user cut $v_{\rm cut} \geq v_{\max} = T/(T+\mu)$, the total average energy loss is calculated. Integration is done using Gaussian quadratures, and binning provides an accuracy better than about 0.03% for $T = 1$ GeV, $Z = 1$. This rapidly improves with increasing T and Z.

Total Cross Section

The integration of the differential cross section over $d\epsilon$ gives the total cross section for muon bremsstrahlung:

$$\sigma_{\rm tot}(E,\epsilon_{\rm cut}) = \int_{\epsilon_{\rm cut}}^{\epsilon_{\max}} \sigma(E,\epsilon)d\epsilon = \int_{\ln v_{\rm cut}}^{\ln v_{\max}} \epsilon\sigma(E,\epsilon)d(\ln v),$$

where $v_{\max} = T/(T+\mu)$. If $v_{\rm cut} \geq v_{\max}$, $\sigma_{\rm tot} = 0$.

Sampling

The photon energy ϵ_p is found by numerically solving the equation :

$$P = \int_{\epsilon_p}^{\epsilon_{\max}} \sigma(E,\epsilon,Z,A)\,d\epsilon \Big/ \int_{\epsilon_{\rm cut}}^{\epsilon_{\max}} \sigma(E,\epsilon,Z,A)\,d\epsilon\ .$$

Here P is the random uniform probability, $\epsilon_{\max} = T$, and $\epsilon_{\rm cut} = (T+\mu)\cdot v_{\rm cut}$. $v_{min.cut} = 10^{-5}$ is the minimal relative energy transfer adopted in the algorithm.

For fast sampling, the solution of the above equation is tabulated at initialization time for selected Z, T and P. During simulation, this table is interpolated in order to find the value of ϵ_p corresponding to the probability P.

The tabulation routine uses accurate functions for the differential cross section. The table contains values of

$$x_p = \ln(v_p/v_{\max})/\ln(v_{\max}/v_{\rm cut}),$$

where $v_p = \epsilon_p/(T+\mu)$ and $v_{\max} = T/(T+\mu)$. Tabulation is performed in the range $1 \le Z \le 128$, $1 \le T \le 1000$ PeV, $10^{-5} \le P \le 1$ with constant logarithmic steps. Atomic weight (which is a required parameter in the cross section) is estimated here with an iterative solution of the approximate relation:

$$A = Z\,(2 + 0.015\,A^{2/3}).$$

For $Z = 1$, $A = 1$ is used.

To find x_p (and thus ϵ_p) corresponding to a given probability P, the sampling method performs a linear interpolation in $\ln Z$ and $\ln T$, and a cubic, 4 point Lagrangian interpolation in $\ln P$. For $P \le P_{\min}$, a linear interpolation in (P, x) coordinates is used, with $x = 0$ at $P = 0$. Then the energy ϵ_p is obtained from the inverse transformation of [mubrem.c] :

$$\epsilon_p = (T+\mu) v_{\max} (v_{\max}/v_{\rm cut})^{x_p}$$

The algorithm with the parameters described above has been tested for various Z and T. It reproduces the differential cross section to within 0.2 – 0.7 % for $T \ge 10$ GeV. The average total energy loss is accurate to within 0.5%. While accuracy improves with increasing T, satisfactory results are also obtained for $1 \le T \le 10$ GeV.

It is important to note that this sampling scheme allows the generation of ϵ_p for different user cuts on v which are above $v_{\rm min.cut}$. To perform such a simulation, it is sufficient to define a new probability variable

$$P' = P\,\sigma_{\rm tot}\,(v_{\rm user.cut})/\sigma_{\rm tot}(v_{\rm min.cut})$$

and use it in the sampling method. Time consuming re-calculation of the 3-dimensional table is therefore not required because only the tabulation of $\sigma_{\rm tot}(v_{\rm user.cut})$ is needed.

The small-angle, ultrarelativistic approximation is used for the simulation (with about 20% accuracy at $\theta \le \theta^* \approx 1$) of the angular distribution of the final state muon and photon. Since the target recoil is small, the muon and photon are directed symmetrically (with equal transverse momenta and coplanar with the initial muon):

$$p_{\perp\mu} = p_{\perp\gamma}, \quad \text{where} \quad p_{\perp\mu} = E'\theta_\mu, \quad p_{\perp\gamma} = \epsilon\theta_\gamma.$$

θ_μ and θ_γ are muon and photon emission angles. The distribution in the variable $r = E\theta_\gamma/\mu$ is given by

$$f(r)dr \sim rdr/(1+r^2)^2.$$

Random angles are sampled as follows:

$$\theta_\gamma = \frac{\mu}{E} r \quad \theta_\mu = \frac{\epsilon}{E'}\theta_\gamma,$$

where

$$r = \sqrt{\frac{a}{1-a}}\,, \quad a = \xi\,\frac{r_{\max}^2}{1+r_{\max}^2}\,, \quad r_{\max} = \min(1, E'/\epsilon)\cdot E\,\theta^*/\mu\,,$$

and ξ is a random number uniformly distributed between 0 and 1.

4.4.3 Muon Ionization

The class *G4MuIonisation* provides the continuous energy loss due to ionization and simulates the 'discrete' part of the ionization, that is, delta rays produced by muons. Inside this class the following models are used:

- *G4BraggModel* (valid for protons with $T < 0.2\ MeV$)
- *G4BetherBlochModel* (valid for protons with $0.2\ MeV < T < 1\ GeV$)
- *G4MuBetherBlochModel* (valid for protons with $T > 1\ GeV$)

The limit energy $0.2\ MeV$ is equivalent to the proton limit energy $2MeV$ because of scaling relation ([enloss.sc]), which allows simulation for muons with energy below $1\ GeV$ in the same way as for point-like hadrons with spin 1/2 described in the section [en_loss].

For higher energies the *G4MuBetherBlochModel* is applied, in which leading radiative corrections are taken into account *[2]*. Simple analytical formula for the cross section, derived with the logarithmic are used. Calculation results appreciably differ from usual elastic $\mu - e$ scattering in the region of high energy transfers $m_e << T < T_{max}$ and give non-negligible correction to the total average energy loss of high-energy muons. The total cross section is written as following:

$$\sigma(E,\epsilon) = \sigma_{BB}(E,\epsilon)\left[1 + \frac{\alpha}{2\pi} ln\left(1 + \frac{2\epsilon}{m_e}\right) ln\left(\frac{4m_e E(E-\epsilon)}{m_\mu^2(2\epsilon + m_e)}\right)\right],$$

here $\sigma(E,\epsilon)$ is the differential cross sections, $\sigma(E,\epsilon)_{BB}$ is the Bethe-Bloch cross section ([hion.i]), m_e is the electron mass, m_μ is the muon mass, E is the muon energy, ϵ is the energy transfer, $\epsilon = \omega + T$, where T is the electron kinetic energy and ω is the energy of radiative gamma.

For computation of the truncated mean energy loss ([comion.a]) the partial integration of the expression ([muion.c]) is performed

$$S(E,\epsilon_{up}) = S_{BB}(E,\epsilon_{up}) + S_{RC}(E,\epsilon_{up}), \quad \epsilon_{up} = min(\epsilon_{max},\epsilon_{cut}),$$

where term S_{BB} is the Bethe-Bloch truncated energy loss ([hion.d]) for the interval of energy transfer $(0 - \epsilon_{up})$ and term S_{RC} is a correction due to radiative effects. The function become smooth after log-substitution and is computed by numerical integration

$$S_{RC}(E,\epsilon_{up}) = \int_{\ln\epsilon_1}^{\ln\epsilon_{up}} \epsilon^2(\sigma(E,\epsilon) - \sigma_{BB}(E,\epsilon))d(\ln\epsilon),$$

where lower limit ϵ_1 does not effect result of integration in first order and in the class *G4MuBetheBlochModel* the default value $\epsilon_1 = 100keV$ is used.

For computation of the discrete cross section ([comion.b]) another substitution is used in order to perform numerical integration of a smooth function

$$\sigma(E) = \int_{1/\epsilon_{max}}^{1/\epsilon_{up}} \epsilon^2\sigma(E,\epsilon)d(1/\epsilon).$$

The sampling of energy transfer is performed between $1/\epsilon_{up}$ and $1/\epsilon_{max}$ using rejection constant for the function $\epsilon^2\sigma(E,\epsilon)$. After the successful sampling of the energy transfer, the direction of the scattered electron is generated with respect to the direction of the incident particle. The energy of radiative gamma is neglected. The azimuthal electron angle ϕ is generated isotropically. The polar angle θ is calculated from energy-momentum conservation. This information is used to calculate the energy and momentum of both scattered particles and to transform them into the *global* coordinate system.

4.4.4 Muon Photonuclear Interaction

The inelastic interaction of muons with nuclei is important at high muon energies ($E \geq 10$ GeV), and at relatively high energy transfers ν ($\nu/E \geq 10^{-2}$). It is especially important for light materials and for the study of detector response to high energy muons, muon propagation and muon-induced hadronic background. The average energy loss for this process increases almost lineary with energy, and at TeV muon energies constitutes about 10% of the energy loss rate. The main contribution to the cross section $\sigma(E,\nu)$ and energy loss comes from the low Q^2–region ($Q^2 \ll 1$ GeV^2). In this domain, many simplifications can be made in the theoretical consideration of the process in order to obtain convenient and simple formulae for the cross section. Most widely used are the expressions given by Borog and Petrukhin *[1]*, and Bezrukov and Bugaev *[2]*. Results from these authors agree within 10% for the differential cross section and within about 5% for the average energy loss, provided the same photonuclear cross section, $\sigma_{\gamma N}$, is used in the calculations.

Differential Cross Section

The Borog and Petrukhin formula for the cross section is based on:

- Hand's formalism *[3]* for inelastic muon scattering,
- a semi-phenomenological inelastic form factor, which is a Vector Dominance Model with parameters estimated from experimental data, and
- nuclear shadowing effects with a reasonable theoretical parameterization *[4]*.

For $E \geq 10$ GeV, the Borog and Petrukhin cross section, differential in transferred energy, is

$$\sigma(E,\nu) = \Psi(\nu)\Phi(E,v),$$

$$\Psi(\nu) = \frac{\alpha}{\pi}\frac{A_{\text{eff}}N_{AV}}{A}\sigma_{\gamma N}(\nu)\frac{1}{\nu},$$

$$\Phi(E,v) = v - 1 + \left[1 - v + \frac{v^2}{2}\left(1 + \frac{2\mu^2}{\Lambda^2}\right)\right]\ln\frac{\dfrac{E^2(1-v)}{\mu^2}\left(1 + \dfrac{\mu^2 v^2}{\Lambda^2(1-v)}\right)}{1 + \dfrac{Ev}{\Lambda}\left(1 + \dfrac{\Lambda}{2M} + \dfrac{Ev}{\Lambda}\right)},$$

where ν is the energy lost by the muon, $v = \nu$/E, and μ and M are the muon and nucleon (proton) masses, respectively. Λ is a Vector Dominance Model parameter in the inelastic form factor which is estimated to be $\Lambda^2 = 0.4$ GeV^2. For A_{eff}, which includes the effect of nuclear shadowing, the parameterization *[4]*

$$A_{\text{eff}} = 0.22A + 0.78A^{0.89}$$

is chosen. A reasonable choice for the photonuclear cross section, $\sigma_{\gamma N}$, is the parameterization obtained by Caldwell et al. *[5]* based on the experimental data on photoproduction by real photons:

$$\sigma_{\gamma N} = (49.2 + 11.1\ln K + 151.8/\sqrt{K}) \cdot 10^{-30}\text{cm}^2 \quad K \text{ in GeV}.$$

The upper limit of the transferred energy is taken to be $\nu_{\max}$ = $E - M/2$. The choice of the lower limit $\nu_{\min}$ is less certain since the formula [munu.1], [munu.2], [munu.3] is not valid in this domain. Fortunately, $\nu_{\min}$ influences the total cross section only logarithmically and has no practical effect on the average energy loss for high energy muons. Hence, a reasonable choice for $\nu_{\min}$ is 0.2 GeV. In Eq. [munu.2], A_{eff} and $\sigma_{\gamma N}$ appear as factors. A more rigorous theoretical approach may lead to some dependence of the shadowing effect on ν and E; therefore in the differential cross section and in the sampling procedure, this possibility is forseen and the atomic weight A of the element is kept as an explicit parameter. The total cross section is obtained by integration of Eq. [munu.1] between $\nu_{\min}$ and $\nu_{\max}$; to facilitate the computation, a $\ln(\nu)$–substitution is used.

Sampling

Sampling the Transferred Energy

The muon photonuclear interaction is always treated as a discrete process with its mean free path determined by the total cross section. The total cross section is obtained by the numerical integration of Eq. [munu.1] within the limits $\nu_{\min}$ and $\nu_{\max}$. The process is considered for muon energies $1\text{GeV} \leq \text{T} \leq 1000\text{PeV}$, though it should be noted that above 100 TeV the extrapolation (Eq. [munu.5]) of $\sigma_{\gamma N}$ may be too crude. The random transferred energy, ν_p, is found from the numerical solution of the equation :

$$P = \int_{\nu_p}^{\nu_{\max}} \sigma(E,\nu)d\nu \Big/ \int_{\nu_{\min}}^{\nu_{\max}} \sigma(E,\nu)d\nu \ .$$

Here P is the random uniform probability, with $\nu_{\max} = E - M/2$ and $\nu_{\min} = 0.2$ GeV. For fast sampling, the solution of Eq. [munu.6] is tabulated at initialization time. During simulation, the sampling method returns a value of ν_p corresponding to the probability P, by interpolating the table. The tabulation routine uses Eq. [munu.1] for the differential cross section. The table contains values of

$$x_p = \ln(\nu_p/\nu_{\max})/\ln(\nu_{\max}/\nu_{\min}),$$

calculated at each point on a three-dimensional grid with constant spacings in $\ln(T)$, $\ln(A)$ and $\ln(P)$. The sampling uses linear interpolations in $\ln(T)$ and $\ln(A)$, and a cubic interpolation in $\ln(P)$. Then the transferred energy is calculated from the inverse transformation of Eq. [munu.7], $\nu_p = \nu_{\max}(\nu_{\max}/\nu_{\min})^{x_p}$. Tabulated parameters reproduce the theoretical dependence to better than 2% for $T > 1$ GeV and better than 1% for $T > 10$ GeV.

Sampling the Muon Scattering Angle

According to Refs. *[1]*[munu.bor77], in the region where the four-momentum transfer is not very large ($Q^2 \leq 3\text{GeV}^2$), the t – dependence of the cross section may be described as:

$$\frac{d\sigma}{dt} \sim \frac{(1 - t/t_{\max})}{t(1 + t/\nu^2)(1 + t/m_0^2)}[(1 - y)(1 - t_{\min}/t) + y^2/2],$$

where t is the square of the four-momentum transfer, $Q^2 = 2(EE' - PP'\cos\theta - \mu^2)$. Also, $t_{\min} = (\mu y)^2/(1 - y)$, $y = \nu/E$ and $t_{\max} = 2M\nu$. $\nu = E - E'$ is the energy lost by the muon and E is the total initial muon energy. M is the nucleon (proton) mass and $m_0^2 \equiv \Lambda^2 \simeq 0.4\ \text{GeV}^2$ is a phenomenological parameter determing the behavior of the inelastic form factor. Factors which depend weakly, or not at all, on t are omitted. To simulate random t and hence the random muon deflection angle, it is convenient to represent Eq. [munu.8] in the form :

$$\sigma(t) \sim f(t)g(t),$$

where

$$f(t) = \frac{1}{t(1 + t/t_1)},$$
$$g(t) = \frac{1 - t/t_{\max}}{1 + t/t_2} \cdot \frac{(1 - y)(1 - t_{\min}/t) + y^2/2}{(1 - y) + y^2/2},$$

and

$$t_1 = \min(\nu^2, m_0^2) \quad t_2 = \max(\nu^2, m_0^2).$$

t_P is found analytically from Eq. [munu.10] :

$$t_P = \frac{t_{\max}t_1}{(t_{\max} + t_1)\left[\dfrac{t_{\max}(t_{\min} + t_1)}{t_{\min}(t_{\max} + t_1)}\right]^P - t_{\max}},$$

where P is a random uniform number between 0 and 1, which is accepted with probability $g(t)$. The conditions of Eq. [munu.11] make use of the symmetry between ν^2 and m_0^2 in Eq. [munu.8] and allow increased selection efficiency, which is typically ≥ 0.7. The polar muon deflection angle θ can easily be found from [1]

$$\sin^2(\theta/2) = \frac{t_P - t_{\min}}{4\,(EE' - \mu^2) - 2\,t_{\min}}.$$

The hadronic vertex is generated by the hadronic processes taking into account the four-momentum transfer.

4.4.5 Positron - Electron Pair Production by Muons

Direct electron pair production is one of the most important muon interaction processes. At TeV muon energies, the pair production cross section exceeds those of other muon interaction processes over a range of energy transfers between 100 MeV and $0.1E_\mu$. The average energy loss for pair production increases linearly with muon energy, and in the TeV region this process contributes more than half the total energy loss rate.

To adequately describe the number of pairs produced, the average energy loss and the stochastic energy loss distribution, the differential cross section behavior over an energy transfer range of 5 MeV $\leq \epsilon \leq 0.1 \cdot E_\mu$ must be accurately reproduced. This is is because the main contribution to the total cross section is given by transferred energies 5 MeV $\leq \epsilon \leq 0.01 \cdot E_\mu$, and because the contribution to the average muon energy loss is determined mostly in the region $0.001 \cdot E_\mu \leq \epsilon \leq 0.1 \cdot E_\mu$.

For a theoretical description of the cross section, the formulae of Ref. *[1]* are used, along with a correction for finite nuclear size *[2]*. To take into account electron pair production in the field of atomic electrons, the inelastic atomic form factor contribution of Ref. *[3]* is also applied.

Differential Cross Section

Definitions and Applicability

In the following discussion, these definitions are used:

- m and μ are the electron and muon masses, respectively
- $E \equiv E_\mu$ is the total muon energy, $E = T + \mu$
- Z and A are the atomic number and weight of the material
- ϵ is the total pair energy or, approximately, the muon energy loss $(E - E')$
- $v = \epsilon/E$
- $e = 2.718\ldots$
- $A^\star = 183$.

The formula for the differential cross section applies when:

- $E_\mu \gg \mu$ ($E \geq 2$ – 5 GeV) and $E_\mu \leq 10^{15}$ – 10^{17} eV. If muon energies exceed this limit, the LPM (Landau Pomeranchuk Migdal) effect may become important, depending on the material
- the muon energy transfer ϵ lies between $\epsilon_{\min} = 4\,m$ and $\epsilon_{\max} = E_\mu - \frac{3\sqrt{e}}{4}\,\mu\,Z^{1/3}$, although the formal lower limit is $\epsilon \gg 2\,m$, and the formal upper limit requires $E'_\mu \gg \mu$.
- $Z \leq 40$ – 50. For higher Z, the Coulomb correction is important but has not been sufficiently studied theoretically.

Formulae

The differential cross section for electron pair production by muons $\sigma(Z, A, E, \epsilon)$ can be written as :

$$\sigma(Z, A, E, \epsilon) = \frac{4}{3\pi} \frac{Z(Z+\zeta)}{A} N_A (\alpha r_0)^2 \frac{1-v}{\epsilon} \int_0^{\rho_{\max}} G(Z, E, v, \rho)\, d\rho,$$

where

$$G(Z, E, v, \rho) = \Phi_e + (m/\mu)^2 \Phi_\mu,$$

$$\Phi_{e,\mu} = B_{e,\mu} L'_{e,\mu}$$

and

$$\Phi_{e,\mu} = 0 \quad \text{whenever} \quad \Phi_{e,\mu} < 0.$$

B_e and B_μ do not depend on Z, A, and are given by

$$B_e = [(2+\rho^2)(1+\beta) + \xi(3+\rho^2)] \ln\left(1 + \frac{1}{\xi}\right) + \frac{1-\rho^2-\beta}{1+\xi} - (3+\rho^2);$$

$$B_e \approx \frac{1}{2\xi}\left[(3-\rho^2) + 2\beta(1+\rho^2)\right] \quad \text{for} \quad \xi \geq 10^3;$$

$$B_\mu = \left[(1+\rho^2)\left(1 + \frac{3\beta}{2}\right) - \frac{1}{\xi}(1+2\beta)(1-\rho^2)\right] \ln(1+\xi) + \frac{\xi(1-\rho^2-\beta)}{1+\xi} + (1+2\beta)(1-\rho^2);$$

$$B_\mu \approx \frac{\xi}{2}\left[(5-\rho^2) + \beta(3+\rho^2)\right] \quad \text{for} \quad \xi \leq 10^{-3};$$

Also,

$$\xi = \frac{\mu^2 v^2}{4m^2} \frac{(1-\rho^2)}{(1-v)}; \quad \beta = \frac{v^2}{2(1-v)};$$

$$L'_e = \ln \frac{A^* Z^{-1/3} \sqrt{(1+\xi)(1+Y_e)}}{1 + \frac{2m\sqrt{e} A^* Z^{-1/3}(1+\xi)(1+Y_e)}{Ev(1-\rho^2)}} - \frac{1}{2} \ln\left[1 + \left(\frac{3mZ^{1/3}}{2\mu}\right)^2 (1+\xi)(1+Y_e)\right];$$

$$L'_\mu = \ln \frac{(\mu/m) A^* Z^{-1/3} \sqrt{(1+1/\xi)(1+Y_\mu)}}{1 + \frac{2m\sqrt{e} A^* Z^{-1/3}(1+\xi)(1+Y_\mu)}{Ev(1-\rho^2)}} - \ln\left[\frac{3}{2} Z^{1/3} \sqrt{(1+1/\xi)(1+Y_\mu)}\right].$$

For faster computing, the expressions for $L'_{e,\mu}$ are further algebraically transformed. The functions $L'_{e,\mu}$ include the nuclear size correction *[2]* in comparison with parameterization *[1]* :

$$Y_e = \frac{5 - \rho^2 + 4\,\beta\,(1+\rho^2)}{2(1+3\beta)\ln(3+1/\xi) - \rho^2 - 2\beta(2-\rho^2)};$$

$$Y_\mu = \frac{4 + \rho^2 + 3\,\beta\,(1+\rho^2)}{(1+\rho^2)(\frac{3}{2}+2\beta)\ln(3+\xi) + 1 - \frac{3}{2}\rho^2};$$

$$\rho_{\max} = [1 - 6\mu^2/E^2(1-v)]\sqrt{1 - 4m/Ev}.$$

Comment on the Calculation of the Integral $\int d\rho$ in Eq. [mupair.a]

The integral $\int_0^{\rho_{\max}} G(Z,E,v,\rho)\, d\rho$ is computed with the substitutions:

$$\begin{aligned} t &= \ln(1-\rho), \\ 1-\rho &= \exp(t), \\ 1+\rho &= 2-\exp(t), \\ 1-\rho^2 &= e^t\,(2-e^t). \end{aligned}$$

After that,

$$\int_0^{\rho_{\max}} G(Z,E,v,\rho)\, d\rho = \int_{t_{\min}}^{0} G(Z,E,v,\rho)\, e^t\, dt,$$

where

$$t_{\min} = \ln \frac{\dfrac{4m}{\epsilon} + \dfrac{12\mu^2}{EE'}\left(1-\dfrac{4m}{\epsilon}\right)}{1+\left(1-\dfrac{6\mu^2}{EE'}\right)\sqrt{1-\dfrac{4m}{\epsilon}}}.$$

To compute the integral of Eq. [mupair.b] with an accuracy better than 0.5%, Gaussian quadrature with $N = 8$ points is sufficient.

The function $\zeta(E,Z)$ in Eq. [mupair.a] serves to take into account the process on atomic electrons (inelastic atomic form factor contribution). To treat the energy loss balance correctly, the following approximation, which is an algebraic transformation of the expression in Ref. *[3]*, is used:

$$\zeta(E,Z) = \frac{0.073 \ln \dfrac{E/\mu}{1+\gamma_1 Z^{2/3} E/\mu} - 0.26}{0.058 \ln \dfrac{E/\mu}{1+\gamma_2 Z^{1/3} E/\mu} - 0.14};$$

$$\zeta(E,Z) = 0 \quad \text{if the numerator is negative.}$$

For E $\leq 35\,\mu$, $\zeta(E,Z) = 0$. Also $\gamma_1 = 1.95 \cdot 10^{-5}$ and $\gamma_2 = 5.30 \cdot 10^{-5}$.

The above formulae make use of the Thomas-Fermi model which is not good enough for light elements. For hydrogen ($Z = 1$) the following parameters must be changed: $A^* = 183 \Rightarrow 202.4$; $\gamma_1 = 1.95 \cdot 10^{-5} \Rightarrow 4.4 \cdot 10^{-5}$; $\gamma_2 = 5.30 \cdot 10^{-5} \Rightarrow 4.8 \cdot 10^{-5}$.

Total Cross Section and Restricted Energy Loss

If the user's cut for the energy transfer ϵ_{cut} is greater than $\epsilon_{\min}$, the process is represented by continuous restricted energy loss for interactions with $\epsilon \leq \epsilon_{\text{cut}}$, and discrete collisions with $\epsilon > \epsilon_{\text{cut}}$. Respective values of the total cross section and restricted energy loss rate are defined as:

$$\sigma_{\text{tot}} = \int_{\epsilon_{\text{cut}}}^{\epsilon_{\max}} \sigma(E,\epsilon)\, d\epsilon; \quad (dE/dx)_{\text{restr}} = \int_{\epsilon_{\min}}^{\epsilon_{\text{cut}}} \epsilon\, \sigma(E,\epsilon)\, d\epsilon.$$

For faster computing, $\ln \epsilon$ substitution and Gaussian quadratures are used.

Sampling of Positron - Electron Pair Production

The e^+e^- pair energy ϵ_P, is found numerically by solving the equation

$$P = \int_{\epsilon_P}^{\epsilon_{\max}} \sigma(Z,A,T,\epsilon)d\epsilon \quad / \int_{cut}^{\epsilon_{\max}} \sigma(Z,A,T,\epsilon)d\epsilon$$

or

$$1-P = \int_{cut}^{\epsilon_P} \sigma(Z,A,T,\epsilon)d\epsilon \quad / \int_{cut}^{\epsilon_{\max}} \sigma(Z,A,T,\epsilon)d\epsilon$$

To reach high sampling speed, solutions of Eqs. [mupair.c], [mupair.d] are tabulated at initialization time. Two 3-dimensional tables (referred to here as A and B) of $\epsilon_P(P,T,Z)$ are created, and then interpolation is used to sample ϵ_P.

The number and spacing of entries in the table are chosen as follows:

- a constant increment in $\ln T$ is chosen such that there are four points per decade in the range $T_{\min} - T_{\max}$. The default range of muon kinetic energies in Geant4 is $T = 1\,\text{GeV} - 1000\,\text{PeV}$.
- a constant increment in $\ln Z$ is chosen. The shape of the sampling distribution does depend on Z, but very weakly, so that eight points in the range $1 \le Z \le 128$ are sufficient. There is practically no dependence on the atomic weight A.
- for probabilities $P \le 0.5$, Eq. [mupair.c] is used and Table A is computed with a constant increment in $\ln P$ in the range $10^{-7} \le P \le 0.5$. The number of points in $\ln P$ for Table A is about 100.
- for $P \ge 0.5$, Eq. [mupair.d] is used and Table B is computed with a constant increment in $\ln(1-P)$ in the range $10^{-5} \le (1-P) \le 0.5$. In this case 50 points are sufficient.

The values of $\ln(\epsilon_P - cut)$ are stored in both Table A and Table B.

To create the "probability tables" for each (T,Z) pair, the following procedure is used:

- a temporary table of ~ 2000 values of $\epsilon \cdot \sigma(Z,A,T,\epsilon)$ is constructed with a constant increment (~ 0.02) in $\ln\epsilon$ in the range $(cut, \epsilon_{\max})$. ϵ is taken in the middle of the corresponding bin in $\ln\epsilon$.
- the accumulated cross sections

$$\sigma_1 = \int_{\ln\epsilon}^{\ln\epsilon_{\max}} \epsilon\,\sigma(Z,A,T,\epsilon)\,d(\ln\epsilon)$$

$$and$$

$$\sigma_2 = \int_{\ln(cut)}^{\ln\epsilon} \epsilon\,\sigma(Z,A,T,\epsilon)\,d(\ln\epsilon)$$

  are calculated by summing the temporary table over the values above $\ln\epsilon$ (for σ_1) and below $\ln\epsilon$ (for σ_2) and then normalizing to obtain the accumulated probability functions.
- finally, values of $\ln(\epsilon_P - cut)$ for corresponding values of $\ln P$ and $\ln(1-P)$ are calculated by linear interpolation of the above accumulated probabilities to form Tables A and B. The monotonic behavior of the accumulated cross sections is very useful in speeding up the interpolation procedure.

The random transferred energy corresponding to a probability P, is then found by linear interpolation in $\ln Z$ and $\ln T$, and a cubic interpolation in $\ln P$ for Table A or in $\ln(1-P)$ for Table B. For $P \le 10^{-7}$ and $(1-P) \le 10^{-5}$, linear extrapolation using the entries at the edges of the tables may be safely used. Electron pair energy is related to the auxiliary variable $x = \ln(\epsilon_P - cut)$ found by the trivial interpolation $\epsilon_P = e^x + cut$.

Similar to muon bremsstrahlung (section [secmubrem]), this sampling algorithm does not re-initialize the tables for user cuts greater than cut_{min}. Instead, the probability variable is redefined as

$$P' = P\sigma_{\text{tot}}(cut_{user})/\sigma_{\text{tot}}(cut_{min}),$$

and P' is used for sampling.

In the simulation of the final state, the muon deflection angle (which is of the order of m/E) is neglected. The procedure for sampling the energy partition between e^+ and e^- and their emission angles is similar to that used for the $\gamma \to e^+ e^-$ conversion.

4.5 Precision

4.5.1 Overview

The physics simulation tools grouped in this domain reflect ongoing research in key issues of particle transport:

- multi-scale simulation and its implications on condensed and discrete transport schemes [tns_pixe], [n5_mc2009], [n5_nss2009], [nss_mutants], [mc_mutants],
- epistemic uncertainties in physics models and parameters [tns_epistemic],
- innovative software design techniques [chep_photons], [mc_photons], [nss_photons], [mc_datamanagement], [nss_datamanagement] in support of physics modeling,
- the assessment of the accuracy of data libraries used by Monte Carlo simulation codes [tns_relax_prob], [nss_binding], [nss_datalib], [mc_datalib], [mc_beb], [nss_beb],
- precision models of particle interactions with matter, quantitatively assessed through comparison with experimental measurements of the model constituents [tns_pixe], [mc_beb], [nss_beb].

The main features of the simulation tools developed in this research context, which are so far released in Geant4, are summarized below. They concern impact ionisation by protons and α particles, and the following particle induced X-ray emission (PIXE), which are encompassed in the Geant4 "electromagnetic/pii" package.

4.5.2 Impact ionisation by hadrons and PIXE

Despite the simplicity of its nature as a physical effect, PIXE represents a conceptual challenge for general-purpose Monte Carlo codes, since it involves an intrinsically discrete effect (the atomic relaxation) intertwined with a process (ionisation) affected by infrared divergence, therefore usually treated in Monte Carlo codes by means of con The largely incomplete knowledge of ionisation cross sections by hadron impact, limited to the innermost atomic shells both as theoretical calculations and experimental measurements, further complicates the achievement of a conceptually consistent description of this process.

Early developments of proton and α particle impact ionisation cross sections in Geant4 are reviewed in a detailed paper devoted to PIXE simulation with Geant4 [tns_pixe]. This article also presents new, extensive developments for PIXE simulation, their validation with respect to experimental data and the first Geant4-based simulation involving PIXE in a concrete experimental use case: the optimization of the graded shielding of the X-ray detectors of the eROSITA [erosita] mission. The new developments described in [tns_pixe] are released in Geant4 in the *pii* package (in *source/processes/electromagnetic/pii*).

The developments for PIXE simulation described in [tns_pixe] provide a variety of proton and α particle cross sections for the ionisation of K, L and M shells:

- theoretical calculations based on the ECPSSR [ecpssr] model and its variants (with Hartree-Slater corrections [ecpssr_hs], with the "united atom" approximation [ecpssr_ua] and specialized for high energies [ecpssr_he]),
- theoretical calculations based on plane wave Born approximation (PWBA),
- empirical models based on fits to experimental data collected by Paul and Sacher [paul_sacher] (for protons, K shell), Paul and Bolik [paul_bolik] (for α, K shell), Kahoul et al. [kahoul]) (for protons, K, shell), Miyagawa et al. [miyagawa], Orlic et al. [orlic_semiemp] and Sow et al. [sow] for L shell.

The cross section models available in Geant4 are listed in Table [tab_models].

|lll|c|
Model & Z range
ECPSSR & 6-92
ECPSSR High Energy & 6-92
ECPSSR Hartree-Slater & 6-92
ECPSSR United Atom & 6-92
ECPSSR reference [paul_sacher] & 6-92
PWBA & 6-92
Paul and Sacher & 6-92
Kahoul et al. & 6-92
Model & Z range
ECPSSR & 6-92
ECPSSR United Atom & 6-92
PWBA & 6-92
Miyagawa et al. & 40-92
Orlic et al. & 43-92
Sow et al. & 43-92
Model & Z range
ECPSSR & 6-92
PWBA & 6-92
Model & Z range
ECPSSR & 6-92
ECPSSR Hartree-Slater & 6-92
ECPSSR reference [paul_bolik] & 6-92
PWBA & 6-92
Paul and Bolik & 6-92
Model & Z range
ECPSSR & 6-92
PWBA & 6-92

The calculation of cross sections in the course of the simulation is based on the interpolation of tabulated values, which are collected in a data library. The tabulations corresponding to theoretical calculations span the energy range between 10 keV and 10 GeV; empirical models are tabulated consistently with the energy range of validity documented by their authors, that corresponds to the range of the data used in the empirical fits and varies along with the atomic number and sub-shell.

ECPSSR tabulations have been produced using the ISICS software [isics][isics2006], 2006 version; an extended version, kindly provided by ISICS author S. Cipolla [isics2008], has been exploited to produce tabulations associated with recent high energy modelling developments [ecpssr_he].

An example of the characteristics of different cross section models is illustrated in Fig. [fig_crossk29]. Fig. [fig_crossk6] shows various cross section models for the ionisation of carbon K shell by proton, compared to experimental data reported in [paul_sacher].

The implemented cross section models have been subject to rigorous statistical analysis to evaluate their compatibility with experimental measurements reported in [paul_sacher], [orlic_exp], [sokhi] and to compare the relative accuracy of the various modelling options.

The validation process involved two stages: first goodness-of-fit analysis based on the χ^2 test to evaluate the hypothesis of compatibility with experimental data, then categorical analysis exploiting contingency tables to determine whether the various modelling options differ significantly in accuracy. Contingency tables were analyzed with the χ^2 test and with Fisher's exact test.

The complete set of validation results is documented in [tns_pixe]. Only the main ones are summarized here; Geant4 users interested in detailed results, like the accuracy of different cross section models for specific target elements, should should refer to [tns_pixe] for detailed information.

Regarding the K shell, the statistical analysis identified the ECPSSR model with Hartree-Slater correction as the most accurate in the energy range up to approximately 10 MeV; at higher energies the ECPSSR model in its plain formulation or the empirical Paul and Sacher one (within its range of applicability) exhibit the best performance. The scarceness of high energy data prevents a definitive appraisal of the ECPSSR specialization for high energies.

Regarding the L shell, the ECPSSR model with "united atom" approximation exhibits the best accuracy among the various implemented models; its compatibility with experimental measurements at 95% confidence level ranges from approximately 90% of the test cases for the L_3 sub-shell to approximately 65% for the L_1 sub-shell. According to the results of the categorical analysis, the ECPSSR model in its original formulation can be considered an equivalently accurate alternative. The Orlic et al. model exhibits the worst accuracy with respect to experimental data; its accuracy is significantly different from the one of the ECPSSR model in the "united atom" variant.

In the current Geant4 release the implementation of the hadron impact ionisation process (*G4ImpactIonisation*) is largely based on the original *G4hLowEnergyIonisation* process [lowe_chep],:cite:*lowe_nss*, [tns_antiprotons]. Thanks to the adopted component-based software design, the simulation of PIXE currently exploits the existing Geant4 atomic relaxation [relax] component to produce secondary X-rays resulting from impact ionisation.

4.6 Utils

4.6.1 Density effect

x is a kinetic variable of the particle : $x = \log_{10}(\gamma\beta) = \ln(\gamma^2\beta^2)/4.606$, and $\delta(x)$ is defined by

$$\begin{array}{lll} \text{for} \quad x < x_0 : & \delta(x) = 0 \\ \text{for} \quad x \in [x_0,\, x_1] : & \delta(x) = 4.606x - C + a(x_1 - x)^m \\ \text{for} \quad x > x_1 : & \delta(x) = 4.606x - C \end{array}$$

where the matter-dependent constants are calculated as follows:

$$\begin{array}{lcl} h\nu_p & = & \text{plasma energy of the medium } = \sqrt{4\pi n_{el} r_e^3} mc^2/\alpha = \sqrt{4\pi n_{el} r_e}\hbar c \\ C & = & 1 + 2\ln(I/h\nu_p) \\ x_a & = & C/4.606 \\ a & = & 4.606(x_a - x_0)/(x_1 - x_0)^m \\ m & = & 3. \end{array}$$

For condensed media

$$\begin{array}{ll} I < 100\,\text{eV} & \begin{cases} \text{for } C \le 3.681 & x_0 = 0.2 \quad x_1 = 2 \\ \text{for } C > 3.681 & x_0 = 0.326C - 1.0 \quad x_1 = 2 \end{cases} \\ I \ge 100\,\text{eV} & \begin{cases} \text{for } C \le 5.215 & x_0 = 0.2 \quad x_1 = 3 \\ \text{for } C > 5.215 & x_0 = 0.326C - 1.5 \quad x_1 = 3 \end{cases} \end{array}$$

and for gaseous media

$$
\begin{array}{llll}
\text{for} & C < 10. & x_0 = 1.6 & x_1 = 4 \\
\text{for} & C \in [10.0,\ 10.5[& x_0 = 1.7 & x_1 = 4 \\
\text{for} & C \in [10.5,\ 11.0[& x_0 = 1.8 & x_1 = 4 \\
\text{for} & C \in [11.0,\ 11.5[& x_0 = 1.9 & x_1 = 4 \\
\text{for} & C \in [11.5,\ 12.25[& x_0 = 2. & x_1 = 4 \\
\text{for} & C \in [12.25,\ 13.804[& x_0 = 2. & x_1 = 5 \\
\text{for} & C \geq 13.804 & x_0 = 0.326C - 2.5 & x_1 = 5.
\end{array}
$$

4.6.2 Introduction

All processes of gamma interaction with media in Geant4 are happen at the end of the step, so these interactions are $discrete$ and corresponding processes are following $G4VDiscreteProcess$ interface.

General Interfaces

There are a number of similar functions for discrete electromagnetic processes and for electromagnetic (EM) packages an additional base classes were designed to provide common computations *[1]*. Common calculations for discrete EM processes are performed in the class $G4VEmProcess$. Derived classes ([discrete:table1]) are concrete processes providing initialisation. The physics models are implemented using the $G4VEmModel$ interface. Each process may have one or many models defined to be active over a given energy range and set of $G4Regions$. Models are implementing computation of energy loss, cross section and sampling of final state. The list of EM processes and models for gamma incident is shown in Table [discrete:table1].

EM process	EM model	Ref.
G4PhotoElectricEffect	G4PEEffectFluoModel	[sec:em.pee]
	G4LivermorePhotoElectricModel	[secphoto]
	G4LivermorePolarizedPhotoElectricModel	
	G4PenelopePhotoElectricModel	[pen:phot]
G4PolarizedPhotoElectricEffect	G4PolarizedPEEffectModel	[sec:pol.intro]
G4ComptonScattering	G4KleinNishinaCompton	[sec:em.compton]
	G4KleinNishinaModel	[sec:em.compton]
	G4LivermoreComptonModel	[le:comp]
	G4LivermoreComptonModelRC	
	G4LivermorePolarizedComptonModel	[le:polcomp]
	G4LowEPComptonModel	[sec:em.monash]
	G4PenelopeComptonModel	[pen:comp]
G4PolarizedCompton	G4PolarizedComptonModel	[sec:pol.intro]
G4GammaConversion	G4BetheHeitlerModel	[sec:em.conv]
	G4PairProductionRelModel	
	G4LivermoreGammaConversionModel	[le:conv]
	G4BoldyshevTripletModel	[le:3conv]
	G4LivermoreNuclearGammaConversionModel	
	G4LivermorePolarizedGammaConversionModel	
	G4PenelopeGammaConvertion	[pen:conv]
G4PolarizedGammaConversion	G4PolarizedGammaConversionModel	[sec:pol.intro]
G4RayleighScattering	G4LivermoreRayleighModel	[le:rayleigh]
	G4LivermorePolarizedRayleighModel	
	G4PenelopeRayleighModel	[pen:rayl]
G4GammaConversionToMuons		[sec:em.gmumu]

Table: List of process and model classes for gamma.

4.6.3 Mean Energy Loss

Energy loss processes are very similar for $e+/e-$, $\mu+/\mu-$ and charged hadrons, so a common description for them was a natural choice in Geant4 *[1]*, *[1]*. Any energy loss process must calculate the continuous and discrete energy loss in a material. Below a given energy threshold the energy loss is continuous and above it the energy loss is simulated by the explicit production of secondary particles - gammas, electrons, and positrons.

Method

Let

$$\frac{d\sigma(Z,E,T)}{dT}$$

be the differential cross-section per atom (atomic number Z) for the ejection of a secondary particle with kinetic energy T by an incident particle of total energy E moving in a material of density ρ. The value of the *kinetic energy cut-off* or *production threshold* is denoted by T_{cut}. Below this threshold the soft secondaries ejected are simulated as continuous energy loss by the incident particle, and above it they are explicitly generated. The mean rate of energy loss is given by:

$$\frac{dE_{soft}(E,T_{cut})}{dx} = n_{at}\cdot\int_0^{T_{cut}}\frac{d\sigma(Z,E,T)}{dT}T\,dT$$

where n_{at} is the number of atoms per volume in the material. The total cross section per atom for the ejection of a secondary of energy $T > T_{cut}$ is

$$\sigma(Z,E,T_{cut}) = \int_{T_{cut}}^{T_{max}}\frac{d\sigma(Z,E,T)}{dT}\,dT$$

where T_{max} is the maximum energy transferable to the secondary particle.

If there are several processes providing energy loss for a given particle, then the total continuous part of the energy loss is the sum:

$$\frac{dE^{tot}_{soft}(E,T_{cut})}{dx} = \sum_i \frac{dE_{soft,i}(E,T_{cut})}{dx}.$$

These values are pre-calculated during the initialization phase of Geant4 and stored in the dE/dx table. Using this table the ranges of the particle in given materials are calculated and stored in the $Range$ table. The $Range$ table is then inverted to provide the $InverseRange$ table. At run time, values of the particle's continuous energy loss and range are obtained using these tables. Concrete processes contributing to the energy loss are not involved in the calculation at that moment. In contrast, the production of secondaries with kinetic energies above the production threshold is sampled by each concrete energy loss process.

The default energy interval for these tables extends from $100eV$ to $10TeV$ and the default number of bins is 77. For muons and for heavy particles energy loss processes models are valid for higher energies and can be extended. For muons uppper limit may be set to $1000PeV$.

General Interfaces

There are a number of similar functions for discrete electromagnetic processes and for electromagnetic (EM) packages an additional base classes were designed to provide common computations *[1]*. Common calculations for discrete EM processes are performed in the class $G4VEnergyLossProcess$. Derived classes ([enloss:table1]) are concrete

processes providing initialisation. The physics models are implemented using the $G4VEmModel$ interface. Each process may have one or many models defined to be active over a given energy range and set of $G4Regions$. Models are implementing computation of energy loss, cross section and sampling of final state. The list of EM processes and models for gamma incident is shown in Table [enloss:table1].

EM process	EM model	Ref.
G4eIonisation	G4MollerBhabhaModel	[sec:em.eion]
	G4LivermoreIonisationModel	[secioni2]
	G4PenelopeIonisationModel	[pen:eioni]
	G4PAIModel	[secpai]
	G4PAIPhotModel	[secpai]
G4ePolarizedIonisation	G4PolarizedMollerBhabhaModel	[sec:pol.intro]
G4MuIonisation	G4MuBetheBlochModel	[muioni]
	G4PAIModel	[secpai]
	G4PAIPhotModel	[secpai]
G4hIonisation	G4BetheBlochModel	[hion]
	G4BraggModel	[hion]
	G4ICRU73QOModel	[lowneg]
	G4PAIModel	[secpai]
	G4PAIPhotModel	[secpai]
G4ionIonisation	G4BetheBlochModel	[hion]
	G4BetheBlochIonGasModel	[hion]
	G4BraggIonModel	[hion]
	G4BraggIonGasModel	[hion]
	G4IonParametrisedLossModel	[ion:ICRU73]
G4NuclearStopping	G4ICRU49NuclearStoppingModel	[nuclstop]
G4mplIonisation	G4mplIonisationWithDeltaModel	
G4eBremsstrahlung	G4SeltzerBergerModel	[sec:em.ebrem.sbnew]
	G4eBremsstrahlungRelModel	[sec:em.ebrem.lpm]
	G4LivermoreBremsstrahlungModel	[lowebrems]
	G4PenelopeBremsstrahlungModel	[pen:bremss]
G4ePolarizedBremsstrahlung	G4PolarizedBremsstrahlungModel	[sec:pol.intro]
G4MuBremsstrahlung	G4MuBremsstrahlungModel	[secmubrem]
G4hBremsstrahlung	G4hBremsstrahlungModel	
G4ePairProduction	G4MuPairProductionModel	[muee]
G4MuPairProduction	G4MuPairProductionModel	[muee]
G4hPairProduction	G4hPairProductionModel	

Table: List of process and model classes for charged particles.

Step-size Limit

Continuous energy loss imposes a limit on the step-size because of the energy dependence of the cross sections. It is generally assumed in MC programs (for example, Geant3) that the cross sections are approximately constant along a step, i.e. the step size should be small enough, so that the change in cross section along the step is also small. In principle one must use very small steps in order to insure an accurate simulation, however the computing time increases as the step-size decreases.

For EM processes the exact solution is available (see [integral]) but is is not implemented yet for all physics processes including hadronics. A good compromise is to limit the step-size by not allowing the stopping range of the particle to decrease by more than ~ 20 % during the step. This condition works well for particles with kinetic energies > 1 MeV, but for lower energies it gives too short step-sizes, so must be relaxed. To solve this problem a lower limit on

the step-size was introduced. A smooth *StepFunction*, with 2 parameters, controls the step size. At high energy the maximum step size is defined by Step/Range $\sim \alpha_R$ (parameter *dRoverRange*). By default $\alpha_R = 0.2$. As the particle travels the maximum step size decreases gradually until the range becomes lower than ρ_R (parameter *finalRange*). Default *finalRange* $\rho_R = 1mm$. For the case of a particle range $R > \rho_R$ the *StepFunction* provides limit for the step size ΔS_{lim} by the following formula:

$$\Delta S_{lim} = \alpha_R R + \rho_R(1 - \alpha_R)\left(2 - \frac{\rho_R}{R}\right).$$

In the opposite case of a small range $\Delta S_{lim} = R$. The figure below shows the ratio step/range as a function of range if step limitation is determined only by the expression ([comion.d]).

[width=,height=0.4,draft=false] electromagnetic/utils/steplimit.eps

The parameters of *StepFunction* can be overwritten using an UI command: */process/eLoss/StepFunction 0.2 1 mm* To provide more accurate simulation of particle ranges in physics constructors *G4EmStandardPhysics_option3* and *G4EmStandardPhysics_option4* more strict step limitation is chosen for different particle types.

Run Time Energy Loss Computation

The computation of the *mean energy loss* after a given step is done by using the dE/dx, $Range$, and $InverseRange$ tables. The dE/dx table is used if the energy deposition (ΔT) is less than allowed limit $\Delta T < \xi T_0$, where ξ is $linearLossLimit$ parameter (by default $\xi = 0.01$), T_0 is the kinetic energy of the particle. In that case

$$\Delta T = \frac{dE}{dx}\Delta s,$$

where ΔT is the energy loss, Δs is the *true step length*. When a larger percentage of energy is lost, the mean loss can be written as

$$\Delta T = T_0 - f_T(r_0 - \Delta s)$$

where r_0 the range at the beginning of the step, the function $f_T(r)$ is the inverse of the $Range$ table (i.e. it gives the kinetic energy of the particle for a range value of r). By default spline approximation is used to retrieve a value from dE/dx, $Range$, and $InverseRange$ tables. The spline flag can be changed using an UI command: */process/em/spline false* After the mean energy loss has been calculated, the process computes the *actual* energy loss, i.e. the loss with fluctuations. The fluctuation models are described in Section [gen_fluctuations].

If deexcitation module (see [relax]) is enabled then simulation of atomic deexcitation is performed using information on step length and ionisation cross section. Fluorescence gamma and Auger electrons are produced above the same threshold energy as δ-electrons and bremsstrahlung gammas. Following UI commands can be used to enable atomic relaxation: */process/em/deexcitation myregion true true true /process/em/fluo true /process/em/auger true /process/em/pixe true /process/em/deexcitationIgnoreCut true* The last command means that production threshold for electrons and gammas are not checked, so full atomic de-excitation decay chain is simulated.

After the step a kinetic energy of a charged particle is compered with the *lowestEnergy*. In the case if final kinetic energy is below the particle is stooped and remaining kinetic energy is assigned to the local energy deposit. The default value of the limit is $1keV$. It may be changed separately for electron/positron and muon/hadron using UI commands: */process/em/lowestElectronEnergy 100 eV /process/em/lowestMuHadEnergy 50 eV* These values may be also can be set to zero.

Energy Loss by Heavy Charged Particles

To save memory in the case of positively charged hadrons and ions energy loss, dE/dx, $Range$ and $InverseRange$ tables are constructed only for *proton, antiproton, muons, pions, kaons, and Generic Ion*. The energy loss for other particles is computed from these tables at the *scaled kinetic energy* T_{scaled} :

$$T_{scaled} = T\frac{M_{base}}{M_{particle}},$$

where T is the kinetic energy of the particle, M_{base} and $M_{particle}$ are the masses of the base particle (*proton or kaon*) and particle. For positively changed hadrons with non-zero spin *proton* is used as a based particle, for negatively charged hadrons with non-zero spin - *antiproton*, for charged particles with zero spin - K^+ or K^- correspondingly. The virtual particle *Generic Ion* is used as a base particle for for all ions with $Z > 2$. It has mass, change and other quantum numbers of the *proton*. The energy loss can be defined via scaling relation:

$$\frac{dE}{dx}(T) = q_{eff}^2(F_1(T)\frac{dE}{dx}_{base}(T_{scaled}) + F_2(T, q_{eff})),$$

where q_{eff} is particle effective change in units of positron charge, F_1 and F_2 are correction function taking into account Birks effect, Block correction, low-energy corrections based on data from evaluated data bases *[1]*. For a hadron q_{eff} is equal to the hadron charge, for a slow ion effective charge is different from the charge of the ion's nucleus, because of electron exchange between transporting ion and the media. The effective charge approach is used to describe this effect *[2]*. The scaling relation ([enloss.sc]) is valid for any combination of two heavy charged particles with accuracy corresponding to high order mass, charge and spin corrections *[3]*.

4.6.4 Energy Loss Fluctuations

The total continuous energy loss of charged particles is a stochastic quantity with a distribution described in terms of a straggling function. The straggling is partially taken into account in the simulation of energy loss by the production of δ-electrons with energy $T > T_{cut}$ (Eq.[comion.b]). However, continuous energy loss (Eq.[comion.a]) also has fluctuations. Hence in the current GEANT4 implementation different models of fluctuations implementing the $G4VEmFluctuationModel$ interface:

- G4BohrFluctuations;
- G4IonFluctuations;
- G4PAIModel;
- G4PAIPhotModel;
- G4UniversalFluctuation.

The last model is the default one used in main Physics List and will be described below. Other models have limited applicability and will be described in chapters for ion ionisation and PAI models.

Fluctuations in Thick Absorbers

The total continuous energy loss of charged particles is a stochastic quantity with a distribution described in terms of a straggling function. The straggling is partially taken into account in the simulation of energy loss by the production of δ-electrons with energy $T > T_c$. However, continuous energy loss also has fluctuations. Hence in the current GEANT4 implementation two different models of fluctuations are applied depending on the value of the parameter κ which is the lower limit of the number of interactions of the particle in a step. The default value chosen is $\kappa = 10$. In the case of a high range cut (i.e. energy loss without delta ray production) for thick absorbers the following condition should be fulfilled:

$$\Delta E > \kappa\, T_{max}$$

where ΔE is the mean continuous energy loss in a track segment of length s, and T_{max} is the maximum kinetic energy that can be transferred to the atomic electron. If this condition holds the fluctuation of the total (unrestricted) energy loss follows a Gaussian distribution. It is worth noting that this condition can be true only for heavy particles, because for electrons, $T_{max} = T/2$, and for positrons, $T_{max} = T$, where T is the kinetic energy of the particle. In order to simulate the fluctuation of the continuous (restricted) energy loss, the condition should be modified. After a study, the following conditions have been chosen:

$$\Delta E > \kappa\, T_c$$

$$T_{max} <= 2\,T_c$$

where T_c is the cut kinetic energy of δ-electrons. For thick absorbers the straggling function approaches the Gaussian distribution with Bohr's variance *[3]*:

$$\Omega^2 = 2\pi r_e^2 m_e c^2 N_{el} \frac{Z_h^2}{\beta^2} T_c s \left(1 - \frac{\beta^2}{2}\right),$$

where r_e is the classical electron radius, N_{el} is the electron density of the medium, Z_h is the charge of the incident particle in units of positron charge, and β is the relativistic velocity.

Fluctuations in Thin Absorbers

If the conditions [cond2] and [cond3] are not satisfied the model of energy fluctuations in thin absorbers is applied. The formulas used to compute the energy loss fluctuation (straggling) are based on a very simple physics model of the atom. It is assumed that the atoms have only two energy levels with binding energies E_1 and E_2. The particle-atom interaction can be an excitation with energy loss E_1 or E_2, or ionisation with energy loss distributed according to a function $g(E) \sim 1/E^2$:

$$\int_{E_0}^{T_{up}} g(E)\,dE = 1 \Longrightarrow g(E) = \frac{E_0 T_{up}}{T_{up} - E_0} \frac{1}{E^2}.$$

The macroscopic cross section for excitation $(i = 1, 2)$ is

$$\Sigma_i = C \frac{f_i}{E_i} \frac{\ln[2mc^2\,(\beta\gamma)^2/E_i] - \beta^2}{\ln[2mc^2\,(\beta\gamma)^2/I] - \beta^2}\,(1 - r)$$

and the ionisation cross section is

$$\Sigma_3 = C \frac{T_{up} - E_0}{E_0 T_{up} \ln(\frac{T_{up}}{E_0})}\,r$$

where E_0 denotes the ionisation energy of the atom, I is the mean ionisation energy, T_{up} is the production threshold for delta ray production (or the maximum energy transfer if this value smaller than the production threshold), E_i and f_i are the energy levels and corresponding oscillator strengths of the atom, and C and r are model parameters.

The oscillator strengths f_i and energy levels E_i should satisfy the constraints

$$f_1 + f_2 = 1$$

$$f_1 \cdot lnE_1 + f_2 \cdot lnE_2 = lnI.$$

The cross section formulas [fluct.eqn1],[fluct.eqn2] and the sum rule equations [fluct.eqn3],[fluct.eqn4] can be found e.g. in Ref. [straggling.bichsel]. The model parameter C can be defined in the following way. The numbers of collisions (n_i, $i = 1, 2$ for excitation and 3 for ionisation) follow the Poisson distribution with a mean value $\langle n_i \rangle$. In a step of length Δx the mean number of collisions is given by

$$\langle n_i \rangle = \Delta x\,\Sigma_i$$

The mean energy loss in a step is the sum of the excitation and ionisation contributions and can be written as

$$\frac{dE}{dx} \cdot \Delta x = \left\{ \Sigma_1 E_1 + \Sigma_2 E_2 + \int_{E_0}^{T_{up}} E g(E) dE \right\} \Delta x.$$

From this, using Eq. [fluct.eqn1] - [fluct.eqn4], one can see that

$$C = dE/dx.$$

The other parameters in the fluctuation model have been chosen in the following way. $Z \cdot f_1$ and $Z \cdot f_2$ represent in the model the number of loosely/tightly bound electrons

$$f_2 = 0 \quad for \quad Z = 1$$

$$f_2 = 2/Z \quad for \quad Z \geq 2$$

$$E_2 = 10 \text{ eV } Z^2$$

$$E_0 = 10 \text{ eV } .$$

Using these parameter values, E_2 corresponds approximately to the K-shell energy of the atoms (and $Zf_2 = 2$ is the number of K-shell electrons). The parameters f_1 and E_1 can be obtained from Eqs. [fluct.eqn3] and [fluct.eqn4]. The parameter r is the only variable in the model which can be tuned. This parameter determines the relative contribution of ionisation and excitation to the energy loss. Based on comparisons of simulated energy loss distributions to experimental data, its value has been fixed as

$$r = 0.55$$

Width Correction Algorithm

This simple parametrization and sampling in the model give good values for the most probable energy loss in thin layers. The width of the energy loss distribution (Full Width at Half Maximum, FWHM) in most of the cases is too small. In order to get good FWHM values a relatively simple width correction algorithm has been applied. This algorithm rescales the energy levels E_1, E_2 and the number of excitations n_1, n_2 in such a way that the mean energy loss remains the same. Using this width correction scheme the model gives not only good most probable energy loss, but good FWHM value too.

Width correction algorithm is in the model since version 9.2. The updated version in the model (in version 9.4) causes an important change in the behaviour of the model: the results become much more stable, i.e. the results do not change practically when the cuts and/or the stepsizes are changing. Another important change: the (unphysical) second peak or shoulder in the energy loss distribution which can be seen in some cases (energy loss in thin gas layers) in older versions of the model disappeared. Limit of validity of the model for thin targets: the model gives good (reliable) energy loss distribution if the mean energy loss in the target is $\geq (few \ \ times) * I_{exc}$, where I_{exc} is the mean excitation energy of the target material.

This simple model of energy loss fluctuations is rather fast and can be used for any thickness of material. This has been verified by performing many simulations and comparing the results with experimental data, such as those in Ref.:cite:*straggling.lassila*. As the limit of validity of Landau's theory is approached, the loss distribution approaches the Landau form smoothly.

Sampling of Energy Loss

If the mean energy loss and step are in the range of validity of the Gaussian approximation of the fluctuation ([cond2] and [cond3]), the Gaussian sampling is used to compute the actual energy loss ([sig.fluc]). For smaller steps the energy loss is computed in the model under the assumption that the step length (or relative energy loss) is small and, in consequence, the cross section can be considered constant along the step. The loss due to the excitation is

$$\Delta E_{exc} = n_1 E_1 + n_2 E_2$$

where n_1 and n_2 are sampled from a Poisson distribution. The energy loss due to ionisation can be generated from the distribution $g(E)$ by the inverse transformation method :

$$u = F(E) = \int_{E_0}^{E} g(x)dx$$

$$E = F^{-1}(u) = \frac{E_0}{1 - u\frac{T_{up}-E_0}{T_{up}}}$$

where u is a uniformly distributed random number $\in [0,\ 1]$. The contribution coming from the ionisation will then be

$$\Delta E_{ion} = \sum_{j=1}^{n3} \frac{E_0}{1 - u_j\frac{T_{up}-E_0}{T_{up}}}$$

where n_3 is the number of ionisations sampled from the Poisson distribution. The total energy loss in a step will be $\Delta E = \Delta E_{exc} + \Delta E_{ion}$ and the energy loss fluctuation comes from fluctuations in the number of collisions n_i and from the sampling of the ionisation loss.

4.6.5 Correcting the Cross Section for Energy Variation

As described in Sections [en_loss] and [ip] the step size limitation is provided by energy loss processes in order to insure the precise calculation of the probability of particle interaction. It is generally assumed in Monte Carlo programs that the particle cross sections are approximately constant during a step, hence the reaction probability p at the end of the step can be expressed as

$$p = 1 - \exp\left(-ns\sigma(E_i)\right),$$

where n is the density of atoms in the medium, s is the step length, E_i is the energy of the incident particle at the beginning of the step, and $\sigma(E_i)$ is the reaction cross section at the beginning of the step.

However, it is possible to sample the reaction probability from the exact expression

$$p = 1 - \exp\left(-\int_{E_i}^{E_f} n\sigma(E)ds\right),$$

where E_f is the energy of the incident particle at the end of the step, by using the integral approach to particle transport. This approach is available for processes implemented via the $G4VEnergyLossProcess$ and $G4VEmProcess$ interfaces.

The Monte Carlo method of integration is used for sampling the reaction probability [int.unimod]. It is assumed that during the step the reaction cross section smaller, than some value $\sigma(E) < \sigma_m$. The mean free path for the given step is computed using σ_m. If the process is chosen as the process happens at the step, the sampling of the final state is performed only with the probability $p = \sigma(E_f)/\sigma_m$, alternatively no interaction happen and tracking of the particle is continued. To estimate the maximum value σ_m for the given tracking step at Geant4 initialisation the energy E_m of absoluted maximum σ_{max} of the cross section for given material is determined and stored. If at the tracking time particle energy $E < E_m$, then $\sigma_m = \sigma(E)$. For higher initial energies if $\xi E > E_m$ then $\sigma_m = max(\sigma(E), \sigma(\xi E))$, in the opposit case, $\sigma_m = \sigma_{max}$. Here ξ is a parameter of the algorithm. Its optimal value is connected with the value of the *dRoverRange* parameter (see sub-chapter [en_loss]), by default $\xi = 1 - \alpha_R = 0.8$. Note, that described method is precise if the cross section has only one maximum, which is a typical case for electromagnetic processes.

The integral variant of step limitation is the default for the $G4eIonisation$, $G4eBremsstrahlung$ and some otehr process but is not automatically activated for others. To do so the boolean UI command can be used: */process/eLoss/integral true* The integral variant of the energy loss sampling process is less dependent on values of the production cuts [int.g403] and allows to have less step limitation, however it should be applied on a case-by-case basis because may require extra CPU.

4.7 Xrays

4.7.1 Čerenkov Effect

The radiation of Čerenkov light occurs when a charged particle moves through a dispersive medium faster than the speed of light in that medium. A dispersive medium is one whose index of refraction is an increasing function of photon energy. Two things happen when such a particle slows down:

1. a cone of Čerenkov photons is emitted, with the cone angle (measured with respect to the particle momentum) decreasing as the particle loses energy;
2. the momentum of the photons produced increases, while the number of photons produced decreases.

When the particle velocity drops below the local speed of light, photons are no longer emitted. At that point, the Čerenkov cone collapses to zero. In order to simulate Čerenkov radiation the number of photons per track length must be calculated. The formulae used for this calculation can be found below and in *[1]*[pdg2]. Let n be the refractive index of the dielectric material acting as a radiator. Here $n = c/c'$ where c' is the group velocity of light in the material, hence $1 \leq n$. In a dispersive material n is an increasing function of the photon energy ϵ ($dn/d\epsilon \geq 0$). A particle traveling with speed $\beta = v/c$ will emit photons at an angle θ with respect to its direction, where θ is given by

$$\cos\theta = \frac{1}{\beta n}.$$

From this follows the limitation for the momentum of the emitted photons:

$$n(\epsilon_{min}) = \frac{1}{\beta}.$$

Photons emitted with an energy beyond a certain value are immediately re-absorbed by the material; this is the window of transparency of the radiator. As a consequence, all photons are contained in a cone of opening angle $\cos\theta_{max} = 1/(\beta n(\epsilon_{max}))$. The average number of photons produced is given by the relations :

$$\begin{aligned} dN = & \frac{\alpha z^2}{\hbar c}\sin^2\theta d\epsilon dx = \frac{\alpha z^2}{\hbar c}(1 - \frac{1}{n^2\beta^2})d\epsilon dx \\ \approx & \quad 370 z^2 \frac{photons}{eV\ cm}(1 - \frac{1}{n^2\beta^2})d\epsilon dx \end{aligned}$$

and the number of photons generated per track length is

$$\frac{dN}{dx} \approx 370 z^2 \int_{\epsilon_{min}}^{\epsilon_{max}} d\epsilon \left(1 - \frac{1}{n^2\beta^2}\right) = 370 z^2 \left[\epsilon_{max} - \epsilon_{min} - \frac{1}{\beta^2}\int_{\epsilon_{min}}^{\epsilon_{max}} \frac{d\epsilon}{n^2(\epsilon)}\right]$$

.

The number of photons produced is calculated from a Poisson distribution with a mean of $\langle n \rangle =$ StepLength dN/dx. The energy distribution of the photon is then sampled from the density function

$$f(\epsilon) = \left[1 - \frac{1}{n^2(\epsilon)\beta^2}\right]$$

.

4.7.2 Scintillation

Every scintillating material has a characteristic light yield, :math:)‘(Y, (photons/MeV‘), and an intrinsic resolution which generally broadens the statistical distribution, $\sigma_i/\sigma_s > 1$, due to impurities which are typical for doped crystals

like NaI(Tl) and CsI(Tl). The average yield can have a non-linear dependence on the local energy deposition. Scintillators also have a time distribution spectrum with one or more exponential decay time constants, τ_i, with each decay component having its intrinsic photon emission spectrum. These are empirical parameters typical for each material. The generation of scintillation light can be simulated by sampling the number of photons from a Poisson distribution. This distribution is based on the energy lost during a step in a material and on the scintillation properties of that material. The frequency of each photon is sampled from the empirical spectra. The photons are generated evenly along the track segment and are emitted uniformly into 4π with a random linear polarization.

4.7.3 Transition radiation

The Relationship of Transition Radiation to X-ray Cherenkov Radiation

X-ray transition radiation (XTR) occurs when a relativistic charged particle passes from one medium to another of a different dielectric permittivity. In order to describe this process it is useful to begin with an explanation of X-ray Cherenkov radiation, which is closely related.

The mean number of X-ray Cherenkov radiation (XCR) photons of frequency ω emitted into an angle θ per unit distance along a particle trajectory is *[1]*

$$\frac{d^3\bar{N}_{xcr}}{\hbar d\omega\, dx\, d\theta^2} = \frac{\alpha}{\pi\hbar c}\frac{\omega}{c}\theta^2 \mathrm{Im}\left\{Z\right\}.$$

Here the quantity Z is introduced as the *complex formation zone* of XCR in the medium:

$$Z = \frac{L}{1 - i\dfrac{L}{l}}, \quad L = \frac{c}{\omega}\left[\gamma^{-2} + \frac{\omega_p^2}{\omega^2} + \theta^2\right]^{-1}, \quad \gamma^{-2} = 1 - \beta^2.$$

with l and ω_p the photon absorption length and the plasma frequency, respectively, in the medium. For the case of a transparent medium, $l \to \infty$ and the complex formation zone reduces to the *coherence length* L of XCR. The coherence length roughly corresponds to that part of the trajectory in which an XCR photon can be created.

Introducing a complex quantity Z with its imaginary part proportional to the absorption cross-section ($\sim l^{-1}$) is required in order to account for absorption in the medium. Usually, $\omega_p^2/\omega^2 \gg c/\omega l$. Then it can be seen from Eqs. [Nxcr] and [Zj] that the number of emitted XCR photons is considerably suppressed and disappears in the limit of a transparent medium. This is caused by the destructive interference between the photons emitted from different parts of the particle trajectory.

The destructive interference of X-ray Cherenkov radiation is removed if the particle crosses a boundary between two media with different dielectric permittivities, ϵ, where

$$\epsilon = 1 - \frac{\omega_p^2}{\omega^2} + i\frac{c}{\omega l}.$$

Here the standard high-frequency approximation for the dielectric permittivity has been used. This is valid for energy transfers larger than the K-shell excitation potential.

If layers of media are alternated with spacings of order L, the X-ray radiation yield from a trajectory of unit length can be increased by roughly l/L times. The radiation produced in this case is called X-ray transition radiation (XTR).

Calculating the X-ray Transition Radiation Yield

Using the methods developed in Ref. *[2]* one can derive the relation describing the mean number of XTR photons generated per unit photon frequency and θ^2 *inside* the radiator for a general XTR radiator consisting of n different

absorbing media with fluctuating thicknesses:

$$\frac{d^2\bar{N}_{in}}{\hbar d\omega\, d\theta^2} = \frac{\alpha}{\pi\hbar c^2}\omega\theta^2 \mathrm{Re}\left\{\sum_{i=1}^{n-1}(Z_i - Z_{i+1})^2 + \right.$$

$$\left. + \quad 2\sum_{k=1}^{n-1}\sum_{i=1}^{k-1}(Z_i - Z_{i+1})\left[\prod_{j=i+1}^{k} F_j\right](Z_k - Z_{k+1})\right\},\ F_j = \exp\left[-\frac{t_j}{2Z_j}\right].$$

In the case of gamma distributed gap thicknesses (foam or fiber radiators) the values F_j, $(j = 1, 2)$ can be estimated as:

$$F_j = \int_0^\infty dt_j \left(\frac{\nu_j}{\bar{t}_j}\right)^{\nu_j} \frac{t_j^{\nu_j - 1}}{\Gamma(\nu_j)} \exp\left[-\frac{\nu_j t_j}{\bar{t}_j} - i\frac{t_j}{2Z_j}\right] = \left[1 + i\frac{\bar{t}_j}{2Z_j\nu_j}\right]^{-\nu_j},$$

where Z_j is the complex formation zone of XTR (similar to relation [Zj] for XCR) in the j-th medium *[2][3]*. Γ is the Euler gamma function, $\bar{t}_j$ is the mean thickness of the j-th medium in the radiator and $\nu_j > 0$ is the parameter roughly describing the relative fluctuations of t_j. In fact, the relative fluctuation is $\delta t_j/\bar{t}_j \sim 1/\sqrt{\nu_j}$.

In the particular case of n foils of the first medium (Z_1, F_1) interspersed with gas gaps of the second medium (Z_2, F_2), one obtains:

$$\frac{d^2\bar{N}_{in}}{\hbar d\omega\, d\theta^2} = \frac{2\alpha}{\pi\hbar c^2}\omega\theta^2 \mathrm{Re}\left\{\langle R^{(n)}\rangle\right\}, \quad F = F_1F_2,$$

$$\langle R^{(n)}\rangle = (Z_1 - Z_2)^2\left\{n\frac{(1-F_1)(1-F_2)}{1-F} + \frac{(1-F_1)^2F_2[1-F^n]}{(1-F)^2}\right\}.$$

Here $\langle R^{(n)}\rangle$ is the stack factor reflecting the radiator geometry. The integration of ([Nn1]) with respect to θ^2 can be simplified for the case of a regular radiator ($\nu_{1,2} \to \infty$), transparent in terms of XTR generation media, and $n \gg 1$ *[4]*. The frequency spectrum of emitted XTR photons is given by:

$$\frac{d\bar{N}_{in}}{\hbar d\omega} = \int_0^{\sim 10\gamma^{-2}} d\theta^2 \frac{d^2\bar{N}_{in}}{\hbar d\omega\, d\theta^2} = \frac{4\alpha n}{\pi\hbar\omega}(C_1 + C_2)^2$$

$$\cdot \sum_{k=k_{min}}^{k_{max}} \frac{(k - C_{min})}{(k - C_1)^2(k + C_2)^2} \sin^2\left[\frac{\pi t_1}{t_1 + t_2}(k + C_2)\right],$$

$$C_{1,2} = \frac{t_{1,2}(\omega_1^2 - \omega_2^2)}{4\pi c\omega}, \quad C_{min} = \frac{1}{4\pi c}\left[\frac{\omega(t_1 + t_2)}{\gamma^2} + \frac{t_1\omega_1^2 + t_2\omega_2^2}{\omega}\right].$$

The sum in ([Nntr]) is defined by terms with $k \geq k_{min}$ corresponding to the region of $\theta \geq 0$. Therefore k_{min} should be the nearest to C_{min} integer $k_{min} \geq C_{min}$. The value of k_{max} is defined by the maximum emission angle $\theta^2_{max} \sim 10\gamma^{-2}$. It can be evaluated as the integer part of

$$C_{max} = C_{min} + \frac{\omega(t_1 + t_2)}{4\pi c}\frac{10}{\gamma^2}, \quad k_{max} - k_{min} \sim 10^2 \div 10^3 \gg 1.$$

Numerically, however, only a few tens of terms contribute substantially to the sum, that is, one can choose $k_{max} \sim k_{min} + 20$. Equation ([Nntr]) corresponds to the spectrum of the total number of photons emitted inside a regular transparent radiator. Therefore the mean interaction length, λ_{XTR}, of the XTR process in this kind of radiator can be introduced as:

$$\lambda_{XTR} = n(t_1 + t_2)\left[\int_{\hbar\omega_{min}}^{\hbar\omega_{max}} \hbar d\omega \frac{d\bar{N}_{in}}{\hbar d\omega}\right]^{-1},$$

where $\hbar\omega_{min} \sim 1$ keV, and $\hbar\omega_{max} \sim 100$ keV for the majority of high energy physics experiments. Its value is constant along the particle trajectory in the approximation of a transparent regular radiator. The spectrum of the total number of XTR photons *after* regular transparent radiator is defined by ([Nntr]) with:

$$n \to n_{eff} = \sum_{k=0}^{n-1} \exp[-k(\sigma_1 t_1 + \sigma_2 t_2)] = \frac{1 - \exp[-n(\sigma_1 t_1 + \sigma_2 t_2)]}{1 - \exp[-(\sigma_1 t_1 + \sigma_2 t_2)]},$$

where σ_1 and σ_2 are the photo-absorption cross-sections corresponding to the photon frequency ω in the first and the second medium, respectively. With this correction taken into account the XTR absorption in the radiator ([Nntr]) corresponds to the results of *[5]*. In the more general case of the flux of XTR photons *after* a radiator, the XTR absorption can be taken into account with a calculation based on the stack factor derived in *[6]*:

$$\langle R^{(n)}_{flux} \rangle = (L_1 - L_2)^2 \left\{ \frac{1-Q^n}{1-Q} \frac{(1+Q_1)(1+F) - 2F_1 - 2Q_1F_2}{2(1-F)} + \frac{(1-F_1)(Q_1-F_1)F_2(Q^n-F^n)}{(1-F)(Q-F)} \right\},$$

$$Q = Q_1 \cdot Q_2, \quad Q_j = \exp\left[-t_j/l_j\right] = \exp\left[-\sigma_j t_j\right], \quad j = 1, 2.$$

Both XTR energy loss ([Rn]) and flux ([Rflux]) models can be implemented as a discrete electromagnetic process (see below).

Simulating X-ray Transition Radiation Production

A typical XTR radiator consits of many ($\sim$ 100) boundaries between different materials. To improve the tracking performance in such a volume one can introduce an artificial material *[3]*, which is the geometrical mixture of foil and gas contents. Here is an example:

```
// In DetectorConstruction of an application
// Preparation of mixed radiator material
foilGasRatio  = fRadThickness/(fRadThickness+fGasGap);
foilDensity   = 1.39*g/cm3;     // Mylar
gasDensity    = 1.2928*mg/cm3 ; // Air
totDensity    = foilDensity*foilGasRatio +
                gasDensity*(1.0-foilGasRatio);
fractionFoil =  foilDensity*foilGasRatio/totDensity;
fractionGas  =  gasDensity*(1.0-foilGasRatio)/totDensity;
G4Material* radiatorMat = new G4Material("radiatorMat",
                                         totDensity,
                                         ncomponents = 2 );
radiatorMat->AddMaterial( Mylar, fractionFoil );
radiatorMat->AddMaterial( Air,   fractionGas  );
G4cout << *(G4Material::GetMaterialTable()) << G4endl;
// materials of the TR radiator
fRadiatorMat = radiatorMat;   // artificial for geometry
fFoilMat     = Mylar;
fGasMat      = Air;
```

This artificial material will be assigned to the logical volume in which XTR will be generated:

```
solidRadiator = new G4Box("Radiator",
                          1.1*AbsorberRadius ,
                          1.1*AbsorberRadius,
                          0.5*radThick        );
logicRadiator = new G4LogicalVolume( solidRadiator,
                                     fRadiatorMat,  // !!!
                                    "Radiator");
physiRadiator = new G4PVPlacement(0,
                                  G4ThreeVector(0,0,zRad),
                                  "Radiator", logicRadiator,
                                  physiWorld, false, 0       );
```

XTR photons generated by a relativistic charged particle intersecting a radiator with $2n$ interfaces between different media can be simulated by using the following algorithm. First the total number of XTR photons is estimated using a

Poisson distribution about the mean number of photons given by the following expression:

$$\bar{N}^{(n)} = \int_{\omega_1}^{\omega_2} d\omega \int_0^{\theta^2_{max}} d\theta^2 \frac{d^2\bar{N}^{(n)}}{d\omega\, d\theta^2} = \frac{2\alpha}{\pi c^2} \int_{\omega_1}^{\omega_2} \omega d\omega \int_0^{\theta^2_{max}} \theta^2 d\theta^2 \mathrm{Re}\left\{\langle R^{(n)}\rangle\right\}.$$

Here $\theta^2_{max} \sim 10\gamma^{-2}$, $\hbar\omega_1 \sim 1$ keV, $\hbar\omega_2 \sim 100$ keV, and $\langle R^{(n)}\rangle$ correspond to the geometry of the experiment. For events in which the number of XTR photons is not equal to zero, the energy and angle of each XTR quantum is sampled from the integral distributions obtained by the numerical integration of expression ([Nn1]). For example, the integral energy spectrum of emitted XTR photons, $\bar{N}^{(n)}_{>\omega}$, is defined from the following integral distribution:

$$\bar{N}^{(n)}_{>\omega} = \frac{2\alpha}{\pi c^2} \int_{\omega}^{\omega_2} \omega d\omega \int_0^{\theta^2_{max}} \theta^2 d\theta^2 \mathrm{Re}\left\{\langle R^{(n)}\rangle\right\}.$$

In Geant4 XTR generation *inside* or *after* radiators is described as a discrete electromagnetic process. It is convenient for the description of tracks in magnetic fields and can be used for the cases when the radiating charge experiences a scattering inside the radiator. The base class G4VXTRenergyLoss is responsible for the creation of tables with integral energy and angular distributions of XTR photons. It also contains the PostDoIt function providing XTR photon generation and motion (if fExitFlux=true) through a XTR radiator to its boundary. Particular models like G4RegularXTRadiator implement the pure virtual function GetStackFactor, which calculates the response of the XTR radiator reflecting its geometry. Included below are some comments for the declaration of XTR in a user application.

In the physics list one should pass to the XTR process additional details of the XTR radiator involved:

```
// In PhysicsList of an application
else if (particleName == "e-")  // Construct processes for electron with XTR
{
   pmanager->AddProcess(new G4MultipleScattering, -1, 1,1 );
   pmanager->AddProcess(new G4eBremsstrahlung(),  -1,-1,1 );
   pmanager->AddProcess(new Em10StepCut(),        -1,-1,1 );
// in regular radiators:
   pmanager->AddDiscreteProcess(
   new G4RegularXTRadiator        // XTR dEdx in general regular radiator
// new G4XTRRegularRadModel        - XTR flux after general regular radiator
// new G4TransparentRegXTRadiator  - XTR dEdx in transparent
//                                   regular radiator
// new G4XTRTransparentRegRadModel - XTR flux after transparent
//                                   regular radiator
                          (pDet->GetLogicalRadiator(), // XTR radiator

                           pDet->GetFoilMaterial(), // real foil
                           pDet->GetGasMaterial(),  // real gas
                           pDet->GetFoilThick(),    // real geometry
                           pDet->GetGasThick(),
                           pDet->GetFoilNumber(),
                           "RegularXTRadiator"));
// or for foam/fiber radiators:
   pmanager->AddDiscreteProcess(
   new G4GammaXTRadiator    - XTR dEdx in general foam/fiber radiator
// new G4XTRGammaRadModel   - XTR flux after general foam/fiber radiator
                           ( pDet->GetLogicalRadiator(),
                             1000.,
                             100.,
                             pDet->GetFoilMaterial(),
                             pDet->GetGasMaterial(),
                             pDet->GetFoilThick(),
                             pDet->GetGasThick(),
                             pDet->GetFoilNumber(),
                             "GammaXTRadiator"));
}
```

Here for the foam/fiber radiators the values 1000 and 100 are the ν parameters (which can be varied) of the Gamma distribution for the foil and gas gaps, respectively. Classes G4TransparentRegXTRadiator and G4XTRTransparentRegRadModel correspond ([Nntr]) to n and n_{eff}, respectively.

BIBLIOGRAPHY

[1] A.G. Bogdanov et al. Geant4 simulation of production and interaction of muons. *IEEE Trans. Nucl. Sci. 53, 513*, 2006.

[2] S. Kelner, H. Burkhardt and R. Kokoulin. Production of muon pairs in annihilation of high-energy positrons with resting electrons. *CERN-AB-2003-002 (ABP) and CLIC Note 554*, January 2003.

[4] H. Messel and D. Crawford. *Electron-Photon shower distribution*. Pergamon Press, 1970.

[3] W.R. Nelson, H. Hirayama, and D.W.O. Rogers. *EGS4 code system*. SLAC, Dec 1985. SLAC-265, UC-32.

[1] W. Heitler. *The Quantum Theory of Radiation*. Oxford Clarendon Press, edition, 1954.

[1] A.G. Bogdanov et al. Geant4 simulation of production and interaction of muons. *IEEE Trans. Nucl. Sci. 53, 513*, 2006.

[3] J.C. Butcher and H. Messel. *Nucl. Phys.*, 20(15):, 1960.

[4] H. Messel and D. Crawford. *Electron-Photon shower distribution*. Pergamon Press, 1970.

[3] W.R. Nelson, H. Hirayama, and D.W.O. Rogers. *EGS4 code system*. SLAC, Dec 1985. SLAC-265, UC-32.

[4] J. H. Hubbell, H. A. Gimm, and I. Øverbø. Pair, Triplet, and Total Atomic Cross Sections (and Mass Attenuation Coefficients) for 1 MeV-100 GeV Photons in Elements Z=1 to 100. *Journal of Physical and Chemical Reference Data*, 9:1023–1148, October 1980. doi:10.1063/1.555629.

[1] Y. Tsai. Pair production and bremsstrahlung of charged leptons. *Rev. Mod. Phys.*, 46():815, 1974.

[2] Y. Tsai. Pair production and bremsstrahlung of charged leptons. *Rev. Mod. Phys.*, 49():421, 1977.

[4] H. Messel and D. Crawford. *Electron-Photon shower distribution*. Pergamon Press, 1970.

[5] René et al. Brun. *GEANT: Detector Description and Simulation Tool; Oct 1994*. CERN Program Library. CERN, Geneva, 1993. Long Writeup W5013. URL: https://cds.cern.ch/record/1082634.

[6] Richard L. Ford and W. Ralph Nelson. The egs code system: computer programs for the monte carlo simulation of electromagnetic cascade showers (version 3). Technical Report, SLAC, 1978.

[4] J. H. Hubbell, H. A. Gimm, and I. Øverbø. Pair, Triplet, and Total Atomic Cross Sections (and Mass Attenuation Coefficients) for 1 MeV-100 GeV Photons in Elements Z=1 to 100. *Journal of Physical and Chemical Reference Data*, 9:1023–1148, October 1980. doi:10.1063/1.555629.

[1] W. Heitler. *The Quantum Theory of Radiation*. Oxford Clarendon Press, edition, 1954.

[1] Y. Tsai. Pair production and bremsstrahlung of charged leptons. *Rev. Mod. Phys.*, 46():815, 1974.

[2] Y. Tsai. Pair production and bremsstrahlung of charged leptons. *Rev. Mod. Phys.*, 49():421, 1977.

[3] S.M. Seltzer and M.J. Berger. Bremsstrahlung energy spectra from electrons with kinetic energy 1 kev - 100 gev incident on screened nuclei and orbital electrons of neutral atoms with z = 1–100. *Atomic Data and Nuclear Data Tables*, 35():345, 1986.

[4] Stephen M. Seltzer and Martin J. Berger. Bremsstrahlung spectra from electron interactions with screened atomic nuclei and orbital electrons. *Nuclear Instruments and Methods in Physics Research Section B: Beam Interactions with Materials and Atoms*, 12(1):95–134, aug 1985. URL: https://doi.org/10.1016/0168-583X(85)90707-4, doi:10.1016/0168-583x(85)90707-4.

[5] R.H. Pratt, H.K. Tseng, C.M. Lee, Lynn Kissel, Crawford MacCallum, and Merle Riley. Bremsstrahlung energy spectra from electrons of kinetic energy 1 keV $\leq$ t1 $\leq$ 2000 keV incident on neutral atoms 2 $\leq$ z $\leq$ 92. *Atomic Data and Nuclear Data Tables*, 20(2):175–209, aug 1977. URL: https://doi.org/10.1016/0092-640X(77)90045-6, doi:10.1016/0092-640x(77)90045-6.

[6] Martin L. Perl. Notes on the Landau, Pomeranchuk, Migdal effect: Experiment and theory. In *8th Les Rencontres de Physique de la Vallee d'Aoste: Results and Perspectives in Particle Physics La Thuile, Italy, March 6-12, 1994*. 1994. URL: http://www-public.slac.stanford.edu/sciDoc/docMeta.aspx?slacPubNumber=SLAC-PUB-6514.

[7] Spencer Klein. Suppression of bremsstrahlung and pair production due to environmental factors. *Reviews of Modern Physics*, 71(5):1501–1538, oct 1999. URL: https://doi.org/10.1103/RevModPhys.71.1501, doi:10.1103/revmodphys.71.1501.

[8] Todor Stanev, Ch. Vankov, R. E. Streitmatter, R. W. Ellsworth, and Theodore Bowen. Development of ultrahigh-energy electromagnetic cascades in water and lead including the landau-pomeranchuk-migdal effect. *Physical Review D*, 25(5):1291–1304, mar 1982. URL: https://doi.org/10.1103/PhysRevD.25.1291, doi:10.1103/physrevd.25.1291.

[9] C. Amsler et al. Review of particle physics. *Physics Letters B*, 667(1-5):1–6, sep 2008. URL: https://doi.org/10.1016/j.physletb.2008.07.018, doi:10.1016/j.physletb.2008.07.018.

[10] V. M. Galitsky and I. I. Gurevich. Coherence effects in ultra-relativistic electron bremsstrahlung. *Il Nuovo Cimento (1955-1965)*, 32(2):396–407, Apr 1964. URL: https://doi.org/10.1007/BF02733969, doi:10.1007/BF02733969.

[11] A. B. Migdal. Bremsstrahlung and pair production in condensed media at high energies. *Physical Review*, 103(6):1811–1820, sep 1956. URL: https://doi.org/10.1103/PhysRev.103.1811, doi:10.1103/physrev.103.1811.

[12] P. L. Anthony, R. Becker-Szendy, P. E. Bosted, M. Cavalli-Sforza, L. P. Keller, L. A. Kelley, S. R. Klein, G. Niemi, M. L. Perl, L. S. Rochester, and J. L. White. Bremsstrahlung suppression due to the landau-pomeranchuk-migdal and dielectric effects in a variety of materials. *Physical Review D*, 56(3):1373–1390, aug 1997. URL: https://doi.org/10.1103/PhysRevD.56.1373, doi:10.1103/physrevd.56.1373.

[13] ML TERMIKAELYAN. * spektr tormoznogo izlucheniya v srede. *DOKLADY AKADEMII NAUK SSSR*, 94(6):1033–1036, 1954.

[14] M.L. Ter-Mikaelian. *High-energy Electromagnetic Processes in Condensed Media*. Wiley, 1972.

[1] M. J. Berger, M. Inokuti, H. H. Anderson, H. Bichsel, J. A. Dennis, D. Powers, S. M. Seltzer, and J. E. Turner. Icru report 37. *Journal of the International Commission on Radiation Units and Measurements*, os19(2):NP–NP, dec 1984. URL: https://doi.org/10.1093/jicru/os19.2.Report37, doi:10.1093/jicru/os19.2.report37.

[2] R. M. Sternheimer and R. F. Peierls. General expression for the density effect for the ionization loss of charged particles. *Physical Review B*, 3(11):3681–3692, jun 1971. URL: https://doi.org/10.1103/PhysRevB.3.3681, doi:10.1103/physrevb.3.3681.

[3] M. J. Berger, M. Inokuti, H. H. Andersen, H. Bichsel, D. Powers, S . M. Seltzer, D . Thwaites, and D. E. Watt. Report 49. *Journal of the International Commission on Radiation Units and Measurements*, os25(2):NP–NP, may 1993. ICRU Report 49. URL: https://doi.org/10.1093/jicru/os25.2.Report49, doi:10.1093/jicru/os25.2.report49.

[1] M. J. Berger, M. Inokuti, H. H. Anderson, H. Bichsel, J. A. Dennis, D. Powers, S. M. Seltzer, and J. E. Turner. Icru report 37. *Journal of the International Commission on Radiation Units and Measurements*, os19(2):NP–NP, dec 1984. URL: https://doi.org/10.1093/jicru/os19.2.Report37, doi:10.1093/jicru/os19.2.report37.

[2] R. M. Sternheimer and R. F. Peierls. General expression for the density effect for the ionization loss of charged particles. *Physical Review B*, 3(11):3681–3692, jun 1971. URL: https://doi.org/10.1103/PhysRevB.3.3681, doi:10.1103/physrevb.3.3681.

[4] W-M Yao et al. Review of particle physics. *Journal of Physics G: Nuclear and Particle Physics*, 33(1):1–1232, jul 2006. URL: https://doi.org/10.1088/0954-3899/33/1/001, doi:10.1088/0954-3899/33/1/001.

[5] Steven P. Ahlen. Theoretical and experimental aspects of the energy loss of relativistic heavily ionizing particles. *Reviews of Modern Physics*, 52(1):121–173, jan 1980. URL: https://doi.org/10.1103/RevModPhys.52.121, doi:10.1103/revmodphys.52.121.

[6] M. C. Walske. The stopping power ofK-electrons. *Physical Review*, 88(6):1283–1289, dec 1952. URL: https://doi.org/10.1103/PhysRev.88.1283, doi:10.1103/physrev.88.1283.

[7] M. C. Walske. Stopping power ofL-electrons. *Physical Review*, 101(3):940–944, feb 1956. URL: https://doi.org/10.1103/PhysRev.101.940, doi:10.1103/physrev.101.940.

[8] Govind S. Khandelwal. Shell corrections for k- and l-electrons. *Nuclear Physics A*, 116(1):97–111, jul 1968. URL: https://doi.org/10.1016/0375-9474(68)90485-5, doi:10.1016/0375-9474(68)90485-5.

[9] Hans Bichsel. Stopping power and ranges of fast ions in heavy elements. *Physical Review A*, 46(9):5761–5773, nov 1992. URL: https://doi.org/10.1103/PhysRevA.46.5761, doi:10.1103/physreva.46.5761.

[10] J. C. Ashley, R. H. Ritchie, and Werner Brandt. Z13-dependent stopping power and range contributions. *Physical Review A*, 8(5):2402–2408, nov 1973. URL: https://doi.org/10.1103/PhysRevA.8.2402, doi:10.1103/physreva.8.2402.

[3] M. J. Berger, M. Inokuti, H. H. Andersen, H. Bichsel, D. Powers, S . M. Seltzer, D . Thwaites, and D. E. Watt. Report 49. *Journal of the International Commission on Radiation Units and Measurements*, os25(2):NP–NP, may 1993. ICRU Report 49. URL: https://doi.org/10.1093/jicru/os25.2.Report49, doi:10.1093/jicru/os25.2.report49.

[2] M.J. Boschini et al. Nuclear and non-ionizing energy-loss for coulomb scattered particles from low energy up to relativistic regime in space radiation environment. In *Cosmic Rays for Particle and Astroparticle Physics*, 9–23. WORLD SCIENTIFIC, jun 2011. IBSN: 978-981-4329-02-6; arXiv 1011.4822. URL: https://doi.org/10.1142/9789814329033_0002, doi:10.1142/9789814329033_0002.

[3] C. Leroy and P.G. Rancoita. *Principles of Radiation Interaction in Matter and Detection*. World Scientific (Singapore), 2nd edition edition, 2009.

[4] G. Wentzel. Zwei bemerkungen über die zerstreuung korpuskularer strahlen als beugungserscheinung. *Zeitschrift für Physik*, 40(8):590–593, aug 1926. URL: https://doi.org/10.1007/BF01390457, doi:10.1007/bf01390457.

[5] J.P. Biersack J.F. Ziegler, M.D. Ziegler. The stopping and range of ions in matter, \em SRIM version 2008.03 (2008). http://www.srim.org/, 2008. [Online; accessed 26-october-2017].

[6] James F Ziegler, Jochen P Biersack, and Matthias D Ziegler. *SRIM: the stopping and range of ions in matter*. Cadence Design Systems, Raleigh, NC, 2008. URL: https://cds.cern.ch/record/1525729.

[7] Claude Leroy and Pier-Giorgio Rancoita. Particle interaction and displacement damage in silicon devices operated in radiation environments. *Reports on Progress in Physics*, 70(4):493–625, mar 2007. URL: https://doi.org/10.1088/0034-4885/70/4/R01, doi:10.1088/0034-4885/70/4/r01.

[1] J. Apostolakis et al. Geometry and physics of the geant4 toolkit for high and medium energy applications. *Radiation Physics and Chemistry*, 78(10):859–873, oct 2009. URL: https://doi.org/10.1016/j.radphyschem.2009.04.026, doi:10.1016/j.radphyschem.2009.04.026.

[2] G. Molière. Theorie der Streuung schneller geladener Teilchen II. Mehrfach- und Vielfachstreuung. *Zeitschrift Naturforschung Teil A*, 3:78–97, February 1948. doi:10.1515/zna-1948-0203.

[3] J. M. Fernández-Varea, R. Mayol, J. Baró, and F. Salvat. On the theory and simulation of multiple elastic scattering of electrons. *Nuclear Instruments and Methods in Physics Research B*, 73:447–473, April 1993. doi:10.1016/0168-583X(93)95827-R.

[4] S. Goudsmit and J. L. Saunderson. Multiple scattering of electrons. *Physical Review*, 57(1):24–29, jan 1940. URL: https://doi.org/10.1103/PhysRev.57.24, doi:10.1103/physrev.57.24.

[5] O. Kadri, V. Ivanchenko, F. Gharbi, and A. Trabelsi. Incorporation of the goudsmit–saunderson electron transport theory in the geant4 monte carlo code. *Nuclear Instruments and Methods in Physics Research Section B: Beam Interactions with Materials and Atoms*, 267(23-24):3624–3632, dec 2009. URL: https://doi.org/10.1016/j.nimb.2009.09.015, doi:10.1016/j.nimb.2009.09.015.

[6] László Urbán. A model for multiple scattering in GEANT4. Technical Report CERN-OPEN-2006-077, CERN, Geneva, Dec 2006. URL: http://cds.cern.ch/record/1004190.

[7] H. W. Lewis. Multiple scattering in an infinite medium. *Physical Review*, 78(5):526–529, jun 1950. URL: https://doi.org/10.1103/PhysRev.78.526, doi:10.1103/physrev.78.526.

[8] V N Ivanchenko, O Kadri, M Maire, and L Urban. Geant4 models for simulation of multiple scattering. *Journal of Physics: Conference Series*, 219(3):032045, apr 2010. URL: https://doi.org/10.1088/1742-6596/219/3/032045, doi:10.1088/1742-6596/219/3/032045.

[9] I. Kawrakow and Alex F. Bielajew. On the condensed history technique for electron transport. *Nuclear Instruments and Methods in Physics Research Section B: Beam Interactions with Materials and Atoms*, 142(3):253–280, jul 1998. URL: https://doi.org/10.1016/S0168-583X(98)00274-2, doi:10.1016/s0168-583x(98)00274-2.

[10] RICARDO MAYOL and FRANCESC SALVAT. TOTAL AND TRANSPORT CROSS SECTIONS FOR ELASTIC SCATTERING OF ELECTRONS BY ATOMS. *Atomic Data and Nuclear Data Tables*, 65(1):55–154, jan 1997. URL: https://doi.org/10.1006/adnd.1997.0734, doi:10.1006/adnd.1997.0734.

[11] V. L. Highland. Some practical remarks on multiple scattering. *Nuclear Instruments and Methods*, 129:497–499, November 1975. doi:10.1016/0029-554X(75)90743-0.

[12] G. R. Lynch and O. I. Dahl. Approximations to multiple Coulomb scattering. *Nuclear Instruments and Methods in Physics Research B*, 58:6–10, May 1991. doi:10.1016/0168-583X(91)95671-Y.

[13] D. Attwood, P. Bell, S. Bull, T. McMahon, J. Wilson, R. Fernow, P. Gruber, A. Jamdagni, K. Long, E. McKigney, P. Savage, M. Curtis-Rouse, T.R. Edgecock, M. Ellis, J. Lidbury, W. Murray, P. Norton, K. Peach, K. Ishida, Y. Matsuda, K. Nagamine, S. Nakamura, G.M. Marshall, S. Benveniste, D. Cline, Y. Fukui, K. Lee, Y. Pischalnikov, S. Holmes, and A. Bogacz. The scattering of muons in low-z materials. *Nuclear Instruments and Methods in Physics Research Section B: Beam Interactions with Materials and Atoms*, 251(1):41–55, sep 2006. URL: https://doi.org/10.1016/j.nimb.2006.05.006, doi:10.1016/j.nimb.2006.05.006.

[1] M.H. Mendenhall and R.A. Weller. An algorithm for computing screened coulomb scattering in geant4. *Nuclear Instruments and Methods in Physics Research B*, 227():420, 2005.

[2] M.H. Mendenhall and R.A. Weller. Algorithms for the rapid computation of classical cross sections for screened coulomb collisions. *Nuclear Instruments and Methods in Physics Research B*, 58():11, 1991.

[3] J.P. Biersack and L.G. Haggmark. A monte carlo computer program for the transport of energetic ions in amorphous targets. *Nuclear Instruments and Methods in Physics Research*, 174():257, 1980.

[4] I. Stegun (Eds.) M. Abramowitz. *Handbook of Mathematical Functions*. Dover, New York, edition, 1965.

[1] F Biggs and R Lighthill. Analytical approximations for x-ray cross sections III. Technical Report, Sandia Lab, aug 1988. Preprint Sandia Laboratory, SAND 87-0070. URL: https://doi.org/10.2172/7124946, doi:10.2172/7124946.

[2] Mihai Gavrila. RelativisticK-shell photoeffect. *Physical Review*, 113(2):514–526, jan 1959. URL: https://doi.org/10.1103/PhysRev.113.514, doi:10.1103/physrev.113.514.

[1] H. W. Koch and J. W. Motz. Bremsstrahlung cross-section formulas and related data. *Rev. Mod. Phys.*, 31(4):920–955, 1959.

[2] H. Davies et al. Theory of bremsstrahlung and pair production. ii. integral cross section for pair production. *Phys. Rev.*, 93(4):788–795, 1954.

[1] H. W. Koch and J. W. Motz. Bremsstrahlung cross-section formulas and related data. *Rev. Mod. Phys.*, 31(4):920–955, 1959.

[2] H. Davies et al. Theory of bremsstrahlung and pair production. ii. integral cross section for pair production. *Phys. Rev.*, 93(4):788–795, 1954.

[1] H. W. Koch and J. W. Motz. Bremsstrahlung cross-section formulas and related data. *Rev. Mod. Phys.*, 31(4):920–955, 1959.

[2] H. Davies et al. Theory of bremsstrahlung and pair production. ii. integral cross section for pair production. *Phys. Rev.*, 93(4):788–795, 1954.

[1] H. W. Koch and J. W. Motz. Bremsstrahlung cross-section formulas and related data. *Rev. Mod. Phys.*, 31(4):920–955, 1959.

[2] H. Davies et al. Theory of bremsstrahlung and pair production. ii. integral cross section for pair production. *Phys. Rev.*, 93(4):788–795, 1954.

[1] H. W. Koch and J. W. Motz. Bremsstrahlung cross-section formulas and related data. *Rev. Mod. Phys.*, 31(4):920–955, 1959.

[2] H. Davies et al. Theory of bremsstrahlung and pair production. ii. integral cross section for pair production. *Phys. Rev.*, 93(4):788–795, 1954.

[1] H. W. Koch and J. W. Motz. Bremsstrahlung cross-section formulas and related data. *Rev. Mod. Phys.*, 31(4):920–955, 1959.

[2] H. Davies et al. Theory of bremsstrahlung and pair production. ii. integral cross section for pair production. *Phys. Rev.*, 93(4):788–795, 1954.

[1] H. W. Koch and J. W. Motz. Bremsstrahlung cross-section formulas and related data. *Rev. Mod. Phys.*, 31(4):920–955, 1959.

[2] H. Davies et al. Theory of bremsstrahlung and pair production. ii. integral cross section for pair production. *Phys. Rev.*, 93(4):788–795, 1954.

[3] J. M. Fernández-Varea, R. Mayol, J. Baró, and F. Salvat. On the theory and simulation of multiple elastic scattering of electrons. *Nuclear Instruments and Methods in Physics Research B*, 73:447–473, April 1993. doi:10.1016/0168-583X(93)95827-R.

[1] G.A. Korn and T.M. Korn. *Mathematical Handbook for scientists and engineers*. McGraw-Hill Book Company, Inc., edition, 1961.

[1] SR Kelner, RP Kokoulin, and AA Petrukhin. About cross section for high-energy muon bremsstrahlung. Technical Report, MEphI, 1995. Preprint MEPhI 024-95, Moscow, 1995, CERN SCAN-9510048.

[1] S.M.Seltzer S.T.Perkins, D.E.Cullen. Tables and graphs of electron-interaction cross-sections from 10 ev to 100 gev derived from the llnl evaluated electron data library (eedl), z=1-100. Technical Report UCRL-50400 Vol.31, Lawrence Livermore National Laboratory, 1989.

[2] J.Apostolakis et al. Geant4 low energy electromagnetic models for electrons and photons. Technical Report, CERN, CERN/INFN, 1999. CERN-OPEN-99-034(1999), INFN/AE-99/18.

[1] René et al. Brun. *GEANT: Detector Description and Simulation Tool; Oct 1994*. CERN Program Library. CERN, Geneva, 1993. Long Writeup W5013. URL: https://cds.cern.ch/record/1082634.

[1] Y. Tsai. Pair production and bremsstrahlung of charged leptons. *Rev. Mod. Phys.*, 46():815, 1974.

[2] Y. Tsai. Pair production and bremsstrahlung of charged leptons. *Rev. Mod. Phys.*, 49():421, 1977.

[1] H. W. Koch and J. W. Motz. Bremsstrahlung cross-section formulas and related data. *Rev. Mod. Phys.*, 31(4):920–955, 1959.

[7] R. Mohan A. F. Bielajew and C.-S. Chui. Improved bremsstrahlung photon angular sampling in the egs4 code system. Technical Report, 1989. Report NRCC/PIRS-0203.

[8] C. A. Quarls L. Kissel and R. H. Pratt. Bremsstrahlung from electron collisions with neutral atoms. *At. Data Nucl. Data Tables*, 28():382, 1983.

[9] R. H. Pratt H. K. Tseng and C. M. Lee. Electron bremsstrahlung angular distributions in the 1-500 kev energy range. *Phys. Rev. A*, 19():187, 1979.

[10] P. Rodrigues et al. Geant4 applications and developments for medical physics experiments. *IEEE NSS/MIC Conference Record*, ():, 2003.

[1] J.H. Hubbell. Summary of existing information on the incoherent scattering of photons, particularly on the validity of the use of the incoherent scattering function. *Radiation Physics and Chemistry*, 50(1):113–124, jul 1997. URL: https://doi.org/10.1016/S0969-806X(97)00049-2, doi:10.1016/s0969-806x(97)00049-2.

[2] D.E. Cullen. A simple model of photon transport. *Nucl. Instr. Meth. in Phys. Res. B*, 101():499–510, 1995.

[3] J.C. Butcher and H. Messel. *Nucl. Phys.*, 20(15):, 1960.

[4] H. Messel and D. Crawford. *Electron-Photon shower distribution*. Pergamon Press, 1970.

[3] W.R. Nelson, H. Hirayama, and D.W.O. Rogers. *EGS4 code system*. SLAC, Dec 1985. SLAC-265, UC-32.

[6] J. Stepanek. New photon, positron and electron interaction data for geant in energy range from 1 ev to 10 tev. ():. Draft to be submitted for publication.

[1] Y. Tsai. Pair production and bremsstrahlung of charged leptons. *Rev. Mod. Phys.*, 46():815, 1974.

[2] Y. Tsai. Pair production and bremsstrahlung of charged leptons. *Rev. Mod. Phys.*, 49():421, 1977.

[3] J.C. Butcher and H. Messel. *Nucl. Phys.*, 20(15):, 1960.

[4] H. Messel and D. Crawford. *Electron-Photon shower distribution*. Pergamon Press, 1970.

[5] René et al. Brun. *GEANT: Detector Description and Simulation Tool; Oct 1994*. CERN Program Library. CERN, Geneva, 1993. Long Writeup W5013. URL: https://cds.cern.ch/record/1082634.

[6] Richard L. Ford and W. Ralph Nelson. The egs code system: computer programs for the monte carlo simulation of electromagnetic cascade showers (version 3). Technical Report, SLAC, 1978.

[1] P. Sigmund et al. Stopping of ions heavier than helium. *Journal of the International Commission on Radiation Units and Measurements*, jun 2005. ICRU Report 73. URL: https://doi.org/10.1093/jicru/ndi001, doi:10.1093/jicru/ndi001.

[2] J.F. Ziegler and J.M. Manoyan. *Nucl. Instr. and Meth.*, B35():215, 1988.

[3] M. J. Berger, M. Inokuti, H. H. Andersen, H. Bichsel, D. Powers, S . M. Seltzer, D . Thwaites, and D. E. Watt. Report 49. *Journal of the International Commission on Radiation Units and Measurements*, os25(2):NP–NP, may 1993. ICRU Report 49. URL: https://doi.org/10.1093/jicru/os25.2.Report49, doi:10.1093/jicru/os25.2.report49.

[4] Z. Wang Q. Yang, D.J. O'Connor. *Nucl. Instr. and Meth.*, B61():149, 1991.

[5] in: W.K. Chu. *Ion Beam Handbook for Material Analysis, edt. J.W.~Mayer and E.~Rimini*. Academic Press, NY, edition, 1977.

[6] P. Sigmund and A. Schinner. *Nucl. Instr. Meth. in Phys. Res. B*, 195():64, 2002.

[7] P. Sigmund and A. Schinner. *Eur. Phys. J. D*, 12():425, 2000.

[8] A. Schinner P. Sigmund and H. Paul. Stopping of ions heavier than helium. Technical Report Errata and Addenda for ICRU Report 73, 2009.

[9] P.Sigmund. Personal communication. ():, 2009.

[1] René et al. Brun. *GEANT: Detector Description and Simulation Tool; Oct 1994*. CERN Program Library. CERN, Geneva, 1993. Long Writeup W5013. URL: https://cds.cern.ch/record/1082634.

[4] H. Messel and D. Crawford. *Electron-Photon shower distribution*. Pergamon Press, 1970.

[1] S. Incerti. Geant4-microelec online available at:. Technical Report. URL: https://twiki.cern.ch/twiki/bin/view/Geant4/LoweMuElec.

[2] J.-E. Sauvestre et al. A. Valentin, M. Raine. Geant4 physics processes for microdosimetry simulation: very low energy electromagnetic models for electrons in silicon. *Nuclear Instruments and Methods in Physics Research B*, 288():66–73, 2012.

[3] M. Gaillardin A. Valentin, M. Raine and P. Paillet. Geant4 physics processes for microdosimetry simulation: very low energy electromagnetic models for protons and heavy ions in silicon. *Nuclear Instruments and Methods in Physics Research B*, 287():124–129, 2012.

[1] Ribberfors R. *Phys. Rev. B.*, 12():2067–2074, 1975.

[2] Brusa D. et al. *Nucl. Instrum. Methods Phys. Res. A*, 379():167–175, 1996.

[3] R. M. Kippen. *New Astro. Reviews*, 48():221–225, 2004.

[4] Salvat F. et al. Penelope, a code system for monte carlo simulation of electron and photon transport. Technical Report Proceedings of a Workshop/Training Course, OECD/NEA, 5-7 November 2001.

[5] Du Mond J. W. M. *Phys. Rev.*, 33():643–658, 1929.

[6] Brown J. M. C. et al. *Nucl. Instrum. Methods Phys. Res. B*, 338():77–88, 2014.

[1] S.M.Seltzer S.T.Perkins, D.E.Cullen. Tables and graphs of electron-interaction cross-sections from 10 ev to 100 gev derived from the llnl evaluated electron data library (eedl), z=1-100. Technical Report UCRL-50400 Vol.31, Lawrence Livermore National Laboratory, 1989.

[2] J.Apostolakis et al. Geant4 low energy electromagnetic models for electrons and photons. Technical Report, CERN/INFN, 1999. CERN-OPEN-99-034(1999), INFN/AE-99/18.

[1] L.Kissel D.Cullen, J.H.Hubbell. Epdl97: the evaluated photon data library, '97 version. *UCRL–50400*, 6(Rev.5):, 1989. http://reddog1.llnl.gov/homepage.red/photon.htm.

[1] M.H.Chen et al S.T.Perkins, D.E.Cullen. Tables and graphs of atomic subshell and relaxation data derived from the llnl evaluated atomic data library (eadl), z=1-100. Technical Report UCRL-50400 Vol.30.

[5] J.H. Scofield. *"Radiative Transitions", in "Atomic Inner-Shell Processes", B.Crasemann ed.* Academic Press, New York, 1975.

[6] NEA:. Evaluated nuclear reaction data. http://www.oecd-nea.org/dbdata/data/evaluated.htm. [Online; accessed 26-october-2017].

[7] J. Stepanek. New photon, positron and electron interaction data for geant in energy range from 1 ev to 10 tev. ():. Draft to be submitted for publication.

[1] S.M.Seltzer S.T.Perkins, D.E.Cullen. Tables and graphs of electron-interaction cross-sections from 10 ev to 100 gev derived from the llnl evaluated electron data library (eedl), z=1-100. Technical Report UCRL-50400 Vol.31, Lawrence Livermore National Laboratory, 1989.

[1] L.Kissel D.Cullen, J.H.Hubbell. Epdl97: the evaluated photon data library, '97 version. *UCRL–50400*, 6(Rev.5):, 1989. http://reddog1.llnl.gov/homepage.red/photon.htm.

[3] F. Salvat et al. Penelope - a code system for monte carlo simulation of electron and photon transport. Technical Report, Workshop Proceedings Issy-les-Moulineaux, France; AEN-NEA, 5-7 November 2001.

[4] J. Sempau et al. Experimental benchmarks of the monte carlo code penelope. *submitted to NIM B*, ():, 2002.

[5] D. Brusa et al. Fast sampling algorithm for the simulation of photon compton scattering. *NIM A*, 379():167, 1996.

[6] F.Biggs et al. Hartree-fock compton profiles for the elements. *At. Data Nucl. Data Tables*, 16():201, 1975.

[7] M. Born. *Atomic physics*. Ed. Blackie and Sons, edition, 1969.

[8] J.Baró et al. Analytical cross sections for monte carlo simulation of photon transport. *Radiat. Phys. Chem.*, 44():531, 1994.

[9] J.H. Hubbel et al. Atomic form factors, incoherent scattering functions and photon scattering cross sections. *Phys. Chem. Ref. Data*, 4():471, 1975. Erratum: ibid. 6,615 (1977).

[10] M.J. Berger and J.H. Hubbel. Xcom: photom cross sections on a personal computer. Technical Report Report NBSIR 87-3597, National Bureau of Standards, 1987.

[4] J. H. Hubbell, H. A. Gimm, and I. Øverbø. Pair, Triplet, and Total Atomic Cross Sections (and Mass Attenuation Coefficients) for 1 MeV-100 GeV Photons in Elements Z=1 to 100. *Journal of Physical and Chemical Reference Data*, 9:1023–1148, October 1980. doi:10.1063/1.555629.

[2] H. Davies et al. Theory of bremsstrahlung and pair production. ii. integral cross section for pair production. *Phys. Rev.*, 93(4):788–795, 1954.

[13] J.W. Motz et al. Pair production by photons. *Rev. Mod. Phys*, 41():581, 1969.

[2] Fritz Sauter. Über den atomaren photoeffekt bei großer härte der anregenden strahlung. *Annalen der Physik*, 401(2):217–248, 1931. URL: https://doi.org/10.1002/andp.19314010205, doi:10.1002/andp.19314010205.

[3] S.M. Seltzer and M.J. Berger. Bremsstrahlung energy spectra from electrons with kinetic energy 1 kev - 100 gev incident on screened nuclei and orbital electrons of neutral atoms with z = 1–100. *Atomic Data and Nuclear Data Tables*, 35():345, 1986.

[16] Lynn Kissel, C.A. Quarles, and R.H. Pratt. Shape functions for atomic-field bremsstrahlung from electrons of kinetic energy 1–500 keV on selected neutral atoms $1 \leq z \leq 92$. *Atomic Data and Nuclear Data Tables*, 28(3):381–460, May 1983. URL: https://doi.org/10.1016/0092-640X(83)90001-3, doi:10.1016/0092-640x(83)90001-3.

[17] M.J. Berger and S.M. Seltzer. Stopping power of electrons and positrons. Technical Report Report NBSIR 82-2550, National Bureau of Standards, 1982.

[18] L.Kim et al. Ratio of positron to electron bremsstrahlung energy loss: an approximate scaling law. *Phys. Rev. A*, 33():2002, 1986.

[19] U. Fano. Penetration of protons, alpha particles and mesons. *Ann. Rev. Nucl. Sci.*, 13():1, 1963.

[1] W. Heitler. *The Quantum Theory of Radiation*. Oxford Clarendon Press, edition, 1954.

[1] L.Kissel D.Cullen, J.H.Hubbell. Epdl97: the evaluated photon data library, '97 version. *UCRL–50400*, 6(Rev.5):, 1989. http://reddog1.llnl.gov/homepage.red/photon.htm.

[2] Fritz Sauter. Über den atomaren photoeffekt bei großer härte der anregenden strahlung. *Annalen der Physik*, 401(2):217–248, 1931. URL: https://doi.org/10.1002/andp.19314010205, doi:10.1002/andp.19314010205.

[3] R L Pexton R H Pratt, R D Levee and W Aron. K-shell photoelectric cross sections from 200 kev to 2 mev. *Phys. Rev.*, 134(4A):, 1964.

[4] M. Gavrila. Relativistic k-shell photoeffect. *Phys. Rev.*, 113(2):, 1959.

[5] M. Gavrila. Relativistic l-shell photoeffect. *Phys. Rev.*, 124(4):, 1961.

[6] A. Trindade L. Peralta, P. Rodrigues. Monte carlo generation of 2bnbremsstrahlung distribution. *CERN EXT-2004-039*, (039):, July 2003.

[7] G.O. Depaola and F. Longo. Measuring polarization in the x-ray range: new simulation method for gaseous detectors. *NIMA*, 566():590, 2006.

[1] W. Heitler. *The Quantum Theory of Radiation*. Oxford Clarendon Press, edition, 1954.

[2] G.O. Depaola. New monte carlo method for compton and rayleigh scattering by polarized gamma rays. *Nuclear Instruments and Methods A*, 512():619, 2003.

[1] C.N.Kozameh G.O.Depaola and M.H.Tiglio. A method to determine the polarization of high energy gamma rays. *Astroparticle Physics*, 10():175, 1999.

[1] J.H. Hubbell et al. Relativistic atom form factors and photon coherent scattering cross sections. *J. Phys. Chem. Ref. Data*, 8():69, 1979.

[2] D.E. Cullen. A simple model of photon transport. *Nucl. Instr. Meth. in Phys. Res. B*, 101():499–510, 1995.

[1] M.H.Chen et al S.T.Perkins, D.E.Cullen. Tables and graphs of atomic subshell and relaxation data derived from the llnl evaluated atomic data library (eadl), z=1-100. Technical Report UCRL-50400 Vol.30.

[1] E.A. Vinokurov and E.A. Kuraev. *Zh. Eksp. Teor. Fiz.*, 63():1142, 1972. in Russian.

[2] E.A. Vinokurov and E.A. Kuraev. *Sov. Phys. JETP*, 36():602, 1973. in Russian.

[3] N.P. Merenkov V.F. Boldyshev, E.A. Vinokurov and Yu.P. Peresunko. *Phys. Part. Nucl.*, 25():292, 1994.

[4] G.O. Depaola M.L. Iparraguirre. *The European Physical Journal C*, 71():1778, 2011.

[1] S. Agostinelli et al. Geant4—a simulation toolkit. *Nuclear Instruments and Methods in Physics Research Section A: Accelerators, Spectrometers, Detectors and Associated Equipment*, 506(3):250–303, jul 2003. URL: https://doi.org/10.1016/S0168-9002(03)01368-8, doi:10.1016/s0168-9002(03)01368-8.

[1] J. Apostolakis et al. Geometry and physics of the geant4 toolkit for high and medium energy applications. *Radiation Physics and Chemistry*, 78(10):859–873, oct 2009. URL: https://doi.org/10.1016/j.radphyschem.2009.04.026, doi:10.1016/j.radphyschem.2009.04.026.

[1] S. Agostinelli et al. Geant4—a simulation toolkit. *Nuclear Instruments and Methods in Physics Research Section A: Accelerators, Spectrometers, Detectors and Associated Equipment*, 506(3):250–303, jul 2003. URL: https://doi.org/10.1016/S0168-9002(03)01368-8, doi:10.1016/s0168-9002(03)01368-8.

[2] J. Allison et al. Recent developments in g eant 4. *Nuclear Instruments and Methods in Physics Research Section A: Accelerators, Spectrometers, Detectors and Associated Equipment*, 835:186–225, nov 2016. URL: https://doi.org/10.1016/j.nima.2016.06.125, doi:10.1016/j.nima.2016.06.125.

[2] G. Molière. Theorie der Streuung schneller geladener Teilchen II. Mehrfach- und Vielfachstreuung. *Zeitschrift Naturforschung Teil A*, 3:78–97, February 1948. doi:10.1515/zna-1948-0203.

[3] J. M. Fernández-Varea, R. Mayol, J. Baró, and F. Salvat. On the theory and simulation of multiple elastic scattering of electrons. *Nuclear Instruments and Methods in Physics Research B*, 73:447–473, April 1993. doi:10.1016/0168-583X(93)95827-R.

[4] S. Goudsmit and J. L. Saunderson. Multiple scattering of electrons. *Physical Review*, 57(1):24–29, jan 1940. URL: https://doi.org/10.1103/PhysRev.57.24, doi:10.1103/physrev.57.24.

[4] D. Liljequist, M. Ismail, F. Salvat, R. Mayol, and J. D. Martinez. Transport mean free path tabulated for the multiple elastic scattering of electrons and positrons at energies $\leq$20 MeV. *Journal of Applied Physics*, 68(7):3061–3065, oct 1990. URL: https://doi.org/10.1063/1.346399, doi:10.1063/1.346399.

[1] SR Kelner, RP Kokoulin, and AA Petrukhin. About cross section for high-energy muon bremsstrahlung. Technical Report, MEphI, 1995. Preprint MEPhI 024-95, Moscow, 1995, CERN SCAN-9510048.

[2] S. R. Kelner, R. P. Kokoulin, and A. A. Petrukhin. Bremsstrahlung from muons scattered by atomic electrons. *Physics of Atomic Nuclei*, 60:576–583, April 1997.

[3] A. A. Petrukhin and V. V. Shestakov. The influence of the nuclear and atomic form factors on the muon bremsstrahlung cross section. *Canadian Journal of Physics*, 46(10):S377–S380, may 1968. URL: https://doi.org/10.1139/p68-251, doi:10.1139/p68-251.

[4] Y. M. Andreev, L. B. Bezrukov, and E. V. Bugaev. Excitation of a target in muon bremsstrahlung. *Physics of Atomic Nuclei*, 57:2066–2074, December 1994.

[5] Yu. M. Andreev and E. V. Bugaev. Muon bremsstrahlung on heavy atoms. *Physical Review D*, 55(3):1233–1243, feb 1997. URL: https://doi.org/10.1103/PhysRevD.55.1233, doi:10.1103/physrevd.55.1233.

[2] S. R. Kelner, R. P. Kokoulin, and A. A. Petrukhin. Bremsstrahlung from muons scattered by atomic electrons. *Physics of Atomic Nuclei*, 60:576–583, April 1997.

[1] V. V. Borog and A. A. Petrukhin. The Cross-Section of the Nuclear Interaction of High Energy Muons. *International Cosmic Ray Conference*, 6:1949–1954, August 1975.

[2] Leonid B. Bezrukov and E. V. Bugaev. Nucleon shadowing effects in photon nucleus interaction. (in russian). *Yad. Fiz.*, 33:1195–1207, 1981. Sov. J. Nucl. Phys. 33, 635 (1981) - english translation.

[3] L. N. Hand. Experimental investigation of pion electroproduction. *Physical Review*, 129(4):1834–1846, feb 1963. URL: https://doi.org/10.1103/PhysRev.129.1834, doi:10.1103/physrev.129.1834.

[4] Stanley J. Brodsky, Francis E. Close, and J. F. Gunion. Phenomenology of photon processes, vector dominance, and crucial tests for parton models. *Physical Review D*, 6(1):177–189, jul 1972. URL: https://doi.org/10.1103/PhysRevD.6.177, doi:10.1103/physrevd.6.177.

[5] D. O. Caldwell et al. Measurement of shadowing in photon-nucleus total cross sections from 20 to 185 GeV. *Physical Review Letters*, 42(9):553–556, feb 1979. URL: https://doi.org/10.1103/PhysRevLett.42.553, doi:10.1103/physrevlett.42.553.

[1] R. P. Kokoulin and A. A. Petrukhin. Analysis of the cross-section of direct pair production by fast muons. *International Cosmic Ray Conference*, 4:277–284, 1970. Proc. 11th International Cosmic Ray Conference, Acta Phys. Acad. Sci. Hung.,\bf 29, Suppl.4.

[2] R.P.Kokoulin and A.A.Petrukhin. Influence of the nuclear formfactor on the cross-section of electron pair production by high energy muons. In *Cosmic Ray Conference Papers*, volume 6, 2436–2444. Hobart, Tasmania, Australia, 16-25 August 1971. 12th International Conference on Cosmic Rays.

[3] S. R. Kelner. Pair production in collisions between muons and atomic electrons. *Physics of Atomic Nuclei*, 61:448–456, March 1998.

[1] J. Apostolakis et al. Geometry and physics of the geant4 toolkit for high and medium energy applications. *Radiation Physics and Chemistry*, 78(10):859–873, oct 2009. URL: https://doi.org/10.1016/j.radphyschem.2009.04.026, doi:10.1016/j.radphyschem.2009.04.026.

[1] P. Sigmund et al. Stopping of ions heavier than helium. *Journal of the International Commission on Radiation Units and Measurements*, jun 2005. ICRU Report 73. URL: https://doi.org/10.1093/jicru/ndi001, doi:10.1093/jicru/ndi001.

[2] J.F. Ziegler and J.M. Manoyan. *Nucl. Instr. and Meth.*, B35():215, 1988.

[3] M. J. Berger, M. Inokuti, H. H. Andersen, H. Bichsel, D. Powers, S . M. Seltzer, D . Thwaites, and D. E. Watt. Report 49. *Journal of the International Commission on Radiation Units and Measurements*, os25(2):NP–NP, may 1993. ICRU Report 49. URL: https://doi.org/10.1093/jicru/os25.2.Report49, doi:10.1093/jicru/os25.2.report49.

[1] S. Agostinelli et al. Geant4—a simulation toolkit. *Nuclear Instruments and Methods in Physics Research Section A: Accelerators, Spectrometers, Detectors and Associated Equipment*, 506(3):250–303, jul 2003. URL: https://doi.org/10.1016/S0168-9002(03)01368-8, doi:10.1016/s0168-9002(03)01368-8.

[1] J. Apostolakis et al. Geometry and physics of the geant4 toolkit for high and medium energy applications. *Radiation Physics and Chemistry*, 78(10):859–873, oct 2009. URL: https://doi.org/10.1016/j.radphyschem.2009.04.026, doi:10.1016/j.radphyschem.2009.04.026.

[3] M. J. Berger, M. Inokuti, H. H. Andersen, H. Bichsel, D. Powers, S . M. Seltzer, D . Thwaites, and D. E. Watt. Report 49. *Journal of the International Commission on Radiation Units and Measurements*, os25(2):NP–NP, may 1993. ICRU Report 49. URL: https://doi.org/10.1093/jicru/os25.2.Report49, doi:10.1093/jicru/os25.2.report49.

[1] J.D.Jackson. *Classical Electrodynamics*. John Wiley and Sons, third edition, 1998.

[1] V.M. Grichine. *Nucl. Instr. and Meth.*, A482():629, 2002.

[2] V.M. Grichine. *Physics Letters*, B525():225–239, 2002.

[3] V. Grichine et al. J. Apostolakis, S. Giani. *Comput. Phys. Commun.*, 132():241, 2000.

[4] G.M. Garibyan. *Sov. Phys. JETP*, 32():23, 1971.

[5] C.W. Fabian and W. Struczinski. *Physics Letters*, B57():483, 1975.

[6] L.A. Gevorgian, G.M. Garibian and C. Yang. *Sov. Phys.- JETP*, 39():265, 1975.

CHAPTER

FIVE

OPTICAL

5.1 Interactions of optical photons

Optical photons are produced when a charged particle traverses:

1. a dielectric material with velocity above the Čerenkov threshold;
2. a scintillating material.

5.1.1 Physics processes for optical photons

A photon is called optical when its wavelength is much greater than the typical atomic spacing, for instance when $\lambda \geq 10nm$ which corresponds to an energy $E \leq 100eV$. Production of an optical photon in a HEP detector is primarily due to:

1. Čerenkov effect;
2. Scintillation.

Optical photons undergo three kinds of interactions:

1. Elastic (Rayleigh) scattering;
2. Absorption;
3. Medium boundary interactions.

Rayleigh scattering

For optical photons Rayleigh scattering is usually unimportant. For $\lambda = .2\mu m$ we have $\sigma_{Rayleigh} \approx .2b$ for N_2 or O_2 which gives a mean free path of $\approx 1.7km$ in air and $\approx 1m$ in quartz. Two important exceptions are aerogel, which is used as a Čerenkov radiator for some special applications and large water Čerenkov detectors for neutrino detection.

The differential cross section in Rayleigh scattering, $d\sigma/d\Omega$, is proportional to $1 + \cos^2\theta$, where θ is the polar angle of the new polarization with respect to the old polarization.

Absorption

Absorption is important for optical photons because it determines the lower λ limit in the window of transparency of the radiator. Absorption competes with photo-ionization in producing the signal in the detector, so it must be treated properly in the tracking of optical photons.

Medium boundary effects

When a photon arrives at the boundary of a dielectric medium, its behaviour depends on the nature of the two materials which join at that boundary:

- Case dielectric → dielectric.
  The photon can be transmitted (refracted ray) or reflected (reflected ray). In case where the photon can only be reflected, total internal reflection takes place.
- Case dielectric → metal.
  The photon can be absorbed by the metal or reflected back into the dielectric. If the photon is absorbed it can be detected according to the photoelectron efficiency of the metal.
- Case dielectric → black material.
  A black material is a tracking medium for which the user has not defined any optical property. In this case the photon is immediately absorbed undetected.

5.1.2 Photon polarization

The photon polarization is defined as a two component vector normal to the direction of the photon:

$$\begin{pmatrix} a_1 e^{i\Phi_1} \\ a_2 e^{i\Phi_2} \end{pmatrix} = e^{\Phi_o} \begin{pmatrix} a_1 e^{i\Phi_c} \\ a_2 e^{-i\Phi_c} \end{pmatrix}$$

where $\Phi_c = (\Phi_1 - \Phi_2)/2$ is called circularity and $\Phi_o = (\Phi_1 + \Phi_2)/2$ is called overall phase. Circularity gives the left- or right-polarization characteristic of the photon. RICH materials usually do not distinguish between the two polarizations and photons produced by the Čerenkov effect and scintillation are linearly polarized, that is $\Phi_c = 0$.

The overall phase is important in determining interference effects between coherent waves. These are important only in layers of thickness comparable with the wavelength, such as interference filters on mirrors. The effects of such coatings can be accounted for by the empirical reflectivity factor for the surface, and do not require a microscopic simulation. GEANT4 does not keep track of the overall phase.

Vector polarization is described by the polarization angle $\tan \Psi = a_2/a_1$. Reflection/transmission probabilities are sensitive to the state of linear polarization, so this has to be taken into account. One parameter is sufficient to describe vector polarization, but to avoid too many trigonometrical transformations, a unit vector perpendicular to the direction of the photon is used in GEANT4. The polarization vector is a data member of `G4DynamicParticle`.

5.1.3 Tracking of the photons

Optical photons are subject to in flight absorption, Rayleigh scattering and boundary action. As explained above, the status of the photon is defined by two vectors, the photon momentum ($\vec{p} = \hbar\vec{k}$) and photon polarization ($\vec{e}$). By convention the direction of the polarization vector is that of the electric field. Let also $\vec{u}$ be the normal to the material boundary at the point of intersection, pointing out of the material which the photon is leaving and toward the one which the photon is entering. The behaviour of a photon at the surface boundary is determined by three quantities:

1. refraction or reflection angle, this represents the kinematics of the effect;
2. amplitude of the reflected and refracted waves, this is the dynamics of the effect;
3. probability of the photon to be refracted or reflected, this is the quantum mechanical effect which we have to take into account if we want to describe the photon as a particle and not as a wave.

As said above, we distinguish three kinds of boundary action, dielectric → black material, dielectric → metal, dielectric → dielectric. The first case is trivial, in the sense that the photon is immediately absorbed and it goes undetected.

To determine the behaviour of the photon at the boundary, we will at first treat it as an homogeneous monochromatic plane wave:

$$\vec{E} = \vec{E}_0 e^{i\vec{k}\cdot\vec{x} - i\omega t}$$

$$\vec{B} = \sqrt{\mu\epsilon}\frac{\vec{k}\times\vec{E}}{k}$$

Case dielectric → dielectric

In the classical description the incoming wave splits into a reflected wave (quantities with a double prime) and a refracted wave (quantities with a single prime). Our problem is solved if we find the following quantities:

$$\vec{E}' = \vec{E}'_0 e^{i\vec{k}'\cdot\vec{x} - i\omega t}$$

$$\vec{E}'' = \vec{E}''_0 e^{i\vec{k}''\cdot\vec{x} - i\omega t}$$

For the wave numbers the following relations hold:

$$|\vec{k}| = |\vec{k}''| = k = \frac{\omega}{c}\sqrt{\mu\epsilon}$$

$$|\vec{k}'| = k' = \frac{\omega}{c}\sqrt{\mu'\epsilon'}$$

Where the speed of the wave in the medium is $v = c/\sqrt{\mu\epsilon}$ and the quantity $n = c/v = \sqrt{\mu\epsilon}$ is called refractive index of the medium. The condition that the three waves, refracted, reflected and incident have the same phase at the surface of the medium, gives us the well known Fresnel law:

$$(\vec{k}\cdot\vec{x})_{surf} = (\vec{k}'\cdot\vec{x})_{surf} = (\vec{k}''\cdot\vec{x})_{surf}$$

$$k\sin i = k'\sin r = k''\sin r'$$

where i, r, r' are, respectively, the angle of the incident, refracted and reflected ray with the normal to the surface. From this formula the well known condition emerges:

$$i = r'$$

$$\frac{\sin i}{\sin r} = \sqrt{\frac{\mu'\epsilon'}{\mu\epsilon}} = \frac{n'}{n}$$

The dynamic properties of the wave at the boundary are derived from Maxwell's equations which impose the continuity of the normal components of $\vec{D}$ and $\vec{B}$ and of the tangential components of $\vec{E}$ and $\vec{H}$ at the surface boundary. The resulting ratios between the amplitudes of the the generated waves with respect to the incoming one are expressed in the two following cases:

1. a plane wave with the electric field (polarization vector) perpendicular to the plane defined by the photon direction and the normal to the boundary:

$$\frac{E'_0}{E_0} = \frac{2n\cos i}{n\cos i = \frac{\mu}{\mu'}n'\cos r} = \frac{2n\cos i}{n\cos i + n'\cos r}$$

$$\frac{E''_0}{E_0} = \frac{n\cos i - \frac{\mu}{\mu'}n'\cos r}{n\cos i + \frac{\mu}{\mu'}n'\cos r} = \frac{n\cos i - n'\cos r}{n\cos i + n'\cos r}$$

   where we suppose, as it is legitimate for visible or near-visible light, that $\mu/\mu' \approx 1$;

2. a plane wave with the electric field parallel to the above surface:

$$\frac{E_0'}{E_0} = \frac{2n\cos i}{\frac{\mu}{\mu'}n'\cos i + n\cos r} = \frac{2n\cos i}{n'\cos i + n\cos r}$$

$$\frac{E_0''}{E_0} = \frac{\frac{\mu}{\mu'}n'\cos i - n\cos r}{\frac{\mu}{\mu'}n'\cos i + n\cos r} = \frac{n'\cos i - n\cos r}{n'\cos i + n\cos r}$$

with the same approximation as above.

We note that in case of photon perpendicular to the surface, the following relations hold:

$$\frac{E_0'}{E_0} = \frac{2n}{n'+n} \qquad \frac{E_0''}{E_0} = \frac{n'-n}{n'+n}$$

where the sign convention for the parallel field has been adopted. This means that if $n' > n$ there is a phase inversion for the reflected wave.

Any incoming wave can be separated into one piece polarized parallel to the plane and one polarized perpendicular, and the two components treated accordingly.

To maintain the particle description of the photon, the probability to have a refracted or reflected photon must be calculated. The constraint is that the number of photons be conserved, and this can be imposed via the conservation of the energy flux at the boundary, as the number of photons is proportional to the energy. The energy current is given by the expression:

$$\vec{S} = \frac{1}{2}\frac{c}{4\pi}\sqrt{\mu\epsilon}\vec{E}\times\vec{H} = \frac{c}{8\pi}\sqrt{\frac{\epsilon}{\mu}}E_0^2\hat{k}$$

and the energy balance on a unit area of the boundary requires that:

$$\vec{S}\cdot\vec{u} = \vec{S}'\cdot\vec{u} - \vec{S}''\cdot\vec{u}$$

$$S\cos i = S'cosr + S''cosi$$

$$\frac{c}{8\pi}\frac{1}{\mu}nE_0^2\cos i = \frac{c}{8\pi}\frac{1}{\mu'}n'E_0'^2\cos r + \frac{c}{8\pi}\frac{1}{\mu}nE_0''^2\cos i$$

If we set again $\mu/\mu' \approx 1$, then the transmission probability for the photon will be:

$$T = (\frac{E_0'}{E_0})^2\frac{n'\cos r}{n\cos i}$$

and the corresponding probability to be reflected will be $R = 1 - T$.

In case of reflection, the relation between the incoming photon $(\vec{k}, \vec{e})$, the refracted one $(\vec{k}', \vec{e}')$ and the reflected one $(\vec{k}'', \vec{e}'')$ is given by the following relations:

$$\vec{q} = \vec{k}\times\vec{u}$$

$$\vec{e}_\perp = (\frac{\vec{e}\cdot\vec{q}}{|\vec{q}|})\frac{\vec{q}}{|\vec{q}|}$$

$$\vec{e}_\parallel = \vec{e} - \vec{e}_\perp$$

$$e_\parallel' = e_\parallel\frac{2n\cos i}{n'\cos i + n\cos r}$$

$$e_{\perp|}' = e_\perp\frac{2n\cos i}{n\cos i + n'\cos r}$$

$$e_\parallel'' = \frac{n'}{n}e_\parallel' - e_\parallel$$

$$e''_{\perp} = e'_{\perp} - e_{\perp}$$

After transmission or reflection of the photon, the polarization vector is re-normalized to 1. In the case where $\sin r = n \sin i/n' > 1$ then there cannot be a refracted wave, and in this case we have a total internal reflection according to the following formulas:

$$\vec{k}'' = \vec{k} - 2(\vec{k} \cdot \vec{u})\vec{u}$$

$$\vec{e}'' = -\vec{e} + 2(\vec{e} \cdot \vec{u})\vec{u}$$

Case dielectric → metal

In this case the photon cannot be transmitted. So the probability for the photon to be absorbed by the metal is estimated according to the table provided by the user. If the photon is not absorbed, it is reflected.

5.1.4 Mie Scattering in Henyey-Greensterin Approximation

(Author: X. Qian, 2010-07-04)

Mie Scattering (or Mie solution) is an analytical solution of Maxwell's equations for the scattering of optical photon by spherical particles. The general introduction of Mie scattering can be found in Ref. *[1]*. The analytical express of Mie Scattering are very complicated since they are a series sum of Bessel functions *[2]*. Therefore, the exact expression of Mie scattering is not suitable to be included in the Monte Carlo simulation.

One common approximation made is called "Henyey-Greensterin" *[3]*. It has been used by Vlasios Vasileiou in GEANT4 simulation of Milagro experiment *[4]*. In the HG approximation,

$$\frac{d\sigma}{d\Omega} \sim \frac{1 - g^2}{(1 + g^2 - 2g\cos(\theta))^{3/2}}$$

where

$$d\Omega = d\cos(\theta)d\phi$$

and $g =< \cos(\theta) >$ can be viewed as a free constant labeling the angular distribution.

Therefore, the normalized density function of HG approximation can be expressed as:

$$P(\cos(\theta_0)) = \frac{\int_{-1}^{\cos(\theta_0)} \frac{d\sigma}{d\Omega} d\cos(\theta)}{\int_{-1}^{1} \frac{d\sigma}{d\Omega} d\cos(\theta)} = \frac{1 - g^2}{2g}\left(\frac{1}{(1 + g^2 - 2g\cos(\theta_0))} - \frac{1}{1 + g}\right)$$

Therefore,

$$\cos(\theta) = \frac{1}{2g} \cdot \left(1 + g^2 - \left(\frac{1 - g^2}{1 - g + 2g \cdot p}\right)^2\right) = 2p\frac{(1 + g)^2(1 - g + gp)}{(1 - g + 2gp)^2} - 1$$

where p is a uniform random number between 0 and 1.

Similarly, the backward angle where $\theta_b = \pi - \theta_f$ can also be simulated by replacing θ_f to θ_b. Therefore the final differential cross section can be viewed as:

$$\frac{d\sigma}{d\Omega} = r\frac{d\sigma}{d\Omega}(\theta_f, g_f) + (1 - r)\frac{d\sigma}{d\Omega}(\theta_b, g_b)$$

This is the exact approach used in Ref. *[5]*. Here r is the ratio factor between the forward angle and backward angle.

In implementing the above MC method into GEANT4, the treatment of polarization and momentum are similar to that of Rayleigh scattering. We require the final polarization direction to be perpendicular to the momentum direction. We also require the final momentum, initial polarization and final polarization to be in the same plane.

BIBLIOGRAPHY

[1] wikipedia. Mie scattering. http://en.wikipedia.org/wiki/Mie_scattering, 2017. [Online; accessed 26-october-2017].

[2] Richard Fitzpatrick. Mie scattering lectures. http://farside.ph.utexas.edu/teaching/jk1/lectures/node103.html, 2014. [Online; accessed 26-october-2017].

[3] Guangyuan Zhao and Xianming Sun. Error analysis of using henyey-greensterin [sic] in monte carlo radiative transfer simulations. In *Progress In Electromagnetics Research Symposium Proceedings*, 1449–1452. Xi'an, China, March 22nd 2010. download: http://piers.org/piersproceedings/download.php?file=cGllcnMyMDEwWGlhbnw0QVBfMTQ0OS5wZGZ8MDkwOTAyMDg1NTE
URL: http://piers.org/piersproceedings/piers2010XianProc.php?start=300.

[4] Milagro Collaboration. Tev all-sky gamma ray observatory. http://umdgrb.umd.edu/cosmic/milagro.html, 2007. [Online; accessed 26-october-2017].

[5] Vlasios Vasileiou. \it private communication.

CHAPTER

SIX

PHONON

6.1 Introduction

Phonons are quantized vibrations in solid-state lattices or amorphous solids, of interest to the low-temperature physics community. Phonons are typically produced when a heat source excites lattice vibrations, or when energy from radiation is deposited through elastic interactions with nuclei of lattice atoms. Below 1 K, thermal phonons are highly suppressed; this leaves only *acoustic* and *optical* phonons to propagate.

There is significant interest from the condensed-matter community and direct dark-matter searches to integrate phonon production and propagation with the excellent nuclear and electromagnetic simulations available in Geant4. An effort in this area began in 2011 by the SuperCDMS Collaboration:cite:*Brandt* and is continuing; initial developments in phonon propagation have been incorporated into the Geant4 toolkit for Release 10.0.

As quasiparticles, phonons at low temparatures may be treated in the Geant4 particle-tracking framework, carrying well defined momenta, and propagating in specific directions until they interact:cite:*Brandt*. The present implementation handles ballistic transport, scattering with mode-mixing, and anharmonic downcoversion:cite:*Tamura1[1][2]* of acoustic phonons. Optical phonon transport and interactions between propagating phonons and thermal background phonons are not treated.

Production of phonons from charged particle energy loss or by photon-lattice interactions are in development, but are not yet included in the Geant4 toolkit.

6.2 Phonon Propagation

The propagation of phonons is governed by the three-dimensional wave equation:cite:*Wolfe*:

$$\rho\omega^2 e_i = C_{ijlm}k_j k_m e_l$$

where ρ is the crystal mass density and C_{ijml} is the elasticity tensor; the phonon is described by its wave vector $\vec{k}$, frequency ω and polarization $\vec{e}$.

For a given wave vector $\vec{k}$, Eq. [eq:3DWave] has three eigenvalues ω and three polarization eigenvectors $\vec{e}$. The three polarization states are labelled *Fast Transverse (FT)*, *Slow Transverse (ST)* and *Longitudinal (L)*. The direction and speed of propagation of the phonon are given by the *group velocity* $\vec{v_g} = d\omega/dk$, which may be computed from Eq. [eq:3DWave]:

$$\vec{v_g} = \frac{d\omega(\vec{k})}{d\vec{k}} = \nabla_k \omega(\vec{k}) \; .$$

Since the lattice tensor C_{ijml} is anisotropic in general, the phonon group velocity $\vec{v_g}$ is not parallel to the momentum vector $\hbar\vec{k}$. This anisotropic transport leads to a focussing effect, where phonons are driven to directions which correspond to the highest density of eigenvectors $\vec{k}$. Experimentally, this is seen:cite:*Nothrop* as caustics in the energy distribution resulting from a point-like phonon source isotropic in $\vec{k}$-space, as shown in Figure [fig:caustics].

6.3 Lattice Parameters

6.4 Scattering and Mode Mixing

In a pure crystal, *isotope scattering* occurs when a phonon interacts with an isotopic substitution site in the lattice. We treat it as an elastic scattering process, where the phonon momentum direction (wave vector) and polarization are both randomized. The scattering rate for a phonon of frequency ν ($\omega/2\pi$) is given by:cite:*Tamura2*

$$\Gamma_{scatter} = B\nu^4$$

where $\Gamma_{scatter}$ is the number of scattering events per unit time, and B is a constant of proportionality derived from the elasticity tensor (see Eq. 11 and Table 1 in *[2]*). For germanium, $B = 3.67 \times 10^{-41}$ s:math:*(^3)*. *[2]*

At each scattering event, the phonon polarziation may change between any of the three states L, ST, FT. The branching ratios for the polarizations are determined by the relative density of allowed states in the lattice. This process is often referred to as *mode mixing*.

6.5 Anharmonic Downconversion

An energetic phonon may interact in the crystal to produce two phonons of reduced energy. This *anharmonic downconversion* conserves energy ($\vec{k} = \vec{k'} + \vec{k''}$), but not momentum, since momentum is exchanged with the bulk lattice. In principle, all three polarization states may decay through downconversion. In practice, however, the rate for L-phonons completely dominates the energy evolution of the system, with downconversion events from other polarization states being negligigible:cite:*Tamura2*.

The total downconversion rate Γ_{anh} for an L-phonon of frequency ν is given by:cite:*Tamura2*

$$\Gamma_{anh} = A\nu^5$$

where (as in Eq. [eq:ScatterRate]) A is a constant of proportionality derived from the elasticity tensor (see Eq. 11 and Table 1 in *[2]*). For germanium, $A = 6.43 \times 10^{-55}$ s:math:*(^4)*. *[2]*

Downconversion may produce either two transversely polarized phonons, or one transverse and one longitudinal. The relative rates are determined by dynamical constants derived from the elasticity tensor C_{ijkl}.

As can be seen from Eqs. [eq:ScatterRate] and [eq:anhRate], phonon interactions depend strongly on energy $\hbar\nu$. High energy phonons ($\nu \sim$ THz) start out in a diffusive regime with high isotope scattering and downconversion rates and mean free paths of order microns. After several such interactions, mean free paths increase to several centimeters or more. This transition from a diffuse to a ballistic transport mode is commonly referred to as "quasi-diffuse" and it controls the time evolution of phonon heat pulses.

Simulation of heat pulse propagation using our Geant4 transport code has been described previously:cite:*Brandt* and shows good agreement with experiment.

BIBLIOGRAPHY

[1] Shin-ichiro Tamura. Quasidiffusive propagation of phonons in silicon: monte carlo calculations. *Physical Review B*, 48(18):13502–13507, nov 1993. URL: https://doi.org/10.1103/PhysRevB.48.13502, doi:10.1103/physrevb.48.13502.

[2] Shin-ichiro Tamura. Spontaneous decay rates of LA phonons in quasi-isotropic solids. *Physical Review B*, 31(4):2574–2577, feb 1985. URL: https://doi.org/10.1103/PhysRevB.31.2574, doi:10.1103/physrevb.31.2574.

CHAPTER

SEVEN

HADRONIC

7.1 Elastic

7.1.1 Coherent elastic scattering

Nucleon-Nucleon elastic Scattering

The classes G4LEpp and G4LEnp provide data-driven models for proton-proton (or neutron-neutron) and neutron-proton elastic scattering over the range 10-1200 MeV. Final states (primary and recoil particle) are derived by sampling from tables of the cumulative distribution function of the centre-of-mass scattering angle, tabulated for a discrete set of lab kinetic energies from 10 MeV to 1200 MeV. The CDF's are tabulated at 1 degree intervals and sampling is done using bi-linear interpolation in energy and CDF values. The data are derived from differential cross sections obtained from the SAID database, R. Arndt, 1998.

In class G4LEpp there are two data sets: one including Coulomb effects (for p-p scattering) and one with no Coulomb effects (for n-n scattering or p-p scattering with Coulomb effects suppressed). The method G4LEpp::SetCoulombEffects can be used to select the desired data set:

- SetCoulombEffects(0): No Coulomb effects (the default)
- SetCoulombEffects(1): Include Coulomb effects

The recoil particle will be generated as a new secondary particle. In class G4LEnp, the possiblity of a charge-exchange reaction is included, in which case the incident track will be stopped and both the primary and recoil particles will be generated as secondaries.

7.2 Elastic_he

7.2.1 Hadron-nucleus Elastic Scattering at Medium and High Energy

Method of Calculation

The Glauber model *[1]* is used as an alternative method of calculating differential cross sections for elastic and quasi-elastic hadron-nucleus scattering at high and intermediate energies.

For high energies this includes corrections for inelastic screening and for quasi-elastic scattering the exitation of a discrete level or a state in the continuum is considered.

The usual expression for the Glauber model amplitude for multiple scattering was used

$$F(q) = \frac{ik}{2\pi} \int d^2b e^{\vec{q}\cdot\vec{b}} M(\vec{b}).$$

Here $M(\vec{b})$ is the hadron-nucleus amplitude in the impact parameter representation

$$M(\vec{b}) = 1 - [1 - e^{-A\int d^3 r \Gamma(\vec{b}-\vec{s})\rho(\vec{r})}]^A,$$

k is the incident particle momentum, $\vec{q} = \vec{k}' - \vec{k}$ is the momentum transfer, and $\vec{k}'$ is the scattered particle momentum. Note that $|\vec{q}|^2 = -t$ - invariant momentum transfer squared in the center of mass system. $\Gamma(\vec{b})$ is the hadron-nucleon amplitude of elastic scattering in the impact-parameter representation

$$\Gamma(\vec{b}) = \frac{1}{2\pi i k^{hN}} \int d\vec{q} e^{-\vec{q}\cdot\vec{b}} f(\vec{q}).$$

The exponential parameterization of the hadron-nucleon amplitude is usually used:

$$f(\vec{q}) = \frac{ik^{hN}\sigma^{hN}}{2\pi} e^{-0.5q^2 B}.$$

Here $\sigma^{hN} = \sigma_{tot}^{hN}(1 - i\alpha)\,\sigma_{tot}^{hN}$ is the total cross section of a hadron-nucleon scattering, B is the slope of the diffraction cone and α is the ratio of the real to imaginary parts of the amplitude at $q = 0$. The value k^{hN} is the hadron momentum in the hadron-nucleon coordinate system.

The important difference of these calculations from the usual ones is that the two-gaussian form of the nuclear density was used

$$\rho(r) = C(e^{-(r/R_1)^2} - pe^{-(r/R_2)^2}),$$

where R_1 R_2 and p are the fitting parameters and C is a normalization constant.

This density representation allows the expressions for amplitude and differential cross section to be put into analytical form. It was earlier used for light *[2]*[helast.2b][helast.2c][helast.3] and medium *[3][4]* nuclei. Described below is an extension of this method to heavy nuclei. The form [helast.eq5] is not physical for a heavy nucleus, but nevertheless works rather well (see figures below). The reason is that the nucleus absorbs the hadrons very strongly, especially at small impact parameters where the absorption is full. As a result only the peripherial part of the nucleus participates in elastic scattering. Eq. [helast.eq5] therefore describes only the edge of a heavy nucleus.

Substituting Eqs. [helast.eq5] and [helast.eq4] into Eqs. [helast.eq1], [helast.eq2] and [helast.eq3] yields the following formula

$$\begin{aligned} F(q) = \frac{ik\pi}{2} \sum_{k=1}^{A} (-1)^k \binom{A}{k} [\frac{\sigma^{hN}}{2\pi(R_1^3 - pR_2^3)}]^k \sum_{m=0}^{k} (-1)^m \binom{k}{m} \left[\frac{R_1^3}{R_1^2 + 2B}\right]^{k-m} \\ \times \quad \left[\frac{pR_2^3}{R_2^2 + 2B}\right]^m \left(\frac{m}{R_2^2 + 2B} + \frac{k-m}{R_1^2 + 2B}\right)^{-1} \\ \times \quad \exp\left[-\frac{-q^2}{4}\left(\frac{m}{R_2^2 + 2B} + \frac{k-m}{R_1^2 + 2B}\right)^{-1}\right]. \end{aligned}$$

An analogous procedure can be used to get the inelastic screening corrections to the hadron-nucleus amplitude $\Delta M(\vec{b})$ *[5]*. In this case an intermediate inelastic diffractive state is created which rescatters on the nucleons of the nucleus and then returns into the initial hadron. Hence it is nessesary to integrate the production cross section over the mass distribution of the exited system $\frac{d\sigma^{diff}}{dtdM_x^2}$. The expressions for the corresponding amplitude are quite long and so are not presented here. The corrections for the total cross-sections can be found in *[5]*.

The full amplitude is the sum $M(\vec{b}) + \Delta M(\vec{b})$.

The differential cross section is connected with the amplitude in the following way

$$\frac{d\sigma}{d\Omega_{CM}} = |F(q)|^2, \qquad \frac{d\sigma}{|dt|} = \frac{d\sigma}{dq_{CM}^2} = \frac{\pi}{k_{CM}^2} |F(q)|^2.$$

The main energy dependence of the hadron-nucleus elastic scattering cross section comes from the energy dependence of the parameters of hadron-nucleon scattering ($\sigma_{tot}^{hN}\alpha$ B and $\frac{d\sigma^{diff}}{dtdM_x^2}$). At interesting energies these parameters were fixed at their well-known values. The fitting of the nuclear density parameters was performed over a wide range of atomic numbers $(A = 4 - 208)$ using experimental data on proton-nuclei elastic scattering at a kinetic energy of $T_p = 1GeV$.

The fitting was perfomed both for individual nuclei and for the entire set of nuclei at once. It is necessary to note that for every nucleus an optimal set of density parameters exists and it differs slightly from the one derived for the full set of nuclei.

A comparision of the phenomenological cross sections *[6]* with experiment is presented in Figs. [helast.fig1] - [helast.fig9]

In this comparison, the individual nuclei parameters were used. The experimental data were obtained in Gatchina (Russia) and in Saclay (France) *[6]*. The horizontal axis is the scattering angle in the center of mass system Θ_{CM} and the vertical axis is $\frac{d\sigma}{d\Omega_{CM}}$ in $\frac{mb}{Ster}$. Comparisions were also made for p^4He elastic scatering at $T_{=}1GeV$[7], $45GeV$ and $301GeV$ [3]. The resulting cross sections $\frac{d\sigma}{d|t|}$ are shown in the Figs. [helast.fig10] - [helast.fig12].

In order to generate events the distribution function $\mathcal{F}$ of a corresponding process must be known. The differential cross section is proportional to the density distribution. Therefore to get the distribution function it is sufficient to integrate the differential cross section and normalize it:

$$\mathcal{F}(q^2) = \frac{\int_0^{q^2} d(q^2)\frac{d\sigma}{d(q^2)}}{\int_0^{q^2_{max}} d(q^2)\frac{d\sigma}{d(q^2)}}.$$

Expressions [helast.eq6] and [helast.eq7] allow analytic integration in Eq. [helast.eq8] but the result is too long to be given here.

For light and medium nuclei the analytic expression is more convenient for calculations than the numerical integration of Eq. [helast.eq8], but for heavy nuclei the latter is preferred due to the large number of terms in the analytic expression.

7.3 LowEnergyChargedParticles

7.3.1 Low Energy Charged Particle Interactions

Introduction

The low energy charged particle transport class library described here simulates the interactions of protons, deuterons, tritons, He-3 and alpha particle with kinetic energies up to 200 MeV. The upper limit is set by the comprehensive evaluated neutron scattering data libraries that the simulation is based on. It reuses the code of the low energy neutron interactions package, with some small modifications to take into account the change of incident particle.

Only the inelastic interactions are included in this model, while the elastic interaction is treated approximately by other Geant4 models, and the interference between Coulumb and nuclear elastic is neglected.

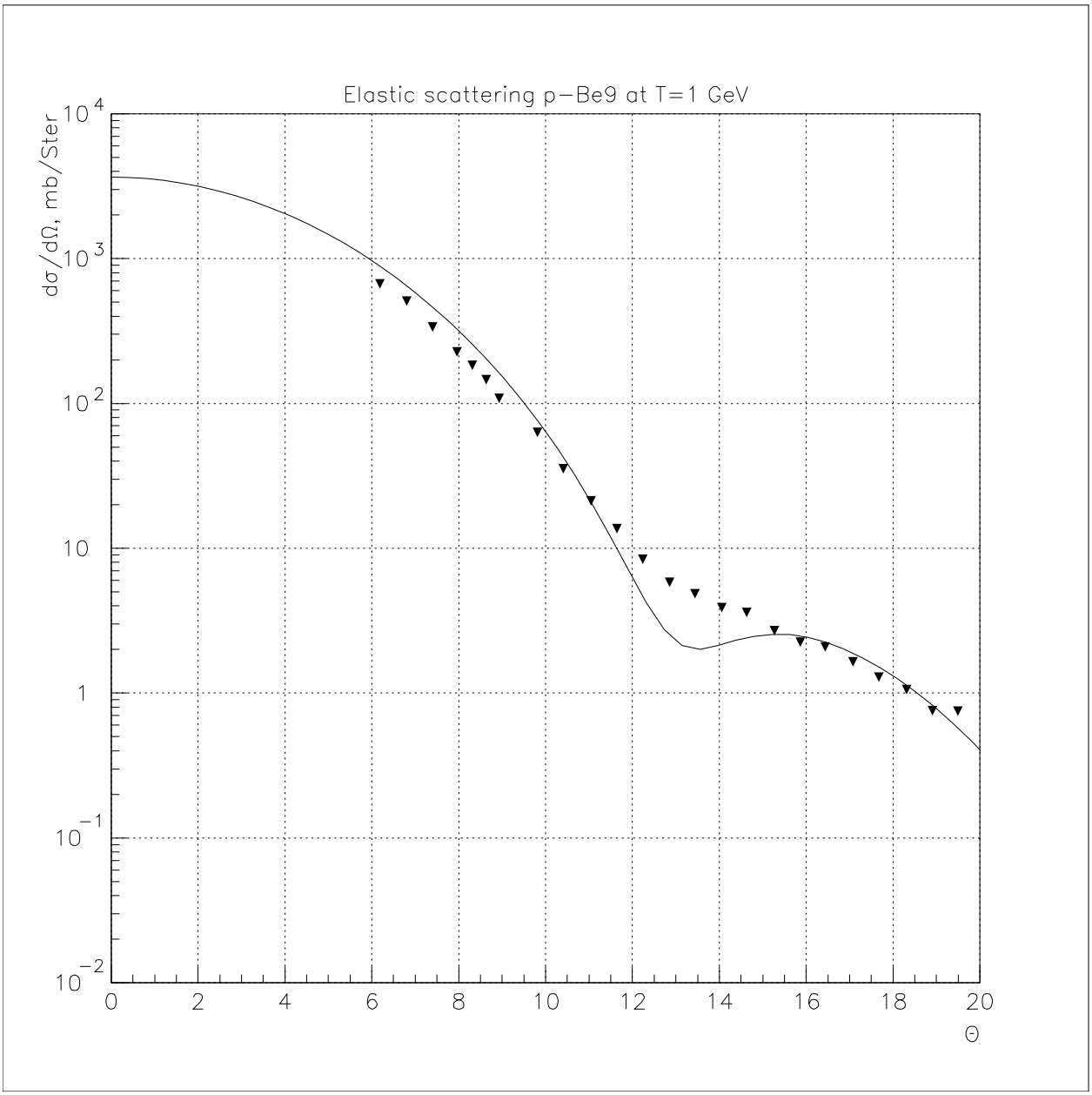

Fig. 7.1: Elastic proton scattering on ^{9}Be at 1 GeV

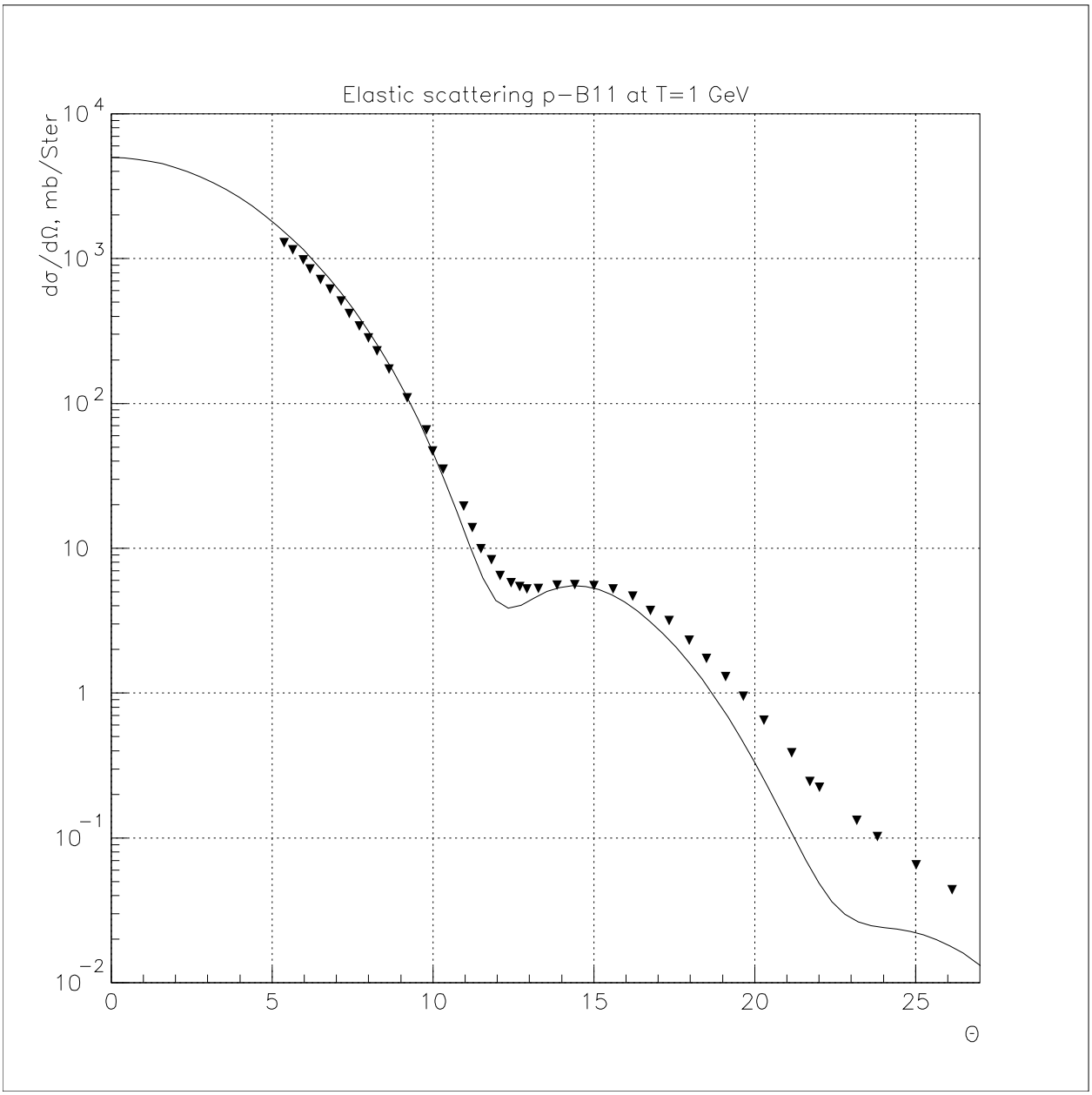

Fig. 7.2: Elastic proton scattering on ^{11}B at 1 GeV

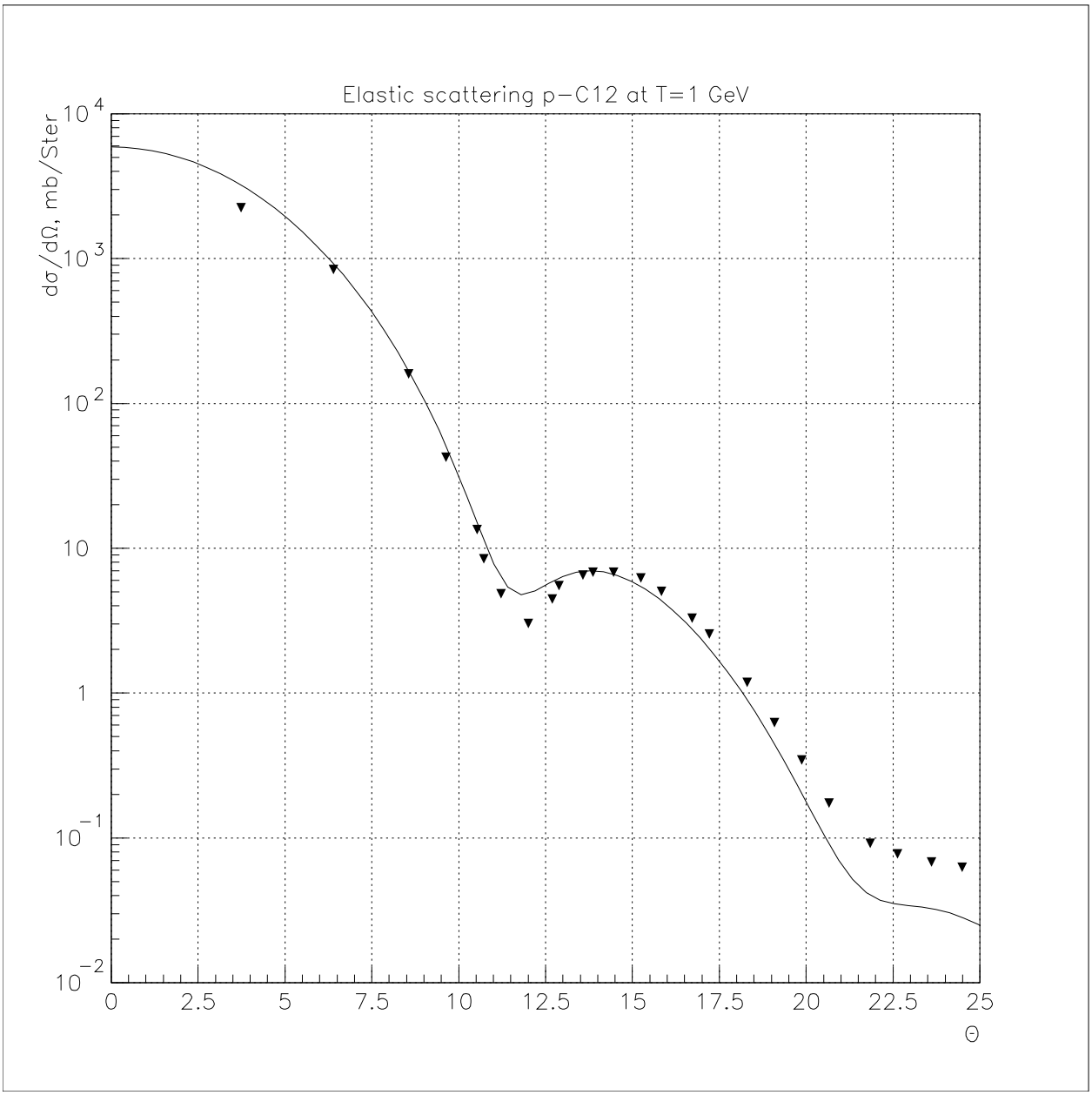

Fig. 7.3: Elastic proton scattering on ^{12}C at 1 GeV

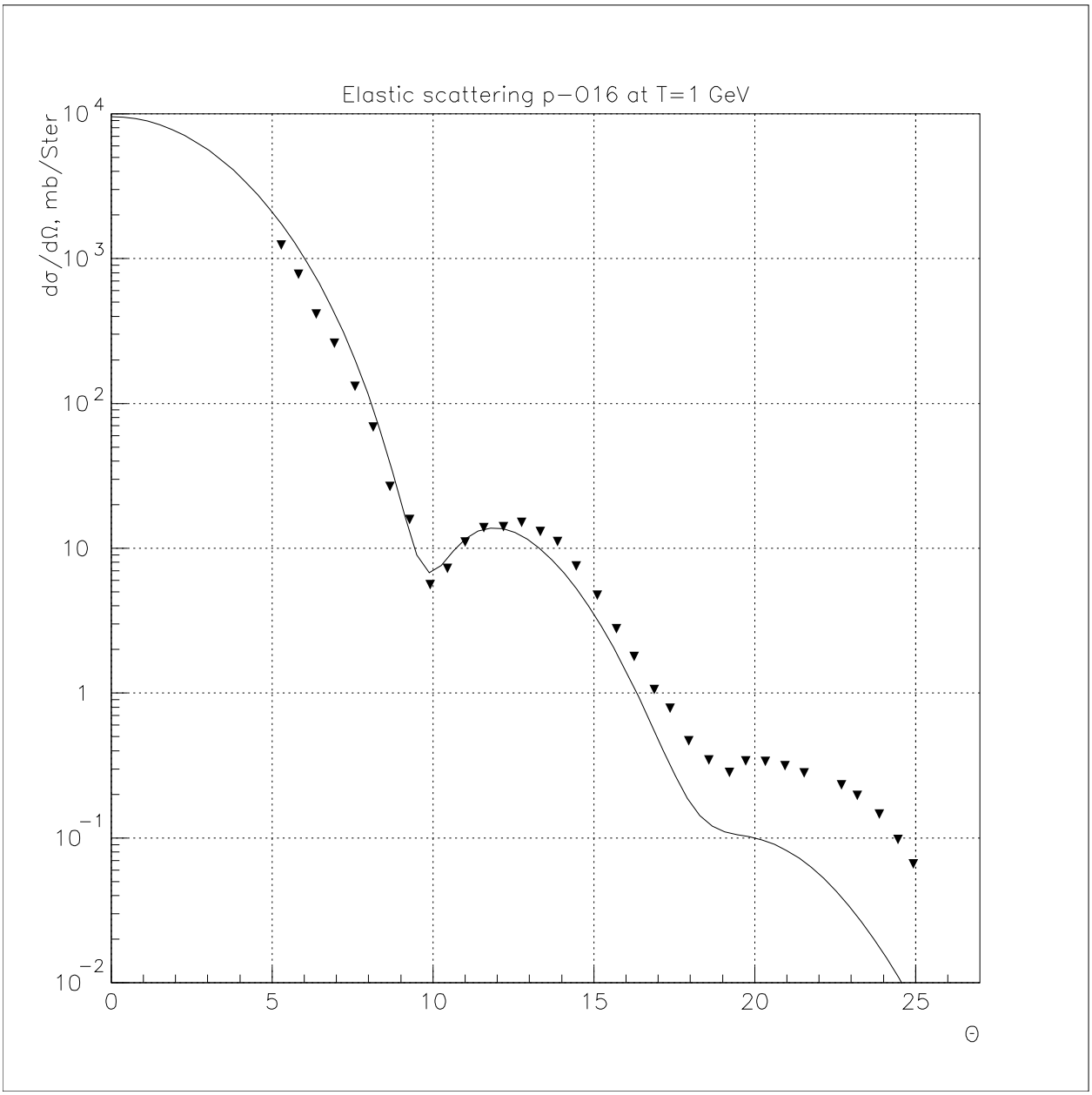

Fig. 7.4: Elastic proton scattering on ^{16}O at 1 GeV

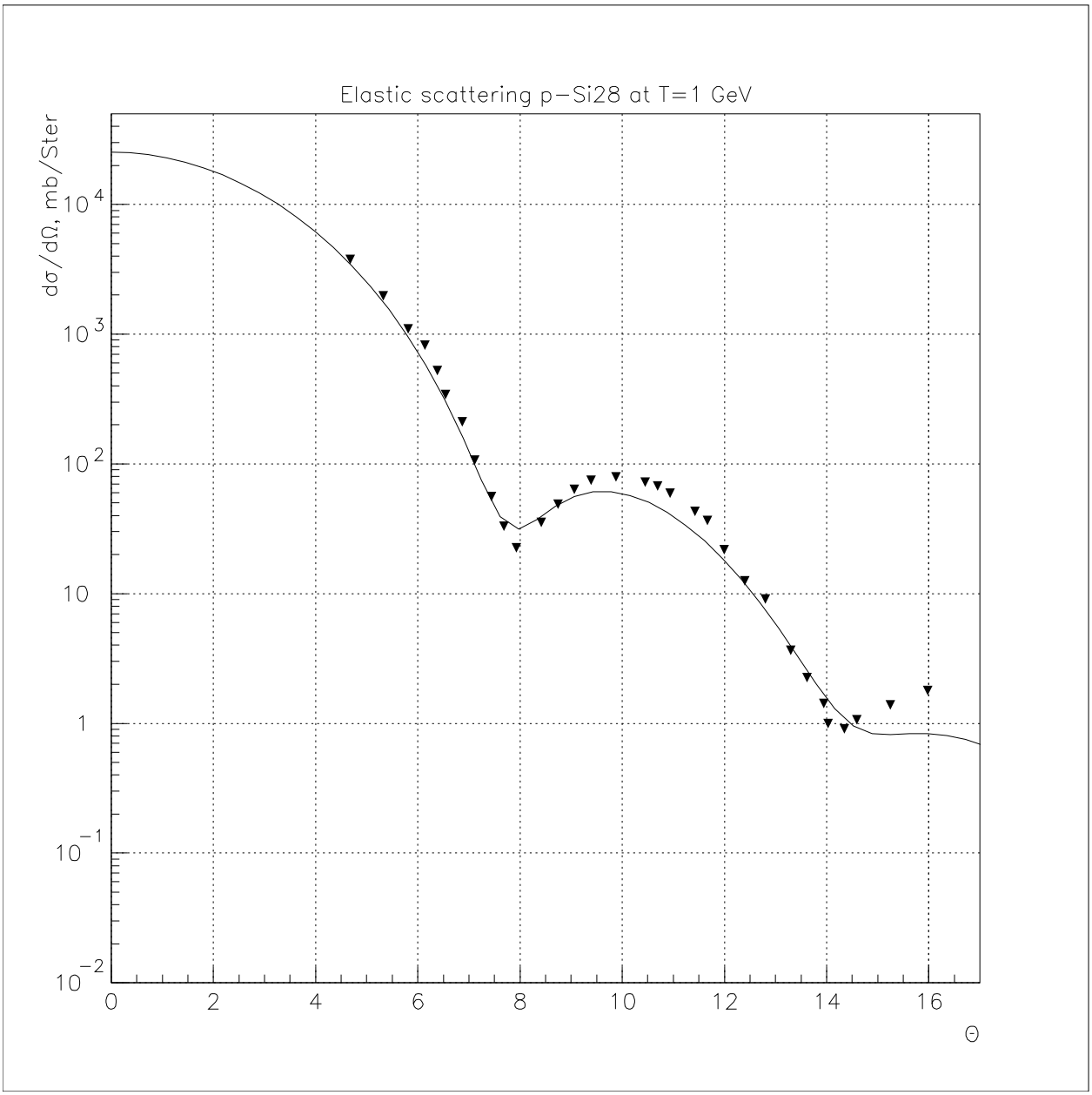

Fig. 7.5: Elastic proton scattering on ^{28}Si at 1 GeV

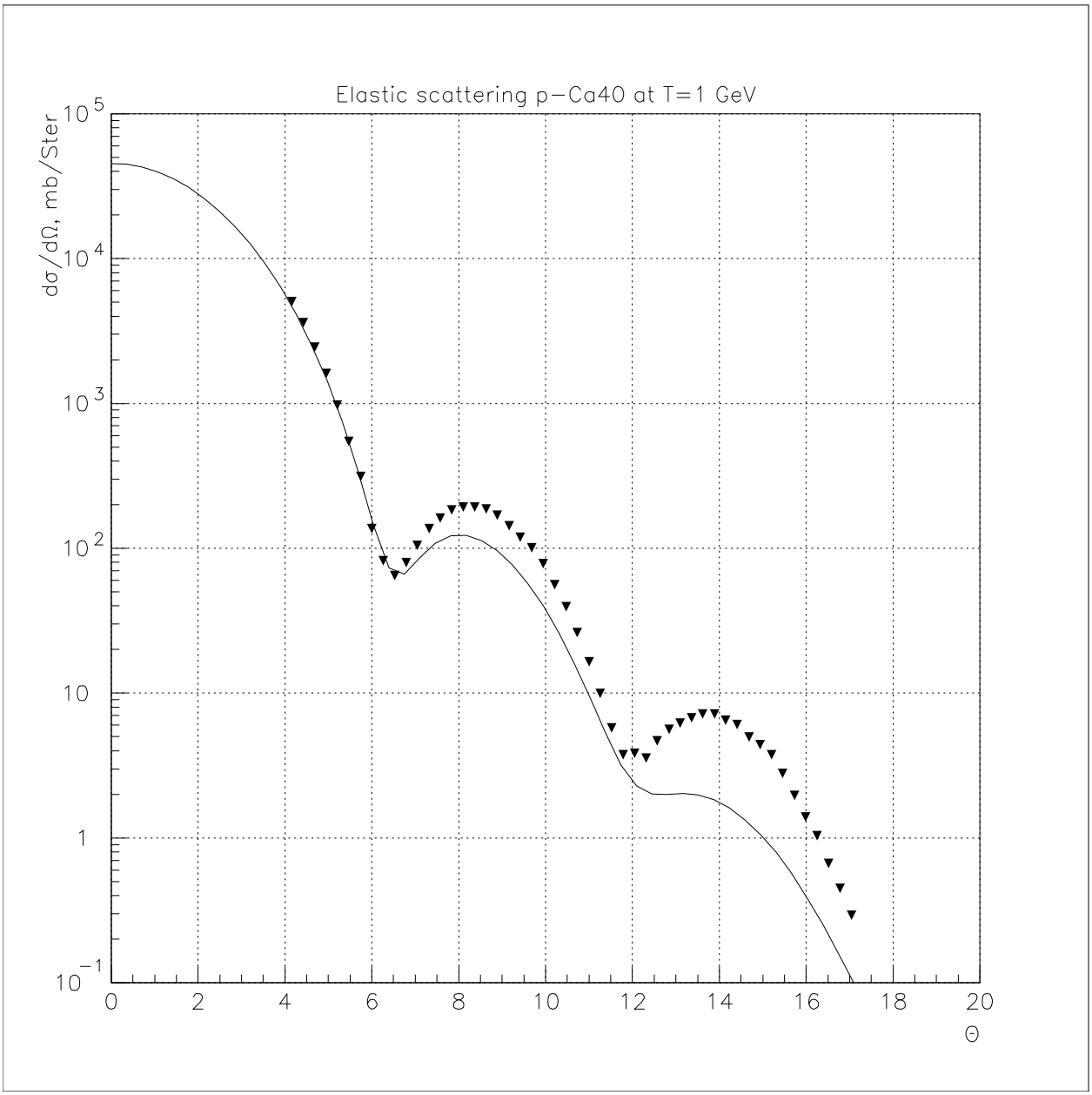

Fig. 7.6: Elastic proton scattering on ^{40}Ca at 1 GeV

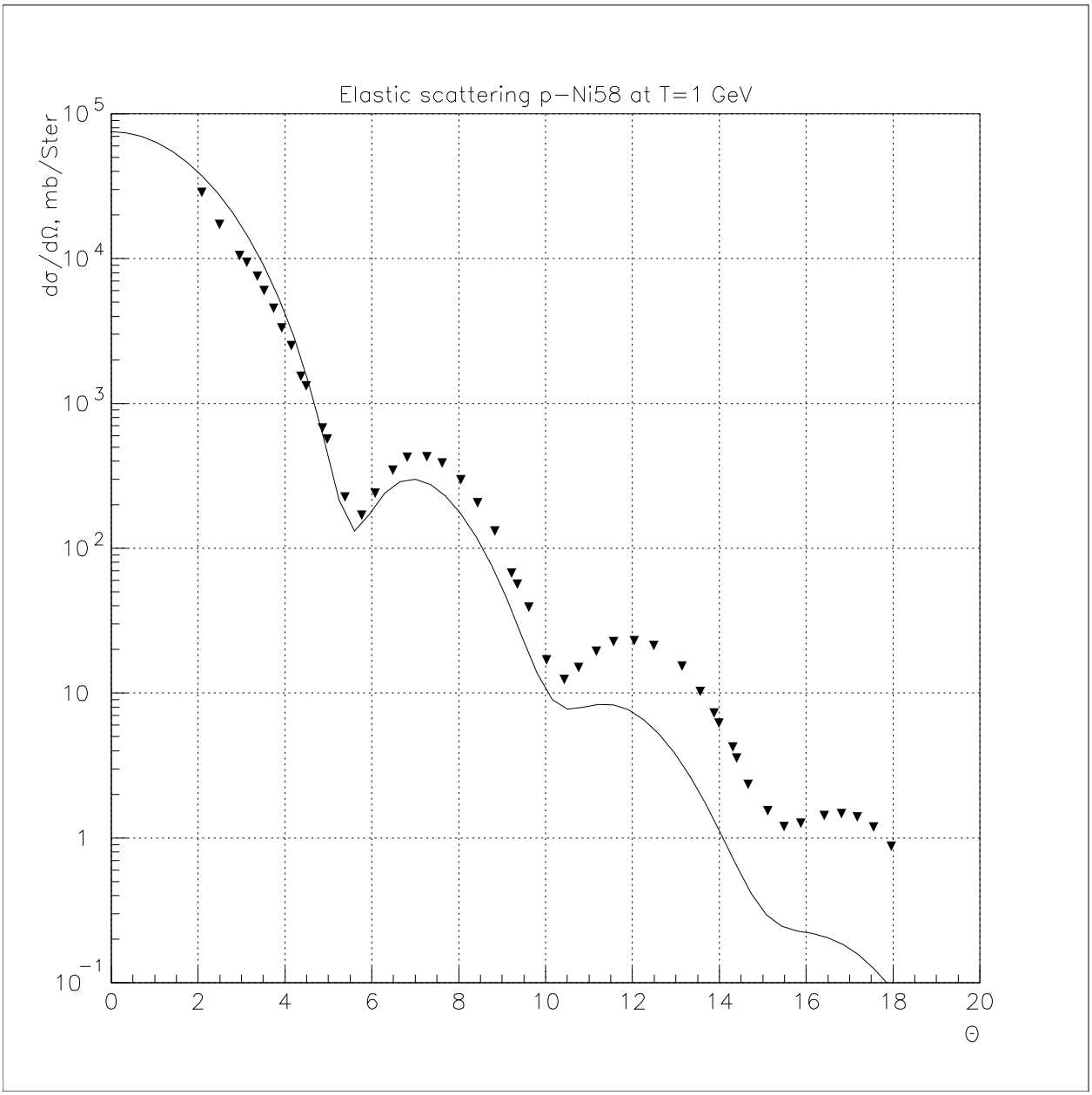

Fig. 7.7: Elastic proton scattering on ^{58}Ni at 1 GeV

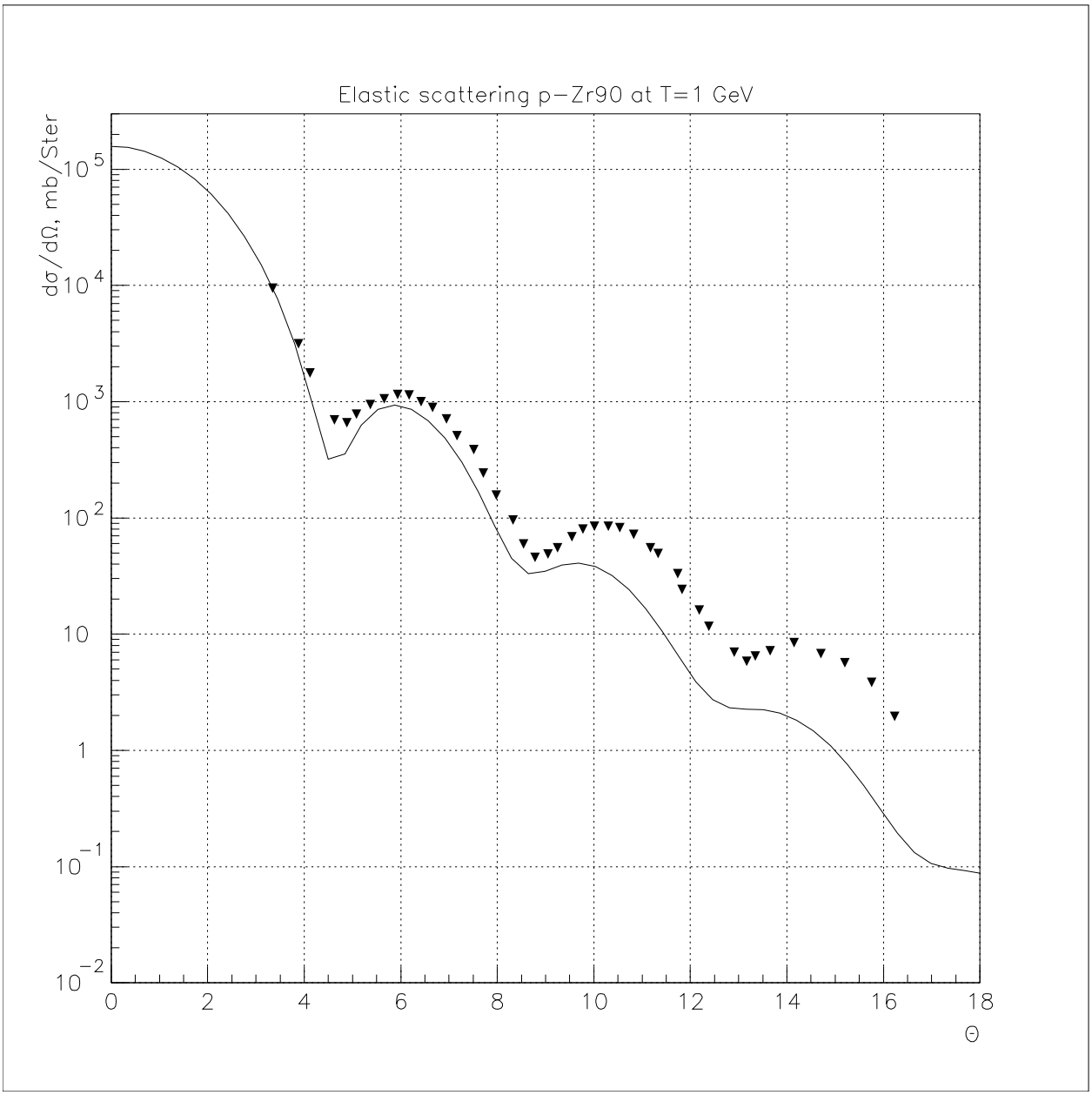

Fig. 7.8: Elastic proton scattering on ^{90}Zr at 1 GeV

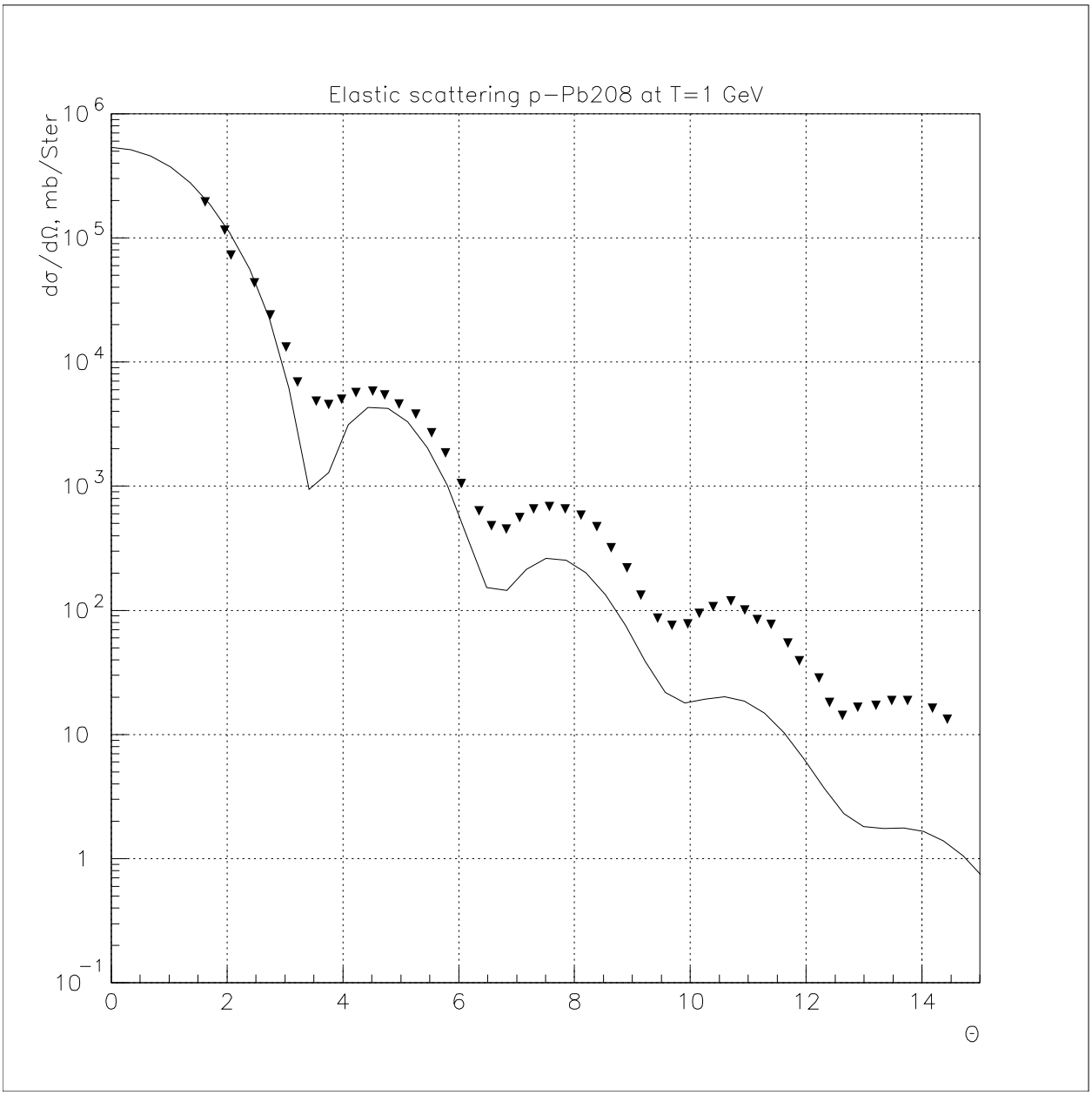

Fig. 7.9: Elastic proton scattering on ^{208}Pb at 1 GeV

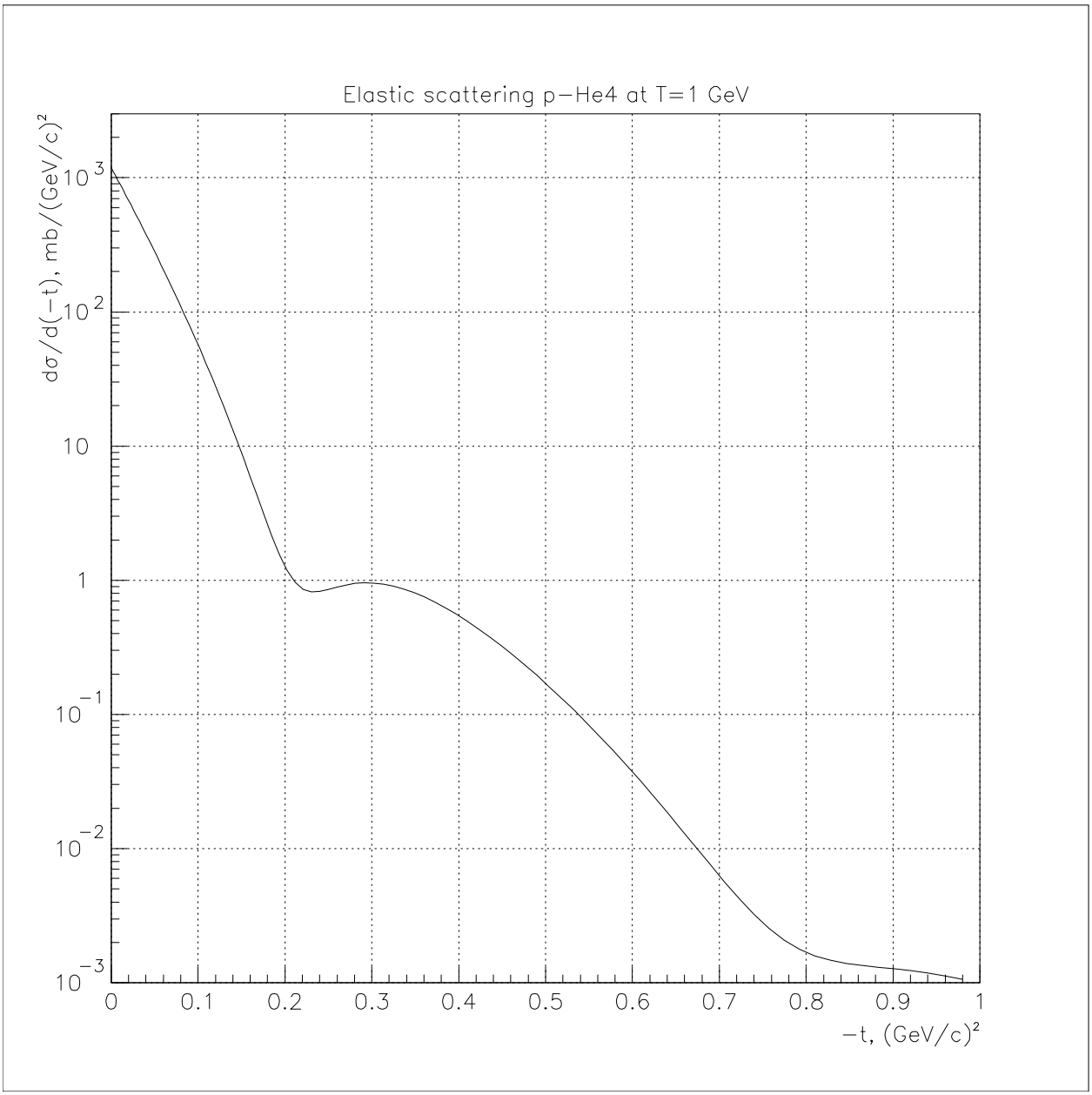

Fig. 7.10: Elastic proton scattering on ^{4}He at 1 GeV

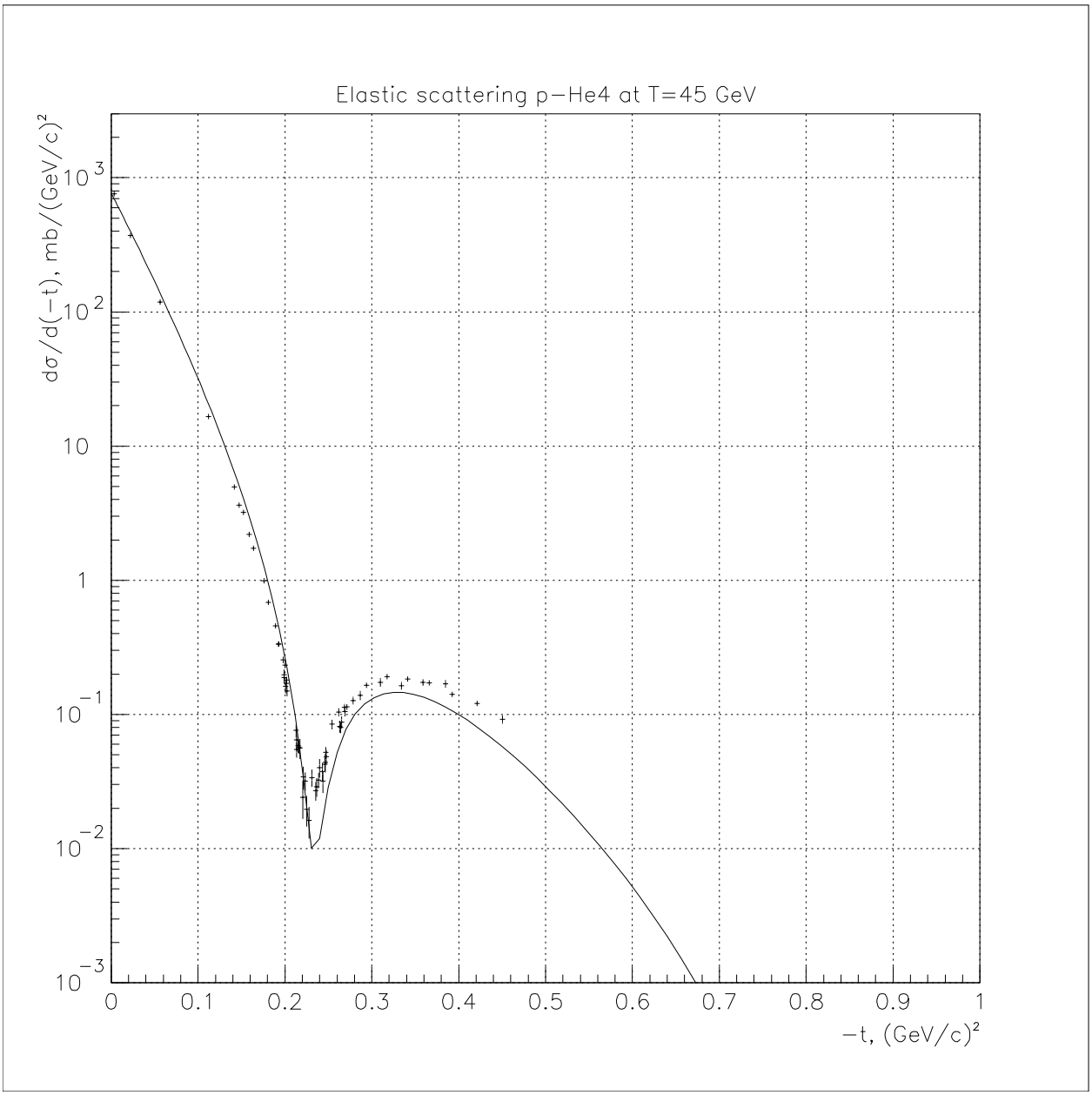

Fig. 7.11: Elastic proton scattering on ^{4}He at 45 GeV

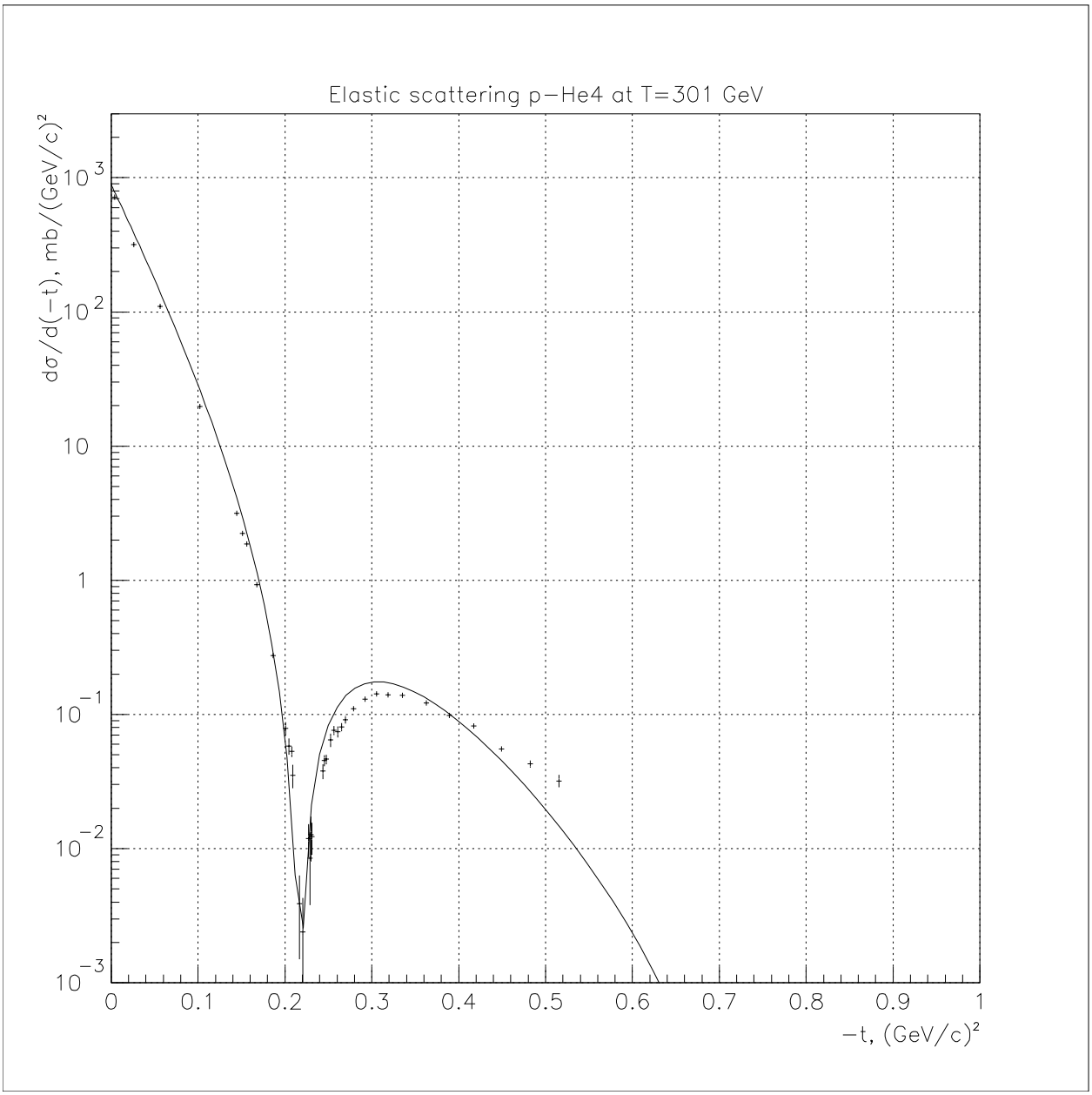

Fig. 7.12: Elastic proton scattering on ^{4}He at 301 GeV

Physics and Verification

Inclusive Cross-sections

Cross-section data is taken from the ENDF/B-VII.r1:cite:*ENDF* evaluated data library for those few elements where data exist. As these isotopes are only a few, most of the isotopes data are taken from the TENDL data library, which uses the TALYS nuclear model. The format is exactly the same as for the low energy neutron data libraries. While the energy of the TENDL files goes up to 200 MeV, in the case of ENDF it only reaches 150 MeV for most isotopes and for some is even less.

The treatment of this data is done with the same code as for the low energy neutron package. It should be mentioned that for all except a few low Z isotopes in the ENDF data library, there is no information about individual decay channels, but only about the total cross section plus particle yields. Therefore the same remark as for the neutron package holds: there is no event-by-event conservation of energy, nor of atomic or mass number.

The absence of treatment of the correlation between inelastic and elastic interactions affects the emission of charged particles, while it does not for neutron and gamma emission. The effect is expected to increase with incident energy and modify the secondary particle spectra.

7.4 LowEnergyNeutrons

7.4.1 Geant4 Low Energy Nuclear Data (LEND) Package

Low Energy Nuclear Data

Geant4 Low Energy Nuclear Data (LEND) Package G4LEND is a set of low energy nuclear interaction models in Geant4. The LEND package uses Generalized Nuclear Data (GND) which is a modern format for storing nuclear data. To use the package, users must download data from and set the environment variable "G4LENDDATA" to point to the directory where the data is unpacked. **GNDv1.3.tar.gz** is a tar ball which can be downloaded from the ftp site and includes GND-formatted nuclear data for incident neutrons and gammas which are converted from the ENDF/B-VII.r1 library. A total of 421 target nuclides from H to Es are available for the neutron- incident data and 162 nuclides from H to Pt for the gamma-incident data. The cross sections and final state products of the interactions are extracted from the data using the General Interaction Data Interface (GIDI). G4LEND then allow them to be used in Geant4 hadronic cross section and model. G4LEND is a data-driven model; therefore the data library quality is crucial for its physics performance. Energy range of the package is also a function of data library. In the case of the data which converted from ENDF/B-VII.r1, it can handle neutrons interaction from below thermal energy up to 20MeV for most target nuclides. The upper limit of the energy enhances up to 150 MeV for some target nuclides. One important limitation of the model is that it does not guarantee conservation laws beyond the 2 body interaction.

7.4.2 Neutrons

Capture

The final state of radiative capture is described by either photon multiplicities, or photon production cross-sections, and the discrete and continuous contributions to the photon energy spectra, along with the angular distributions of the emitted photons.

For the description of the photon multiplicity there are two supported data representations. It can either be tabulated as a function of the energy of the incoming neutron for each discrete photon as well as the eventual continuum contribution, or the full transition probability array is known, and used to determine the photon yields. If photon production cross-sections are used, only a tabulated form is supported.

The photon energies E_γ are associated to the multiplicities or the cross-sections for all discrete photon emissions. For the continuum contribution, the normalised emission probability f is broken down into a weighted sum of normalised distributions g.

$$f\left(E \to E_\gamma\right) \;=\; \sum_i p_i(E) g_i(E \to E_\gamma)$$

The weights p_i are tabulated as a function of the energy E of the incoming neutron. For each neutron energy, the distributions g are tabulated as a function of the photon energy. As in the ENDF/B-VI data formats:cite:*ENDF*, several interpolation laws are used to minimise the amount of data, and optimise the descriptive power. All data are derived from evaluated data libraries.

The techniques used to describe and sample the angular distributions are identical to the case of elastic scattering, with the difference that there is either a tabulation or a set of legendre coefficients for each photon energy and continuum distribution.

As an example of the results is shown in figure[capture] the energy distribution of the emitted photons for the radiative capture of 15 MeV neutrons on Uranium (^{238}U). Similar comparisons for photon yields, energy and angular distributions have been performed for capture on ^{238}U, ^{235}U, ^{23}Na, and ^{14}N for a set of incoming neutron energies. In all cases investigated the agreement between evaluated data and Monte Carlo is very good.

Cross-sections

All cross-section data are taken from the ENDF/B-VI:cite:*ENDF* evaluated data library.

All inclusive cross-sections are treated as point-wise cross-sections for reasons of performance. For this purpose, the data from the evaluated data library have been processed, to explicitly include all neutron nuclear resonances in the form of point-like cross-sections rather than in the form of parametrisations. The resulting data have been transformed into a linearly interpolable format, such that the error due to linear interpolation between adjacent data points is smaller than a few percent.

The inclusive cross-sections comply with the cross-sections data set interface of the Geant4 hadronic design. They are, when registered with the tool-kit at initialisation, used to select the basic process. In the case of fission and inelastic scattering, point-wise semi-inclusive cross-sections are also used in order to decide on the active channel for an individual interaction. As an example, in the case of fission this could be first, second, third, or forth chance fission.

Elastic

The final state of elastic scattering is described by sampling the differential scattering cross-sections $\frac{\mathrm{d}\sigma}{\mathrm{d}\Omega}$. Two representations are supported for the normalised differential cross-section for elastic scattering. The first is a tabulation of the differential cross-section, as a function of the cosine of the scattering angle θ and the kinetic energy E of the incoming neutron.

$$\frac{\mathrm{d}\sigma}{\mathrm{d}\Omega} \;=\; \frac{\mathrm{d}\sigma}{\mathrm{d}\Omega}\left(\cos\theta,\; E\right)$$

The tabulations used are normalised by $\sigma/(2\pi)$ so the integral of the differential cross-sections over the scattering angle yields unity.

In the second representation, the normalised cross-section are represented as a series of legendre polynomials $P_l(\cos\theta)$, and the legendre coefficients a_l are tabulated as a function of the incoming energy of the neutron.

$$\frac{2\pi}{\sigma(E)}\frac{\mathrm{d}\sigma}{\mathrm{d}\Omega}\left(\cos\theta,\; E\right) \;=\; \sum_{l=0}^{n_l} \frac{2l+1}{2} a_l(E) P_l(\cos\theta)$$

Describing the details of the sampling procedures is outside the scope of this paper.

An example of the result we show in figure [elastic] for the elastic scattering of 15 MeV neutrons off Uranium a comparison of the simulated angular distribution of the scattered neutrons with evaluated data. The points are the evaluated data, the histogram is the Monte Carlo prediction.

In order to provide full test-coverage for the algorithms, similar tests have been performed for ^{72}Ge, ^{126}Sn, ^{238}U, ^{4}He, and ^{27}Al for a set of neutron kinetic energies. The agreement is very good for all values of scattering angle and neutron energy investigated.

Fission

For neutron induced fission, we take first chance, second chance, third chance and forth chance fission into account.

Neutron yields are tabulated as a function of both the incoming and outgoing neutron energy. The neutron angular distributions are either tabulated, or represented in terms of an expansion in legendre polynomials, similar to the angular distributions for neutron elastic scattering. In case no data are available on the angular distribution, isotropic emission in the centre of mass system of the collision is assumed.

There are six different possibilities implemented to represent the neutron energy distributions. The energy distribution of the fission neutrons $f(E \rightarrow E')$ can be tabulated as a normalised function of the incoming and outgoing neutron energy, again using the ENDF/B-VI interpolation schemes to minimise data volume and maximise precision.

The energy distribution can also be represented as a general evaporation spectrum,

$$f(E \rightarrow E') \; = \; f\left(E'/\Theta(E)\right).$$

Here E is the energy of the incoming neutron, E' is the energy of a fission neutron, and $\Theta(E)$ is effective temperature used to characterise the secondary neutron energy distribution. Both the effective temperature and the functional behaviour of the energy distribution are taken from tabulations.

Alternatively energy distribution can be represented as a Maxwell spectrum,

$$f(E \rightarrow E') \; \propto \; \sqrt{E'}\mathrm{e}^{E'/\Theta(E)},$$

$$or a evaporation spectrum$$

$$f(E \rightarrow E') \; \propto \; E'\mathrm{e}^{E'/\Theta(E)}.$$

$$In both these cases, the temperature is tabulated as a function of the$$

incoming neutron energy.

The last two options are the energy dependent Watt spectrum, and the Madland Nix spectrum. For the energy dependent Watt spectrum, the energy distribution is represented as

$$f(E \rightarrow E') \; \propto \; \mathrm{e}^{-E'/a(E)} \sinh\sqrt{b(E)E'}.$$

$$Here both the parameters a, and b are used from tabulation as function$$

of the incoming neutron energy. In the case of the Madland Nix spectrum, the energy distribution is described as

$$f(E \rightarrow E') \; = \; \frac{1}{2}\left[g(E', < K_l >) \; + \; g(E', < K_h >)\right].$$

$$Here$$

$$g(E', < K >) \; = \; \frac{1}{3\sqrt{< K >}\Theta}\left[u_2^{3/2}E_1(u_2) - u_1^{3/2}E_1(u_1) + \gamma(3/2, u_2) - \gamma(3/2, u_1)\right],$$

$$u_1(E', < K >) = \frac{(\sqrt{E'} - \sqrt{< K >})^2}{\Theta}, \text{ and}$$

$$u_2(E', < K >) = \frac{(\sqrt{E'} + \sqrt{< K >})^2}{\Theta}.$$

$Here$

K_l is the kinetic energy of light fragments and K_h the kinetic energy of heavy fragments, $E_1(x)$ is the exponential integral, and $\gamma(x)$ is the incomplete gamma function. The mean kinetic energies for light and heavy fragments are assumed to be energy independent. The temperature Θ is tabulated as a function of the kinetic energy of the incoming neutron.

Fission photons are describes in analogy to capture photons, where evaluated data are available. The measured nuclear excitation levels and transition probabilities are used otherwise, if available.

As an example of the results is shown in figure[fission] the energy distribution of the fission neutrons in third chance fission of 15 MeV neutrons on Uranium (^{238}U). This distribution contains two evaporation spectra and one Watt spectrum. Similar comparisons for neutron yields, energy and angular distributions, and well as fission photon yields, energy and angular distributions have been performed for ^{238}U, ^{235}U, ^{234}U, and ^{241}Am for a set of incoming neutron energies. In all cases the agreement between evaluated data and Monte Carlo is very good.

This document describes the format of G4NDL4.5. The previous version of G4NDL does not have entries for data library identification and names of original data libraries, but other formats are same, i.e., the first element of the old version is equivalent to the 3rd element of a new version.

Since G4NDL4.4, files in the data library are compressed by zlib:cite:*zlib*. In this section, we will explain the format of G4NDL in its pre-compressed form.

Cross Section

Each file in the cross section directories has the following entries:

- the first entry is identification of library (in this case G4NDL)
- the second entry original data library from which the file came
- the third entry is a dummy entry but the value usually corresponds to the MT number of reaction in ENDF formats (2:Elastic, 102:Capture, 18:Fission; files in the directory of inelastic cross section usually have 0 for this entry). [1]
- the fourth entry is also a dummy
- the fifth entry represents the number of (energy, cross section) pairs (in eV, barn) to follow.

This is an example of cross section file format:

```
G4NDL           (1st entry)
ENDF/B-VII.1    (2nd entry)
             2  (3rd entry)            \\MT
             0  (4th entry)
           682  (5th entry)            \\number of E-XS pairs
  1.000000e-05  2.043634e+01 1.062500e-05  2.043634e+01 ,,,,,
  (1st pair of E and XS)     (2nd pair of E and XS)
  2.000000e+07  4.827462e-01
  (682th pair of E and XS)
```

Final State

Unlike the format of the cross section files, the format of the final state files is not straightforward and pretty complicated. Even though each of these files follows the same format rules, the actual length and appearance of each file will depend on the specific data. The format rules of the final state files are a subset of the ENDF-6 format and a deep

understanding of the format is required to correctly interpret the content of the files. Because of limited resources, we do not plan to provide a complete documentation on this part in the near future.

Thermal Scattering Cross Section

The format of the thermal scattering cross section data is similar to that of the cross section data described above:

- the 1st and 2nd entries have the same meaning
- the 3rd and 4th entries are also dummies and not used in simulation. However the 3rd entry has the value of 3 that represents MF number of ENDF-6 format and the 4th entry has the value of MT numbers of ENDF-6 format.
- the 5th entry is the temperature (in Kelvin)
- the 6th entry represents the number of (energy, cross section) pairs given for the temperature in entry 5.
- If there are multiple temperatures listed, which is typical, then for each temperature there is a corresponding data block which consists of MF, MT, temperature, number of pairs, and paired E and cross section data.

This is an example of thermal scattering cross section file format:

```
G4NDL           (1st entry)
ENDF/B-VII.1    (2nd entry)
           3    (3rd entry)            \\MF
         223    (4th entry)            \\MT
         296    (5th entry)            \\temperature
        2453    (6th entry)            \\number of E-XS pairs
 1.000000e-5 3.456415e+2 1.125000e-5 3.272908e+2 ,,,,,
 (1st pair of E and XS)  (2nd pair of E and XS)
 4.000040e+0 0.000000e+0 2.000000e+7 0.000000e+0
(2452nd pair of E and XS)(2453rd pair of E and XS)
           3    (MF)
         223    (MT)
         350    (temperature)
        2789    (Number of E-XS pair)
 1.000000e-5 4.457232e+2 1.125000e-5 4.220525e+2 ,,,,,,
 (1st pair of E and XS)  (2nd pair of E and XS)
```

Coherent Final State

The final state files have a similar format:

- the 1st and 2nd entries have the same meaning before
- the 3rd and 4th entries are also dummy entries and not used in simulation. However the 3rd entry has the value of 7 that represents MF number of ENDF-6 format and the 4th entry has the value 2 as MT number of the ENDF-6 format.
- the 5th entry represents temperature
- the 6th entry shows the number of Bragg edges given. This is followed by pairs of Bragg edge energies in eV and structure factors.
- If there are multiple temperatures listed, which is typical, then for each temperature there is a corresponding data block which consists of MF, MT, temperature, number of Bragg edges, and paired energy of Bragg edge and structure factors. However the energies of the Bragg edges only appear in the first data block.

This is an example of thermal scattering coherent final state file:

```
G4NDL           (1st entry)
ENDF/B-VII.1    (2nd entry)
           7    (3rd entry)            // MF
           2    (4th entry)            // MT
         296    (5th entry)            // temperature
         248    (6th entry)            // number of Bragg edges
 4.555489e-4 0.000000e+0 1.822196e-3 1.347465e-2 ,,,,,,
 (1st pair of E and S)   (2nd pair of E and S)
 1.791770e+0 6.259710e-1 5.000000e+0 6.259711e-1
 (247th pair of E, S)    (248th pair of E, S)
           7    (MF)
           2    (MT)
         400    (temperature)
         248    (# of Bragg edge structure factors without energies)
 0.000000e+0 1.342127e-2 ,,,,,
 (1st pair of E and S)
 4.994888e-1 4.994889e-1
 (247th pair of E and S)
```

Incoherent Final State

The incoherent final state files have a similar format:

- the 1st and 2nd entry has same meaning before
- the 3rd and 4th entries are dummy entries and not used in simulation. However the 3rd entry has the value of 6 that represents the MF number of the ENDF-6 format and the 4th entry is the MT number of the ENDF-6 format.
- the 5th entry is the temperature of this data block
- the 6th entry is the number of isoAngle data sets, described below.
- If there are multiple temperatures listed, which is typical, then for each temperature there is a corresponding data block which consists of MF, MT, temperature, number of isoAngle data sets and the isoAngle data sets.

The format of the isoAngle data set is following.

- Up to the 8th entry, only 2nd and 5th entry has real meaning in simulation and the 2nd entry has energy of incidence neutron and 5th entry is the number of equal probability bins (N) in mu.
- 9th to (9+N-2)th entries are the boundary values of the equal probability bins. The lowest and highest boundary of -1 and 1 are obvious thus they are omitted from entries.

This is an example of isoAngle data set

```
0.000000e+0 1.000000e-5         0         0         10        10
(1st entry) (2nd entry)(3rd entry)(4th entry)(5th entry)(6th entry)
 1.000000e-05 1.000000e+00 -8.749199e-01 -6.247887e-01 ,,,
(7th entry)    (8th entry) (2nd boundary) (3rd boundary)
6.252111e-01  8.750801e-01
(9th boundary)(10th boundary)
```

This is an example of thermal scattering incoherent final state file

```
G4NDL               (1st entry)
ENDF/B-VII.1        (2nd entry)
           6        (3rd entry)        \\MF
         224        (4th entry)        \\MT
```

```
         296        (5th entry)        \\temperature
        2452        (6th entry)        \\number of isoAngle data sets
 0.000000e+0 1.000000e-5           0           0          10          10
 (1st isoAngle data set)
 1.000000e-05  1.000000e+00 -8.749199e-01 -6.247887e-01 -3.747014e-01
   -1.246577e-01  1.253423e-01  3.752985e-01  6.252111e-01  8.750801e-01
''''''''''''''''''
 0.000000e+0 1.125000e-5           0           0          10          10
(2452st isoAngle data set)
4.000040e+00  1.000000e+00  9.889886e-01  9.939457e-01  9.958167e-01
  9.970317e-01  9.979352e-01  9.986553e-01  9.992540e-01  9.997666e-01
           6        (MF)
         224        (MT)
         350        (temperature)
        2788        (sumber of isoAngle data sets)
 0.000000e+0 1.000000e-5           0           0          10          10
 1.000000e-05  1.000000e+00 -8.749076e-01 -6.247565e-01 -3.746559e-01
   -1.246055e-01  1.253944e-01  3.753440e-01  6.252433e-01  8.750923e-01
''''''''''''''''''
```

Inelastic Final State

As before, the top six entries are similar:

- the 1st and 2nd entries have the same meaning.
- the 3rd and 4th entries are dummy entries and not used in simulation. However the 3rd entry has the value of 6 that represents the MF number of ENDF-6 format and the 4th entry corresponding to MT number of ENDF-6 format.
- the 5th entry is the temperature [K] of this data block
- the 6th entry is number of E-(E'-isoAngle) data sets, where E is the energy of the incident neutron and E' is energy of the scattered neutron.
- If there are multiple temperatures listed, which is typical, then for each temperature there is a corresponding data block which consists of MF, MT, temperature, number of E-(E'-isoAngle) data set and E-(E'-isoAngle) data.

The format of E-(E'-isoAngle) is following.

- The 1st, 3rd and 4th entries are dummies and not be used in simulation.
- The 2nd entry is the energy of the incident neutron(E)
- the 5th entry is the number of entries to be found after the 6th entry.
- the 6th entry corresponds to the number of entries of each E'-isoAngle data set. The first entry of E'-isoAngle data set represents energy of scattered neutron(E') and 2nd entry is probability of E->E' scattering. Following entries correspond to boundaries of iso-probability bins in mu. The lowest and highest boundaries are also omitted. The first and last E'-isoAng set should always have all 0 values excepting for energy of scattering neutron.

This is an example of E-(E'-isoAngle) data set

```
0.000000e+0 1.000000e-5          0          0       2080         10
(1st entry) (2nd entry)(3rd entry)(4th entry)(5th entry)(6th entry)
0.000000e+00  0.000000e+00  0.000000e+00  0.000000e+00  0.000000e+00
  0.000000e+00  0.000000e+00  0.000000e+00  0.000000e+00  0.000000e+00
(1st E'-isoAng data set)
```

```
6.103500e-10  3.127586e+00 -8.741139e-01 -6.226646e-01 -3.716976e-01
  -1.212145e-01  1.287860e-01  3.783033e-01  6.273366e-01  8.758833e-01
(2nd E'-isoAng data set)
''''''''''''''''''''

7.969600e-01  5.411300e-13 -8.750360e-01 -6.254547e-01 -3.755898e-01
  -1.257686e-01  1.241790e-01  3.742614e-01  6.242919e-01  8.753607e-01
(207th E'-isoAng data set)
8.199830e-01  0.000000e+00  0.000000e+00  0.000000e+00  0.000000e+00
  0.000000e+00  0.000000e+00  0.000000e+00  0.000000e+00  0.000000e+00
(208th E'-isoAng data set)
```

This is an example of thermal scattering inelastic final state file

```
G4NDL               (1st entry)
ENDF/B-VII.1        (2nd entry)
           6        (3rd entry)        \\MF
         222        (4th entry)        \\MT
       293.6        (5th entry)        \\temperature
         107        (6th entry)        \\number of  E-(E'-isoAngle) data sets
 0.000000e+0 1.000000e-5           0           0        2080          10
 0.000000e+00  0.000000e+00  0.000000e+00  0.000000e+00  0.000000e+00
   0.000000e+00  0.000000e+00  0.000000e+00  0.000000e+00  0.000000e+00
 6.103500e-10  3.127586e+00 -8.741139e-01 -6.226646e-01 -3.716976e-01
   -1.212145e-01  1.287860e-01  3.783033e-01  6.273366e-01  8.758833e-01
 1.220700e-09  4.423091e+00 -8.737468e-01 -6.216975e-01 -3.703295e-01
   -1.196465e-01  1.303546e-01  3.796722e-01  6.283050e-01  8.762478e-01
```

Further Information

A detailed description of the file format has been created by reverse engineering the code by a user, Wesley Ford, who was a masters student at McMaster University [g4ndl-format] under the supervision of Prof. Adriaan Buijs and has kindly agreed for its inclusion here:

The link provides a document which describes G4NDL format and as a consequence readers and expert users may obtain useful information from it. Especially detailed descriptions of variable names used in the package and their meanings will be useful to developers who consider extensions of the package.

HPorLEP

The high precision neutron models discussed in the previous section depend on an evaluated neutron data library (G4NDL) for cross sections, angular distributions and final state information. However the library is not complete because there are no data for several key elements. In order to use the high precision models, users must develop their detectors using only elements which exist in the library. In order to avoid this difficulty, alternative models were developed which use the high precision models when data are found in the library, but use the low energy parameterized neutron models when data are missing.

The alternative models cover the same types of interaction as the originals, that is elastic and inelastic scattering, capture and fission. Because the low energy parameterized part of the models is independent of G4NDL, results will not be as precise as they would be if the relevant data existed.

Inelastic

For inelastic scattering, the currently supported final states are (nA:math:*(rightarrow)*) nγs (discrete and continuum), np, nd, nt, n^{3}He, nα, nd2α, nt2α, n2p, n2α, npα, n3α, 2n, 2np, 2nd, 2nα, 2n2α, nX, 3n, 3np, 3nα, 4n, p, pd, pα, 2p d, dα, d2α, dt, t, t2α, ^{3}He, α, 2α, and 3α.

The photon distributions are again described as in the case of radiative capture.

The possibility to describe the angular and energy distributions of the final state particles as in the case of fission is maintained, except that normally only the arbitrary tabulation of secondary energies is applicable.

In addition, we support the possibility to describe the energy angular correlations explicitly, in analogy with the ENDF/B-VI data formats. In this case, the production cross-section for reaction product n can be written as

$$\sigma_n(E, E', \cos(\theta)) \; = \; \sigma(E) Y_n(E) p(E, E', \cos(\theta)).$$

Here $Y_n(E)$ is the product multiplicity, $\sigma(E)$ is the inelastic cross-section, and $p(E, E', \cos(\theta))$ is the distribution probability. Azimuthal symmetry is assumed.

The representations for the distribution probability supported are isotropic emission, discrete two-body kinematics, N-body phase-space distribution, continuum energy-angle distributions, and continuum angle-energy distributions in the laboratory system.

The description of isotropic emission and discrete two-body kinematics is possible without further information. In the case of N-body phase-space distribution, tabulated values for the number of particles being treated by the law, and the total mass of these particles are used. For the continuum energy-angle distributions, several options for representing the angular dependence are available. Apart from the already introduced methods of expansion in terms of legendre polynomials, and tabulation (here in both the incoming neutron energy, and the secondary energy), the Kalbach-Mann systematic is available. In the case of the continuum angle-energy distributions in the laboratory system, only the tabulated form in incoming neutron energy, product energy, and product angle is implemented.

First comparisons for product yields, energy and angular distributions have been performed for a set of incoming neutron energies, but full test coverage is still to be achieved. In all cases currently investigated, the agreement between evaluated data and Monte Carlo is very good.

Introduction

The neutron transport class library described here simulates the interactions of neutrons with kinetic energies from thermal energies up to O(20 MeV). The upper limit is set by the comprehensive evaluated neutron scattering data libraries that the simulation is based on. The result is a set of secondary particles that can be passed on to the tracking sub-system for further geometric tracking within Geant4.

The interactions of neutrons at low energies are split into four parts in analogy to the other hadronic processes in Geant4. We consider radiative capture, elastic scattering, fission, and inelastic scattering as separate models. These models comply with the interface for use with the Geant4 hadronic processes which enables their transparent use within the Geant4 tool-kit together with all other Geant4 compliant hadronic shower models.

Summary

By the way of abstraction and code reuse we minimised the amount of code to be written and maintained. The concept of container-sampling lead to abstraction and encapsulation of data representation and the corresponding random number generators. The Object Oriented design allows for easy extension of the cross-section base of the system, and the ENDF-B VI data evaluations have already been supplemented with evaluated data on nuclear excitation levels, thus improving the energy spectra of de-excitation photons. Other established data evaluations have been investigated, and extensions based on the JENDL:cite:*JENDL*, CENDL:cite:*CENDL*, and Brond:cite:*Brond* data libraries are foreseen for next year.

Followings are important remark of the NeutornHP package. Correlation between final state particles is not included in tabulated data. The method described here does not included necessary correlation or phase space constrains needed to conserver momentum and energy. Such conservation is not guarantee either in single event or averaged over many events.

7.5 LPBias

7.5.1 Leading Particle Bias

Overview

G4Mars5GeV is an inclusive event generator for hadron(photon) interactions with nuclei, and translated from the MARS code system(MARS13(98)). To construct a cascade tree, only a fixed number of particles are generated at each vertex. A corresponding statistical weight is assigned to each secondary particle according to its type and phase-space. Rarely-produced particles or interesting phase-space region can be enhanced. [2mm] N.B. This inclusive simulation is implemented in Geant4 partially for the moment, not completed yet. [3mm] **MARS Code System** MARS is a set of Monte Carlo programs for inclusive simulation of particle interactions, and high multiplicity or rare events can be simulated fast with its sophisticated biasing techniques. For the details on the MARS code system, see *[1]*[MARSWWW].

Method

In *G4Mars5GeV*, three secondary hadrons are generated in the final state of an hadron(photon)-nucleus inelastic interaction, and a statistical weight is assigned to each particle according to its type, energy and emission angle. In this code, energies, momenta and weights of the secondaries are sampled, and the primary particle is simply terminated at the vertex. The allowed projectile kinetic energy is $E_0 \leq 5$ GeV, and following particles can be simulated;

$$p,\ n,\ \pi^+,\ \pi^-,\ K^+,\ K^-,\ \gamma,\ \bar{p}\ .$$

Prior to a particle generation, a Coulomb barrier is considered for projectile charged hadrons(p, π^+, K^+ and $\bar{p}$) with kinetic energy of less than 200 MeV. The coulomb potential $V_{\rm coulmb}$ is given by

$$V_{\rm columb} = 1.11 \times 10^{-3} \times Z/A^{1/3} \quad ({\rm GeV}),$$

where Z and A are atomic and mass number, respectivelly. [2mm]

Inclusive hadron production

The following three steps are carried out in a sequence to produce secondary particles:

- nucleon production,
- charged pion/kaon production and
- neutral pion production.

These processes are performed independently, i.e. the energy and momentum conservation law is broken at each event, however, fulfilled on the average over a number of events simulated. [5mm] **nucleon production** [1mm] Projectiles $K^\pm$ and $\bar{p}$ are replaced with $\pi^\pm$ and p, individually to generate the secondary nucleon. Either of neutron or proton is selected randomly as the secondary except for the case of gamma projectiling. The gamma is handled as a pion. [5mm] **charged pion/kaon production** [1mm] If the incident nucleon does not have enough energy to produce the pion(> 280 MeV), charged and neutral pions are not produced. A charged pion is selected with the equal probability, and a bias is eliminated with the appropriate weight which is assigned taking into account the difference between π^+

and π^- both for production probability and for inclusive spectra. It is replaced with a charged kaon a certain fraction of the time, that depends on the projectile energy if $E_0 > 2.1$ GeV. The ratio of kaon replacement is given by

$$R_{\rm kaon} = 1.3 \times \left\{ C_{\rm min} + (C - C_{\rm min}) \frac{\log(E_0/2)}{\log(100/2)} \right\} \quad (2.1 \leq E_0 \leq 5.2 \text{ GeV}),$$

where $C_{\rm min}$ is 0.03(0.08) for nucleon(others) projectiling, and *Produced particle Projectile particle*

$$C = \left\{ \begin{array}{ll} 0.071 & (\pi^+) \\ 0.083 & (\pi^-) \end{array} \right\} \times \left\{ \begin{array}{ll} 1.3 & (\pi^\pm) \\ 2.0 & (K^\pm) \\ 1.0 & (\text{others}) \end{array} \right\}$$

A similar strangeness replacement is not considered for nucleon production. [3mm]

Sampling of energy and emission angle of the secondary

The energy and emission angle of the secondary particle depends on projectile energy. There are formulae depending on whether or not the interaction particle(IP) is identical to the secondary(JP). [2mm] For IP $\neq$ JP, the secondary energy E_2 is simply given by

$$E_2 = E_{\rm th} \times \left(\frac{E_{\rm max}}{E_{\rm th}} \right)^\epsilon \qquad (\text{MeV}) \,,$$

where $E_{\rm max} = max\,(E_0, 0.5\,\text{MeV})$, $E_{\rm th} = 1$ MeV, and ϵ is a uniform random between 0 and 1. [2mm] For IP = JP,

$$E_2 = \left\{ \begin{array}{ll} E_{\rm th} + \epsilon\,(E_{\rm max} - E_{\rm th}) & \\ E_{\rm th} \times e^{\epsilon\,(\beta+99)} & (\text{MeV}) \\ E_0 \times \big(\beta\,(\epsilon - 1) + 1 + 99\epsilon\big)/100 & \end{array} \right. \begin{array}{l} E_0 < 100\,E_{\rm th} \text{ MeV} \\ E_0 \geq 100\,E_{\rm th} \text{ and } \epsilon < \eta \\ E_0 \geq 100\,E_{\rm th} \text{ and } \epsilon \geq \eta \end{array}$$

Here, $\beta = \log(E_0/100\,E_{\rm th})$ and $\eta = \beta/(99 + \beta)$. If resulting E_2 is less than 0.5 MeV, nothing is generated. [5mm] **Angular distribution** [1mm] The angular distribution is mainly determined by the energy ratio of the secondary to the projectile(i.e. the emission angle and probability of the occurrence increase as the energy ratio decreases). The emission angle of the secondary particle with respect to the incident direction is given by

$$\theta = -\log\big(1 - \epsilon(1 - e^{-\pi\,\tau})\big)/\tau \,,$$

where $\tau = E_0/5(E_0 + 1/2)$.

Sampling statistical weight

The kinematics of the secondary particle are determined randomly using the above formulae([eq:energy],[eq:angle]). A statistical weight is calculated and assigned to each generated particle to reproduce a true inclusive spectrum in the event. The weight is given by

$$D2N = V10(\text{JP}) \times DW\,(E) \times DA\,(\theta) \times V1\,(E, \theta, \text{JP}),$$

where • $V10$ is the statistical weight for the production rate based on neutral pion production($V10 = 1$).

$$V10 = \left\{ \begin{array}{ll} 2.0\,(2.5) & \text{nucleon production (the case of gamma projectile)} \\ 2.1 & \text{charged pion/kaon production} \end{array} \right.$$

• DW and DA are dominantly determined by the secondary energy and emission angle, individually. [2mm] • V1 is a true double-differential production cross-section (divided by the total inelastic cross-section) *[1]*, calculated in *G4Mars5GeV::D2N2* according to the projectile type and energy, target atomic mass, and simulated secondary energy, emission angle and particle type.

7.6 Radioactive Decay

7.6.1 Radioactive Decay

The Radioactive Decay Module

G4RadioactiveDecay and associated classes are used to simulate the decay, either in-flight or at rest, of radioactive nuclei by α, β^+, and β^- emission and by electron capture (EC). The simulation model depends on data taken from the Evaluated Nuclear Structure Data File (ENSDF) *[1]* which provides information on:

- nuclear half-lives,
- nuclear level structure for the parent or daughter nuclide,
- decay branching ratios, and
- the energy of the decay process.

If the daughter of a nuclear decay is an excited isomer, its prompt nuclear de-excitation is treated using the *G4PhotoEvaporation* class (see Section *Photon evaporation*).

Alpha Decay

The final state of alpha decay consists of an α and a recoil nucleus with $(Z-2, A-4)$. The two particles are emitted back-to-back in the center of mass with the energy of the α taken from the ENSDF data entry for the decaying isotope.

Beta Decay

Beta decay is modeled by the emission of a β^- or β^+, an anti-neutrino or neutrino, and a recoil nucleus of either $Z+1$ or $Z-1$. The energy of the β is obtained by sampling either from histogrammed data or from the theoretical three-body phase space spectral shapes. The latter include allowed, first, second and third unique forbidden, and first non-unique forbidden transitions.

The shape of the energy spectrum of the emitted lepton is given by

$$\frac{d^2n}{dEdp_e} = (E_0 - E_e)^2 E_e p_e F(Z, E_e) S(Z, E_0, E_e)$$

where, in units of electron mass, E_0 is the endpoint energy of the decay taken from the ENSDF data, E_e and p_e are the emitted electron energy and momentum, Z is the atomic number, F is the Fermi function and S is the shape factor.

The Fermi function F accounts for the effect of the Coulomb barrier on the probability of $\beta^\pm$ emission. Its relativistic form is

$$F(Z, E_e) = 2(1+\gamma)(2p_eR)^{2\gamma-2} e^{\pm\pi\alpha Z E_e/p_e} \frac{|\Gamma(\gamma + i\alpha Z E_e/p_e)|^2}{\Gamma(2\gamma+1)^2}$$

where R is the nuclear radius, $\gamma = \sqrt{1-(\alpha Z)^2}$, and α is the fine structure constant. The squared modulus of Γ is computed using approximation B of Wilkinson *[2]*.

The factor S determines whether or not additional corrections are applied to the decay spectrum. When $S = 1$ the decay spectrum takes on the so-called allowed shape which is just the phase space shape modified by the Fermi function. For this type of transition the emitted lepton carries no angular momentum and the nuclear spin and parity do not change. When the emitted lepton carries angular momentum and nuclear size effects are not negligible, the factor S is no longer unity and the transitions are called "forbidden". Corrections are then made to the spectrum shape which take into account the energy dependence of the nuclear matrix element. The form of S used in the spectrum sampling is that of Konopinski *[3]*.

Electron Capture

Electron capture from the atomic K, L and M shells is simulated by producing a recoil nucleus of $(Z-1, A)$ and an electron-neutrino back-to-back in the center of mass. Since this leaves a vacancy in the electron orbitals, the atomic relaxation model (ARM) is triggered in order to produce the resulting x-rays and Auger electrons. More information on the ARM can be found in the Electromagnetic section of this manual.

In the electron capture decay mode, internal conversion is also enabled so that atomic electrons may be ejected when interacting with the nucleus.

Recoil Nucleus Correction

Due to the level of imprecision of the rest-mass energy of the nuclei generated by *G4IonTable::GetNucleusMass*, the mass of the parent nucleus is modified to a minor extent just before performing the two- or three-body decay so that the Q for the transition process equals that identified in the ENSDF data.

Biasing Methods

By default, sampling of the times of radioactive decay and branching ratios is done according to standard, analogue Monte Carlo modeling. The user may switch on one or more of the following variance reduction schemes, which can provide significant improvement in the modelling efficiency:

1. The decays can be biased to occur more frequently at certain times, for example, corresponding to times when measurements are taken in a real experiment. The statistical weights of the daughter nuclides are reduced according to the probability of survival to the time of the event, t, which is determined from the decay rate. The decay rate of the n^{th} nuclide in a decay chain is given by the recursive formulae:

$$R_n(t) = \sum_{i=1}^{n-1} A_{n:i} f(t, \tau_i) + A_{n:n} f(t, \tau_n)$$

where:

$$A_{n:i} = \frac{\tau_i}{\tau_i - \tau_n} A_{n:i} \quad \forall i < n$$

$$A_{n:n} = -\sum_{i=1}^{n-1} \frac{\tau_n}{\tau_i - \tau_n} A_{n:i} - y_n$$

$$f(t, \tau_i) = \frac{e^{-\frac{t}{\tau_i}}}{\tau_i} \int_{-\inf}^{t} F(t') e^{\frac{t'}{\tau_i}} dt'.$$

The values τ_i are the mean life-times for the nuclei, y_i is the yield of the i^{th} nucleus, and $F(t)$ is a function identifying the time profile of the source. The above expression for decay rate is simplified, since it assumes that the i^{th} nucleus undergoes 100% of the decays to the $(i+1)^{th}$ nucleus. Similar expressions which allow for branching and merging of different decay chains can be found in Ref. *[4]*.

A consequence of the form of equations [rdk.eq4] and [rdk.eq6] is that the user may provide a source time profile so that each decay produced as a result of a simulated source particle incident at time $t = 0$ is convolved over the source time profile to derive the actual decay rate for that source function.

This form of variance reduction is only appropriate if the radionuclei can be considered to be at rest with respect to the geometry when decay occurs.

2. For a given decay mode (α, $\beta^+ + EC$, or β^-) the branching ratios to the daughter nuclide can be sampled with equal probability, so that some low probability branches which may have a disproportionately greater effect on the measurement are sampled with increased probability.

3. Each parent nuclide can be split into a user-defined number of nuclides (of proportionally lower statistical weight) prior to treating decay in order to increase the sampling of the effects of the daughter products.

7.7 Stopping

7.7.1 Complementary parameterised and theoretical treatment

Absorption of negative pions and kaons at rest from a nucleus is described in literature *[1]*, *[2]*, *[3]*, *[4]* as consisting of two main components:

- a primary absorption process, involving the interaction of the incident stopped hadron with one or more nucleons of the target nucleus;
- the deexcitation of the remnant nucleus, left in an excitated state as a result of the occurrence of the primary absorption process.

This interpretation is supported by several experiments *[5]*, *[6]*, *[7]*, *[8]*, *[9]*, *[10]*, *[11]*, that have measured various features characterizing these processes. In many cases the experimental measurements are capable to distinguish the final products originating from the primary absorption process and those resulting from the nuclear deexcitation component.

A set of stopped particle absorption processes is implemented in GEANT4, based on this two-component model (PiMinusAbsorptionAtRest and KaonMinusAbsorptionAtRest classes, for π^- and K^- respectively. Both implementations adopt the same approach: the primary absorption component of the process is parameterised, based on available experimental data; the nuclear deexcitation component is handled through the theoretical models described elsewhere in this Manual.

7.7.2 Pion absorption at rest

The absorption of stopped negative pions in nuclei is interpreted *[1]*, *[2]*, *[3]*, *[4]* as starting with the absorption of the pion by two or more correlated nucleons; the total energy of the pion is transferred to the absorbing nucleons, which then may leave the nucleus directly, or undergo final-state interactions with the residual nucleus. The remaining nucleus de-excites by evaporation of low energetic particles.

G4PiMinusAbsorptionAtRest generates the primary absorption component of the process through the parameterisation of existing experimental data; the primary absorption component is handled by class G4PiMinusStopAbsorption. In the current implementation only absorption on a nucleon pair is considered, while contributions from absorption on nucleon clusters are neglected; this approximation is supported by experimental results *[1]*, *[12]* showing that it is the dominating contribution.

Several features of stopped pion absorption are known from experimental measurements on various materials *[5]*, *[6]*, *[7]*, *[8]*, *[9]*, *[10]*, *[11]*, *[13]*:

- the average number of nucleons emitted, as resulting from the primary absorption process;
- the ratio of nn vs np as nucleon pairs involved in the absorption process;
- the energy spectrum of the resulting nucleons emitted and their opening angle distribution.

The corresponding final state products and related distributions are generated according to a parameterisation of the available experimental measurements listed above. The dependence on the material is handled by a strategy pattern: the features pertaining to material for which experimental data are available are treated in G4PiMinusStopX classes (where X represents an element), inheriting from G4StopMaterial base class. In case of absorption on an element for which experimental data are not available, the experimental distributions for the elements closest in Z are used.

The excitation energy of the residual nucleus is calculated by difference between the initial energy and the energy of the final state products of the primary absorption process.

Another strategy handles the nucleus deexcitation; the current default implementation consists in handling the deexcitatoin component of the process through the evaporation model described elsewhere in this Manual.

7.7.3 Interactions of Stopping Particles

7.8 Theory-Driven

7.8.1 Abla

ABLA V3 evaporation/fission model

The ABLA V3 evaporation model takes excited nucleus parameters, excitation energy, mass number, charge number and nucleus spin, as input. It calculates the probabilities for emitting proton, neutron or alpha particle and also probability for fission to occur. The summary of Geant4 ABLA V3 implementation is represented in Table [tbl:ablasummary].

The probabilities for emission of particle type j are calculated using formula:

$$W_j(N,Z,E) = \frac{\Gamma_j(N,Z,E)}{\sum_k \Gamma_k(N,Z,E)},$$

where Γ_j is emission width for particle j, N is neutron number, Z charge number and E excitation energy. Possible emitted particles are *protons*, *neutrons* and *alphas*. Emission widths are calculated using the following formula:

$$\Gamma_j = \frac{1}{2\pi\rho_c(E)}\frac{4m_jR^2}{\hbar^2}T_j^2\rho_j(E - S_j - B_j),$$

where $\rho_c(E)$ and $\rho_j(E - S_j - B_j)$ are the level densities of the compound nucleus and the exit channel, respectively. B_j is the height of the Coulomb barrier, S_j the separation energy, R is the radius and T_j the temperature of the remnant nucleus after emission and m_j the mass of the emitted particle.

The fission width is calculated from:

$$\Gamma_i = \frac{1}{2\pi\rho_c(E)}T_f\rho_f(E - B_f),$$

where $\rho_f(E)$ is the level density of transition states in the fissioning nucleus, B_f the height of the fission barrier and T_f the temperature of the nucleus.

Table: ABLA V3 (located in the Geant4 directory source/processes/hadronic/models/abla) feature summary.

Level densities

Nuclear level densities are calculated using the following formula:

$$a = 0.073A[MeV^{-1}] + 0.095B_sA^{2/3}[MeV^{-2}],$$

where A the nucleus mass number and B_s dimensionless surface area of the nucleus.

Fission

Fission barrier, used to calculate fission width [eqn:fissionwidth], is calculated using a semi-empirical model fitting to data obtained from nuclear physics experiments.

External data file required

ABLA V3 needs specific data files. These files contain ABLA V3 shell corrections and nuclear masses. To enable this data set, the environment variable G4ABLADATA needs to be set, and the relevant data should be installed on your machine. You can download them from the Geant4 web site or you can have CMake download them for you during installation. For Geant4 10.0 we use the `G4ABLA3.0` data files.

How to use ABLA V3

None of the stock physics lists use the ABLA V3 model by default. It should also be understood that ABLA V3 is a nuclear de-excitation model and must be used as a secondary reaction stage; the first, dynamical reaction stage must be simulated using some other model, typically an intranuclear-cascade (INC) model. The coupling of the ABLA V3 to the INCL++ model (Chapter [cha:inclxx]) has been somewhat tested and seems to work, but no extensive benchmarking has been realized at the time of writing. Coupling to the Binary-Cascade model (Chapter [BinaryCascade]) should in principle be possible, but has never been tested. The technique to realize the coupling is described in the Application Developer Guide.

Finally, please note that the ABLA V3 model is in alpha status. The code may crash and be affected by bugs.

7.8.2 AbrasionAblation

Abrasion-ablation Model

Introduction

The abrasion model is a simplified macroscopic model for nuclear-nuclear interactions based largely on geometric arguments rather than detailed consideration of nucleon-nucleon collisions. As such the speed of the simulation is found to be faster than models such as G4BinaryCascade, but at the cost of accuracy. The version of the model implemented is interpreted from the so-called abrasion-ablation model described by Wilson *et al* [aaWilson],:cite:*aaTownsend* together with an algorithm from Cucinotta to approximate the secondary nucleon energy spectrum [aaCucinotta]. By default, instead of performing an ablation process to simulate the de-excitation of the nuclear pre-fragments, the Geant4 implementation of the abrasion model makes use of existing and more detailed nuclear de-excitation models within Geant4 (G4Evaporation, G4FermiBreakup, G4StatMF) to perform this function (see section [deexcitation]). However, in some cases cross sections for the production of fragments with large ΔA from the pre-abrasion nucleus are more accurately determined using a Geant4 implementation of the ablation model (see section [ablation]).

The abrasion interaction is the initial fast process in which the overlap region between the projectile and target nuclei is sheered-off (see figure [fig:1]) The spectator nucleons in the projectile are assumed to undergo little change in momentum, and likewise for the spectators in the target nucleus. Some of the nucleons in the overlap region do suffer a change in momentum, and are assumed to be part of the original nucleus which then undergoes de-excitation.

Less central impacts give rise to an overlap region in which the nucleons can suffer significant momentum change, and zones in the projectile and target outside of the overlap where the nucleons are considered as spectators to the initial energetic interaction.

The initial description of the interaction must, however, take into consideration changes in the direction of the projectile and target nuclei due to Coulomb effects, which can then modify the distance of closest approach compared with the initial impact parameter. Such effects can be important for low-energy collisions.

Initial nuclear dynamics and impact parameter

For low-energy collisions, we must consider the deflection of the nuclei as a result of the Coulomb force (see figure [fig:2]). Since the dynamics are non-relativistic, the motion is governed by the conservation of energy equation:

$$E_{tot} = \frac{1}{2}\mu\dot{r}^2 + \frac{l^2}{2\mu r^2} + \frac{Z_P Z_T e^2}{r}$$

where:

E_{tot} = total energy in the centre of mass frame;

r,$\dot{r}$ = distance between nuclei, and rate of change of distance;

l = angular momentum;

μ = reduced mass of system *i.e.* $m_1 m_2/(m_1 + m_2)$;

e = electric charge (units dependent upon the units for E_{tot} and r);

Z_P, Z_T = charge numbers for the projectile and target nuclei.

The angular momentum is based on the impact parameter between the nuclei when their separation is large, *i.e.*

$$E_{tot} = \frac{1}{2}\frac{l^2}{\mu b^2} \;\Rightarrow\; l^2 = 2E_{tot}\mu b^2$$

At the point of closest approach, $\dot{r}$=0, therefore:

$$E_{tot} = \frac{E_{tot} b^2}{r^2} + \frac{Z_P Z_T e^2}{r}$$
$$r^2 = b^2 + \frac{Z_P Z_T e^2}{E_{tot}} r$$

Rearranging this equation results in the expression:

$$b^2 = r(r - r_m)$$

where:

$$r_m = \frac{Z_P Z_T e^2}{E_{tot}}$$

In the implementation of the abrasion process in Geant4, the square of the far-field impact parameter, b, is sampled uniformly subject to the distance of closest approach, r, being no greater than r_P + r_T (the sum of the projectile and target nuclear radii).

Abrasion process

In the abrasion process, as implemented by Wilson *et al* [aaWilson] it is assumed that the nuclear density for the projectile is constant up to the radius of the projectile (r_P) and zero outside. This is also assumed to be the case for the target nucleus. The amount of nuclear material abraded from the projectile is given by the expression:

$$\Delta_{abr} = F A_P \left[1 - \exp\left(-\frac{C_T}{\lambda}\right)\right]$$

where F is the fraction of the projectile in the interaction zone, λ is the nuclear mean-free-path, assumed to be:

$$\lambda = \frac{16.6}{E^{0.26}}$$

E is the energy of the projectile in MeV/nucleon and C_T is the chord-length at the position in the target nucleus for which the interaction probability is maximum. For cases where the radius of the target nucleus is greater than that of the projectile (*i.e.* $r_T > r_P$):

$$C_T = \begin{cases} 2\sqrt{r_T^2 - x^2} & : x > 0 \\ 2\sqrt{r_T^2 - r^2} & : x \leq 0 \end{cases}$$

where:

$$x = \frac{r_P^2 + r^2 - r_T^2}{2r}$$

In the event that $r_P > r_T$ then C_T is:

$$C_T = \begin{cases} 2\sqrt{r_T^2 - x^2} & : x > 0 \\ 2r_T & : x \leq 0 \end{cases}$$

where:

$$x = \frac{r_T^2 + r^2 - r_P^2}{2r}$$

The projectile and target nuclear radii are given by the expression:

$$r_P \approx 1.29\sqrt{r_{RMS,P}^2 - 0.84^2}$$
$$r_T \approx 1.29\sqrt{r_{RMS,T}^2 - 0.84^2}$$

The excitation energy of the nuclear fragment formed by the spectators in the projectile is assumed to be determined by the excess surface area, given by:

$$\Delta S = 4\pi r_P^2 \left[1 + P - (1 - F)^{2/3}\right]$$

where the functions P and F are given in section [PandF]. Wilson *et al* equate this surface area to the excitation to:

$$E_S = 0.95\Delta S$$

if the collision is peripheral and there is no significant distortion of the nucleus, or

$$E_S = 0.95\left\{1 + 5F + \Omega F^3\right\}\Delta S$$
$$\Omega = \begin{cases} 0 & : A_P > 16 \\ 1500 & : A_P < 12 \\ 1500 - 320\,(A_P - 12) & : 12 \leq A_P \leq 16 \end{cases}$$

if the impact separation is such that $r << r_P$+r_T. E_S is in MeV provided ΔS is in fm^2.

For the abraded region, Wilson *et al* assume that fragments with a nucleon number of five are unbounded, 90% of fragments with a nucleon number of eight are unbound, and 50% of fragments with a nucleon number of nine are unbound. This was not implemented within the Geant4 version of the abrasion model, and disintegration of the pre-fragment was only simulated by the subsequent de-excitation physics models in the G4DeexcitationHandler (evaporation, *etc.* or G4WilsonAblationModel) since the yields of lighter fragments were already underestimated compared with experiment.

In addition to energy as a result of the distortion of the fragment, some energy is assumed to be gained from transfer of kinetic energy across the boundaries of the nuclei. This is approximated to the average energy transferred to a nucleon per unit intersection pathlength (assumed to be 13 MeV/fm) and the longest chord-length, C_l, and for half of the nucleon-nucleon collisions it is assumed that the excitation energy is:

$$E_X^* = \begin{cases} 13 \cdot \left[1 + \frac{C_t - 1.5}{3}\right] C_l & : C_t > 1.5\text{fm} \\ 13 \cdot \mathrm{C}_l & : C_t \leq 1.5\text{fm} \end{cases}$$

where:

$$C_l = \begin{cases} 2\sqrt{r_P^2 + 2rr_T - r^2 - r_T^2} & r > r_T \\ 2r_P & r \leq r_T \end{cases}$$

$$C_t = 2\sqrt{r_P^2 - \frac{\left(r_P^2 + r^2 - r_T^2\right)^2}{4r^2}}$$

For the remaining events, the projectile energy is assumed to be unchanged. Wilson *et al* assume that the energy required to remove a nucleon is 10MeV, therefore the number of nucleons removed from the projectile by ablation is:

$$\Delta_{abl} = \frac{E_S + E_X}{10} + \Delta_{spc}$$

where Δ_{spc} is the number of loosely-bound spectators in the interaction region, given by:

$$\Delta_{spc} = A_P F \exp\left(-\frac{C_T}{\lambda}\right)$$

Wilson *et al* appear to assume that for half of the events the excitation energy is transferred into one of the nuclei (projectile or target), otherwise the energy is transferred in to the other (target or projectile respectively).

The abrasion process is assumed to occur without preference for the nucleon type, *i.e.* the probability of a proton being abraded from the projectile is proportional to the fraction of protons in the original projectile, therefore:

$$\Delta Z_{abr} = \Delta_{abr} \frac{Z_P}{A_P}$$

In order to calculate the charge distribution of the final fragment, Wilson *et al* assume that the products of the interaction lie near to nuclear stability and therefore can be sampled according to the Rudstam equation (see section [ablation]). The other obvious condition is that the total charge must remain unchanged.

Abraded nucleon spectrum

Cucinotta has examined different formulae to represent the secondary protons spectrum from heavy ion collisions [aaCucinotta]. One of the models (which has been implemented to define the final state of the abrasion process) represents the momentum distribution of the secondaries as:

$$\psi(p) \propto \sum_{i=1}^{3} C_i \exp\left(-\frac{p^2}{2p_i^2}\right) + d_0 \frac{\gamma p}{\sinh(\gamma p)}$$

where:

$\psi(p)$ = number of secondary protons with momentum p per unit of momentum phase space [c:math:*(^3)*/MeV:math:*(^3)*];

p = magnitude of the proton momentum in the rest frame of the nucleus from which the particle is projected [MeV/c];

$C1$, $C2$, $C3$ = 1.0, 0.03, and 0.0002;

$p1$, $p2$, $p3$ = $\sqrt{\frac{2}{5}}p_F$, $\sqrt{\frac{6}{5}}p_F$, 500 [MeV/c]

p_F = Momentum of nucleons in the nuclei at the Fermi surface [MeV/c]

d_0 = 0.1

$\frac{1}{\gamma}$ = 90 [MeV/c];

G4WilsonAbrasionModel approximates the momentum distribution for the neutrons to that of the protons, and as mentioned above, the nucleon type sampled is proportional to the fraction of protons or neutrons in the original nucleus.

The angular distribution of the abraded nucleons is assumed to be isotropic in the frame of reference of the nucleus, and therefore those particles from the projectile are Lorentz-boosted according to the initial projectile momentum.

De-excitation of the projectile and target nuclear pre-fragments by standard Geant4 de-excitation physics

Unless specified otherwise, G4WilsonAbrasionModel will instantiate the following de-excitation models to treat subsequent particle emission of the excited nuclear pre-fragments (from both the projectile and the target):

1 G4Evaporation, which will perform nuclear evaporation of (α-particles, ^{3}He, ^{3}H, ^{2}H, protons and neutrons, in competition with photo-evaporation and nuclear fission (if the nucleus has sufficiently high A).

2 G4FermiBreakUp, for nuclei with $A \leq 12$ and $Z \leq 6$.

3 G4StatMF, for multi-fragmentation of the nucleus (minimum energy for this process set to 5 MeV).

As an alternative to using this de-excitation scheme, the user may provide to the G4WilsonAbrasionModel a pointer to her own de-excitation handler, or invoke instantiation of the ablation model (G4WilsonAblationModel).

De-excitation of the projectile and target nuclear pre-fragments by nuclear ablation

A nuclear ablation model, based largely on the description provided by Wilson *et al* [aaWilson], has been developed to provide a better approximation for the final nuclear fragment from an abrasion interaction. The algorithm implemented in G4WilsonAblationModel uses the same approach for selecting the final-state nucleus as NUCFRG2 and determining the particles evaporated from the pre-fragment in order to achieve that state. However, use is also made of classes in Geant4's evaporation physics to determine the energies of the nuclear fragments produced.

The number of nucleons ablated from the nuclear pre-fragment (whether as nucleons or light nuclear fragments) is determined based on the average binding energy, assumed by Wilson *et al* to be 10 MeV, *i.e.*:

$$A_{abl} = \begin{cases} Int\left(\frac{E_x}{10MeV}\right) & : A_{PF} > Int\left(\frac{E_x}{10MeV}\right) \\ A_{PF} & : otherwise \end{cases}$$

Obviously, the nucleon number of the final fragment, A_F, is then determined by the number of remaining nucleons. The proton number of the final nuclear fragment (Z_F) is sampled stochastically using the Rudstam equation:

$$\sigma(A_F, Z_F) \propto \exp\left(-R\left|Z_F - SA_F - TA_F^2\right|^{3/2}\right)$$

Here R=$11.8/AF^{0.45}$, S=0.486, and T=$3.8 \cdot 10^{-4}$. Once Z_F and A_F have been calculated, the species of the ablated (evaporated) particles are determined again using Wilson's algorithm. The number of α-particles is determined first, on the basis that these have the greatest binding energy:

$$N_\alpha = \begin{cases} Int\left(\frac{Z_{abl}}{2}\right) & : Int\left(\frac{Z_{abl}}{2}\right) < Int\left(\frac{A_{abl}}{4}\right) \\ Int\left(\frac{A_{abl}}{4}\right) & : Int\left(\frac{Z_{abl}}{2}\right) \geq Int\left(\frac{A_{abl}}{4}\right) \end{cases}$$

Calculation of the other ablated nuclear/nucleon species is determined in a similar fashion in order of decreasing binding energy per nucleon of the ablated fragment, and subject to conservation of charge and nucleon number.

Once the ablated particle species are determined, use is made of the Geant4 evaporation classes to sample the order in which the particles are ejected (from G4AlphaEvaporationProbability, G4He3EvaporationProbability, G4TritonEvaporationProbability, G4DeuteronEvaporationProbability, G4ProtonEvaporationProbability and G4NeutronEvaporationProbability) and the energies and momenta of the evaporated particle and the residual nucleus at each two-body decay (using G4AlphaEvaporationChannel, G4He3EvaporationChannel, G4TritonEvaporationChannel, G4DeuteronEvaporationChannel, G4ProtonEvaporationChannel and G4NeutronEvaporationChannel). If at any stage the probability for evaporation of any of the particles selected by the ablation process is zero, the evaporation is forced, but no significant momentum is imparted to the particle/nucleus. Note, however, that any particles ejected from the projectile will be Lorentz boosted depending upon the initial energy per nucleon of the projectile.

Definition of the functions P and F used in the abrasion model

In the first instance, the form of the functions P and F used in the abrasion model are dependent upon the relative radii of the projectile and target and the distance of closest approach of the nuclear centres. Four radius condtions are treated.

:

$$P = 0.125\sqrt{\mu\nu}\left(\frac{1}{\mu} - 2\right)\left(\frac{1-\beta}{\nu}\right)^2 - 0.125\left[0.5\sqrt{\mu\nu}\left(\frac{1}{\mu} - 2\right) + 1\right]\left(\frac{1-\beta}{\nu}\right)^3$$

$$F = 0.75\sqrt{\mu\nu}\left(\frac{1-\beta}{\nu}\right)^2 - 0.125\left[3\sqrt{\mu\nu} - 1\right]\left(\frac{1-\beta}{\nu}\right)^3$$

where:

$$\nu = \frac{r_P}{r_P + r_T}$$
$$\beta = \frac{r}{r_P + r_T}$$
$$\mu = \frac{r_T}{r_P}$$

:

$$P = -1$$

$$F = 1$$

:

$$P = 0.125\sqrt{\mu\nu}\left(\frac{1}{\mu} - 2\right)\left(\frac{1-\beta}{\nu}\right)^2$$

$$-0.125\left\{0.5\sqrt{\frac{\nu}{\mu}}\left(\frac{1}{\mu} - 2\right) - \left[\frac{\sqrt{1-\mu^2}}{\nu} - 1\right]\sqrt{\frac{2-\mu}{\mu^5}}\right\}\left(\frac{1-\beta}{\nu}\right)^3$$

$$F = 0.75\sqrt{\mu\nu}\left(\frac{1-\beta}{\nu}\right)^2$$

$$-0.125\left[3\sqrt{\frac{\nu}{\mu}} - \frac{\left[1 - \left(1-\mu^2\right)^{3/2}\right]\sqrt{1-(1-\mu)^2}}{\mu^3}\right]\left(\frac{1-\beta}{\nu}\right)^3$$

:

$$P = \left[\frac{\sqrt{1-\mu^2}}{\nu} - 1\right]\sqrt{1 - \left(\frac{\beta}{\nu}\right)^2}$$

$$F = \left[1 - \left(1-\mu^2\right)^{3/2}\right]\sqrt{1 - \left(\frac{\beta}{\nu}\right)^2}$$

7.8.3 BinaryCascade

Angular Distributions

Angular distributions for final states other than nucleon elastic scattering are calculated analytically, derived from the collision term of the in-medium relativistic Boltzmann-Uehling-Uhlenbeck equation, absed on the nucleon nucleon elastic scattering cross-sections:

$$\sigma_{NN\to NN}(s,t) = \frac{1}{(2\pi)^2 s}\left(D(s,t) + E(s,t) + (invertedt, u)\right)$$

Here s, t, u are the Mandelstamm variables, $D(s,t)$ is the direct term, and $E(s,t)$ is the exchange term, with

$$\begin{aligned} D(s,t) =& \frac{(g^{\sigma}_{NN})^4(t-4m^{*}2)^2}{2(t-m^2_{\sigma})^2} + \frac{(g^{\omega}_{NN})^4(2s^2+2st+t^2-8m^{*2}s+8m^{*4})}{(t-m^2_{\omega})^2} + \\ & \frac{24(g^{\pi}_{NN})^4 m^{*2}t^2}{(t-m^2_{\pi})^2} - \frac{4(g^{\sigma}_{NN}g^{\omega}_{NN})^2(2s+t-4m^{*2})m^{*2}}{(t-m^2_{\sigma})(t-m^2_{\omega})}, \end{aligned}$$

and

$$\begin{aligned} E(s,t) =& \frac{(g^{\sigma}_{NN})^4\left(t(t+s)+4m^{*2}(s-t)\right)}{8(t-m^2_{\sigma})(u-m^2_{\sigma})} + \frac{(g^{\omega}_{NN})^4(s-2m^{*2})(s-6m^{*2}))}{2(t-m^2_{\omega})(u-m^2_{\omega})} - \\ & \frac{6(g^{\pi}_{NN})^4(4m^{*2}-s-t)m^{*4}t}{(t-m^2_{\pi})(u=m_p i^2)} + \frac{3(g^{\sigma}_{NN}g^{\pi}_{NN})^2 m^{*2}(4m^{*2}-s-t)(4m^{*2}-t)}{(t-m^2_{\sigma})(u-m^2_{\pi})} + \\ & \frac{3(g^{\sigma}_{NN}g^{\pi}_{NN})^2 t(t+s)m^{*2}}{2(t-m^2_{\pi})(u-m^2_{\sigma})} + \frac{(g^{\sigma}_{NN}g^{\omega}_{NN})^2 t^2 - 4m^{*2}s - 10m^{*2}t + 24m^{*4}}{4(t-m^2_{\sigma})(u-m^2_{\omega})} + \\ & \frac{(g^{\sigma}_{NN}g^{\omega}_{NN})^2(t+s)^2 - 2m^{*2}s + 2m^{*2}t}{4(t-m^2_{\omega})(u-m^2_{\sigma})} + \frac{3(g^{\omega}_{NN}g^{\pi}_{NN})^2(t+s-4m^{*2})(t+s-2m^{*2})}{(t-m^2_{\omega})(u-m^2_{\pi})} + \\ & \frac{3(g^{\omega}_{NN}g^{\pi}_{NN})^2 m^{*2}(t^2-2m^{*2}t)}{(t-m^2_{\pi})(u-m^2_{\omega})}. \end{aligned}$$

Here, in this first release, the in-medium mass was set to the free mass, and the nucleon nucleon coupling constants used were 1.434 for the π, 7.54 for the ω, and 6.9 for the σ. This formula was used for elementary hadron-nucleon differential cross-sections by scaling teh center of mass energy squared accordingly.

Finite size effects were taken into account at the meson nucleon vertex, using a phenomenological form factor (cut-off) at each vertex.

The Geant4 Binary Cascade

Comparison with experiments

We add here a set of preliminary results produced with this code, focusing on neutron and pion production. Given that we are still in the process of writing up the paper, we apologize for the at release time still less then publication quality plots.

Decay

In the simulation of decay of strong resonances, we use the nominal decay branching ratios from the particle data book. The stochastic mass of a individual resonance created is sampled at creation time from the Breit-Wigner form, under the mass constraints posed by center of mass energy of the scattering, and the mass in the lightest decay channel. The decay width from the particle data book are then adjusted according to equation [width], to take the stochastic mass value into account.

All decay channels with nominal branching ratios greater than 1% are simulated.

Escape

When a nucleon other than the incident particle leaves the nucleus, the ground state of the nucleus changes. The energy of the outgoing particle cannot be such that the total mass of the new nucleus would be below its ground state mass. To avoid this, we reduce the energy of an outgoing nucleons by the mass-difference of old and new nucleus.

Furthermore, the momentum of the final exited nucleus derived from energy momentum balance may be such that its mass is below its ground state mass. In this case, we arbitrarily scale the momenta of all outgoing particles by a factor derived from the mass of the nucleus and the mass of the system of outgoing particles.

Excitation Fragment

At the end of the cascade, we form a fragment for further treatment in precompound and nuclear de-excitation models ([deexcitation]).

These models need information about the nuclear fragment created by the cascade. The fragment is characterized by the number of nucleons in the fragment, the charge of the fragment, the number of holes, the number of all excitons, and the number of charged excitons, and the four momentum of the fragment.

The number of holes is given by the difference of the number of nucleons in the original nucleus and the number of non-excited nucleons left in the fragment. An exciton is a nucleon captured in the fragment at the end of the cascade.

The momentum of the fragment calculated by the difference between the momentum of the primary and the outgoing secondary particles must be split in two components. The first is the momentum acquired by coherent elastic effects, and the second is the momentum of the excitons in the nucleus rest frame. Only the later part is passed to the de-excitation models. Secondaries arising from de-excitation models, including the final nucleus, are transformed back the frame of the moving fragment.

Experimental data are used in the calculation of the total, inelastic and elastic cross-section wherever available.

hadron-nucleon scattering

For the case of proton-proton(pp) and proton-neutron(pn) collisions, as well as $\pi^=$ and π^- nucleon collisions, experimental data are readily available as collected by the Particle Data Group (PDG) for both elastic and inelastic collisions. We use a tabulation based on a sub-set of these data for $\sqrt{S}$ below 3 GeV. For higher energies, parametrizations from the CERN-HERA collection are included.

Channel cross-sections

A large fraction of the cross-section in individual channels involving meson nucleon scattering can be modeled as resonance excitation in the s-channel. This kind of interactions show a resonance structure in the energy dependency of the cross-section, and can be modeled using the Breit-Wigner function

$$\sigma_{res}(\sqrt{s}) = \sum_{FS} \frac{2J+1}{(2S_1+1)(2S_2+1)} \frac{\pi}{k^2} \frac{\Gamma_I S \Gamma_F S}{(\sqrt{s}-M_R)^2 + \Gamma/4},$$

Where $S1$ and $S2$ are the spins of the two fusing particles, J is the spin of the resonance, $\sqrt{(}s)$ the energy in the center of mass system, k the momentum of the fusing particles in the center of mass system, $\Gamma_I S$ and $\Gamma)FS$ the partial width of the resonance for the initial and final state respectively. M_R is the nominal mass of the resonance.

The initial states included in the model are pion and kaon nucleon scattering. The product resonances taken into account are the Delta resonances with masses 1232, 1600, 1620, 1700, 1900, 1905, 1910, 1920, 1930, and 1950 MeV, the excited nucleons with masses of 1440, 1520, 1535, 1650, 1675, 1680, 1700, 1710, 1720, 1900, 1990, 2090, 2190, 2220, and 2250 MeV, the Lambda, and its excited states at 1520, 1600, 1670, 1690, 1800, 1810, 1820, 1830, 1890, 2100, and 2110 MeV, and the Sigma and its excited states at 1660, 1670, 1750, 1775, 1915, 1940, and 2030 MeV.

Mass dependent resonance width and partial width

During the cascading, the resonances produced are assigned reall masses, with values distributed according to the production cross-section described above. The concrete (rather than nominal) masses of these resonances may be small compared to the PDG value, and this implies that some channels may not be open for decay. In general it means, that the partial and total width will depend on the concrete mass of the resonance. We are using the UrQMD:cite:*UrQMD1.BC*[SoH92] approach for calculating these actual width,

$$\Gamma_{R\to 12}(M) = (1+r)\frac{\Gamma_{R\to 12}(M_R)}{p(M_R)^{(2l+1)}}\frac{M_R}{M}\frac{p(M)^{(2l+1)}}{1+r(p(M)/p(M_R))^{2l}}.$$

Here M_R is the nominal mass of the resonance, M the actual mass, p is the momentum in the center of mass system of the particles, L the angular momentum of the final state, and r=0.2.

Resonance production cross-section in the t-channel

In resonance production in the t-channel, single and double resonance excitation in nucleon-nucleon collisions are taken into account. The resonance production cross-sections are as much as possible based on parametrizations of experimental data:cite:*res.BC* for proton proton scattering. The basic formula used is motivated from the form of the exclusive production cross-section of the Δ_{1232} in proton proton collisions:

$$\sigma_{AB} = 2\alpha_{AB}\beta_{AB}\frac{\sqrt{s}-\sqrt{s_0}}{(\sqrt{s}-\sqrt{s_0})^2+\beta_{AB}^2}\left(\frac{\sqrt{s0}+\beta_{AB}}{\sqrt{s}}\right)^{\gamma_{AB}}$$

The parameters of the description for the various channels are given in table[Parameters]. For all other channels, the parametrizations were derived from these by adjusting the threshold behavior.

The reminder of the cross-section are derived from these, applying detailed balance. Iso-spin invariance is assumed. The formalism used to apply detailed balance is

$$\sigma(cd\to ab) = \sum_{J,M}\frac{\langle j_c m_c j_d m_d \parallel JM\rangle^2}{\langle j_a m_a j_b m_b \parallel JM\rangle^2}\frac{(2S_a+1)(2S_b+1)}{(2S_c+1)(2S_d+1)}\frac{\langle p_{ab}^2\rangle}{\langle p_{cd}^2\rangle}\sigma(ab\to cd)$$

Light

In simulating light ion reactions, the initial state of the cascade is prepared in the form of two nuclei, as described in the above section on the nuclear model.

The lighter of the collision partners is selected to be the projectile. The nucleons in the projectile are then entered, with position and momenta, into the initial state of the cascade. Note that before the first scattering of an individual nucleon, a projectile nucleon's Fermi-momentum is not taken into account in the tracking inside the target nucleus. The nucleon distribution inside the projectile nucleus is taken to be a representative distribution of its nucleons in configuration space, rather than an initial state in the sense of QMD. The Fermi momentum and the local field are taken into account in the calculation of the collision probabilities and final states of the binary collisions.

Modelling overview

The Geant4 Binary Cascade is an intranuclear cascade propagating primary and secondary particles in a nucleus. Interactions are between a primary or secondary particle and an individual nucleon of the nucleus, leading to the name

Binary Cascade. Cross section data are used to select collisions. Where available, experimental cross sections are used by the simulation. Propagating of particles is the nuclear field is done by numerically solving the equation of motion. The cascade terminates when the average and maximum energy of secondaries is below threshold. The remaining fragment is treated by precompound and de-excitation models documented in the corresponding chapters.

Modeling overview

The transport algorithm

The description of the target nucleus and fermi motion

Optical and phenomenological potentials

Pauli blocking simulation

The scattering term

Total inclusive cross-sections

Nucleon Nucleon elastic collisions

Generation of transverse momentum

Decay

The escaping particle and coherent effects

Light ion reactions

Transition to pre-compound modeling

Calculation of excitation energies and residuals

Neutrons

nnElastic

Angular distributions for elastic scattering of nucleons are taken as closely as possible from experimental data, i.e. from the result of phase-shift analysis. They are derived from differential cross sections obtained from the SAID database, R. Arndt, 1998.

Final states are derived by sampling from tables of the cumulative distribution function of the centre-of-mass scattering angle, tabulated for a discrete set of lab kinetic energies from 10 MeV to 1200 MeV. The CDF's are tabulated at 1 degree intervals and sampling is done using bi-linear interpolation in energy and CDF values. Coulomb effects are taken into consideration for pp scattering.

Nucleus

The nucleus is constructed from A nucleons and Z protons with nucleon coordinates $\mathbf{r}_i$ and momenta $\mathbf{p}_i$, with $i = 1, 2, ..., A$. We use a common initialization Monte Carlo procedure, which is realized in the most of the high energy nuclear interaction models:

- Nucleon radii r_i are selected randomly in the nucleus rest frame according to nucleon density $\rho(r_i)$. For heavy nuclei with $A > 16$ [GLMP91.BC] nucleon density is

  $$\rho(r_i) = \frac{\rho_0}{1 + \exp\left[(r_i - R)/a\right]}$$

  where

  $$\rho_0 \approx \frac{3}{4\pi R^3}(1 + \frac{a^2\pi^2}{R^2})^{-1}.$$

  Here $R = r_0 A^{1/3}$ fm and $r_0 = 1.16(1 - 1.16A^{-2/3})$ fm and $a \approx 0.545$ fm. For light nuclei with $A < 17$ nucleon density is given by a harmonic oscillator shell model [Elton61.BC], e.g.

  $$\rho(r_i) = (\pi R^2)^{-3/2} \exp\left(-r_i^2/R^2\right),$$

  where $R^2 = 2/3 < r^2 >= 0.8133A^{2/3}$ fm:math:*(^2)*. To take into account nucleon repulsive core it is assumed that internucleon distance $d > 0.8$ fm;

- The nucleus is assumed to be isotropic, i.e. we place each nucleon using a random direction and the previously determined radius r_i.

- The initial momenta of the nucleons p_i are randomly choosen between 0 and $p_F^{max}(r)$, where the maximal momenta of nucleons (in the local Thomas-Fermi approximation [DF74.BC]) depends from the proton or neutron density ρ according to

  $$p_F^{max}(r) = \hbar c(3\pi^2\rho(r))^{1/3}$$

- To obtain momentum components, it is assumed that nucleons are distributed isotropic in momentum space; i.e. the momentum direction is chosen at random.

- The nucleus must be centered in momentum space around $\mathbf{0}$, *i. e.* the nucleus must be at rest, i. e. $\sum_i \mathbf{p_i} = \mathbf{0}$; To achieve this, we choose one nucleon to compensate the sum the remaining nucleon momenta $p_rest = \sum_{i=1}^{i=A-1}$. If this sum is larger than maximum momentum $p_F^{max}(r)$, we change the direction of the momentum of a few nucleons. If this does not lead to a possible momentum value, than we repeat the procedure with a different nucleon having a larger maximum momentum $p_F^{max}(r)$. In the rare case this fails as well, we choose new momenta for all nucleons.

  This procedure gives special for hydrogen ^{1}H, where the proton has momentum $p = 0$, and for deuterium ^{2}H, where the momenta of proton and neutron are equal, and in opposite direction.

- We compute energy per nucleon $e = E/A = m_N + B(A, Z)/A$, where m_N is nucleon mass and the nucleus binding energy $B(A, Z)$ is given by the tabulation of [nucleus_binding]: and find the effective mass of each nucleon $m_i^{eff} = \sqrt{(E/A)^2 - p_i^{2\prime}}$.

Pauli Blocking

The cross sections used in this model are cross sections for free particles. In the nucleus these cross sections are reduced to effective cross sections by Pauli-blocking due to Fermi statistics.

For nucleons created by a collision, ie. an inelastic scattering or from decay, we check that all secondary nucleons occupy a state allowed by Fermi statistics. We assume that the nucleus in its ground state and all states below Fermi

energy are occupied. All secondary nucleons therefore must have a momentum p_i above local Fermi momentum $p_F(r)$, i.e.

$$p_i > p_F^{max}(r).$$

If any of the nucleons of the collision has a momentum below the local Fermi momentum, then the collision is Pauli blocked. The reaction products are discarded, and the original particles continue the cascade.

Potentials

The effect of collective nuclear elastic interaction upon primary and secondary particles is approximated by a nuclear potential.

For projectile protons and neutrons this scalar potential is given by the local Fermi momentum $p_F(r)$

$$V(r) = \frac{p_F^2(r)}{2m}$$

where m is the mass of the neutron m_n or the mass of proton m_p.

For pions the potential is given by the lowest order optical potential [stricker79]

$$V(r) = \frac{-2\pi(\hbar c)^2 A}{\overline{m}_\pi}(1 + \frac{m_\pi}{M})b_0\rho(r)$$

where A is the nuclear mass number, m_π, M are the pion and nucleon mass, $\overline{m}_\pi$ is the reduced pion mass $\overline{m}_\pi = (m_\pi m_N)/(m_\pi + m_N)$, with m_N is the mass of the nucleus, and $\rho(r)$ is the nucleon density distribution. The parameter b_0 is the effective $s-$wave scattering length and is obtained from analysis to pion atomic data to be about $-0.042fm$.

scatteringTerm

The basis of the description of the reactive part of the scattering amplitude are two particle binary collisions (hence binary cascade), resonance production, and decay. Based on the cross-section described later in this paper, collisions will occur when the transverse distance d_t of any projectile target pair becomes smaller than the black disk radium corresponding to the total cross-section σ_t

$$\frac{\sigma_t}{\pi} > d_t^2$$

In case of a collision, all particles will be propagated to the estimated time of the collision, i.e. the time of closest approach, and the collision final state is produced.

toPreCompound

Eventually, the cascade assumptions will break down at low energies, and the state of affairs has to be treated by means of evaporation and pre-equilibrium decay. This transition is not at present studied in depth, and an interesting approach which uses the tracking time, as in the Liege cascade code, remains to be studied in our context.

For this first release, the following algorithm is used to determine when cascading is stopped, and pre-equilibrium decay is called: As long as there are still particles above the kinetic energy threshold (75 MeV), cascading will continue. Otherwise, when the mean kinetic energy of the participants has dropped below a second threshold (15 MeV), the cascading is stopped.

The residual participants, and the nucleus in its current state are then used to define the initial state, i.e. excitation energy, number of excitons, number of holes, and momentum of the exciton system, for pre-equilibrium decay.

In the case of light ion reactions, the projectile excitation is determined from the binary collision participants (P) using the statistical approach towards excitation energy calculation in an adiabatic abrasion process, as described in [GSI1]:

$$E_{ex} = \sum_{P} (E^{P}_{fermi} - E^{P})$$

Given this excitation energy, the projectile fragment is then treated by the evaporation models described previously.

Transport

For the primary particle an impact parameter is chosen random in a disk outside the nucleus perpendicular to a vector passing through the center of the nucleus coordinate system an being parallel to the momentum direction. Using a straight line trajectory, the distance of closest approach d_i^{min} to each target nucleon i and the corresponding time-of-flight t_i^d is calculated. In this calculation the momentum of the target nucleons is ignored, i.e. the target nucleons do not move. The interaction cross section σ_i with target nucleons is calculated using total inclusive cross-sections described below. For calculation of the cross-section the momenta of the nucleons are taken into account. The primary particle may interact with those target nucleons where the distance of closest approach d_i^{min} is smaller than $d_i^{min} < \sqrt{\frac{\sigma_i}{\pi}}$. These candidate interactions are called collisions, and these collisions are stored ordered by time-of-flight t_i^d. In the case no collision is found, a new impact parameter is chosen.

The primary particle is tracked the time-step given by the time to the first collision. As long a particle is outside the nucleus, that is a radius of the outermost nucleon plus $3fm$, particles travel along straight line trajectories. Particles entering the nucleus have their energy corrected for Coulomb effects. Inside the nucleus particles are propagated in the scalar nuclear field. The equation of motion in the field is solved for a given time-step using a Runge-Kutta integration method.

At the end of the step, the primary and the nucleon interact suing the scattering term. The resulting secondaries are checked for the Fermi exclusion principle. If any of the two particles has a momentum below Fermi momentum, the interaction is suppressed, and the original primary is tracked to the next collision. In case interaction is allowed, the secondaries are treated like the primary, that is, all possible collisions are calculated like above, with the addition that these new primary particles may be short-lived and may decay. A decay is treated like others collisions, the collision time being the time until the decay of the particle. All secondaries are tracked until they leave the nucleus, or the until the cascade stops.

7.8.4 CrossSection

Cross section models.

Glauber model at high energies.

We can use Glauber approach [Glauber55] to calculate the total, elastic and differential elastic hadron-nucleus and nucleus- nucleus cross sections at high (more than hundreds of MeV) energies.

The hadron–nucleus and nucleus–nucleus total and elastic cross sections.

The knowledge of the nuclear elastic scattering amplitude $F(\vec{q}, s)$, where s is the total hadron-nucleon or nucleon-nucleon c.m. energy squared and $\vec{q}$ is the momentum transfer vector, gives us a possibility to calculate the total cross section (the optical theorem)

$$\sigma_{tot}(s) = \frac{4\pi}{k} ImF(0, s),$$

where k is a hadron or nucleon projectile momentum in the target nucleus rest frame. Using this amplitude we are also able to calculate the differential elastic cross section

$$\frac{d\sigma_{el}(s)}{d\Omega} = |F(\vec{q},s)|^2$$

or

$$\frac{d\sigma_{el}(s)}{dt} = \frac{\pi}{k^2}|F(\vec{q},s)|^2$$

and total elastic cross section

$$\sigma_{el}(s) = \int d\Omega |F(\vec{q},s)|^2 = \frac{1}{k^2}\int dq |F(\vec{q},s)|^2.$$

The elastic scattering amplitude can be expressed through the profile function

$$\Gamma(\vec{B},s) = 1 - S(\vec{B},s)$$
$$as the following$$

$$F(\vec{q},s) = \frac{ik}{2\pi}\int d^2\vec{B}\exp\left[i\vec{q}\Gamma(\vec{B},s)\right],$$

where $S(\vec{B},s)$ is the S-matrix and $\vec{B}$ is the impact parameter vector perpendicular to the incident momentum $\vec{k}$.

The total and elastic cross sections can be obtained from the profile function $\Gamma(\vec{B},s)$:

$$\sigma_{tot}(s) = 2\int d^2\vec{B} Re\Gamma(\vec{B},s)$$

and

$$\sigma_{el}(s) = \int d^2\vec{B}|\Gamma(\vec{B},s)|^2.$$

Thus to calculate the total, elastic and differential cross sections we need to know S-matrix $S(\vec{B},s)$.

The hadron–nucleus and nucleus–nucleus S-matrix.

Let us consider the nucleus-nucleus scattering at given impact parameter $\vec{B}$ and at given squared total c.m. nucleon–nucleon energy s.

In Glauber approach [Glauber55] an elastic nucleus–nucleus interaction is a result of the interactions between nucleons from the projectile and target nuclei. Thus, the S-scattering matrix $S^{AB}(\vec{B},s)$ for nucleus A on nucleus B collision in the impact parameter representation can be expressed as follows:

$$S^{AB}(\vec{B},s) = < \prod_{i=1}^{A}\prod_{j=1}^{B}[1-\Gamma_{ij}(\vec{B}+\vec{b}_i^A-\vec{b}_j^B,s)] >$$

where $< ... >$ means integration over the sets $\{\vec{b}_i^A\}$ and $\{\vec{b}_j^B\}$ with weight functions $T_A(\{\vec{b}^A\})$ and $T_B(\{\vec{b}^B\})$. These functions

$$T_{A,B}(\vec{b}_i^{A,B}) = \int \rho((\vec{b}_i^{A,B}z_i)dz_i$$

can be obtained from the nucleon densities $\rho((\vec{b}_i^{A,B},z_i)$. The nucleon profile function is

$$\Gamma_{ij}(\vec{B}+\vec{b}_i^A-\vec{b}_j^B,s) = \frac{\sigma_{ij}(s)}{4\pi\beta_{ij}(s)}\exp\left[-\frac{(\vec{B}+\vec{b}_i^A-\vec{b}_j^B)^2}{2\beta_{ij}(s)}\right].$$

The last equation can be obtained in the case of nucleon-nucleon amplitude parametrization:

$$f_{ij}(q,s) = \frac{ik\sigma_{ij}(s)}{4\pi}\exp\left[-\frac{1}{2}\beta_{ij}(s)q^2\right].$$

The equation (7.8.4) is a result of the assumptions that the AB-scattering phase is sum of the nucleon–nucleon scattering phases and no correlations between nucleons inside a nucleus are taken into account.

The hadron-nucleus S-matrix is calculated in similar way using Eq. (7.8.4) for $i = 1$ and $\vec{b}_i = 0$. In this case we need to use the corresponding parameter $\sigma_{hN}(s)$ and $\beta_{hN}(s)$ in nucleon profile function.

As we will show below the hadron-nucleon and nucleon–nucleon elastic scattering amplitudes at high energies can be expressed through the reggeon-nucleon vertex parameters and the parameters of the reggeon trajectory:cite:*BT76*.

High energy MC cross section algorithm.

To obtain total (see Eq. (7.8.4)) and elastic (see Eq. (7.8.4)) hadron-nucleus or nucleus-nucleus cross section at given initial energy we have to integrate the nucleon profile function $\Gamma(\vec{B},s) = 1-S(\vec{B},s)$. This is done by the Monte Carlo averaging procedure [Shabelski90], [ZSU84] to obtain the S-matrix values using Eq. (7.8.4). These values depend on the squared total c.m. energy of the colliding (i,j) pair $s_{ij} = (p_i + p_j)^2$, where p_i and p_j are the particle 4-momenta, respectively. Performing the Monte Carlo averaging one has to pick up projectile and target nucleons randomly according to the weight functions $T([\vec{b}_i^A])$ and $T([\vec{b}_j^B])$, respectively. The last functions represent probability densities to find sets of the nucleon impact parameters $[\vec{b}_i^A]$, where $i = 1,2,...,A$ and $[\vec{b}_j^B]$, where $j = 1,2,...,B$. Then by integration over $\vec{B}$ we find the total and elastic cross sections. To obtain the elastic differential cross section from the Eqs. (7.8.4) and (7.8.4) we have at first to perform the back Fourier transform of the nucleon profile function (see Eq. (7.8.4)).

Total Reaction Cross Section in Nucleus-nucleus Reactions

The transportation of heavy ions in matter is a subject of much interest in several fields of science. An important input for simulations of this process is the total reaction cross section, which is defined as the total (σ_T) minus the elastic (σ_{el}) cross section for nucleus-nucleus reactions:

$$\sigma_R = \sigma_T - \sigma_{el}.$$

The total reaction cross section has been studied both theoretically and experimentally and several empirical parameterizations of it have been developed. In Geant4 the total reaction cross sections are calculated using four such parameterizations: the Sihver:cite:*nnc.Sihver93*, Kox:cite:*nnc.Kox87*, Shen:cite:*nnc.Shen89* and Tripathi:cite:*nnc.Tripathi97* formulae. Each of these is discussed in order below.

Sihver Formula

Of the four parameterizations, the Sihver formula has the simplest form:

$$\sigma_R = \pi r_0^2[A_p^{1/3} + A_t^{1/3} - b_0[A_p^{-1/3} + A_t^{-1/3}]]^2$$

where A_p and A_t are the mass numbers of the projectile and target nuclei, and

$$b_0 = 1.581 - 0.876(A_p^{-1/3} + A_t^{-1/3}),$$

$$r_0 = 1.36fm.$$

It consists of a nuclear geometrical term $(A_p^{1/3} + A_t^{1/3})$ and an overlap or transparency parameter (b_0) for nucleons in the nucleus. The cross section is independent of energy and can be used for incident energies greater than 100 MeV/nucleon.

Kox and Shen Formulae

Both the Kox and Shen formulae are based on the strong absorption model. They express the total reaction cross section in terms of the interaction radius R, the nucleus-nucleus interaction barrier B, and the center-of-mass energy of the colliding system E_{CM}:

$$\sigma_R = \pi R^2[1 - \frac{B}{E_{CM}}].$$

Kox formula: Here B is the Coulomb barrier (B_c) of the projectile-target system and is given by

$$B_c = \frac{Z_t Z_p e^2}{r_C(A_t^{1/3} + A_p^{1/3})},$$

where r_C = 1.3 fm, e is the electron charge and Z_t, Z_p are the atomic numbers of the target and projectile nuclei. R is the interaction radius R_{int} which in the Kox formula is divided into volume and surface terms:

$$R_{int} = R_{vol} + R_{surf}.$$

R_{vol} and R_{surf} correspond to the energy-independent and energy-dependent components of the reactions, respectively. Collisions which have relatively small impact parameters are independent of both energy and mass number. These core collisions are parameterized by R_{vol}. Therefore R_{vol} can depend only on the volume of the projectile and target nuclei:

$$R_{vol} = r_0(A_t^{1/3} + A_p^{1/3}).$$

The second term of the interaction radius is a nuclear surface contribution and is parameterized by

$$R_{surf} = r_0[a\frac{A_t^{1/3}A_p^{1/3}}{A_t^{1/3} + A_p^{1/3}} - c] + D.$$

The first term in brackets is the mass asymmetry which is related to the volume overlap of the projectile and target. The second term c is an energy-dependent parameter which takes into account increasing surface transparency as the projectile energy increases. D is the neutron-excess which becomes important in collisions of heavy or neutron-rich targets. It is given by

$$D = \frac{5(A_t - Z_t)Z_p}{A_p A_r}.$$

The surface component (R_{surf}) of the interaction radius is actually not part of the simple framework of the strong absorption model, but a better reproduction of experimental results is possible when it is used.

The parameters r_0, a and c are obtained using a χ^2 minimizing procedure with the experimental data. In this procedure the parameters r_0 and a were fixed while c was allowed to vary only with the beam energy per nucleon. The best χ^2 fit is provided by r_0 = 1.1 fm and $a = 1.85$ with the corresponding values of c listed in Table III and shown in Fig. 12 of Ref. [nnc.Kox87] as a function of beam energy per nucleon. This reference presents the values of c only in chart and figure form, which is not suitable for Monte Carlo calculations. Therefore a simple analytical function is used to calculate c in Geant4. The function is:

$$c = -\frac{10}{x^5} + 2.0 \text{ for x} \geq 1.5$$

$$c = (-\frac{10}{1.5^5} + 2.0) \times (\frac{x}{1.5})^3 \text{ for x} < 1.5,$$

$$x = log(KE),$$

where KE is the projectile kinetic energy in units of MeV/nucleon in the laboratory system. **Shen formula:** as mentioned earlier, this formula is also based on the strong absorption model, therefore it has a structure similar to the Kox formula:

$$\sigma_R = 10\pi R^2[1 - \frac{B}{E_{CM}}].$$

However, different parameterized forms for R and B are applied. The interaction radius R is given by

$$R = r_0[A_t^{1/3} + A_p^{1/3} + 1.85\frac{A_t^{1/3}A_p^{1/3}}{A_t^{1/3} + A_p^{1/3}} - C'(KE)]$$
$$+\alpha\frac{5(A_t - Z_t)Z_p}{A_pA_r} + \beta E_{CM}^{-1/3}\frac{A_t^{1/3}A_p^{1/3}}{A_t^{1/3} + A_p^{1/3}}$$

where α, β and r_0 are

$$\alpha = 1fm$$

$$\beta = 0.176MeV^{1/3} \cdot fm$$

$$r_0 = 1.1fm$$

In Ref. [nnc.Shen89] as well, no functional form for $C'(KE)$ is given. Hence the same simple analytical function is used by Geant4 to derive c values.

The second term B is called the nuclear-nuclear interaction barrier in the Shen formula and is given by

$$B = \frac{1.44Z_tZ_p}{r} - b\frac{R_tR_p}{R_t + R_p}(MeV)$$

where r, b, R_t and R_p are given by

$$r = R_t + R_p + 3.2fm$$

$$b = 1MeV \cdot fm^{-1}$$

$$R_i = 1.12A_i^{1/3} - 0.94A_i^{-1/3}\ (i = t, p)$$

The difference between the Kox and Shen formulae appears at energies below 30 MeV/nucleon. In this region the Shen formula shows better agreement with the experimental data in most cases.

Tripathi formula

Because the Tripathi formula is also based on the strong absorption model its form is similar to the Kox and Shen formulae:

$$\sigma_R = \pi r_0^2(A_p^{1/3} + A_t^{1/3} + \delta_E)^2[1 - \frac{B}{E_{CM}}],$$

where r_0 = 1.1 fm. In the Tripathi formula B and R are given by

$$B = \frac{1.44Z_tZ_p}{R}$$

$$R = r_p + r_t + \frac{1.2(A_p^{1/3} + A_t^{1/3})}{E_{CM}^{1/3}}$$

where r_i is the equivalent sphere radius and is related to the $r_{rms,i}$ radius by

$$r_i = 1.29 r_{rms,i} \; (i = p, t).$$

δ_E represents the energy-dependent term of the reaction cross section which is due mainly to transparency and Pauli blocking effects. It is given by

$$\delta_E = 1.85S + (0.16S/E_{CM}^{1/3}) - C_{KE} + [0.91(A_t - 2Z_t)Z_p/(A_p A_t)],$$

where S is the mass asymmetry term given by

$$S = \frac{A_p^{1/3} A_t^{1/3}}{A_p^{1/3} + A_t^{1/3}}.$$

This is related to the volume overlap of the colliding system. The last term accounts for the isotope dependence of the reaction cross section and corresponds to the D term in the Kox formula and the second term of R in the Shen formula.

The term C_{KE} corresponds to c in Kox and $C'(KE)$ in Shen and is given by

$$C_E = D_{Pauli}[1 - \exp(-KE/40)] - 0.292 \exp(-KE/792) \times \cos(0.229 KE^{0.453}).$$

Here D_{Pauli} is related to the density dependence of the colliding system, scaled with respect to the density of the ^{12}C+^{12}C colliding system:

$$D_{Pauli} = 1.75 \frac{\rho_{A_p} + \rho_{A_t}}{\rho_{A_C} + \rho_{A_C}}.$$

The nuclear density is calculated in the hard sphere model. D_{Pauli} simulates the modifications of the reaction cross sections caused by Pauli blocking and is being introduced to the Tripathi formula for the first time. The modification of the reaction cross section due to Pauli blocking plays an important role at energies above 100 MeV/nucleon. Different forms of D_{Pauli} are used in the Tripathi formula for alpha-nucleus and lithium-nucleus collisions. For alpha-nucleus collisions,

$$D_{Pauli} = 2.77 - (8.0 \times 10^{-3} A_t) + (1.8 \times 10^{-5} A_t^2) \\ -0.8/\{1 + \exp[(250 - KE)/75]\}$$

For lithium-nucleus collisions,

$$D_{Pauli} = D_{Pauli}/3.$$

Note that the Tripathi formula is not fully implemented in Geant4 and can only be used for projectile energies less than 1 GeV/nucleon.

Representative Cross Sections

Representative cross section results from the Sihver, Kox, Shen and Tripathi formulae in Geant4 are displayed in Table I and compared to the experimental measurements of Ref. [nnc.Kox87].

Tripathi Formula for "light" Systems

For nuclear-nuclear interactions in which the projectile and/or target are light, Tripathi *et al* [RefTripathiLight] propose an alternative algorithm for determining the interaction cross section (implemented in the new class G4TripathiLightCrossSection). For such systems, Eq.[eqn15.4] becomes:

$$\sigma_R = \pi r_0^2 [A_p^{1/3} + A_t^{1/3} + \delta_E]^2 (1 - R_C \frac{B}{E_{CM}}) X_m$$

R_C is a Coulomb multiplier, which is added since for light systems Eq. [eqn15.4] overestimates the interaction distance, causing B (in Eq. [eqn15.4]) to be underestimated. Values for R_C are given in Table [tab15.1].

$$X_m = 1 - X_1 \exp\left(-\frac{E}{X_1 S_L}\right)$$

where:

$$X_1 = 2.83 - \left(3.1 \times 10^{-2}\right) A_T + \left(1.7 \times 10^{-4}\right) A_T^2$$

except for neutron interactions with ^{4}He, for which X_1 is better approximated to 5.2, and the function S_L is given by:

$$S_L = 1.2 + 1.6\left[1 - \exp\left(-\frac{E}{15}\right)\right]$$

For light nuclear-nuclear collisions, a slightly more general expression for C_E is used:

$$C_E = D\left[1 - \exp\left(-\frac{E}{T_1}\right)\right] - 0.292\exp\left(-\frac{E}{792}\right)\cdot\cos\left(0.229E^{0.453}\right)$$

D and T_1 are dependent on the interaction, and are defined in table [tab15.2].

Table: Representative total reaction cross sections

1. Data measured by Jaros et al. [nnc.Jaros78]
2. Natural silver was used in this measurement.

cc System & R_C
p + d & 13.5
p + ^{3}He & 21
p + ^{4}He & 27
p + Li & 2.2
d + d & 13.5
d + ^{4}He & 13.5
d + C & 6.0
^{4}He + Ta & 0.6
^{4}He + Au & 0.6

cccc System & T1 [MeV] & D & G [MeV]
& & & (^{4}He + X only)
p + X & 23 & $1.85 + \frac{0.16}{1+\exp\left(\frac{500-E}{200}\right)}$ & (Not applicable)
n + X & 18 & $1.85 + \frac{0.16}{1+\exp\left(\frac{500-E}{200}\right)}$ & (Not applicable)
d + X & 23 & $1.65 + \frac{0.1}{1+\exp\left(\frac{500-E}{200}\right)}$ & (Not applicable)
^{3}He + X & 40 & 1.55 & (Not applicable)
^{4}He + ^{4}He & 40 & $D = 2.77 - 8.0\times10^{-3}A_T + 1.8\times10^{-5}A_T^2 - \frac{0.8}{1+\exp\left(\frac{250-E}{G}\right)}$ & 300
^{4}He + Be & 25 & (as for ^{4}He + ^{4}He) & 300
^{4}He + N & 40 & (as for ^{4}He + ^{4}He) & 500

^{4}He + Al & 25 & (as for ^{4}He + ^{4}He) & 300
^{4}He + Fe & 40 & (as for ^{4}He + ^{4}He) & 300
^{4}He + X (general) & 40 & (as for ^{4}He + ^{4}He) & 75

7.8.5 Evaporation

Sampling procedure

The evaporation model algorithm consists from repeating steps on decay channels. The stack of excited nuclear fragments is created and initial excited fragent is stored there. For the each fragment from the stack decay chain is sampled via loop of actions:

1. switch to the next excited fragment in the stack;
2. check if Fermi break-up model [FBU] is applicable and apply this model if it is the case;
3. sort out decay products between store of excited fragments and the list of final products;
4. if Fermi break up is not applicable compute probabilities of all evaporation channels;
5. randomly select of a break-up channel and sample final state for the selected channel;
6. sort out decay products between store of excited fragments and the list of final products;
7. check if the residual fragment is stable, stop the loop if it is the case and store residual fragment to the list of final products;
8. if the fragment is not stable check if Fermi break-up is applicable, if yes then store this residual into the stack of excited fragments, else repeat from (4).

Evaporation Model

Nuclear fission

The fission decay channel (only for nuclei with $A > 65$) is taken into account as a competitor for fragment and photon evaporation channels.

The fission total probability

The fission probability (per unit time) W_{fis} in the Bohr and Wheeler theory of fission [BW39] is proportional to the level density $\rho_{fis}(T)$ (approximation Eq. (7.8.5) is used) at the saddle point, i.e.

$$W_{fis} = \frac{1}{2\pi\hbar\rho_{fis}(E^*)} \int_0^{E^*-B_{fis}} \rho_{fis}(E^* - B_{fis} - T)dT = \\ = \frac{1+(C_f-1)\exp(C_f)}{4\pi a_{fis}\exp(2\sqrt{aE^*})},$$

where B_{fis} is the fission barrier height. The value of $C_f = 2\sqrt{a_{fis}(E^* - B_{fis})}$ and a, a_{fis} are the level density parameters of the compound and of the fission saddle point nuclei, respectively.

The value of the level density parameter is large at the saddle point, when excitation energy is given by initial excitation energy minus the fission barrier height, than in the ground state, i. e. $a_{fis} > a$. $a_{fis} = 1.08a$ for $Z < 85$, $a_{fis} = 1.04a$ for $Z \geq 89$ and $a_f = a[1.04 + 0.01(89. - Z)]$ for $85 \leq Z < 89$ is used.

The fission barrier

The fission barrier is determined as difference between the saddle-point and ground state masses.

We use simple semiphenomenological approach was suggested by Barashenkov and Gereghi [Barash73]. In their approach fission barrier $B_{fis}(A, Z)$ is approximated by

$$B_{fis} = B^0_{fis} + \Delta_g + \Delta_p.$$

The fission barrier height $B^0_{fis}(x)$ varies with the fissility parameter $x = Z^2/A$. $B^0_{fis}(x)$ is given by

$$B^0_{fis}(x) = 12.5 + 4.7(33.5 - x)^{0.75}$$

for $x \leq 33.5$ and

$$B^0_{fis}(x) = 12.5 - 2.7(x - 33.5)^{2/3}$$

for $x > 33.5$. The $\Delta_g = \Delta M(N) + \Delta M(Z)$, where $\Delta M(N)$ and $\Delta M(Z)$ are shell corrections for Cameron's liquid drop mass formula [Cameron_1957][Cameron_1958] and the pairing energy corrections: $\Delta_p = 1$ for odd-odd nuclei, $\Delta_p = 0$ for odd-even nuclei, $\Delta_p = 0.5$ for even-odd nuclei and $\Delta_p = -0.5$ for even-even nuclei.

Introduction

At the end of the pre-equilibrium stage, or a thermalizing process, the residual nucleus is supposed to be left in an equilibrium state, in which the excitation energy E^* is shared by a large number of nucleons. Such an equilibrated compound nucleus is characterized by its mass, charge and excitation energy with no further memory of the steps which led to its formation. If the excitation energy is higher than the separation energy, it can still eject nucleons and fragments (d, t, ^{3}He, α, others). These constitute the low energy and most abundant part of the emitted particles in the rest system of the residual nucleus. The emission of particles by an excited compound nucleus has been successfully described by comparing the nucleus with the evaporation of molecules from a fluid *[1]*. The first statistical theory of compound nuclear decay is due to Weisskopf and Ewing *[2]*.

Evaporation model

The Weisskopf treatment is an application of the detailed balance principle that relates the probabilities to go from a state i to another d and viceversa through the density of states in the two systems:

$$P_{i\to d}\rho(i) = P_{d\to i}\rho(d)$$

where $P_{d\to i}$ is the probability per unit of time of a nucleus d captures a particle j and form a compound nucleus i which is proportional to the compound nucleus cross section $\sigma_{\rm inv}$. Thus, the probability that a parent nucleus i with an excitation energy E^* emits a particle j in its ground state with kinetic energy ε is

$$P_j(\varepsilon)\mathrm{d}\varepsilon = g_j\sigma_{\rm inv}(\varepsilon)\frac{\rho_d(E_{\rm max} - \varepsilon)}{\rho_i(E^*)}\varepsilon\mathrm{d}\varepsilon$$

where $\rho_i(E^*)$ is the level density of the evaporating nucleus, $\rho_d(E_{\rm max} - \varepsilon)$ that of the daugther (residual) nucleus after emission of a fragment j and $E_{\rm max}$ is the maximum energy that can be carried by the ejectile. With the spin s_j and the mass m_j of the emitted particle, g_j is expressed as $g_j = (2s_j + 1)m_j/\pi^2\hbar^2$.

This formula must be implemented with a suitable form for the level density and inverse reaction cross section. We have followed, like many other implementations, the original work of Dostrovsky *et al.* [evap.Dostrovsky59] (which represents the first Monte Carlo code for the evaporation process) with slight modifications. The advantage of the Dostrovsky model is that it leds to a simple expression for equation [evap:2] that can be analytically integrated and used for Monte Carlo sampling.

Cross sections for inverse reactions

The cross section for inverse reaction is expressed by means of empirical equation [evap.Dostrovsky59]

$$\sigma_{\rm inv}(\varepsilon) = \sigma_g \alpha \left(1 + \frac{\beta}{\varepsilon}\right)$$

where $\sigma_g = \pi R^2$ is the geometric cross section.

In the case of neutrons, $\alpha = 0.76 + 2.2A^{-\frac{1}{3}}$ and $\beta = (2.12A^{-\frac{2}{3}} - 0.050)/\alpha$ MeV. This equation gives a good agreement to those calculated from continuum theory [evap.Blatt52] for intermediate nuclei down to $\varepsilon \sim 0.05$ MeV. For lower energies $\sigma_{{\rm inv},n}(\varepsilon)$ tends toward infinity, but this causes no difficulty because only the product $\sigma_{{\rm inv},n}(\varepsilon)\varepsilon$ enters in equation [evap:2]. It should be noted, that the inverse cross section needed in [evap:2] is that between a neutron of kinetic energy ε and a nucleus in an excited state.

For charged particles (p, d, t, ^{3}He and α), $\alpha = (1 + c_j)$ and $\beta = -V_j$, where c_j is a set of parameters calculated by Shapiro [evap.Shapiro53] in order to provide a good fit to the continuum theory [evap.Blatt52] cross sections and V_j is the Coulomb barrier.

Coulomb barriers

Coulomb repulsion, as calculated from elementary electrostatics are not directly applicable to the computation of reaction barriers but must be corrected in several ways. The first correction is for the quantum mechanical phenomenoon of barrier penetration. The proper quantum mechanical expressions for barrier penetration are far too complex to be used if one wishes to retain equation [evap:2] in an integrable form. This can be approximately taken into account by multiplying the electrostatic Coulomb barrier by a coefficient k_j designed to reproduce the barrier penetration approximately whose values are tabulated [evap.Shapiro53].

$$V_j = k_j \frac{Z_j Z_d e^2}{R_c}$$

The second correction is for the separation of the centers of the nuclei at contact, R_c. We have computed this separation as $R_c = R_j + R_d$ where $R_{j,d} = r_c A_{j,d}^{1/3}$ and r_c is given [evap.Iljinov94] by

$$r_c = 2.173 \frac{1 + 0.006103 Z_j Z_d}{1 + 0.009443 Z_j Z_d}$$

Level densities

The simplest and most widely used level density based on the Fermi gas model are those of Weisskopf [evap.Weisskopf37] for a completely degenerate Fermi gas. We use this approach with the corrections for nucleon pairing proposed by Hurwitz and Bethe [evap.Hurwitz51] which takes into account the displacements of the ground state:

$$\rho(E) = C \exp\left(2\sqrt{a(E-\delta)}\right)$$

where C is considered as constant and does not need to be specified since only ratios of level densities enter in equation [evap:2]. δ is the pairing energy correction of the daughter nucleus evaluated by Cook *et al.* [evap.Cook67] and Gilbert and Cameron [evap.Gilbert65] for those values not evaluated by Cook *et al.*. The level density parameter is calculated according to:

$$a(E, A, Z) = \tilde{a}(A)\left\{1 + \frac{\delta}{E}[1 - \exp(-\gamma E)]\right\}$$

and the parameters calculated by Iljinov *et al.* *[1]* and shell corrections of Truran, Cameron and Hilf [evap.Truran70].

Maximum energy available for evaporation

The maximum energy avilable for the evaporation process (*i.e.* the maximum kinetic energy of the outgoing fragment) is usually computed like $E^* - \delta - Q_j$ where is the separation energy of the fragment j: $Q_j = M_i - M_d - M_j$ and M_i, M_d and M_j are the nclear masses of the compound, residual and evporated nuclei respectively. However, that expression does not consider the recoil energy of the residual nucleus. In order to take into account the recoil energy we use the expression

$$\varepsilon_j^{\max} = \frac{(M_i + E^* - \delta)^2 + M_j^2 - M_d^2}{2(M_i + E^* - \delta)} - M_j$$

Total decay width

The total decay width for evaporation of a fragment j can be obtained by integrating equation [evap:2] over kinetic energy

$$\Gamma_j = \hbar \int_{V_j}^{\varepsilon_j^{\max}} P(\varepsilon_j) \mathrm{d}\varepsilon_j$$

This integration can be performed analiticaly if we use equation [evap:6] for level densities and equation [evap:3] for inverse reaction cross section. Thus, the total width is given by

$$\Gamma_j = \frac{g_j m_j R_d^2}{2\pi\hbar^2} \frac{\alpha}{a_d^2} \times \left(\left\{ \left(\beta a_d - \frac{3}{2} \right) + a_d(\varepsilon_j^{\max} - V_j) \right\} \exp\left\{ -\sqrt{a_i(E^* - \delta_i)} \right\} + \left\{ (2\beta a_d - 3)\sqrt{a_d(\varepsilon_j^{\max} - V_j)} + 2a_d(\varepsilon_j^{\max} - V_j) \right\} \times \exp\left\{ 2\left[\sqrt{a_d(\varepsilon_j^{\max} - V_j)} - \sqrt{a_i(E^* - \delta_i)} \right] \right\} \right)$$

where $a_d = a(A_d, Z_d, \varepsilon_j^{\max})$ and $a_i = a(A_i, Z_i, E^*)$.

GEM model

As an alternative model we have implemented the generalized evaporation model (GEM) by Furihata [evap.Furihata00]. This model considers emission of fragments heavier than α particles and uses a more accurate level density function for total decay width instead of the approximation used by Dostrovsky. We use the same set of parameters but for heavy ejectiles the parameters determined by Matsuse *et al.* [evap.Matsuse82] are used.

Based on the Fermi gas model, the level density function is expressed as

$$\rho(E) = \begin{cases} \frac{\sqrt{\pi}}{12} \frac{e^{2\sqrt{a(E-\delta)}}}{a^{1/4}(E-\delta)^{5/4}} & \text{for} \quad \mathrm{E} \geq \mathrm{E_x} \\ \frac{1}{T} e^{(E-E_0)/T} & \text{for} \quad \mathrm{E} < \mathrm{E_x} \end{cases}$$

where $E_x = U_x + \delta$ and $U_x = 150/M_d + 2.5$ (M_d is the mass of the daughter nucleus). Nuclear temperature T is given as $1/T = \sqrt{a/U_x} - 1.5U_x$, and E_0 is defined as $E_0 = E_x - T(\log T - \log a/4 - (5/4)\log U_x + 2\sqrt{aU_x})$.

By substituting equation [evap:11] into equation [evap:2] and integrating over kinetic energy can be obtained the following expression

$$\Gamma_j = \frac{\sqrt{\pi} g_j \pi R_d^2 \alpha}{12\rho(E^*)} \times \begin{cases} \{I_1(t,t) + (\beta + V) I_0(t)\} & \text{for} \quad \varepsilon_{\mathrm{j}}^{\max} - \mathrm{V_j} < \mathrm{E_x} \\ \{I_1(t,t_x) + I_3(s,s_x)e^s + \\ (\beta + V)(I_0(t_x) + I_2(s,s_x)e^s)\} & \text{for} \quad \varepsilon_{\mathrm{j}}^{\max} - \mathrm{V_j} \geq \mathrm{E_x}. \end{cases}$$

$I_0(t)$, $I_1(t, t_x)$, $I_2(s, s_x)$, and $I_3(s, s_x)$ are expressed as:

$$
\begin{aligned}
I_0(t) = & \quad e^{-E_0/T}(e^t - 1) \\
I_1(t, t_x) = & \quad e^{-E_0/T} T\{(t - t_x + 1)e^{t_x} - t - 1\} \\
I_2(s, s_x) = & \quad 2\sqrt{2}\Big\{ s^{-3/2} + 1.5s^{-5/2} + 3.75s^{-7/2} - \\
& \quad (s_x^{-3/2} + 1.5s_x^{-5/2} + 3.75s_x^{-7/2}) \Big\} \\
I_3(s, s_x) = & \quad \frac{1}{2\sqrt{2}} \Bigg[2s^{-1/2} + 4s^{-3/2} + 13.5s^{-5/2} + 60.0s^{-7/2} + \\
& \quad 325.125s^{-9/2} - \Big\{ (s^2 - s_x^2)s_x^{-3/2} + (1.5s^2 + 0.5s_x^2)s_x^{-5/2} + \\
& \quad (3.75s^2 + 0.25s_x^2)s_x^{-7/2} + (12.875s^2 + 0.625s_x^2)s_x^{-9/2} + \\
& \quad (59.0625s^2 + 0.9375s_x^2)s_x^{-11/2} + \\
& \quad (324.8s^2 + 3.28s_x^2)s_x^{-13/2} + \Big\} \Bigg]
\end{aligned}
$$

where $t = (\varepsilon_j^{\max} - V_j)/T$, $t_x = E_x/T$, $s = 2\sqrt{a(\varepsilon_j^{\max} - V_j - \delta_j)}$ and $s_x = 2\sqrt{a(E_x - \delta)}$.

Besides light fragments, 60 nuclides up to ^{28}Mg are considered, not only in their ground states but also in their exited states, are considered. The excited state is assumed to survive if its lifetime $T_{1/2}$ is longer than the decay time, *i. e.*, $T_{1/2}/\ln 2 > \hbar/\Gamma_j^*$, where Γ_j^* is the emission width of the resonance calculated in the same manner as for ground state particle emission. The total emission width of an ejectile j is summed over its ground state and all its excited states which satisfy the above condition.

Simulation of fragment evaporation.

The evaporation of neutron, proton, deutron, thritium and alpha fragments are taken into account.

Evaporation threshold.

One should take into account the energy condition for fragment emission, i. e. the nucleus excitation energy should be higher than the reaction threshold:

$$T_b^{\max} = E^* - Q_b - V_b > 0.$$

Here $T_b^{\max}$ is the maximal kinetic energy carried by emitted fragment b, $Q_b = M(A, Z) - M(A_f, Z_f) - M_b$ is the fragment b binding energy. V_b is the Coulomb potential energy, i. e. the Coulomb barrier for fragment b. $M(A, Z)$ is the mass of the initial nucleus, $M(A_f, Z_f)$ is the mass of the nucleus after emission of fragment b and M_b is the fragment b mass. It should be noted that expression (7.8.5) is only valid, when the recoil kinetic energy equals zero. In our code we apply the condition:

$$T_b^{\max} = E_b^{\max} - M_b - V_b > 0,$$

where

$$E_b^{\max} = \frac{(M(A, Z) + E^*)^2 + M_b^2 - M^2(A_f, Z_f)}{2(M(A, Z) + E^*)}.$$

Coulomb barrier calculation.

The Coulomb barrier:

$$V_b = C_b \frac{Z_b Z_f}{R_f + R_b},$$

where $C_b = 1.44$ MeVfm, Z_b and R_b are charge and radius of nucleus after fragment emission, Z_f and R_f are charge and radius of fragment. The radii of nuclei are approximated by $R = r_C A^{1/3}$, where [IKP94]

$$r_C = 2.173 \frac{1 + 0.006103 Z_b Z_f}{1 + 0.009443 Z_b Z_f}\ fm.$$

The fragment evaporation probability.

Evaporation process has been predicted by the statistical Weisskopf-Ewing model [WE40.evap]. Probability to evaporate particle b in the energy interval $(T_b, T_b + dT_b)$ per unit of time is given

$$W_b(T_b) = \sigma_b(T_b) \frac{(2s_b + 1)m_b}{\pi^2 h^3} \frac{\rho(E^* - Q_b - T_b)}{\rho(E^*)} T_b,$$

where $\sigma_b(T_b)$ is the inverse (absorption of particle b) reaction cross section, s_b and m_b are particle spin and mass, ρ is level densities of nucleus.

The inverse reaction cross section.

To calculate inverse reaction cross section it is assumed to have the form [Dostr59]

$$\sigma_b(T_b) = (1 + C_b)(1 - k_b V_b / T_b)\pi R^2$$

for charged charged fragments with $A_f \leq 4$ interaction, where the k_b is the barrier penetration coefficient (its tabulated values are used), and

$$\sigma_b(T_b) = \alpha(1 + \beta / T_b)\pi R^2$$

for neutrons. Here $R = r_0 A^{1/3}$ denotes the absorption radius, where $r_0 = 1.5$ fm, $\alpha = 0.76 + 2.2A^{-1/3}$ and $\beta = (2.12A^{-2/3} - 0.05)/(0.76 + 2.2A^{-1/3})$.

The level density.

The level density is approximated by Fermi-gas approach [IKP94] for the nuclear level density:

$$\rho(E^*) = C \exp(2\sqrt{aE^*}),$$

where C is a constant, which does not depend from nucleus properties and excitation energy E^* and a is the level density parameter.

The total evaporation probability.

The total probability W_b or total partial width $\Gamma_b = \hbar W_b$ to evaporate particle b can be obtained from Eq. (7.8.5) by integration over T_b:

$$W_b = \int_{V_b}^{E^* - Q_b} W_b(T_b) dT_b.$$

Here the summation is carried out over all excited states of the fragment.

Integration in Eq. (7.8.5) for probability to emit fragment b can be performed analiticaly, if we will use Eq. (7.8.5) for level density and the Eqs. (7.8.5)-(7.8.5) for inverse cross section. The probability to emit a charged particle:

$$W_b = \gamma_b A_b^{2/3} B \exp[-2\sqrt{aE^*}] \frac{(1+C_b)}{a_b^2} \{a_b T_b^{\max} [2\exp(2\sqrt{a_b T_b^{\max}}) + 1] - \\ -3\sqrt{a_b T_b^{\max}} \exp(2\sqrt{a_b T_b^{\max}}) - 3[1 - \exp(2\sqrt{a_b T_b^{\max}})]/2\},$$

where T_b^{max} is defined by the equation (7.8.5). The following notations were introduced: $A_b = A - \Delta A_b$, $B = m_N r_0^2/(2\pi h^2)$, $\gamma_b = (2s_b + 1)m_b/m_N$. ΔA_b is the number of nucleons in b particle. m_b, m_N and s_b are mass of particle b, mass of nucleon and spin of particle b respectively. The a_b is level density parameter for nucleus after emission of fragment b. Similarly for the neutron evaporation probability we obtain the following equation:

$$W_n = \gamma_n A_n^{2/3} B \frac{\alpha}{2a_n^2} \\ \exp[-2\sqrt{aE^*} + 2\sqrt{a_n T_n^{\max}}][4a_n T_n^{\max} + (2a_n\beta - 3)(2\exp(2\sqrt{a_n T_n^{\max}} - 1)].$$

Using probabilities Eq. (7.8.5) and Eq. (7.8.5) we are able to choose randomly the type of emitted fragment.

Kinetic energy of emitted fragment.

The equation (7.8.5) can be used to sample kinetic energies of evaporated fragments. For example, keeping terms in Eq. (7.8.5), which depend from T_b and using the approximations for inverse cross section is given by Eq. (7.8.5) and for level densities are given by Eq. (7.8.5), we obtain for charged fragments

$$W(x) = C_1 x \exp(2\sqrt{a(T_b^{\max} - x)} = C_2 T_b \exp(2\sqrt{aE^*}),$$

where C_1 and C_2 do not depend from T_b, $x = T_b - V_b$. To generate values of x we can use the next procedure, changing the expression for $W(x)$ to have $W(x^{\max}) = 1$ ($x^{\max} = [(a_b + T_b^{\max} + 1/4)^{1/2} - 1/2]/a_b$). Choose two random numbers ξ_1 and ξ_2 (distributed with equal probabilities between 0 and 1) and find kinetic energy of particle b as $T_b = T_b^{\max}\xi_1 + V_b$ at condition $\xi_2 \leq W(\xi_1 T_b^{\max})$. If this condition is not fulfilled we should choose another pair of random numbers.

Angular distribution of evaporated fragments.

We consider the angular distribution for emitted fragments as isotropical since we have no information about spin and polarization of nuclei.

Parameters of residual nucleus.

After fragment emission we update parameter of decaying nucleus:

$$A_f = A - A_b; Z_f = Z - Z_b; P_f = P_0 - p_b; \\ E_f^* = \sqrt{E_f^2 - \vec{P}_f^2} - M(A_f, Z_f).$$

Here p_b is the evaporated fragment four momentum.

Photon evaporation

Photon evaporation main be simulated as a continium gamma transition using dipole approximation and via discrete gamma transition using evaluated database on nuclear gamma transitions.

Computation of probability

As the first approximation we assume that dipole $E1$–transitions is the main source of γ–quanta from highly–excited nuclei *[1]*. The probability to evaporate γ in the energy interval $(\epsilon_\gamma, \epsilon_\gamma + d\epsilon_\gamma)$ per unit of time is given

$$W_\gamma(\epsilon_\gamma) = \frac{1}{\pi^2(\hbar c)^3}\sigma_\gamma(\epsilon_\gamma)\frac{\rho(E^* - \epsilon_\gamma)}{\rho(E^*)}\epsilon_\gamma^2,$$

where $\sigma_\gamma(\epsilon_\gamma)$ is the inverse (absorption of γ) reaction cross section, ρ is a nucleus level density is defined by Eq. (7.8.5).

The photoabsorption reaction cross section is given by the expression

$$\sigma_\gamma(\epsilon_\gamma) = \frac{\sigma_0\epsilon_\gamma^2\Gamma_R^2}{(\epsilon_\gamma^2 - E_{GDP}^2)^2 + \Gamma_R^2\epsilon_\gamma^2},$$

where $\sigma_0 = 2.5A$ mb, $\Gamma_R = 0.3E_{GDP}$ and $E_{GDP} = 40.3A^{-1/5}$ MeV are empirical parameters of the giant dipole resonance *[1]*. The total radiation probability is

$$W_\gamma = \frac{1}{\pi^2(\hbar c)^3}\int_0^{E^*}\sigma_\gamma(\epsilon_\gamma)\frac{\rho(E^* - \epsilon_\gamma)}{\rho(E^*)}\epsilon_\gamma^2 d\epsilon_\gamma.$$

The integration is performed numericaly. The energy of γ-quantum is sampled according to the Eq. (7.8.5) distribution.

Discrete photon evaporation

The last step of evaporation cascade consists of evaporation of photons with discrete energies. The competition between photons and fragments as well as giant resonance photons is neglected at this step. We consider the discrete E1, M1 and E2 photon transitions from tabulated isotopes. There are large number of isotopes *[2]* with the experimentally measured exited level energies, spins, parities and relative transitions probabilities. This information is uploaded for each excited state in run time when corresponding excited state first created.

The list of isotopes included in the photon evaporation data base has been extended from $A <= 240$ to $A <= 250$. The highest atomic number included is $Z = 98$ (this ensures that Americium sources can now be simulated).

Internal conversion electron emission

An important conpetitive channel to photon emission is internal conversion. To take this into account, the photon evaporation data-base was entended to include internal conversion coeffficients.

The above constitute the first six columns of data in the photon evaporation files. The new version of the data base adds eleven new columns corresponding to:

- 7. ratio of internal conversion to gamma-ray emmission probability
- **(8–17) internal conversion coefficients for shells K, L1, L2, L3, M1,** M2, M3, M4, M5 and N+ respectively. These coefficients are normalised to 1.0

The calculation of the Internal Conversion Coefficients (ICCs) is done by a cubic spline interpolation of tabulalted data for the corresponding transition energy. These ICC tables, which we shall label Band [spe.band], Rösel [spe.rosel] and Hager-Seltzer [spe.hagsel], are widely used and were provided in electronic format by staff at LBNL. The reliability of these tabulated data has been reviewed in Ref. [spe.rys]. From tests carried out on these data we find that the ICCs calculated from all three tables are comparable within a 10% uncertainty, which is better than what experimetal measurements are reported to be able to achive.

The range in atomic number covered by these tables is Band: $1 <= Z <= 80$; Rösel: $30 <= Z <= 104$ and Hager-Seltzer: $3, 6, 10, 14 <= Z <= 103$. For simplicity and taking into account the completeness of the tables, we have used the Band table for $Z <= 80$ and Rösel for $81 <= Z <= 98$.

The Band table provides a higher resolution of the ICC curves used in the interpolation and covers ten multipolarities for all elements up to $Z = 80$, but it only includes ICCs for shells up to M5. In order to calculate the ICC of the N+ shell, the ICCs of all available M shells are added together and the total divided by 3. This is the scheme adopted in the LBNL ICC calculation code when using the Band table. The Rösel table includes ICCs for all shells in every atom and for $Z > 80$ the N+ shell ICC is calculated by adding together the ICCs of all shells above M5. In this table only eight multipolarities have ICCs calculated for.

For the production of an internal conversion electron, the energy of the transition must be at least the binding energy of the shell the electron is being released from. The binding energy corresponding to the various shells in all isotopes used in the ICC calculation has been taken from the Geant4 file G4AtomicShells.hh.

The ENSDF data provides information on the multipolarity of the transition. The ICCs included in the photon evaporation data base refer to the multipolarity indicated in the ENSDF file for that transition. Only one type of mixed mulltipolarity is considered (M1+E2) and whenever the mixing ratio is provided in the ENSDF file, it is used to calculate the ICCs corresponding to the mixed multipolarity according to the formula:

- fraction in $M1 = 1/(1 + \delta^2)$
- fraction in $E2 = \delta^2/(1 + \delta^2)$

where δ is the mixing ratio.

7.8.6 Fermi Breakup

Fermi break-up simulation for light nuclei

For light nuclei the values of excitation energy per nucleon are often comparable with nucleon binding energy. Thus a light excited nucleus breaks into two or more fragments with branching given by available phase space. To describe a process of nuclear disassembling the so-called Fermi break-up model is formulated [Fermi50], [Kretz61], [EG67], [Bond95]. This statistical approach was first used by Fermi [Fermi50] to describe the multiple production in high energy nucleon collision. The GEANT4 Fermi break-up model is capable to predict final states as result of an excited nucleus with $Z < 9$ and $A < 17$ statistical break-up.

Allowed channels

The channel will be allowed for decay, if the total kinetic energy E_{kin} of all fragments of the given channel at the moment of break-up is positive. This energy can be calculated according to equation:

$$E_{kin} = U + M(A, Z) - E_{Coulomb} - \sum_{b=1}^{n}(m_b + \epsilon_b),$$

U is primary fragment excitation, m_b and ϵ_b are masses and excitation energies of fragments, respectively, $E_{Coulomb}$ is the Coulomb barrier for a given channel. It is approximated by

$$E_{Coulomb} = \frac{3}{5}\frac{e^2}{r_0}(1 + \frac{V}{V_0})^{-1/3}(\frac{Z^2}{A^{1/3}} - \sum_{b=1}^{n}\frac{Z^2}{A_b^{1/3}}),$$

where V_0 is the volume of the system corresponding to the normal nuclear matter density

$$V_0 = 4\pi R^3/3 = 4\pi r_0^3 A/3,$$

where $r_0 = 1.3fm$ is used. Free parameter of the model is the ratio of the effective volume V to the normal volume, currently

$$\kappa = \frac{V}{V_0} = 6.$$

Break-up probability

The total probability for nucleus to break-up into n componets (nucleons, deutrons, tritons, alphas etc) in the final state is given by

$$W(E,n) = (V/\Omega)^{n-1}\rho_n(E),$$

where $\rho_n(E)$ is the density of a number of final states, $\Omega = (2\pi\hbar)^3$ is the normalization volume. The density $\rho_n(E)$ can be defined as a product of three factors:

$$\rho_n(E) = M_n(E)S_nG_n.$$

The first one is the phase space factor defined as

$$M_n = \int_{-\infty}^{+\infty} ... \int_{-\infty}^{+\infty} \delta(\sum_{b=1}^{n} \mathbf{p_b})\delta(E - \sum_{b=1}^{n} \sqrt{p^2 + m_b^2}) \prod_{b=1}^{n} d^3p_b,$$

where $\mathbf{p_b}$ is fragment b momentum. The second one is the spin factor

$$S_n = \prod_{b=1}^{n}(2s_b + 1),$$

which gives the number of states with different spin orientations. The last one is the permutation factor

$$G_n = \prod_{j=1}^{k} \frac{1}{n_j!},$$

which takes into account identity of components in final state. n_j is a number of components of j- type particles and k is defined by $n = \sum_{j=1}^{k} n_j$).

In non-relativistic case (Eq. (7.8.6) the integration in Eq. (7.8.6) can be evaluated analiticaly (see e. g. [BBB58]). The probability for a nucleus with energy E disassembling into n fragments with masses m_b, where $b = 1, 2, 3, ..., n$ equals

$$W(E_{kin},n) = S_nG_n(\frac{V}{\Omega})^{n-1}(\frac{1}{\sum_{b=1}^{n} m_b} \prod_{b=1}^{n} m_b)^{3/2} \frac{(2\pi)^{3(n-1)/2}}{\Gamma(3(n-1)/2)} E_{kin}^{3n/2-5/2},$$

where $\Gamma(x)$ is the gamma function.

Fragment characteristics

We take into account the formation of fragments in their ground and low-lying excited states, which are stable for nucleon emission. However, several unstable fragments with large lifetimes: ^5He, ^5Li, ^8Be, ^9B etc are also considered. Fragment characteristics A_b, Z_b, s_b and ϵ_b are taken from [AS81]. Recently nuclear level energies were changed to be identical with nuclear levels in the gamma evaporation database (see Chapter [PHOTOEVAP]).

Sampling procedure

The nucleus break-up is described by the Monte Carlo (MC) procedure. We randomly (according to probability Eq. (7.8.6) and condition Eq. (7.8.6)) select decay channel. Then for given channel we calculate kinematical quantities of each fragment according to n-body phase space distribution:

$$M_n = \int_{-\infty}^{+\infty} ... \int_{-\infty}^{+\infty} \delta(\sum_{b=1}^{n} \mathbf{p_b}) \delta(\sum_{b=1}^{n} \frac{p_b^2}{2m_b} - E_{kin}) \prod_{b=1}^{n} d^3 p_b.$$

The Kopylov's sampling procedure [Kopylov70] is applied. The angular distributions for emitted fragments are considered to be isotropical.

Fermi break-up model.

7.8.7 Fermi Breakup

7.8.8 Gamma Interaction

MC procedure.

At intermediate energies γ-nucleon and γ-nucleus interactions are performed within the hadron kinetic model similarly as the hadron-nucleon and hadron-nucleus interactions.

At high energies the Monte Carlo procedure in the case of γ–nucleon collision can be outlined as follows:

- At given c.m. energy squared and at given virtuality Q^2 sample mass M^2 of hadronic $q\bar{q}$ fluctuation according to (7.8.8) and sample its flavor according to statistical weights: $\omega_{u\bar{u}} = 1/2$, $\omega_{d\bar{d}} = 1/4$ and $\omega_{s\bar{s}} = 1/4$ are derived from (7.8.8);
- Sample the momentum fraction x of a valence quark inside a hadronic fluctuation according to

  $$\rho(x) \sim \frac{1}{\sqrt{x(1-x)}}$$

  and transverse momentum of a quark according to the Gaussian distribution as for hadrons;
- Split nucleon into quark and diquark as it was described for hadron-nucleon interaction;
- Create two strings spanned between quark from a hadronic fluctuation and diquark from nucleon and between antiquark from a hadronic fluctuation and quark from nucleon;
- Decay string into hadrons as it was described for hadron-nucleon interactions.

In the case of γ–nucleus collision the MC procedure is follows:

- At given c.m. energy squared and at given virtuality Q^2 sample mass M^2 of hadronic $q\bar{q}$ fluctuation and sample its flavor as it is done for γ–nucleon collision;
- Calculate coherence length d;
- If coherence length less than internucleon distance then simulate inelastic hadron fluctuation-nucleon collision at choosen impact parameter B as was described above;
- If coherence length more than internucleon distance then perform simulation of hadron fluctuation-nucleus collision at choosen impact parameter B using parton string model similarly as for meson-nucleus interactions. For this case the probability of inelastic collision of a hadron fluctuation with nucleon i at given impact parameter $\mathbf{b}_i$ is calculated according to

  $$p_{VN}(s, b^2) = 1 - exp[-2u(s, b^2)];$$

  with the eikonal $u(s, b^2)$ defined by Eq. (7.8.8) at $Q^2 = 0$ and $M^2 = M_\rho$.

Hadronic interaction of photons.

The high energy γ-nucleon and γ-nucleus interactions.

To simulate high energy photon interactions with nucleon and nucleus we use the approach:cite:*PRW95*. We consider the following kinematic variables for γ-nucleon scattering: the Bjorken-x variable defined as $x = Q^2/2m\nu$ with Q^2, ν and m the photon virtuality, the photon energy and nucleon mass, respectively. The the squared total energy of the γ-nucleon system is given by $s = Q^2(1-x)/x + m^2$. We restrict consideration to the range of small x-values and Q^2 is much less than s.

The Generalized Vector Dominance Model (GVDM) [BSY78] assumes that the virtual photon fluctuates into intermediate $q\bar{q}$-states V of mass M which subsequently may interact with a nucleon N. Thus the total photon-nucleon cross section can be expressed by a relation [PRW95]:

$$\sigma_{\gamma N}(s,Q^2) = 4\pi\alpha_{em}\int_{M_0^2}^{M_1^2} dM^2 D(M^2)\times$$
$$\times(\tfrac{M^2}{M^2+Q^2})^2(1+\epsilon\tfrac{Q^2}{M^2})\sigma_{VN}(s,Q^2),$$

where integration over M^2 should be performed between $M_0^2 = 4m_\pi^2$ and $M^2 = s$. Here $\alpha_{em} = e^2/4\pi = 1/137$ and the density of $q\bar{q}$-system per unit mass-squared is given by

$$D(M^2) = \frac{R_{e^+e^-}(M^2)}{12\pi^2 M^2},$$

$$R_{e^+e^-}(M^2) = \frac{\sigma_{e^+e^-\to hadrons}(M^2)}{\sigma_{e^+e^-\to\mu^+\mu^-}(M^2)} \approx 3\Sigma_f e_f^2,$$

where e_f^2 the squared charge of quark with flavor f. ϵ is the ratio between the fluxes of longitudinally and transversally polarized photons.

Similarly the inelastic cross section for the scattering of a γ with virtuality Q^2 and with a nucleus A at impact parameter B and the γ-nucleon c.m. energy squared s is given by [ERR97]:

$$\sigma_{\gamma A}(s,Q^2,B) = 4\pi\alpha_{em}\int_{M_0^2}^{M_1^2} dM^2 D(M^2)\times$$
$$\times(\tfrac{M^2}{M^2+Q^2})^2(1+\epsilon\tfrac{Q^2}{M^2})\sigma_{VA}(s,Q^2,B),$$

To calculate γ-nucleon or γ-nucleus inelastic cross sections we need model for the M^2-, Q^2- and s-dependence of the σ_{VN} or σ_{VA}. For these we apply the Gribov-Regge approach, similarly as it was done for h-nucleon or h-nucleus inelastic cross sections.

The effective cross section for the interaction of a $q\bar{q}$-system with squared mass M^2 with nucleus for the coherence length

$$d = \frac{2\nu}{M^2+Q^2}$$

exceeding the average distance between two nucleons can be written as follows

$$\sigma_{VA}(s,Q^2,B) = \int\prod_{i=1}^{A} d^3r_i\rho_A(\mathbf{r}_i)\times$$
$$\times(1-|\prod_{i=1}^{A}[1-u(s,Q^2,M^2,b_i^2)]|^2).$$

Here the amplitude (eikonal) $u(s,Q^2,M^2,b_i^2)$ for the interaction of the hadronic fluctuation with i-th nucleon is given by [ERR97]

$$u(s,Q^2,M^2,\mathbf{b}_i) = \tfrac{\sigma_{VN}(s,Q^2,M^2)}{8\pi\lambda(s,Q^2,M^2)}\times$$
$$\times(1-i\rho\exp[-\tfrac{b^2}{4\lambda(s,Q^2,M^2)}],$$

where $\rho \approx 0$ is the ratio of real and imaginary parts of scattering amplitude at 0 angle. The amplitude parameters: the effective $q\bar{q}$-nucleon cross section

$$\sigma_{VN}(s, Q^2, M^2) = \frac{\tilde{\sigma}_{VN}(s, Q^2)}{M^2 + Q^2 + C^2},$$

where $C^2 = 2$ GeV:math:*(^2)*, and

$$\lambda(s, Q^2, M^2) = 2 + \frac{m_\rho^2}{M^2 + Q^2} + \alpha'_P \ln\left(\frac{s}{M^2 + Q^2}\right).$$

The values of $\tilde{\sigma}_{VN}(s, Q^2)$ are calculated in paper [ERR97]. It was shown [ERR97] that Q^2 dependence of $\sigma_{VN}(s, Q^2)$ is very week at $Q^2 < m_{rho}^2 + C^2$, where m_ρ is ρ-meson mass, and we omitted this dependence. We also use $\sigma_{VN}(s, Q^2)$ calculated in [ERR97] at $M^2 = m_{rho}^2$.

If coherence length is smaller that an internuclear distance integrated over B then cross section $\sigma_{VA} = A\sigma_{VN}$.

Reaction initial state.

The GEANT4 γ-nucleon and γ-nucleus interaction model is capable to predict final states (produced hadrons which belong to the pseudoscalar meson nonet and the baryon (antibaryon) octet) of reactions on nucleon and nuclear targets. The break-up simulation of the residual excited target nucleus is performed with help of the nucleus deexcitation models. The recommended bombarding energy in the photon–nucleon or photon–nucleus interaction has to be more than 20 MeV in the laboratory frame.

7.8.9 Incl

INCL++: the Liège Intranuclear Cascade model

Introduction

There is a renewed interest in the study of spallation reactions. This is largely due to new technological applications, such as Accelerator-Driven Systems, consisting of sub-critical nuclear reactor coupled to a particle accelerator. These applications require optimized targets as spallation sources. This type of problem typically involves a large number of parameters and thus it cannot be solved by trial and error. One has to rely on simulations, which implies that very accurate tools need to be developed and their validity and accuracy need to be assessed.

Above ∼200 MeV incident energy it is necessary to use reliable models due to the prohibitive number of open channels. The most appropriate modeling technique in this energy region is intranuclear cascade (INC) combined with evaporation model. One such pair of models is the Liège cascade model `INCL++`*[1][2]* coupled with the `G4ExcitationHandler` statistical de-excitation model. The strategy adopted by the `INCL++` cascade is to improve the quasi-classical treatment of physics without relying on too many free parameters.

This chapter introduces the physics provided by `INCL++` as implemented in Geant4. Table [tbl:inclsummary] summarizes the key features and provides references to detailed descriptions of the physics.

The `INCL++` model is available through dedicated physics lists (see Table [tbl:inclsummary]). The `_HP` variants of the physics lists use the `NeutronHP` model (Chapter [cha:low-energy-neutron]) for neutron interactions at low energy; the `QGSP_` and `FTFP_` variants respectively use the `QGSP` and `FTFP` model at high energy. Figure [fig:inclxx_hadmodmap] shows a schematic model map of the `INCL++`-based physics lists.

Finally, the `INCL++` model is directly accessible through its interface (`G4INCLXXInterface`).

The reference paper for the `INCL++` model is Ref. *[2]*. Please make sure you cite it appropriately if you publish any work based on this model.

Table: `INCL++` feature summary.

Suitable application fields

The INCL++-dedicated physics lists are suitable for the simulation of any system where spallation reactions or light-ion-induced reactions play a dominant role. As examples, we include here a non-exhaustive list of possible application fields:

- Accelerator-Driven Systems (ADS);
- spallation targets;
- radioprotection close to high-energy accelerators;
- radioprotection in space;
- proton or carbon therapy;
- production of beams of exotic nuclei.

Generalities of the INCL++ cascade

INCL++ is a Monte-Carlo simulation incorporating the aforementioned cascade physics principles. The INCL++ algorithm consists of an initialization stage and the actual data processing stage.

The INCL++ cascade can be used to simulate the collisions between bullet particles and nuclei. The supported bullet particles and the interface classes supporting them are presented in table [tbl:inclsummary].

The momenta and positions of the nucleons inside the nuclei are determined at the beginning of the simulation run by modeling the nucleus as a free Fermi gas in a static potential well with a realistic density. The cascade is modeled by tracking the nucleons and their collisions.

The possible reactions inside the nucleus are

- $NN \rightarrow NN$ (elastic scattering)
- $NN \rightarrow N\Delta$ and $N\Delta \rightarrow NN$
- $\Delta \rightarrow \pi N$ and $\pi N \rightarrow \Delta$
- $NN \rightarrow NN\,x\pi$ (multiple pion production)
- $\pi N \rightarrow \pi N$ (elastic scattering and charge exchange)
- $\pi N \rightarrow N\,(x+1)\pi$ (multiple pion production)
- $NN \rightarrow NNM$ ($M = \eta$ or ω)
- $NN \rightarrow NNM\,x\pi$ (inclusive production, $M = \eta$ or ω)
- $\pi N \rightarrow MN$ ($M = \eta$ or ω)
- $MN \rightarrow \pi N, \pi\pi N$ ($M = \eta$ or ω)
- $MN \rightarrow MN$ ($M = \eta$ or ω; elastic scattering)

Model limits

The INCL++ model has certain limitations with respect to the bullet particle energy and type, and target-nucleus type. The supported energy range for incident nucleons and pions is 1 MeV–20 GeV. Any target nucleus from deuterium (^{2}H) up is in principle acceptable, but not all areas of the nuclide chart have received equal attention during testing. Heavy nuclei (say above Fe) close to the stability valley have been more thoroughly studied than light or unstable nuclei. The model is anyway expected to accept any existing nucleus as a target.

Light nuclei (from $A = 2$ to $A = 18$ included) can also be used as projectiles. The `G4INCLXXInterface` class can be used for collisions between nuclei of any mass, but it will internally rely on the Binary Cascade model (see chapter [BinaryCascade]) if both reaction partners have $A > 18$. A warning message will be displayed (once) if this happens.

Physics ingredients

The philosophy of the `INCL++` model is to minimize the number of free parameters, which guarantees the predictive power of the model. All `INCL++`parameters are either taken from known phenomenology (e.g. nuclear radii, elementary cross sections, nucleon potentials) or fixed once and for all (stopping time, cluster-coalescence parameters).

The nucleons are modeled as a free Fermi gas in a static potential well. The radius of the well depends on the nucleon momentum, the r-p correlation being determined by the desired spatial density distribution $\rho_r(r)$ according to the following equation:

$$\rho_p(p)p^2dp = -\frac{d\rho_r(r)}{dr}\frac{r^3}{3}dr,$$

where $\rho_p(p)$ is the momentum-space density (a hard-sphere of radius equal to the Fermi momentum).

After the initialization a projectile particle, or bullet, is shot towards the target nucleus. In the following we assume that the projectile is a nucleon or a pion; the special case of composite projectiles will be described in more detail in subsection [sec:inclxx_composite_projectiles].

The impact parameter, i.e. the distance between the projectile particle and the center point of the projected nucleus surface is chosen at random. The value of the impact parameter determines the point where the bullet particle will enter the calculation volume. After this the algorithm tracks the nucleons by determining the times at which an event will happen. The possible events are:

- collision
- decay of a delta resonance
- reflection from the nuclear potential well
- transmission through the nuclear potential well

The particles are assumed to propagate along straight-line trajectories. The algorithm calculates the time at which events will happen and propagates the particles directly to their positions at that particular point in time. This means that the length of the time step in simulation is not constant, and that we do not need to perform expensive numerical integration of the particle trajectories.

Particles in the model are labeled either as *participants* (projectile particles and particles that have undergone a collision with a projectile) or *spectators* (target particles that have not undergone any collision). Collisions between spectator particles are neglected.

Emission of composite particles

`INCL++` is able to simulate the emission of composite particles (up to $A = 8$) during the cascade stage. Clusters are formed by coalescence of nucleons; when a nucleon (the *leading* particle) reaches the surface and is about to leave the system, the coalescence algorithm looks for other nucleons that are "sufficiently close" in phase space; if any are found, a candidate cluster is formed. If several clusters are formed, the algorithm selects the least excited one. Penetration of the Coulomb barrier is tested for the candidate cluster, which is emitted if the test is successful; otherwise, normal transmission of the leading nucleon is attempted.

There are at least two peculiarities of `INCL++`'s cluster-coalescence algorithm. First, it acts in *phase space*, while many existing algorithms act in momentum space only. Second, it is *dynamical*, in the sense that it acts on the instantaneous phase-space distribution of nucleons in the system, and not on the distribution of the escaping nucleons.

Cascade stopping time

Stopping time is defined as the point in time when the cascade phase is finished and the excited remnant is passed to evaporation model. In the INCL++ model the stopping time, t_{stop}, is defined as:

$$t_{\text{stop}} = t_0(A_{\text{target}}/208)^{0.16}.$$

Here A_{target} is the target mass number and $t_0 = 70$ fm/c. The intranuclear cascade also stops if no participants are left in the nucleus.

Conservation laws

The INCL++ model generally guarantees energy and momentum conservation at the keV level, which is compatible with the numerical accuracy of the code. It uses G4ParticleTable and G4IonTable for the masses of particles and ions, which means that the energy balance is guaranteed to be consistent with radiation transport. However, INCL++ can occasionally generate an event such that conservation laws cannot be exactly fulfilled; these corner cases typically happen for very light targets.

Baryon number and charge are always conserved.

Initialisation of composite projectiles

In the case of composite projectiles, the projectile nucleons are initialised off their mass shell, to account for their binding in the projectile. The sum of the four-momenta of the projectile nucleons is equal to the nominal four-momentum of the projectile nucleus.

Given a random impact parameter, projectile nucleons are separated in geometrical spectators (those that do not enter the calculation volume) and geometrical participants (those that do). Geometrical participant that traverse the nucleus without undergoing any collision are coalesced with any existing geometrical spectators to form an excited projectile-like pre-fragment. The excitation energy of the pre-fragment is generated by a simple particle-hole model. At the end of the cascade stage, the projectile-like pre-fragment is handed over to G4ExcitationHandler.

η and ω mesons as new particles

The mesons η and ω can be produced and emitted during the intranuclear cascade phase. The cross sections taken into account are listed in section [sec:inclmodel]. By default in Geant4 the η meson emitted is not decayed by INCL++, while that is the case for the ω meson (then only the decay products (π and γ) are given to Geant4).

De-excitation phase

The INCL++ model simulates only the first part of the nuclear reaction; the de-excitation of the cascade remnant is simulated by default by G4ExcitationHandler. As an alternative, the ABLA V3 model (Chapter [cha:abla-v3-evap]) can be used instead, by employing the technique described in the Application Developer Guide, section "hadronic interactions".

Physics performance

|Left: double-differential cross sections for the production of charged pions in 730-MeV :math:‘\(p\)‘\ +Cu. Right: double-differential cross sections for the production of neutrons in 290-\ :math:‘\(A\)‘\ MeV :math:‘\(^{12}\)‘\ C+\ :math:‘\(^{12}\)‘\ C. Predictions of the ‘‘INCL++‘‘ and Binary-Cascade models are

compared with experimental data from Refs. :cite:‘Cochran_1972,Cochran_1974‘ and :cite:‘Iwata01a‘.||Left: double-differential cross sections for the production of charged pions in 730-MeV :math:‘\(p\)‘\ +Cu. Right: double-differential cross sections for the production of neutrons in 290-\ :math:‘\(A\)‘\ MeV :math:‘\(^{12}\)‘\ C+\ :math:‘\(^{12}\)‘\ C. Predictions of the ‘‘INCL++‘‘ and Binary-Cascade models are compared with experimental data from Refs. :cite:‘Cochran_1972,Cochran_1974‘ and :cite:‘Iwata01a‘.|

INCL++ (coupled with G4ExcitationHandler) provides an accurate modeling tool for spallation studies in the tens of MeV–15 GeV energy range. The INCL++-ABLA07 *[3]* model was recognized as one of the best on the market by the IAEA Benchmark of Spallation Models *[4]* (note however that the ABLA07 de-excitation model is presenty not available in Geant4).

As a sample of the quality of the model predictions of INCL++-G4ExcitationHandler for nucleon-induced reactions, the left panel of Figure [fig:pDoubleDifferential] presents a comparison of double-differential cross sections for pion production in 730-MeV p+Cu, compared with the predictions of the Binary-Cascade model (chapter [BinaryCascade]) and with experimental data.

Reactions induced by light-ion projectiles up to $A = 18$ are also treated by the model. The right panel of Figure [fig:pDoubleDifferential] shows double-differential cross sections for neutron production in 290-AMeV ^{12}C+^{12}C. Figure [fig:BiaxnExcitationCurves] shows excitation curves for ^{209}Bi(α, xn) reactions at very low energy. We stress here that intranuclear-cascade models are supposedly not valid below ~ 150 AMeV. The very good agreement presented in Figure [fig:BiaxnExcitationCurves] is due to the complete-fusion model that smoothly replaces INCL++ at low energy.

INCL++ is continuously updated and validated against experimental data.

7.8.10 Multifragmentation

Multifragmentation process simulation.

The GEANT4 multifragmentation model is capable to predict final states as result of an highly excited nucleus statistical break-up.

The initial information for calculation of multifragmentation stage consists from the atomic mass number A, charge Z of excited nucleus and its excitation energy U. At high excitation energies $U/A > 3$ MeV the multifragmentation mechanism, when nuclear system can eventually breaks down into fragments, becomes the dominant. Later on the excited primary fragments propagate independently in the mutual Coulomb field and undergo de-excitation. Detailed description of multifragmentation mechanism and model can be found in review [BBIMS95].

Multifragmentation probability.

The probability of a breakup channel b is given by the expression (in the so-called microcanonical approach [BBIMS95], [Botvina87]):

$$W_b(U, A, Z) = \frac{1}{\sum_b \exp[S_b(U, A, Z)]} \exp[S_b(U, A, Z)],$$

where $S_b(U, A, Z)$ is the entropy of a multifragment state corresponding to the breakup channel b. The channels $\{b\}$ can be parametrized by set of fragment multiplicities N_{A_f,Z_f} for fragment with atomic number A_f and charge Z_f. All partitions $\{b\}$ should satisfy constraints on the total mass and charge:

$$\sum_f N_{A_f,Z_f} A_f = A$$

and

$$\sum_f N_{A_f,Z_f} Z_f = Z.$$

It is assumed [Botvina87] that thermodynamic equilibrium is established in every channel, which can be characterized by the channel temperature T_b.

The channel temperature T_b is determined by the equation constraining the average energy $E_b(T_b, V)$ associated with partition b:

$$E_b(T_b, V) = U + E_{ground} = U + M(A, Z),$$

where V is the system volume, E_{ground} is the ground state (at $T_b = 0$) energy of system and $M(A, Z)$ is the mass of nucleus.

According to the conventional thermodynamical formulae the average energy of a partitition b is expressed through the system free energy F_b as follows

$$E_b(T_b, V) = F_b(T_b, V) + T_b S_b(T_b, V).$$

Thus, if free energy F_b of a partition b is known, we can find the channel temperature T_b from Eqs. (7.8.10) and (7.8.10), then the entropy $S_b = -dF_b/dT_b$ and hence, decay probability W_b defined by Eq. (7.8.10) can be calculated.

Calculation of the free energy is based on the use of the liquid-drop description of individual fragments [Botvina87]. The free energy of a partition b can be splitted into several terms:

$$F_b(T_b, V) = \sum_f F_f(T_b, V) + E_C(V),$$

where $F_f(T_b, V)$ is the average energy of an individual fragment including the volume

$$F_f^V = [-E_0 - T_b^2/\epsilon(A_f)]A_f,$$

surface

$$F_f^{Sur} = \beta_0[(T_c^2 - T_b^2)/(T_c^2 + T_b^2)]^{5/4} A_f^{2/3} = \beta(T_b)A_f^{2/3},$$

symmetry

$$F_f^{Sim} = \gamma(A_f - 2Z_f)^2/A_f,$$

Coulomb

$$F_f^C = \frac{3}{5}\frac{Z_f^2 e^2}{r_0 A_f^{1/3}}[1 - (1 + \kappa_C)^{-1/3}]$$

and translational

$$F_f^t = -T_b \ln(g_f V_f/\lambda_{T_b}^3) + T_b \ln(N_{A_f,Z_f}!)/N_{A_f,Z_f}$$

terms and the last term

$$E_C(V) = \frac{3}{5}\frac{Z^2 e^2}{R}$$

is the Coulomb energy of the uniformly charged sphere with charge Ze and the radius $R = (3V/4\pi)^{1/3} = r_0 A^{1/3}(1+\kappa_C)^{1/3}$, where $\kappa_C = 2$ [Botvina87].

Parameters $E_0 = 16$ MeV, $\beta_0 = 18$ MeV, $\gamma = 25$ MeV are the coefficients of the Bethe-Weizsacker mass formula at $T_b = 0$. $g_f = (2S_f + 1)(2I_f + 1)$ is a spin S_f and isospin I_f degeneracy factor for fragment (fragments with $A_f > 1$ are treated as the Boltzmann particles), $\lambda_{T_b} = (2\pi h^2/m_N T_b)^{1/2}$ is the thermal wavelength, m_N is the nucleon mass, $r_0 = 1.17$ fm, $T_c = 18$ MeV is the critical temperature, which corresponds to the liquid-gas phase transition. $\epsilon(A_f) = \epsilon_0[1 + 3/(A_f - 1)]$ is the inverse level density of the mass A_f fragment and $\epsilon_0 = 16$ MeV is

considered as a variable model parameter, whose value depends on the fraction of energy transferred to the internal degrees of freedom of fragments [Botvina87]. The free volume $V_f = \kappa V = \kappa \frac{4}{3}\pi r_0^4 A$ available to the translational motion of fragment, where $\kappa \approx 1$ and its dependence on the multiplicity of fragments was taken from [Botvina87]:

$$\kappa = [1 + \frac{1.44}{r_0 A^{1/3}}(M^{1/3} - 1)]^3 - 1.$$

For $M = 1$ $\kappa = 0$.

The light fragments with $A_f < 4$, which have no excited states, are considered as elementary particles characterized by the empirical masses M_f, radii R_f, binding energies B_f, spin degeneracy factors g_f of ground states. They contribute to the translation free energy and Coulomb energy.

Direct simulation of the low multiplicity multifragment disintegration

At comparatively low excitation energy (temperature) system will disintegrate into a small number of fragments $M \leq 4$ and number of channel is not huge. For such situation a direct (microcanonical) sorting of all decay channels can be performed. Then, using Eq. (7.8.10), the average multiplicity value $< M >$ can be found. To check that we really have the situation with the low excitation energy, the obtained value of $< M >$ is examined to obey the inequality $< M > \leq M_0$, where $M_0 = 3.3$ and $M_0 = 2.6$ for $A \sim 100$ and for $A \sim 200$, respectively [Botvina87]. If the discussed inequality is fulfilled, then the set of channels under consideration is belived to be able for a correct description of the break up. Then using calculated according Eq. (7.8.10) probabilities we can randomly select a specific channel with given values of A_f and Z_f.

Fragment multiplicity distribution.

The individual fragment multiplicities N_{A_f,Z_f} in the so-called macrocanonical ensemble [BBIMS95] are distributed according to the Poisson distribution:

$$P(N_{A_f,Z_f}) = \exp(-\omega_{A_f,Z_f}) \frac{\omega_{A_f,Z_f}^{N_{A_f,Z_f}}}{N_{A_f,Z_f}!}$$

with mean value $< N_{A_f,Z_f} > = \omega_{A_f,Z_f}$ defined as

$$< N_{A_f,Z_f} > = g_f A_f^{3/2} \frac{V_f}{\lambda_{T_b}^3} \exp[\frac{1}{T_b}(F_f(T_b,V) - F_f^t(T_b,V) - \mu A_f - \nu Z_f)],$$

where μ and ν are chemical potentials. The chemical potential are found by substituting Eq. (7.8.10) into the system of constraints:

$$\sum_f < N_{A_f,Z_f} > A_f = A$$

and

$$\sum_f < N_{A_f,Z_f} > Z_f = Z$$

and solving it by iteration.

Atomic number distribution of fragments.

Fragment atomic numbers $A_f > 1$ are also distributed according to the Poisson distribution [BBIMS95] (see Eq. (7.8.10)) with mean value $< N_{A_f} >$ defined as

$$< N_{A_f} > = A_f^{3/2} \frac{V_f}{\lambda_{T_b}^3} \exp[\frac{1}{T_b}(F_f(T_b,V) - F_f^t(T_f,V) - \mu A_f - \nu < Z_f >)],$$

where calculating the internal free energy $F_f(T_b,V) - F_f^t(T_b,V)$ one has to substitute $Z_f \rightarrow < Z_f >$. The average charge $< Z_f >$ for fragment having atomic number A_f is given by

$$< Z_f(A_f) >= \frac{(4\gamma+\nu)A_f}{8\gamma + 2[1-(1+\kappa)^{-1/3}]A_f^{2/3}}.$$

$Chargedistributionoffragments.$

At given mass of fragment $A_f > 1$ the charge Z_f distribution of fragments are described by Gaussian

$$P(Z_f(A_f)) \sim \exp\,[-\frac{(Z_f(A_f) - < Z_f(A_f) >)^2}{2(\sigma_{Z_f}(A_f))^2}]$$

with dispertion

$$\sigma_{Z_f(A_f)} = \sqrt{\frac{A_f T_b}{8\gamma + 2[1-(1+\kappa)^{-1/3}]A_f^{2/3}}} \approx \sqrt{\frac{A_f T_b}{8\gamma}}.$$

and the average charge $< Z_f(A_f) >$ defined by Eq. (7.8.10).

Kinetic energy distribution of fragments.

It is assumed [Botvina87] that at the instant of the nucleus break-up the kinetic energy of the fragment T_{kin}^f in the rest of nucleus obeys the Boltzmann distribution at given temperature T_b:

$$\frac{dP(T_{kin}^f)}{dT_{kin}^f} \sim \sqrt{T_{kin}^f}\exp\,(-T_{kin}^f/T_b).$$

Under assumption of thermodynamic equilibrium the fragment have isotropic velocities distribution in the rest frame of nucleus. The total kinetic energy of fragments should be equal $\frac{3}{2}MT_b$, where M is fragment multiplicity, and the total fragment momentum should be equal zero. These conditions are fullfilled by choosing properly the momenta of two last fragments.

The initial conditions for the divergence of the fragment system are determined by random selection of fragment coordinates distributed with equal probabilities over the break-up volume $V_f = \kappa V$. It can be a sphere or prolongated ellipsoid. Then Newton's equations of motion are solved for all fragments in the self-consistent time-dependent Coulomb field [Botvina87]. Thus the asymptotic energies of fragments determined as result of this procedure differ from the initial values by the Coulomb repulsion energy.

Calculation of the fragment excitation energies.

The temparature T_b determines the average excitation energy of each fragment:

$$U_f(T_b) = E_f(T_b) - E_f(0) = \frac{T_b^2}{\epsilon_0}A_f + [\beta(T_b) - T_b\frac{d\beta(T_b)}{dT_b} - \beta_0]A_f^{2/3},$$

where $E_f(T_b)$ is the average fragment energy at given temperature T_b and $\beta(T_b)$ is defined in Eq. (7.8.10). There is no excitation for fragment with $A_f < 4$, for ^4He excitation energy was taken as $U_{^4He} = 4T_b^2/\epsilon_o$.

Multifragmentation model.

7.8.11 Parton string

Kinky string decay simulation.

For kinky string decay simulation we have assumed the two steps process:

1. split gluon $g \to q_1\bar{q}_1$ and create two longitudinal strings;
2. decay longitudunal strings $q\bar{q}_1 \to h$ and $\bar{q}q_1 \to h$ into hadrons h.

The production of $q_1\bar{q}_1$ is considered similar (the same sampling of quark flavors and the same p_t-distribution for the quarks) as a production of $q\bar{q}$-pairs during a longitudinal string decay. We use the $g \to q_1\bar{q}_1$ splitting function [APKW80]:

$$f_g^q(z) = z^2 + (1-z)^2,$$

where $z = \frac{E_q + p_q^z}{E_g + p_g^z}$, derived by Altarelli and Parisi [AP77].

Kinky string excitation.

Having sampled the configuration of kinky strings we generate outgoing gluon–kink momenta.

We assume that kinky strings are produced as result of $gg \to gg$ hard interactions. Our generation of the outgoing gluons (kinks) momenta is based on the two-jets inclusive production cross section:

$$\frac{d\sigma_{gg}}{dx_g^+ dx_g^- d\cos\theta} = f(x_g^+, Q^2) f(x_g^-, Q^2) \frac{d\sigma_{gg}(\hat{s})}{d\cos\theta},$$

where we take $\hat{s} = Q^2 = x_g^+ x_g^- s$ and s is the total colliding system center of mass energy squared, which calculated using x_i and q_{ti} and m_i^2 string end partons. The value of s should be large enough to produce gluons with the transverse momentum cutoff $Q_0^2 = 2\ GeV^2$ choosen. The QCD gluon – gluon interaction cross section

$$\frac{d\sigma_{gg}(\hat{s})}{d\cos\theta} = \frac{9\pi\alpha_s^2(Q^2)}{32s} \frac{(3+\cos^2\theta)^3}{(1-\cos^2\theta)^2}$$

was calculated in the Born approximation [CKR77]. The θ is the scattering angle in the center of mass of the parton-parton system and $-z_0 < \cos\theta < z_0$ with

$$z_0 = \sqrt{1 - \frac{4Q_0^2}{sx^+x^-}}.$$

The QCD running coupling constant

$$\alpha_s(Q^2) = \frac{12\pi}{25\ln(Q^2/\Lambda^2)},$$

which is corresponding to four flavours and $\Lambda^2 = 0.01$ GeV^2 is taken.

$f(x, Q^2)$ is the momentum fraction distribution of gluons in hadron. It is choosen from:cite:*CKMT95*:

$$f(x, Q^2) = A(Q^2) \frac{x^{-\Delta(Q^2)}}{x} (1-x)^{n(Q^2)+3}$$

with parameters $\Delta(Q^2) = \Delta(1 + \frac{2Q^2}{Q^2+1.12})$ and $n(Q^2) = \frac{3}{2}(1 + \frac{Q^2}{Q^2+3.55})$ and $A(Q^2)$ is calculated from energy-momentum conservation sum rule. At $Q_0^2 = 2\ GeV^2$

$$f(x, Q_0^2) = 1.71 \frac{x^{-0.18}}{x} (1-x)^5.$$

Thus the MC procedure to build the kinky strings can be outlined as follows:

- Sample x_i, $\mathbf{q_{it}}$ and m_i^2, where $i = 1, 2, ..., 2n$, for partons, which will be on the $2n$ string ends for both the soft and kinky strings.
- For each pair of kinky string calculate total center of mass energy s and sample $x^+_{min} < x^+$ and $x^-_{min} < x^-$, where $x_{min} = 2Q_0/\sqrt{s}$, for ingoing gluon momenta using gluon distribution function defined by Eq.(7.8.11) at $Q_0^2 = 2$ GeV^2.
- Sample the outgoing gluon center of mass scattering angle θ using Eq. (7.8.11).
- For each kinky string recalculate parton string end energies and momenta.

This procedure should be improved taking into account initial and final state gluon radiation.

Longitudinal string decay.

Hadron production by string fragmentation.

A string is stretched between flying away constituents: quark and antiquark or quark and diquark or diquark and antidiquark or antiquark and antidiquark. From knowledge of the constituents longitudinal $p_{3i} = p_{zi}$ and transversal $p_{1i} = p_{xi}$, $p_{2i} = p_{yi}$ momenta as well as their energies $p_{0i} = E_i$, where $i = 1, 2$, we can calculate string mass squared:

$$M_S^2 = p^\mu p_\mu = p_0^2 - p_1^2 - p_2^2 - p_3^2,$$

where $p_\mu = p_{\mu 1} + p_{\mu 2}$ is the string four momentum and $\mu = 0, 1, 2, 3$.

The fragmentation of a string follows an iterative scheme:

$$string \Rightarrow hadron + new\ string,$$

i.e. a quark-antiquark (or diquark-antidiquark) pair is created and placed between leading quark-antiquark (or diquark-quark or diquark-antidiquark or antiquark-antidiquark) pair.

The values of the strangeness suppression and diquark suppression factors are

$$u : d : s : qq = 1 : 1 : 0.35 : 0.1.$$

A hadron is formed randomly on one of the end-points of the string. The quark content of the hadrons determines its species and charge. In the chosen fragmentation scheme we can produce not only the groundstates of baryons and mesons, but also their lowest excited states. If for baryons the quark-content does not determine whether the state belongs to the lowest octet or to the lowest decuplet, then octet or decuplet are choosen with equal probabilities. In the case of mesons the multiplet must also be determined before a type of hadron can be assigned. The probability of choosing a certain multiplet depends on the spin of the multiplet.

The zero transverse momentum of created quark-antiquark (or diquark-antidiquark) pair is defined by the sum of an equal and opposite directed transverse momenta of quark and antiquark.

The transverse momentum of created quark is randomly sampled according to probability (7.8.11) with the parameter $a = 0.25$ GeV^{-2}. Then a hadron transverse momentum $\mathbf{p_t}$ is determined by the sum of the transverse momenta of its constituents.

The fragmentation function $f^h(z, p_t)$ represents the probability distribution for hadrons with the transverse momenta $\mathbf{p_t}$ to aquire the light cone momentum fraction $z = z^\pm = (E^h \pm p_z^h/(E^q \pm p_z^q)$, where E^h and E^q are the hadron and fragmented quark energies, respectively and p_z^h and p_z^q are hadron and fragmented quark longitudinal momenta, respectively, and $z^\pm_{min} \le z^\pm \le z^\pm_{max}$, from the fragmenting string. The values of $z^\pm_{min,max}$ are determined by hadron m_h and constituent transverse masses and the available string mass. One of the most common fragmentation function is used in the LUND model [LUND83]:

$$f^h(z, p_t) \sim \frac{1}{z}(1 - z)^a \exp\,[-\frac{b(m_h^2 + p_t^2)}{z}].$$

One can use this fragmentation function for the decay of the excited string.

One can use also the fragmentation functions are derived in [Kai87]:

$$f_q^h(z, p_t) = [1 + \alpha_q^h(< p_t >)](1 - z)^{\alpha_q^h(<p_t>)}.$$

The advantage of these functions as compared to the LUND fragmentation function is that they have correct three–reggeon behaviour at $z \to 1$ [Kai87].

The hadron formation time and coordinate.

To calculate produced hadron formation times and longitudinal coordinates we consider the $(1 + 1)$-string with mass M_S and string tension κ, which decays into hadrons at string rest frame. The i-th produced hadron has energy E_i and its longitudinal momentum p_{zi}, respectively. Introducing light cone variables $p_i^{\pm} = E_i \pm p_{iz}$ and numbering string breaking points consecutively from right to left we obtain $p_0^+ = M_S$, $p_i^+ = \kappa(z_{i-1}^+ - z_i^+)$ and $p_i^- = \kappa x_i^-$.

We can identify the hadron formation point coordinate and time as the point in space-time, where the quark lines of the quark-antiquark pair forming the hadron meet for the first time (the so-called 'yo-yo' formation point [LUND83]):

$$t_i = \frac{1}{2\kappa}[M_S - 2\sum_{j=1}^{i-1} p_{zj} + E_i - p_{zi}]$$

and coordinate

$$z_i = \frac{1}{2\kappa}[M_S - 2\sum_{j=1}^{i-1} E_j + p_{zi} - E_i].$$

Longitudinal string excitation

Hadron–nucleon inelastic collision

Let us consider collision of two hadrons with their c. m. momenta $P_1 = \{E_1^+, m_1^2/E_1^+, \mathbf{0}\}$ and $P_2 = \{E_2^-, m_2^2/E_2^-, \mathbf{0}\}$, where the light-cone variables $E_{1,2}^{\pm} = E_{1,2} \pm P_{z1,2}$ are defined through hadron energies $E_{1,2} = \sqrt{m_{1,2}^2 + P_{z1,2}^2}$, hadron longitudinal momenta $P_{z1,2}$ and hadron masses $m_{1,2}$, respectively. Two hadrons collide by two partons with momenta $p_1 = \{x^+ E_1^+, 0, \mathbf{0}\}$ and $p_2 = \{0, x^- E_2^-, \mathbf{0}\}$, respectively.

The diffractive string excitation

In the diffractive string excitation (the Fritiof approach [FRITIOF87]) only momentum can be transferred:

$$P_1' = P_1 + q$$
$$P_2' = P_2 - q,$$

where

$$q = \{-q_t^2/(x^- E_2^-), q_t^2/(x^+ E_1^+), \mathbf{q_t}\}$$

is parton momentum transferred and $\mathbf{q_t}$ is its transverse component. We use the Fritiof approach to simulate the diffractive excitation of particles.

The string excitation by parton exchange

For this case the parton exchange (rearrangement) and the momentum exchange are allowed [QGSM82],:cite:*DPM94*,:cite:*Am86*:

$$P_1' = P_1 - p_1 + p_2 + q$$
$$P_2' = P_2 + p_1 - p_2 - q,$$

where $q = \{0, 0, \mathbf{q_t}\}$ is parton momentum transferred, i. e. only its transverse components $\mathbf{q_t} = 0$ is taken into account.

Transverse momentum sampling

The transverse component of the parton momentum transferred is generated according to probability

$$P(\mathbf{q_t})d\mathbf{q_t} = \sqrt{\frac{a}{\pi}} \exp\left(-aq_t^2\right)d\mathbf{q_t},$$

where parameter $a = 0.6$ GeV^{-2}.

Sampling x-plus and x-minus

Light cone parton quantities x^+ and x^- are generated independently and according to distribution:

$$u(x) \sim x^\alpha (1-x)^\beta,$$

where $x = x^+$ or $x = x^-$. Parameters $\alpha = -1$ and $\beta = 0$ are chosen for the FRITIOF approach [FRITIOF87]. In the case of the QGSM approach [Am86] $\alpha = -0.5$ and $\beta = 1.5$ or $\beta = 2.5$. Masses of the excited strings should satisfy the kinematical constraints:

$$P_1'^+ P_1'^- \geq m_{h1}^2 + q_t^2$$

and

$$P_2'^+ P_2'^- \geq m_{h2}^2 + q_t^2,$$

where hadronic masses m_{h1} and m_{h2} (model parameters) are defined by string quark contents. Thus, the random selection of the values x^+ and x^- is limited by above constraints.

The diffractive string excitation

In the diffractive string excitation (the FRITIOF approach [FRITIOF87]) for each inelastic hadron–nucleon collision we have to select randomly the transverse momentum transferred $\mathbf{q_t}$ (in accordance with the probability given by Eq. (7.8.11)) and select randomly the values of $x^\pm$ (in accordance with distribution defined by Eq. (7.8.11)). Then we have to calculate the parton momentum transferred q using Eq. (7.8.11) and update scattered hadron and nucleon or scatterred nucleon and nucleon momenta using Eq. (7.8.11). For each collision we have to check the constraints (7.8.11) and (7.8.11), which can be written more explicitly:

$$[E_1^+ - \frac{q_t^2}{x^- E_2^-}][\frac{m_1^2}{E_1^+} + \frac{q_t^2}{x^+ E_1^+}] \geq m_{h1}^2 + q_t^2$$

and

$$[E_2^- + \frac{q_t^2}{x^- E_2^-}][\frac{m_2^2}{E_2^-} - \frac{q_t^2}{x^+ E_1^+}] \geq m_{h1}^2 + q_t^2.$$

The string excitation by parton rearrangement

In this approach [Am86] strings (as result of parton rearrangement) should be spanned not only between valence quarks of colliding hadrons, but also between valence and sea quarks and between sea quarks. The each participant hadron or nucleon should be splitted into set of partons: valence quark and antiquark for meson or valence quark (antiquark) and diquark (antidiquark) for baryon (antibaryon) and additionaly the $(n-1)$ sea quark-antiquark pairs (their flavours are selected according to probability ratios $u:d:s=1:1:0.35$), if hadron or nucleon is participating in the n inelastic collisions. Thus for each participant hadron or nucleon we have to generate a set of light cone variables x_{2n}, where $x_{2n}=x_{2n}^{+}$ or $x_{2n}=x_{2n}^{-}$ according to distribution:

$$f^h(x_1,x_2,...,x_{2n})=f_0\prod_{i=1}^{2n}u_{q_i}^h(x_i)\delta(1-\sum_{i=1}^{2n}x_i),$$

where f_0 is the normalization constant. Here, the quark structure functions $u_{q_i}^h(x_i)$ for valence quark (antiquark) q_v, sea quark and antiquark q_s and valence diquark (antidiquark) qq are:

$$u_{q_v}^h(x_v)=x_v^{\alpha_v},\ u_{q_s}^h(x_s)=x_s^{\alpha_s},\ u_{qq}^h(x_{qq})=x_{qq}^{\beta_{qq}},$$

where $\alpha_v=-0.5$ and $\alpha_s=-0.5$ [QGSM82] for the non-strange quarks (antiquarks) and $\alpha_v=0$ and $\alpha_s=0$ for strange quarks (antiquarks), $\beta_{uu}=1.5$ and $\beta_{ud}=2.5$ for proton (antiproton) and $\beta_{dd}=1.5$ and $\beta_{ud}=2.5$ for neutron (antineutron). Usualy x_i are selected between $x_i^{min}\le x_i\le 1$, where model parameter x^{min} is a function of initial energy, to prevent from production of strings with low masses (less than hadron masses), when whole selection procedure should be repeated. Then the transverse momenta of partons $\mathbf{q_{it}}$ are generated according to the Gaussian probability Eq. (7.8.11) with $a=1/4\Lambda(s)$ and under the constraint: $\sum_{i=1}^{2n}\mathbf{q_{it}}=0$. The partons are considered as the off-shell partons, i. e. $m_i^2\neq 0$.

Quark or diquark annihilation in hadronic processes.

We consider also hadron-hadron inelastic processes when antiquark or antidiquark from hadron projectile annihilate with corresponding quark or diquark from hadron target. In this case excitation of one baryonic (string with quark and diquark ends) or mesonic (string with quark and antiquark ends) is created, respectively. These processes in the Regge theory correspond to cut reggeon exchange diagrams. Initial energy $\sqrt{s}$ dependences of these processes cross sections are defined by intercepts of reggeon exchange trajectories. For example $\sigma_{\pi^+p\to S(s)}\sim s^{\alpha_\rho(0)-1}$, S notes string and $\alpha_\rho(0)$ is the intercept of ρ reggeon trajectory. Thus $\sigma_{\pi^+p\to S(s)}$ decreases with energy rise. Cross sections for other quark and diquark proccesses have simiar as $\sigma_{\pi^+p\to S(s)}$ initial energy dependences. Thus quark and diquark annihilation processes are important at relative low initial energies. Another example of these processes is $\bar{p}p\to S$, which is used in the kinetic model to describe final state of $\bar{p}p$ annihilation. Simulation of such kind process is rather simple. We should randomly (according to weight calculated using hadron wave function) choose quark (antiquark) or diquark (antidiquark) from projectile and find suitable (with the same flavor content) partner for annihilation from target. The created string four-momentum will be equal total reaction four-momentum since annihilated system has small neglected momentum (only low momenta quarks are able to annihilate).

To determine statistical weights for quark annihilation processes are leading to a string production and separate them from processes, when two or more strings can be produced we use the Regge motivated total cross section parametrization suggested by Donnachie and Landshoff [DL92]. Using their parametrization the statistical weight for the one string production process is given by

$$W_1=\frac{Y_{hN}s^{-\eta}}{\sigma_{hN}^{tot}(s)}$$

and statistical weight to produce two and more strings is given by

$$W_2=\frac{X_{hN}s^{\epsilon}}{\sigma_{hN}^{tot}(s)},$$

where hadron-nucleon total cross sections $\sigma_{hN}^{tot}(s)$ and its fit parameters Y_{hN}, X_{hN}, which do not depend from the total c.m. energy squared s and depend on type of projectile hadron h and target nucleon N can be found in [PDG96]. The reggeon intercept $\eta \approx 0.45$ and the pomeron intercept $\epsilon \approx 0.08$.

Parton string model MC procedure.

The parton string model algorithm can be considered as a set of steps should be performed:

1. Create two vectors (projectile and target) of particles: assign initial projectile and target particle types, their coordinates and momenta. In the case of hadron-nucleus (or nucleus-nucleus) interaction one should perform target nucleus (or projectile and target nuclei) initial state simulation and sample impact parameter;
2. Sample collision participants and separated them into diffractive and non-diffractive. Store the total interaction four momentum of participants;
3. For non-diffractive inelastic collisions sample the number of the soft longitudinal and hard kinky string can be produced.
4. Excite and reexcite colliding particles in the case of diffractive collisions and create diffractive longitudinal strings, if particles are not participate in further soft or hard collisions;
5. Perform longitudinal and kinky string excitations;
6. Perform string decay simulation;
7. Correct energies and momenta of produced particles, if it is needed.

Parton string model.

Reaction initial state simulation.

Allowed projectiles and bombarding energy range for interaction with nucleon and nuclear targets

The GEANT4 parton string models are capable to predict final states (produced hadrons which belong to the scalar and vector meson nonets and the baryon (antibaryon) octet and decuplet) of reactions on nucleon and nuclear targets with nucleon, pion and kaon projectiles. The allowed bombarding energy $\sqrt{s} > 5$ GeV is recommended. Two approaches, based on diffractive excitation or soft scattering with diffractive admixture according to cross-section, are considered. Hadron-nucleus collisions in the both approaches (diffractive and parton exchange) are considered as a set of the independent hadron-nucleon collisions. However, the string excitation procedures in these approaches are rather different.

MC initialization procedure for nucleus.

The initialization of each nucleus, consisting from A nucleons and Z protons with coordinates $\mathbf{r}_i$ and momenta $\mathbf{p}_i$, where $i = 1, 2, ..., A$ is performed. We use the standard initialization Monte Carlo procedure, which is realized in the most of the high energy nuclear interaction models:

- Nucleon radii r_i are selected randomly in the rest of nucleus according to proton or neutron density $\rho(r_i)$. For heavy nuclei with $A > 16$ [GLMP91] nucleon density is

$$\rho(r_i) = \frac{\rho_0}{1 + \exp\left[(r_i - R)/a\right]}$$

where

$$\rho_0 \approx \frac{3}{4\pi R^3}(1 + \frac{a^2\pi^2}{R^2})^{-1}.$$

Here $R = r_0 A^{1/3}$ fm and $r_0 = 1.16(1 - 1.16A^{-2/3})$ fm and $a \approx 0.545$ fm. For light nuclei with $A < 17$ nucleon density is given by a harmonic oscillator shell model [Elton61], e. g.

$$\rho(r_i) = (\pi R^2)^{-3/2} \exp(-r_i^2/R^2),$$

where $R^2 = 2/3 < r^2 >= 0.8133A^{2/3}$ fm:math:*(^2)*. To take into account nucleon repulsive core it is assumed that internucleon distance $d > 0.8$ fm;

- The initial momenta of the nucleons are randomly choosen between 0 and p_F^{max}, where the maximal momenta of nucleons (in the local Thomas-Fermi approximation [DF74]) depends from the proton or neutron density ρ according to

$$p_F^{max} = \hbar c (3\pi^2 \rho)^{1/3}$$

with $\hbar c = 0.197327$ GeV fm;

- To obtain coordinate and momentum components, it is assumed that nucleons are distributed isotropicaly in configuration and momentum spaces;
- Then perform shifts of nucleon coordinates $\mathbf{r'_j} = \mathbf{r_j} - 1/A \sum_i \mathbf{r_i}$ and momenta $\mathbf{p'_j} = \mathbf{p_j} - 1/A \sum_i \mathbf{p_i}$ of nucleon momenta. The nucleus must be centered in configuration space around $\mathbf{0}$, *i. e.* $\sum_i \mathbf{r}_i = \mathbf{0}$ and the nucleus must be at rest, i. e. $\sum_i \mathbf{p_i} = \mathbf{0}$;
- We compute energy per nucleon $e = E/A = m_N + B(A,Z)/A$, where m_N is nucleon mass and the nucleus binding energy $B(A,Z)$ is given by the Bethe-Weizsäcker formula:cite:*BM69*:

$$B(A,Z) = \\ = -0.01587A + 0.01834A^{2/3} + 0.09286(Z - \tfrac{A}{2})^2 + 0.00071Z^2/A^{1/3},$$

and find the effective mass of each nucleon $m_i^{eff} = \sqrt{(E/A)^2 - p_i^{2\prime}}$.

Random choice of the impact parameter.

The impact parameter $0 \leq b \leq R_t$ is randomly selected according to the probability:

$$P(\mathbf{b}) d\mathbf{b} = b d\mathbf{b},$$

where R_t is the target radius, respectively. In the case of nuclear projectile or target the nuclear radius is determined from condition:

$$\frac{\rho(R)}{\rho(0)} = 0.01.$$

The longitudinal and kinky strings are produced in hadronic collisions.

The number of the cut Pomerons.

In the case of a nondiffractive interaction we can determine n of cut Pomerons or $2n$ produced strings according to probability [AGK74]

$$p_{ij}^{(n)}(\vec{b_i} - \vec{b_j}, s) = c^{-1} \exp\{-2u(b_{ij}^2, s)\} \frac{[2u(b_{ij}^2, s)]^n}{n!}.$$

Separation of the longitudinal soft strings from the kinky hard strings.

We assume [ASGABP95], [WDFHO97] that each cut Pomeron can be substituted either by the two longitudinal soft strings or by the two kinky hard strings.

At the moment it is not completely clear how to choose which cut pomeron should be substituted by longitudinal and which one should be substituted by kinky strings.

One recipe is based on the eikonal model [RCT94], [WDFHO97]

$$u(b_{ij}^2, s) = u_{soft}(b_{ij}^2, s) + u_{hard}(b_{ij}^2, s).$$

The soft eikonal part is defined as

$$u_{soft}(b_{ij}^2, s) = \frac{\gamma_{soft}}{\lambda_{soft}(s)}(s/s_0)^{\Delta_{soft}} \exp(-b_{ij}^2/4\lambda_{soft}(s)).$$

The hard part is calculated according to

$$u_{hard}(b_{ij}^2, s) = \frac{\sigma_{jet}}{8\pi\lambda_{hard}(s)}(s/s_0)^{\Delta_{hard}} \exp(-b_{ij}^2/4\lambda_{hard}(s)).$$

The $\sigma_{jet} = 0.027$ mbarn and $\Delta_{hard} = 0.47$ were found from the fit of the two–jet experimental cross section [UA1]. Then from the global fit of the total and elastic cross sections for pp collisions the values of $\gamma_{soft} = 35.5$ mbarn, $\Delta_{soft} = 0.07$ and $R_{hard}^2 = R_{soft}^2 = 3.56$ GeV^{-2} were found.

Thus we can examine each cut Pomeron and substitute it by two kinky strings with probability

$$P_{hard}(b_{ij}^2, s) = \frac{u_{hard}(b_{ij}^2, s)}{u_{soft}(b_{ij}^2, s) + u_{hard}(b_{ij}^2, s)}.$$

Sample of collision participants in nuclear collisions.

MC procedure to define collision participants.

The inelastic hadron–nucleus interactions at ultra–relativistic energies are considered as independent hadron–nucleon collisions. It was shown long time ago [CK78] for the hadron–nucleus collision that such a picture can be obtained starting from the Regge–Gribov approach [BT76], when one assumes that the hadron-nucleus elastic scattering amplitude is a result of reggeon exchanges between the initial hadron and nucleons from target–nucleus. This result leads to simple and efficient MC procedure [Am86] to define the interaction cross sections and the number of the nucleons participating in the inelastic hadron–nucleus collision:

- We should randomly distribute B nucleons from the target-nucleus on the impact parameter plane according to the weight function $T([\vec{b}_j^B])$. This function represents probability density to find sets of the nucleon impact parameters $[\vec{b}_j^B]$, where $j = 1, 2, ..., B$.
- For each pair of projectile hadron i and target nucleon j with choosen impact parameters $\vec{b}_i$ and $\vec{b}_j^B$ we should check whether they interact inelastically or not using the probability $p_{ij}(\vec{b}_i - \vec{b}_j^B, s)$, where $s_{ij} = (p_i + p_j)^2$ is the squared total c.m. energy of the given pair with the 4–momenta p_i and p_j, respectively.

In the Regge–Gribov approach:cite:*BT76* the probability for an inelastic collision of pair of i and j as a function at the squared impact parameter difference $b_{ij}^2 = (\vec{b}_i - \vec{b}_j^B)^2$ and s is given by

$$p_{ij}(\vec{b}_i - \vec{b}_j^B, s) = c^{-1}[1 - \exp\{-2u(b_{ij}^2, s)\}] = \sum_{n=1}^{\infty} p_{ij}^{(n)}(\vec{b}_i - \vec{b}_j^B, s),$$

where

$$p_{ij}^{(n)}(\vec{b}_i - \vec{b}_j^B, s) = c^{-1} \exp\{-2u(b_{ij}^2, s)\} \frac{[2u(b_{ij}^2, s)]^n}{n!}.$$

is the probability to find the n cut Pomerons or the probability for $2n$ strings produced in an inelastic hadron-nucleon collision. These probabilities are defined in terms of the (eikonal) amplitude of hadron–nucleon elastic scattering with Pomeron exchange:

$$u(b_{ij}^2, s) = \frac{z(s)}{2} \exp(-b_{ij}^2/4\lambda(s)).$$

The quantities $z(s)$ and $\lambda(s)$ are expressed through the parameters of the Pomeron trajectory, $\alpha_P^{'} = 0.25\ GeV^{-2}$ and $\alpha_P(0) = 1.0808$, and the parameters of the Pomeron-hadron vertex R_P and γ_P:

$$z(s) = \frac{2c\gamma_P}{\lambda(s)} (s/s_0)^{\alpha_P(0)-1}$$

$$\lambda(s) = R_P^2 + \alpha_P^{'} \ln(s/s_0),$$

respectively, where s_0 is a dimensional parameter.

In Eqs. ([SP3],[SP4]) the so–called shower enhancement coefficient c is introduced to determine the contribution of diffractive dissociation:cite:*BT76*. Thus, the probability for diffractive dissociation of a pair of nucleons can be computed as

$$p_{ij}^d(\vec{b}_i - \vec{b}_j^B, s) = \frac{c-1}{c}[p_{ij}^{tot}(\vec{b}_i - \vec{b}_j^B, s) - p_{ij}(\vec{b}_i - \vec{b}_j^B, s)],$$

where

$$p_{ij}^{tot}(\vec{b}_i - \vec{b}_j^B, s) = (2/c)[1 - \exp\{-u(b_{ij}^2, s)\}].$$

The Pomeron parameters are found from a global fit of the total, elastic, differential elastic and diffractive cross sections of the hadron–nucleon interaction at different energies.

For the nucleon-nucleon, pion-nucleon and kaon-nucleon collisions the Pomeron vertex parameters and shower enhancement coefficients are found: $R_P^{2N} = 3.56\ GeV^{-2}$, $\gamma_P^N = 3.96\ GeV^{-2}$, $s_0^N = 3.0\ GeV^2$, $c^N = 1.4$ and $R_P^{2\pi} = 2.36\ GeV^{-2}$, $\gamma_P^\pi = 2.17\ GeV^{-2}$, and $R_P^{2K} = 1.96\ GeV^{-2}$, $\gamma_P^K = 1.92\ GeV^{-2}$, $s_0^K = 2.3\ GeV^2$, $c^\pi = 1.8$.

Separation of hadron diffraction excitation.

For each pair of target hadron i and projectile nucleon j with choosen impact parameters $\vec{b}_i$ and $\vec{b}_j^B$ we should check whether they interact inelastically or not using the probability

$$p_{ij}^{in}(\vec{b}_i - \vec{b}_j^B, s) = p_{ij}(\vec{b}_i - \vec{b}_j^B, s) + p_{ij}^d(\vec{b}_i^A - \vec{b}_j^B, s).$$

If interaction will be realized, then we have to consider it to be diffractive or nondiffractive with probabilities

$$\frac{p_{ij}^d(\vec{b}_i - \vec{b}_j^B, s)}{p_{ij}^{in}(\vec{b}_i^A - \vec{b}_j^B, s)}$$

and

$$\frac{p_{ij}(\vec{b}_i - \vec{b}_j^B, s)}{p_{ij}^{in}(\vec{b}_i^A - \vec{b}_j^B, s)}.$$

7.8.12 Parton string

Precompound model.

Reaction initial state.

The GEANT4 precompound model is considered as an extension of the hadron kinetic model. It gives a possibility to extend the low energy range of the hadron kinetic model for nucleon-nucleus inelastic collision and it provides a "smooth" transition from kinetic stage of reaction described by the hadron kinetic model to the equilibrium stage of reaction described by the equilibrium deexcitation models.

The initial information for calculation of pre-compound nuclear stage consists from the atomic mass number A, charge Z of residual nucleus, its four momentum P_0, excitation energy U and number of excitons n equals the sum of number of particles p (from them p_Z are charged) and number of holes h.

At the preequilibrium stage of reaction, we following the [GMT83] approach, take into account all possible nuclear transition the number of excitons n with $\Delta n = +2, -2, 0$ [GMT83], which defined by transition probabilities. Only emmision of neutrons, protons, deutrons, thritium and helium nuclei are taken into account.

7.8.13 QMD

Quantum Molecular Dynamics for Heavy Ions

QMD is the quantum extension of the classical molecular dynamics model and is widely used to analyze various aspects of heavy ion reactions, especially for many-body processes, and in particular the formation of complex fragments. In the previous section, we mentioned several similar and dissimilar points between Binary Cascade and QMD. There are three major differences between them:

1. The definition of a participant particle,
2. The potential term in the Hamiltonian, and
3. Participant-participant interactions.

At first, we will explain how they are each treated in QMD. The entire nucleons in the target and projectile nucleus are considered as participant particles in the QMD model. Therefore each nucleon has its own wave function, however the total wave function of a system is still assumed as the direct product of them. The potential terms of the Hamiltonian in QMD are calculated from the entire relation of particles in the system, in other words, it can be regarded as self-generating from the system configuration. On the contrary to Binary Cascade which tracks the participant particles sequentially, all particles in the system are tracked simultaneously in QMD. Along with the time evolution of the system, its potential is also dynamically changed. As there is no criterion between participant particle and others in QMD, participant-participant scatterings are naturally included. Therefore QMD accomplishes more detailed treatments of the above three points, however with a cost of computing performance.

Equations of Motion

The basic assumption of QMD is that each nucleon state is represented by a Gaussian wave function of width L,

$$\varphi_i(\mathbf{r}) \equiv \frac{1}{(2\pi L)^{3/4}} \exp\left(-\frac{(r-r_i)^2}{4L} + \frac{i}{\hbar} r \cdot p_i\right)$$

where r_i and p_i represent the center values of position and momentum of the i^{th} particle. The total wave function is assumed to be a direct product of them,

$$\Psi(\mathbf{r}_1, \mathbf{r}_2, \ldots, \mathbf{r}_N) \equiv \prod_i \varphi_i(r_i) \, .$$

Equations of the motion of particle derived on the basis of the time dependent variation principle as

$$\dot{r}_i = \frac{\partial H}{\partial p_i}\,, \quad \dot{p}_i = -\frac{\partial H}{\partial r_i}$$

where H is the Hamiltonian which consists particle energy including mass energy and the energy of the two-body interaction.

However, further details in the prescription of QMD differ from author to author and JAERI QMD (JQMD):cite:*Niita95* is selected as a basis for our model. In this model, the Hamiltonian is

$$H = \sum_i \sqrt{m_i^2 + p_i^2} + \hat{V}$$

A Skyrme type interaction, a Coulomb interaction, and a symmetry term are included in the effective Potential ($\hat{V}$). The relativistic form of the energy expression is introduced in the Hamiltonian. The interaction term is a function of the squared spatial distance:

$$R_{ij} = (R_i - R_j)^2$$

This is not a Lorentz scalar. In Relativistic QMD (RQMD):cite:*Sorge89*, they are replaced by the squared transverse four-dimensional distance,

$$-q_{Tij}^2 = -q_{ij}^2 + \frac{(q_{ij} \cdot p_{ij})^2}{p_{ij}^2}$$

where q_{ij} is the four-dimensional distance and p_{ij} is the sum of the four momentum. In JQMD they change the argument by the squared distance in center of mass system of the two particles,

$$\tilde{R} = R_{ij}^2 + \gamma_{ij}^2 (R_{ij} \cdot \beta_{ij})^2$$

with

$$\beta_{ij} = \frac{p_i + p_j}{E_i + E_j}\,, \quad \gamma_{ij} = \frac{1}{\sqrt{1 - \beta_{ij}}}$$

As a result of this, the interaction term in also depends on momentum.

Recently R-JQMD, the Lorentz covariant version of JQMD, has been proposed:cite:*Mancusi09*. The covariant version of Hamiltonian is

$$H_C = \sum_i \sqrt{p_i^2 + m_i^2 + 2 m_i V_i}$$

where V_i is the effective potential felt by the i^{th} particle.

With on-mass-shell constraints and a simple form of the "time fixations" constraint, the entire particle has the same time coordinate. They justified the latter assumption with the following argument "In high-energy reactions, two-body collisions are dominant; the purpose of the Lorentz-covariant formalism is only to describe relatively low energy phenomena between particles in a fast-moving medium"[Mancusi09].

From this assumption, they get following equation of motion together with a big improvement in CPU performance.

$$\begin{aligned}
\dot{r}_i = & \quad \frac{p_i}{2p_i^0} + \sum_j \frac{2m_j}{2p_j^0} \frac{\tilde{V}_j}{\partial p_i} \\
= & \quad \frac{\partial}{\partial p_i} \sum_j \sqrt{p_j^2 + m_j^2 + 2 m_j \tilde{V}} \\
\dot{p}_i = & \quad -\sum_j \frac{2m_j}{2p_j^0} \frac{\tilde{V}_j}{\partial r_i} \\
= & \quad \frac{\partial}{\partial r_i} \sum_j \sqrt{p_j^2 + m_j^2 + 2 m_j \tilde{V}}
\end{aligned}$$

The $i^{\rm th}$ particle has an effective mass of

$$m_i^* = \sqrt{m_i^2 + 2m_i V_i}\ .$$

We follow their prescription and also use the same parameter values, such as the width of the Gaussian L = 2.0 fm^2 and so on.

Ion-ion Implementation

For the case of two body collisions and resonance decay, we used the same codes which the Binary Cascade uses in Geant4. However for the relativistic covariant kinematic case, the effective mass of $i^{\rm th}$ particle depends on the one-particle effective potential, V_i, which also depends on the momentum of the entire particle system. Therefore, in R-JQMD, all the effective masses are calculated iteratively for keeping energy conservation of the whole system. We track their treatment for this.

As already mentioned, the Binary cascade model creates detailed $3r+3p$ dimensional nucleus at the beginning of each reaction. However, we could not use them in our QMD code, because they are not stable enough in time evolution. Also, a real ground state as an energy minimum state of the nucleus is not available in the framework of QMD, because it does not have fermionic properties. However, a reasonably stable "ground state" nucleus is required for the initial phase space distribution of nucleons in the QMD calculation. JQMD succeeded to create such a "ground state" nucleus. We also follow their prescription of generating the ground state nucleus. And "ground state" nuclei for target and projectile will be Lorentz-boosted (construct) to the center-of-mass system between them. By this Lorentz transformation, additional instabilities are introduced into both nuclei in the case of the non-covariant version.

The time evolution of the QMD system will be calculated until a certain time, typically 100 fm/c. The δT of the evolution is 1 fm/c. The user can modify both values from the Physics List of Geant4. After the termination of the time evolution, cluster identification is carried out in the phase space distribution of nucleons in the system. Each identified cluster is considered as a fragmented nucleus from the reaction and it usually has more energy than the ground state. Therefore, excitation energy of the nucleus is calculated and then the nucleus is passed on to other Geant4 models like Binary Cascade. However, unlike Binary Cascade which passes them to Precompound model and Excitation models by calling them inside of the model, the QMD model uses Excitation models directly. There are multiple choices of excitation model and one of them is the GEM model:cite:*Furihata00* which JQMD and RJQMD use. The default excitation model is currently this GEM model.

Figure [fig:qmd-time] shows an example of time evolution of the reaction of 290 MeV/n ^{56}Fe ions bombarding a ^{208}Pb target. Because of the small Lorentz factor (~ 1.3), the Lorentz contractions of both nuclei are not seen clearly.

Cross Sections

Nucleus-Nucleus (NN) cross section is not a fundamental component of either QMD or Binary Light Ions Cascade model. However without the cross section, no meaningful simulation beyond the study of the NN reaction itself can be done. In other words, Geant4 needs the cross section to decide where an NN reaction will happen in simulation geometry.

Many cross section formulae for NN collisions are included in Geant4, such as Tripathi:cite:*Tripathi97* and Tripathi Light System:cite:*Tripathi99*, Shen:cite:*Shen89*, Kox:cite:*Kox87* and Sihver:cite:*Sihver93*. These are empirical and parameterized formulae with theoretical insights and give total reaction cross section of wide variety of combination of projectile and target nucleus in fast. These cross sections are also used in the sampling of impact parameter in the QMD model.

7.8.14 Stopped Absorption

Reaction initial state.

The GEANT4 hadron kinetic model is capable to predict final states particles and nuclear fragments as result of absorption of the stopped π^-, K^- and $\bar{p}$ by a nucleus.

MC procedure.

The stopped particle absorption MC procedure consists from several steps:

1. Sample position inside nucleus, where absorption takes place, according to phenomenological probability distribution;
2. Simulate particle absorption according to particular particle absorption mechanism;
3. Using the hadron kinetic model perform propagation of final state (after absorption) particles;
4. Using corresponding deexcitation model perform decay of residual excited nucleus.

Stopped particle absorption.

Stopped particle absorption simulation.

Mechanism of the stopped particle absorption by a nucleus.

An absorption of a stopped π^--meson, K^--meson and $\bar{p}$ by a nucleus procceeds in several steps [IKP94]:

1. A particle is captured by the Coulomb fiels of a nucleus forming a pionic or a kaonic or $\bar{p}$-atom;
2. Such atom de-excites through the emission of Auger-electrons and X-rays;
3. A stopped particle from the atomic orbit is captured by nucleus (by a pair or more of intranuclear nucleons in the case of a stopped pion or by reaction on a quasifree nucleon producing a pion and Λ or Σ hyperon in the case of a stopped kaon or by annihilation on a quasifree nucleon in the case of $\bar{p}$-capture);
4. Rescatterings of fast nucleons and pions produced in a stopped particle absorption (hadron kinetics);
5. Decay of excited residual nucleus (nucleus deexcitation).

Thus the absorption processes for the stopped pion, kaon and antiproton are similar. However, there are some absorption peculiarities for each type of particles.

Absorption of stopped π^- by nucleus.

It is simulated by the kinetic model. As follows from calculations within the framework of the optical model [INC76] with the Kisslinger potential [Kiss55] the capture a pion from an orbit of atom takes place at radius r in the nuclear surface and absorption probability $P_{abs}(r)$ can be approximated by

$$P_{abs}(r) = P_0 \exp\left[-0.5\left(\frac{r - R_\pi}{D_\pi}\right)^2\right],$$

where parameters of the Gaussian distribution $R_\pi \approx R_{1/2}$, where $R_{1/2}$ is the half-density radius, and D_π for different nuclei can be found in [IKP94].

The absorption of the pion is considered as the s-wave (non-resonant) absorption mainly by the the simplest cluster consisting of two nucleon (np) or (pp).

Once a pion has been absorbed by a nucleon pair, the pion mass is converted into kinetic energy of nucleon. Each nucleon has the energy $E_N = m_\pi/2$ in the center of mass pair. In the center of mass nucleons flay away in opposite direction isotropically. The inital momentum of pair is taken as a sum of nucleon Fermi momenta.

Absorption of stopped K^- by nucleus.

It is simulated in the kinetic model framework. In this case the absorption probability was choosen the same as in annhihilation of the stopped antiprotons.

Annihilation of stopped $\bar{p}$ by nucleus.

In this case the absorption probability was also given by equation of ([SAS1]) with the values of $R_{\bar{p}} = R_\pi$ and dispertion $D^2 = 1$ fm:math:*(^2)* [INC82].

The annhihilation of antiproton on a quasifree nucleon is modelled via the annihilation of a diquark-antidiquark with subsequent fragmentation of the meson string as it was done in the parton string model.

BIBLIOGRAPHY

[1] R.J. Glauber. *High Energy Physics and Nuclear Structure*. Plenum Press, NY, edited by s. devons edition, 1970.

[2] Robert H. Bassel and Colin Wilkin. High-energy proton scattering and the structure of light nuclei. *Physical Review*, 174(4):1179–1199, oct 1968. URL: https://doi.org/10.1103/PhysRev.174.1179, doi:10.1103/physrev.174.1179.

[3] VL KOROTKIKH and NI STARKOV. Photoproduction of heavy vector-mesons on nuclei with excitation of a discrete level. *Soviet Journal of Nuclear Physics*, 37(4):610–613, 1983.

[4] NT ERMEKOV, VL KOROTKIKH, and NI STARKOV. Estimate of the contribution of excitation of the 2+(1.78 mev) level of silicon to the cross-section for the reaction si-28(pi, 3-pi)si-28'. *Soviet Journal of Nuclear Physics*, 33(6):775–777, 1981.

[5] R.A. Nam, S.I. Nikol'skii, N.I. Starkov, V.A. Tsarev, A.P. Chubenko, and V.I. Yakovlev. Proton-proton total cross sections from cosmic ray data. *Sov. J. Nucl. Phys. (Engl. Transl.); (United States)*, 26:5:550–555, Nov 1977. Yad. Fiz. 26 1038 - Russian.

[6] G.D. Alkhazov, S.L. Belostotsky, and A.A. Vorobyov. Scattering of 1 GeV protons on nuclei. *Physics Reports*, 42(2):89–144, jun 1978. URL: https://doi.org/10.1016/0370-1573(78)90083-2, doi:10.1016/0370-1573(78)90083-2.

[1] N.V. Mokhov. The mars code system user's guide, version 13(95). 1995. Fermilab-FN-628.

[1] J.K. Tuli. Evaluated nuclear structure data file. *Nuclear Instruments and Methods in Physics Research Section A: Accelerators, Spectrometers, Detectors and Associated Equipment*, 369(2-3):506–510, Feb 1996. online database: http://www.nndc.bnl.gov/nudat2/. URL: https://doi.org/10.1016/S0168-9002(96)80040-4, doi:10.1016/s0168-9002(96)80040-4.

[2] D.H. Wilkinson. Evaluation of the fermi function$\mathsemicolon $ EO competition. *Nuclear Instruments and Methods*, 82:122–124, may 1970. URL: https://doi.org/10.1016/0029-554X(70)90336-8, doi:10.1016/0029-554x(70)90336-8.

[3] E. Konopinski. *The Theory of Beta Radioactivity*. Oxford Press, 1966.

[4] P.R. Truscott. *PhD Thesis*. University of London, 1996.

[1] E. Gadioli and E. Gadioli Erba. Nuclear reactions induced by$\uppi $-at rest. *Physical Review C*, 36(2):741–757, aug 1987. URL: https://doi.org/10.1103/PhysRevC.36.741, doi:10.1103/physrevc.36.741.

[2] H.C. Chiang and J. Hüfner. Nucleons after pion absorption. *Nuclear Physics A*, 352(3):442–460, feb 1981. URL: https://doi.org/10.1016/0375-9474(81)90422-X, doi:10.1016/0375-9474(81)90422-x.

[3] D Ashery and J P Schiffer. Pion absorption in nuclei. *Annual Review of Nuclear and Particle Science*, 36(1):207–252, dec 1986. URL: https://doi.org/10.1146/annurev.ns.36.120186.001231, doi:10.1146/annurev.ns.36.120186.001231.

[4] Heinz J Weyer. Pion absorption in light nuclei. *Physics Reports*, 195(6):295–367, nov 1990. URL: https://doi.org/10.1016/0370-1573(90)90076-E, doi:10.1016/0370-1573(90)90076-e.

[5] R. Hartmann, H.P. Isaak, R. Engfer, E.A. Hermes, H.S. Pruys, W. Dey, H.J. Pfeiffer, U. Sennhauser, H.K. Walter, and J. Morgenstern. Spectroscopy of single and correlated neutrons following pion absorption in 12c, 59co and 197au. *Nuclear Physics A*, 308(3):345–364, oct 1978. URL: https://doi.org/10.1016/0375-9474(78)90556-0, doi:10.1016/0375-9474(78)90556-0.

[6] R. Madey, T. Vilaithong, B. D. Anderson, J. N. Knudson, T. R. Witten, A. R. Baldwin, and F. M. Waterman. Neutrons from nuclear capture of negative pions. *Physical Review C*, 25(6):3050–3067, jun 1982. URL: https://doi.org/10.1103/PhysRevC.25.3050, doi:10.1103/physrevc.25.3050.

[7] F. W. Schlepütz, J. C. Comiso, T. C. Meyer, and K. O. H. Ziock. Emission of low-energy charged particles following negative-pion capture from rest. *Physical Review C*, 19(1):135–141, jan 1979. URL: https://doi.org/10.1103/PhysRevC.19.135, doi:10.1103/physrevc.19.135.

[8] C. J. Orth, W. R. Daniels, B. J. Dropesky, R. A. Williams, G. C. Giesler, and J. N. Ginocchio. Products of stopped-pion interactions with cu and ta. *Physical Review C*, 21(6):2524–2534, jun 1980. URL: https://doi.org/10.1103/PhysRevC.21.2524, doi:10.1103/physrevc.21.2524.

[9] H.S. Pruys, R. Engfer, R. Hartmann, U. Sennhauser, H.-J. Pfeiffer, H.K. Walter, J. Morgenstern, A. Wyttenbach, E. Gadioli, and E. Gadioli-Erba. Absorption of stopped $\uppi $- in 59co, 75as, 197au and 209bi investigated by in-beam and activation $\upgamma $-ray spectroscopy. *Nuclear Physics A*, 316(3):365–388, mar 1979. URL: https://doi.org/10.1016/0375-9474(79)90043-5, doi:10.1016/0375-9474(79)90043-5.

[10] P. Heusi, H.P. Isaak, H.S. Pruys, R. Engfer, E.A. Hermes, T. Kozlowski, U. Sennhauser, and H.K. Walter. Coincident emission of neutrons and charged particles after $\uppi $- absorption in 6li, 7li, 12c, 59co and 197au. *Nuclear Physics A*, 407(3):429–459, oct 1983. URL: https://doi.org/10.1016/0375-9474(83)90660-7, doi:10.1016/0375-9474(83)90660-7.

[11] H.P. Isaak, A. Zglinski, R. Engfer, R. Hartmann, E.A. Hermes, H.S. Pruys, F.W. Schlepütz, T. Kozlowski, U. Sennhauser, H.K. Walter, K. Junker, and Nimai C. Mukhopadhyay. Inclusive neutron spectra from the absorption of stopped negative pions in heavy nuclei. *Nuclear Physics A*, 392(2-3):368–384, jan 1983. URL: https://doi.org/10.1016/0375-9474(83)90133-1, doi:10.1016/0375-9474(83)90133-1.

[12] H. Machner. Study of particle emission following $\uppi $- absorption at rest. *Nuclear Physics A*, 395(2):457–470, mar 1983. URL: https://doi.org/10.1016/0375-9474(83)90054-4, doi:10.1016/0375-9474(83)90054-4.

[13] H.P. Isaak et al. Single and coincident neutron emission after the absorption of stopped negative pions in ^{6}li, ^{7}li, ^{12}c, ^{59}co ^{197}au. *Helvetica Physica Acta*, 55:477–500, 1982. https://www.e-periodica.ch/digbib/view?pid=hpa-001:1982:55#479.

[1] J Frenkel. On the absorption of light and the trapping of electrons and positive holes in crystalline dielectrics. *Phys. Zs. Sowjetunion*, 9:533–536, 1936.

[2] V. F. Weisskopf and D. H. Ewing. On the yield of nuclear reactions with heavy elements. *Physical Review*, 57(6):472–485, mar 1940. URL: https://doi.org/10.1103/PhysRev.57.472, doi:10.1103/physrev.57.472.

[1] A.S. Iljinov, M.V. Mebel, N. Bianchi, E. De Sanctis, C. Guaraldo, V. Lucherini, V. Muccifora, E. Polli, A.R. Reolon, and P. Rossi. Phenomenological statistical analysis of level densities, decay widths and lifetimes of excited nuclei. *Nuclear Physics A*, 543(3):517–557, jul 1992. URL: https://doi.org/10.1016/0375-9474(92)90278-R, doi:10.1016/0375-9474(92)90278-r.

[2] Evaluated nuclear structure data file (ensdf) - a computer file of evaluated experimental nuclear structure data maintained by the national nuclear data center, brookhaven national laboratory. http://www.nndc.bnl.gov/nudat2/. [Online; accessed 31-october-2017].

[1] A. Boudard, J. Cugnon, J.-C. David, S. Leray, and D. Mancusi. New potentialities of the liège intranuclear cascade model for reactions induced by nucleons and light charged particles. *Physical Review C*, jan 2013. URL: https://doi.org/10.1103/PhysRevC.87.014606, doi:10.1103/physrevc.87.014606.

[2] Davide Mancusi, Alain Boudard, Joseph Cugnon, Jean-Christophe David, Pekka Kaitaniemi, and Sylvie Leray. Extension of the liège intranuclear-cascade model to reactions induced by light nuclei. *Physical Review C*, nov 2014. URL: https://doi.org/10.1103/PhysRevC.90.054602, doi:10.1103/physrevc.90.054602.

[3] Ricciardi M V Kelic A and Schmidt K H. Abla07 — towards a complete description of the decay channels of a nuclear system from spontaneous fission to multifragmentation. In D Filges, S Leray, Y Yariv, A Mengoni, A Stanculescu, and G Mank Eds., editors, *Proceedings of the Joint ICTP-IAEA Advanced Workshop on Model Codes for Spallation Reactions*, number INDC(NDS)-530, 181. ICTP Trieste, Italy, 4-8 February 2008. IAEA, IAEA Vienna, August 2008. download: http://www-nds.iaea.org/reports-new/indc-reports/indc-nds/indc-nds-0530.pdf.

[4] IAEA. Benchmark of spallation models, organized by the iaea. http://www-nds.iaea.org/spallations. [Online; accessed 28-october-2017].

CHAPTER

EIGHT

PHOTOLEPTON

8.1 Introduction

Gamma-nuclear and lepto-nuclear reactions are handled in Geant4 as hybrid processes which typically require both electromagnetic and hadronic models for their implementation. While neutrino-induced reactions are not currently provided, the Geant4 hadronic framework is general enough to include their future implementation as a hybrid of weak and hadronic models.

The general scheme followed is to factor the full interaction into an electromagnetic (or weak) vertex, in which a virtual particle is generated, and a hadronic vertex in which the virtual particle interacts with a target nucleus. In most cases the hadronic vertex is implemented by an existing Geant4 model which handles the intra-nuclear propagation.

The cross sections for these processes are parameterizations, either directly of data or of theoretical distributions determined from the integration of lepton-nucleon cross sections double differential in energy loss and momentum transfer.

8.2 Gamma-nuclear Interactions

8.2.1 Process and Cross Section

Gamma-nuclear reactions in Geant4 are handled by the class *G4PhotoNuclearProcess*. The default cross section class for this process is *G4PhotoNuclearCrossSection*, which was described in detail in the previous chapter.

8.2.2 Final State Generation

Final state generation proceeds by two different models, one for incident gamma energies of a few GeV and below, and one for high energies. For high energy gammas, the QGSP model is used. Indicent gammas are treated as QCD strings which collide with nucleons in the nucleus, forming more strings which later hadronize to produce secondaries. In this particular model the remnant nucleus is de-excited using the Geant4 precompound and de-excitation sub-models.

At lower incident energies, there are two models to choose from. The Bertini-style cascade (*G4CascadeInterface* interacts the incoming gamma with nucleons using measured partial cross sections to decide the final state multiplicity and particle types. Secondaries produced in this initial interaction are then propagated through the nucleus so that they may react with other nucleons before exiting the nucleus. The remnant nucleus is then de-excited to produce low energy fragments. Details of this model are provided in another chapter in this manual.

An alternate handling of low energy gamma interactions is provided by *G4GammaNuclearReaction*, which is based upon the Chiral Invariant Phase Space model (CHIPS [CHIPS1][CHIPS2][CHIPS3]). In Geant4 version 9.6 and earlier a separate CHIPS model was provided for gamma nuclear interactions. Here the incoming gamma is absorbed into a nucleon or cluster of nucleons within the target nucleus. This forms an excited bag of partons which later fuse to form

final state hadrons. Parton fusion continues until there are none left, at which point the final nuclear evaporation stage is invoked to bring the nucleus to its ground state.

8.3 Electro-nuclear Interactions

8.3.1 Process and Cross Section

Electro-nuclear reactions in Geant4 are handled by the classes *G4ElectronNuclearProcess* and *G4PositronNuclearProcess*. The default cross section class for both these processes is *G4ElectroNuclearCrossSection* which was described in detail in an earlier chapter.

8.3.2 Final State Generation

Final state generation proceeds in two steps. In the first step the electromagnetic vertex of the electron/positron-nucleus reaction is calculated. Here the virtual photon spectrum is generated by sampling parameterized Q^2 and ν distributions. The equivalent photon method is used to get a real photon from this distribution.

In the second step, the real photon is interacted with the target nucleus at the hadronic vertex, assuming the photon can be treated as a hadron. Photons with energies below 10 GeV can be interacted directly with nucleons in the target nucleus using the measured (γ, p) partial cross sections to decide the final state multiplicity and particle types. This is currently done by the Bertini-style cascade (*G4CascadeInterface*). Photons with energies above 10 GeV are converted to π^0s and then allowed to interact with nucleons using the FTFP model. In this model the hadrons are treated as QCD strings which collide with nucleons in the nucleus, forming more strings which later hadronize to produce secondaries. In this particular model the remnant nucleus is de-excited using the Geant4 precompound and de-excitation sub-models.

This two-step process is implemented in the *G4ElectroVDNuclearModel*. An alternative model is the CHIPS-based *G4ElectroNuclearReaction* [CHIPS3]. This model also uses the equivalent photon approximation in which the incoming electron or positron generates a virtual photon at the electromagnetic vertex, and the virtual photon is converted to a real photon before it interacts with the nucleus. The real photon interacts with the hadrons in the target using the CHIPS model in which quasmons (generalized excited hadrons) are produced and then decay into final state hadrons. Electrons and positrons of all energies can be handled by this single model.

8.4 Muon-nuclear Interactions

8.4.1 Process and Cross Section

Muon-nuclear reactions in Geant4 are handled by the class *G4MuonNuclearProcess*. The default cross section class for this process is *G4KokoulinMuonNuclearXS*, the details of which are discussed in section [section:muonNuclear].

8.4.2 Final State Generation

Just as for the electro-nuclear models, the final state generation for the muon-nuclear reactions proceeds in two steps. In the first step the electromagnetic vertex of the muon-nucleus reaction is calculated. Here the virtual photon spectrum is generated by sampling parameterized momentum transfer (Q^2) and energy transfer (ν) distributions. In this case the same equations used to generate the process cross section are used to sample Q^2 and ν. The equivalent photon method is then used to get a real photon.

In the second step, the real photon is interacted with the target nucleus at the hadronic vertex, assuming the photon can be treated as a hadron. Photons with energies below 10 GeV can be interacted directly with nucleons in the

target nucleus using the measured (γ, p) partial cross sections to decide the final state multiplicity and particle types. This is currently done by the Bertini-style cascade (*G4CascadeInterface*). Photons with energies above 10 GeV are converted to π^0s and then allowed to interact with nucleons using the FTFP model. In this model the hadrons are treated as QCD strings which collide with nucleons in the nucleus, forming more strings which later hadronize to produce secondaries. In this particular model the remnant nucleus is de-excited using the Geant4 precompound and de-excitation sub-models.

This two-step process is implemented in the *G4MuonVDNuclearModel*.